Interplay between retinal light responses and the circadian clock, and their implications for retinal degenerative diseases



Teele Palumaa

St Cross College

University of Oxford

A thesis submitted for the degree of

Doctor of Philosophy

Hilary 2021

Acknowledgements

I would like to begin by thanking my supervisors Associate Professor Aarti Jagannath and Professor Russell Foster. Thank you for awarding me a studentship in your lab and for all your support and guidance throughout my DPhil.

Next, I want to thank the entire Jagannath Lab and the wider SCNi community. Thank you, Anna, Simona, Norbert, and Steve, for your friendship and support throughout the years and for making the lab such a fun work environment. Thank you, Steve Hughes, for teaching me all the retina-specific lab techniques and for always taking the time to share your vast knowledge of melanopsin. Thank you, Michael Gilhooley and Moritz Lindner, for the valuable input from a clinical perspective. And Lewis. You have been an extremely kind and supportive mentor. Thank you for all the help and advice you have given me throughout the years, for always taking the time to discuss any experiments, and for guiding me in the thesis-writing process.

This page is too short to mention everyone whose care and kindness have helped shape this DPhil into a fantastic experience. I was very fortunate to be part of St Cross College. Thank you for always looking out for me. And thank you to all the amazing people whom I have the fortune to call my friends.

I am very grateful to my family for their love and support. My parents, thank you for being such exceptional role models. And thank you, my brother Priit, for being my best friend, and for colour-blind-proofing all the figures of this thesis.

Most of all, thank you, Mother Ksenia. This thesis is for you.

Abstract

Multiple aspects of mammalian physiology display circadian rhythms, which allow the organism to better adapt to the external environment. Several circadian rhythms, such as the sleep-wake cycle and the retinal function, are primarily regulated by light detection in the retina. The molecular properties of melanopsin, a blue light sensitive photopigment expressed in a subset of retinal ganglion cells, make it ideal for encoding environmental light levels. Indeed, melanopsin has been shown to regulate several aspects of the retinal circadian function. However, the molecular mechanisms underpinning melanopsin's role in retinal circadian rhythms remain unknown. By analysing the circadian transcriptome of wild-type and melanopsin-null retinas, I discovered that the absence of melanopsin leads to dampened rhythmicity in the expression of core clock genes. Furthermore, while the melanopsin-null retinas retained the rhythmic expression of dopamine-related and gap junction genes, the circadian rhythmicity of sphingolipid and phototransduction pathways were aberrant.

Alongside its role in the retinal circadian clock, melanopsin is also modulating functional aspects of retinal light adaption, and it has been suggested that melanopsin may mediate retinoprotection in response to bright light exposure. However, using a mouse model of light-induced retinal damage, I did not detect an increased susceptibility to light damage in animals lacking melanopsin. I further studied how well the mouse model of retinal light damage mirrors the human retinal degenerations. I conducted a meta-analysis of all available datasets probing retinal transcriptome changes in this model and discovered that the genes affected by light damage were enriched for genes implicated in human retinal degenerations, indicating that the model indeed mimics the molecular aspects of human diseases.

Finally, melanopsin signalling also regulates the central light responses in the suprachiasmatic nucleus (SCN), but several reports on its role in retinal light sensitivity are conflicting. Therefore, I further researched how retinal and SCN responses to light are regulated. I found that the retinal light responses of animals lacking melanopsin were slightly attenuated, similarly to what is known about their SCN light responses. However, in a mouse model showing increased SCN light sensitivity, the retinal responses were not enhanced, suggesting differential regulation of the retinal and SCN light sensitivity.

These results provide valuable insights into the molecular and functional aspects of retinal light responses in both local and central circadian rhythms, and dissect their implications for retinal degenerative diseases, together providing a wealth of avenues for future research.

Declaration of Authorship

I declare that this thesis is my own original work, other than where explicitly indicated in the text, and it has not been submitted toward a research degree at this university or any other.

Teele Palumaa
Hilary 2021

Contents

List of Figures **x**

List of Tables **xiv**

List of Abbreviations **xv**

1 Introduction **1**

1.1 The structure and function of the mammalian retina 1

1.1.1 Visual responses 4

1.1.2 Non-visual responses 8

1.2 The structure and function of melanopsin and pRGCs 11

1.2.1 The properties of melanopsin 12

1.2.2 The central projections of pRGCs 14

1.2.3 The diversity of pRGCs 16

1.2.4 Intraretinal connections 18

1.2.5 Role in non-visual responses 19

1.2.6 Role in visual responses 22

1.2.7 Role in retinal development 22

1.3 Circadian rhythms 24

1.3.1 The concepts and terminology of circadian rhythms 24

1.3.2 The suprachiasmatic nucleus and central circadian rhythms . 25

1.3.3 Molecular mechanisms of circadian rhythms 28

1.3.4 Peripheral circadian rhythms 30

1.4 Retinal circadian rhythms 31

1.4.1 Physiological significance of retinal circadian rhythms 32

1.4.2 Retinal connectivity and retinal circadian rhythms: rod-cone coupling 32

1.4.3 Outputs of retinal circadian rhythms 33

1.4.4 Mechanisms of retinal circadian rhythms 34

1.4.5 Circadian rhythms and retinal degenerative diseases 37

1.5 Thesis aims 39

2 Methods **40**
2.1 Animals . . . 40
2.1.1 Animal housing . . . 40
2.1.2 Breeding . . . 40
2.1.3 Genotyping . . . 41
2.2 *In vivo* assessment of circadian and visual function . . . 42
2.2.1 Circadian activity monitoring . . . 42
2.2.2 Phase-shifting protocols . . . 42
2.2.3 Bright light exposure . . . 43
2.2.4 Pupillometry . . . 44
2.2.5 Optomotor response . . . 45
2.2.6 Novel visuospatial context recognition task . . . 47
2.2.7 Electroretinography . . . 49
2.3 RNA expression analysis . . . 52
2.3.1 Tissue collection for RNA analysis . . . 52
2.3.2 RNA extraction . . . 52
2.3.3 RNA quantity and quality analysis . . . 53
2.3.4 Reverse transcription and quantitative reverse transcription PCR . . . 53
2.3.5 RNA sequencing . . . 54
2.4 Mass spectrometry . . . 55
2.5 Cell culture and plasmid transfection . . . 56
2.6 Immunostaining . . . 56
2.6.1 Immunocytochemistry . . . 56
2.6.2 Frozen tissue sections . . . 57
2.6.3 Retinal flat-mounts . . . 58
2.6.4 Confocal microscopy image aquisition . . . 59
2.6.5 Retinal thickness measurements . . . 59
2.6.6 Determining retinal cone distribution . . . 60
2.7 Multielectrode array recordings . . . 60
2.8 Light measurements . . . 61
2.9 Meta-analysis of acute gene expression changes in light-induced retinal damage . . . 62
2.9.1 Identifying studies . . . 62
2.9.2 Data extraction and analysis . . . 62
2.10 Defining retinal cell-specific gene enrichment . . . 63
2.11 Statistical analysis . . . 64

3 The role of melanopsin in retinal and central circadian rhythms 66
3.1 Introduction . . . 66
3.1.1 Retinal circadian rhythms in *Opn4*$^{-/-}$ animals . . . 66
3.1.2 Light-induced phase shifts in *Opn4*$^{-/-}$ animals . . . 73
3.1.3 Retinal development of *Opn4*$^{-/-}$ animals . . . 75
3.2 Aims of this chapter . . . 76
3.3 Results . . . 77
3.3.1 Circadian rhythmicity of the retinal transcriptome is not abolished but altered in *Opn4*$^{-/-}$ animals . . . 77
3.3.2 *Opn4*$^{-/-}$ retinas display dampened circadian rhythmicity of core clock genes . . . 88
3.3.3 There are global differences in retinal gene expression between WT and *Opn4*$^{-/-}$ animals . . . 93
3.3.4 Mouse and baboon rhythmic retinal transcriptomes show little overlap . . . 94
3.3.5 The light responses of the retina, but not the SCN, are affected by the light dose reaching the retinas of WT and *Opn4*$^{-/-}$ animals 98
3.3.6 There are no discernible cone abnormalities in *Opn4*$^{-/-}$ retinas 108
3.4 Discussion . . . 118
3.4.1 Retinal circadian rhythms and the role of melanopsin . . . 118
3.4.2 Retinal and SCN light responses in the absence of melanopsin 121
3.4.3 Melanopsin and retinal cones . . . 122
3.4.4 Limitations of this study and future work . . . 122

4 The role of melanopsin in light-induced retinal damage 124
4.1 Introduction . . . 124
4.1.1 The damaging effect of light on the retina . . . 125
4.1.2 The protective effect of light on the retina . . . 128
4.1.3 The potential role for melanopsin in retinal protection . . . 128
4.2 Aims of this chapter . . . 133
4.3 Results . . . 134
4.3.1 The retinal and visual functions of *Opn4*$^{-/-}$ mice show a transient decline after exposure to a 10,000 lux light pulse . 134
4.3.2 Retinal morphology of WT and *Opn4*$^{-/-}$ mice is not affected by a 10,000 lux light pulse . . . 140
4.3.3 The pupils of *Opn4*$^{-/-}$ mice redilate when exposed to a 10,000 lux light pulse . . . 142
4.3.4 WT mice develop retinal degeneration upon exposure to a 3-hour light pulse of 20,000 lux . . . 144

4.3.5 Retinal transcriptomes of WT and *Opn4*$^{-/-}$ mice are similar after a 20,000 lux light pulse . . . 149
4.3.6 The retinal function of WT and *Opn4*$^{-/-}$ mice deteriorates after exposure to a 20,000 lux light pulse . . . 154
4.3.7 A 20,000 lux light pulse induces retinal degeneration in WT and *Opn4*$^{-/-}$ mice . . . 158
4.4 Discussion . . . 164
4.4.1 Limitations of this study and future work . . . 167

5 Light-induced retinal damage as a model of human retinal degenerative diseases: a meta-analysis of transcriptome profiling studies 169
5.1 Introduction . . . 169
5.1.1 Inherited and acquired retinal degenerations . . . 170
5.1.2 Molecular mechanisms of retinal degenerations . . . 171
5.1.3 Mouse models of retinal degenerations . . . 173
5.2 Aims of this chapter . . . 175
5.3 Results . . . 176
5.3.1 Six publicly available LIRD transcriptomics datasets were identified . . . 176
5.3.2 Meta-analysis revealed 2,944 retinal genes differentially regulated in LIRD . . . 179
5.3.3 LIRD leads to the differential regulation of genes implicated in IRDs and AMD . . . 182
5.3.4 LIRD affects the cellular pathways, but not genes differentially regulated in AMD . . . 182
5.3.5 Retinal cell populations enriched for genes differentially regulated in LIRD and AMD show limited similarity . . . 188
5.3.6 LIRD and AMD do not differentially affect rhythmic retinal genes . . . 190
5.4 Discussion . . . 192
5.4.1 Limitations of this study and future work . . . 195

6 Characterisation of the key circadian protein salt-inducible kinase 1 in the mammalian retina 198
6.1 Introduction . . . 198
6.1.1 Function of SIK1 in the core molecular clock . . . 199
6.1.2 The SIK family and signalling cascade . . . 200
6.1.3 The possible function of SIK1 in the retina . . . 201
6.2 Aims of this chapter . . . 202

6.3 Results 203
6.3.1 SIK family and related transcripts are expressed in the retina and other ocular tissues 203
6.3.2 SIK1 is expressed ubiquitously in the mouse retina 206
6.3.3 Retinal morphology is unaffected by the lack of functional SIK1 212
6.3.4 The distribution of cones is not affected by the lack of functional SIK1 212
6.3.5 Retinal gene induction in response to a light pulse is not enhanced in the absence of functional SIK1 217
6.3.6 Maximum pupil constriction and its diurnal regulation is normal in animals lacking functional SIK1 218
6.4 Discussion 222
6.4.1 Limitations of this study and future work 222

7 Thesis summary and final discussion **225**
7.1 Key findings 225
7.2 Future directions 227

Appendices

A Spectra of lights used in this thesis **231**

B Primers used for RT-qPCR **234**

References **236**

List of Figures

1.1 The general structure of the mammalian retina 3
1.2 Phototransduction cascade of rods and cones 5
1.3 The visual cycle 7
1.4 A simplified schematic of ascending visual pathways in rodents . . . 8
1.5 Phototransduction cascade of pRGCs 13
1.6 Projections of pRGCs and associated physiological processes 15
1.7 pRGC subtypes and intraretinal connections 19
1.8 Terminology of circadian rhythms 26
1.9 The molecular mechanism of the mammalian core circadian clock . 29
1.10 The hierarchical organisation of circadian clocks 31

2.1 Schematic of the optomotor system 46
2.2 Novel visuospatial context recognition task 48

3.1 Diurnal rhythmicity of pupillary light response in WT and *Opn4*$^{-/-}$ animals 68
3.2 Circadian and diurnal rhythmicity of contrast sensitivity in WT and *Opn4*$^{-/-}$ animals 69
3.3 Diurnal rhythmicity of cone ERG in WT and *Opn4*$^{-/-}$ animals . . . 71
3.4 Quality control metrics of the retinal circadian time course RNA-seq samples 78
3.5 Principal component analysis of WT and *Opn4*$^{-/-}$ retinal circadian time course RNA-seq samples 79
3.6 An overview of the circadian transcriptomes of WT and *Opn4*$^{-/-}$ retinas 80
3.7 Genes showing circadian rhythmicity in WT and *Opn4*$^{-/-}$ retinas . . 81
3.8 The distribution in peak phases of circadian transcripts in WT and *Opn4*$^{-/-}$ retinas 82
3.9 Cell-specific gene expression of the markers used for cell sorting by Siegert et al. 83
3.10 Enrichment of circadian genes in retinal cell subpopulations 85
3.11 Analysis of overrepresented pathways in the circadian genes 87

3.12 Cell-specific expression of the circadian genes belonging to differentially regulated pathways 89
3.13 Circadian expression of core clock and related genes in WT and *Opn4*$^{-/-}$ retinas 90
3.14 Circadian expression of core clock genes in WT and *Opn4*$^{-/-}$ retinas 91
3.15 Circadian rhythmicity parameters of clock genes in WT and *Opn4*$^{-/-}$ retinas 92
3.16 Expression of core clock genes in different retinal cell populations . 93
3.17 Global gene expression differences between WT and *Opn4*$^{-/-}$ retinas 94
3.18 Analysis of overrepresented pathways in genes differentially expressed between WT and *Opn4*$^{-/-}$ retinas 95
3.19 Comparison of mouse retinal circadian genes and baboon retinal diurnal genes 97
3.20 Pupil constriction of WT and *Opn4*$^{-/-}$ mice in response to a sustained white light pulse 99
3.21 Expression and light regulation of immediate early genes genes in WT and *Opn4*$^{-/-}$ retinas upon an equal light dose 102
3.22 Representative actograms of mice in diurnal and circadian conditions 103
3.23 Circadian phase shifting of WT and *Opn4*$^{-/-}$ animals in response to CT16 light pulses 104
3.24 Expression and light regulation of immediate early genes genes in WT and *Opn4*$^{-/-}$ SCNs upon an equal light dose 106
3.25 Expression and light regulation of clock genes genes in WT and *Opn4*$^{-/-}$ SCNs upon an equal light dose 107
3.26 Expression of cone genes and proteins in WT and *Opn4*$^{-/-}$ retinas . 108
3.27 Cone distribution in WT and *Opn4*$^{-/-}$ retinas 110
3.28 Number of cones along the dorsoventral axis in WT and *Opn4*$^{-/-}$ retinas 111
3.29 Density of cone subtypes along the dorsoventral axis in WT and *Opn4*$^{-/-}$ retinas 112
3.30 Schematic of chromatic pupillometry experiment setup 114
3.31 Maximum pupil constriction of WT and *Opn4*$^{-/-}$ animals in response to different wavelengths of light 115
3.32 Effect of opsinamide on melanopsin, and rod and cone photoreception 117

4.1 Light-induced transcriptome changes in WT and *Opn4*$^{-/-}$ retinas . . 130
4.2 Light-induced expression of retinal crystallin genes 132
4.3 Timeline of the retinal light damage experiment 136
4.4 Maximum pupil constriction before and after bright light exposure . 137
4.5 Optomotor response before and after bright light exposure 138

4.6 Novel visuospatial context recognition task performance before and after bright light exposure 139
4.7 Immunohistochemical analysis of retinal morphology after bright light exposure 141
4.8 Pupil constriction dynamics in response to a sustained 10,000 lux light pulse 143
4.9 Expression of photoreceptor genes after exposure to 20,000 lux light pulses 145
4.10 Expression of pro-inflammatory genes after exposure to 20,000 lux light pulses of different durations 146
4.11 Retinal morphology of WT animals after exposure to 20,000 lux light pulses of different durations 148
4.12 Quality control metrics of the bright light exposed retinal RNA-seq samples 150
4.13 The genes and pathways differentially regulated between WT and *Opn4*$^{-/-}$ retinas after bright light exposure 151
4.14 The genes of selected pathways differentially regulated between WT and *Opn4*$^{-/-}$ retinas after bright light exposure 152
4.15 Enrichment of differentially expressed genes in retinal cell subpopulations 154
4.16 Pupil response before and after a 20,000 lux light pulse 156
4.17 Electroretinography before and after bright light exposure: first experiment 157
4.18 Electroretinography before and after bright light exposure: second experiment 159
4.19 Retinal gene expression after exposure to a 20,000 lux light pulse . 160
4.20 Gene expression in whole eyes after exposure to a 20,000 lux light pulse 161
4.21 Retinal morphology after bright light exposure 162
4.22 Correlations of retinal function measures after light damage 163

5.1 Principal component analysis of the six studies included in the LIRD meta-analysis 180
5.2 Differentially regulated genes and pathways in LIRD 181
5.3 Overlap of differentially expressed genes in LIRD with genes associated with IRDs and AMD 183
5.4 Principal component analysis of control and AMD retinas 184
5.5 Differentially regulated genes and pathways in AMD retinas 185
5.6 Gene expression and pathway overlap between LIRD and AMD retinal changes 186

5.7 The overlap between retinal genes differentially regulated in AMD and AMD risk genes . . . 188
5.8 Differentially regulated genes and pathways in male and female AMD retinas . . . 189
5.9 Enrichment of differentially regulated genes in retinal cell types . . 190
5.10 Representation of diurnally rhythmic genes in LIRD and AMD retinas 191

6.1 SIK1 acts as a brake on light-induced clock shifts in the SCN 200
6.2 Expression of SIK family and related transcripts in baboon ocular tissues . . . 204
6.3 Expression of *Sik1* in murine retinal cell populations 206
6.4 Immunohistochemical staining pattern of SIK1 in the retina 208
6.5 Immunohistochemical staining pattern of SIK1 in the SCN 209
6.6 Immunocytochemical staining pattern of SIK1 in NIH3T3 cells overexpressing SIK1 . . . 211
6.7 Morphology of cones, bipolar and retinal ganglion cells in WT and SIK1 KI retinas . . . 213
6.8 Morphology of amacrine, horizontal and glial cells in WT and SIK1 KI retinas . . . 214
6.9 Expression of opsins and core clock genes in WT and SIK1 KI retinas 215
6.10 Cone distribution in WT and SIK1 KI retinas 216
6.11 Light-regulation of immediate early genes in SIK1 KI retinas 218
6.12 Light-induced expression of clock genes in SIK1 KI retinas 219
6.13 Characterisation of pupil response in SIK1 KI animals 220
6.14 Diurnal rhythmicity of pupil response in SIK1 KI animals 221

A.1 Spectra of lights used in this thesis 231
A.2 Spectra of lights used in this thesis *(continued)* 232
A.3 Spectra of lights used in this thesis *(continued)* 233

List of Tables

2.1 ERG protocols used 51
2.2 Primary antibodies used 58
2.3 Secondary antibodies used 59

3.1 Differences in light doses between WT and *Opn4*$^{-/-}$ animals at commonly used light pulses 100

5.1 Light-induced retinal damage transcriptome profiling studies identified 178

6.1 Statistical significance of diurnal rhythmicity of individual genes in ocular tissues 205

List of Abbreviations

ABCD4 . . . . . ATP-binding cassette subfamily D member 4

ACO1 . . . . . aconitase 1

ADCY . . . . . adenylate cyclase

AMD . . . . . age-related macular degeneration

AMPK1 . . . . . adenosine monophosphate activated protein kinase 1

ANOVA . . . . . analysis of variance

ARR . . . . . arrestin

bFGF . . . . . basic fibroblast growth factor

BMAL1 . . . . . brain and muscle ARNT-like 1

C2/C3 . . . . . complement components 2/3

cAMP . . . . . cyclic adenosine monophosphate

cGMP . . . . . cyclic guanosine monophosphate

CFB/CFH . . . . complement factor B/H

CHRNA3 . . . . . neuronal acetylcholine receptor subunit alpha-3

CK1 . . . . . casein kinase 1

cl . . . . . a transgenic mouse line expressing attenuated diphteria toxin under the control of the human cone opsin promoter, which leads to cone degeneration

CLOCK . . . . . circadian locomotor output cycles protein kaput gene

CNGC . . . . . cyclic nucleotide–gated ion channel

cNMP . . . . . cyclic nucleotide

CNS . . . . . central nervous system

CNTF . . . . . ciliary neurotrophic factor

cpd . . . . . cycles per degree

CRE . . . . . cAMP response element

CREB . . . . . cAMP response element-binding protein

CREBBP . . . . . CREB binding protein

CRH . . . . . corticotropin-releasing hormone

CRTC . . . . . CREB-regulated transcription coactivator

CRY1/2 . . . . . cryptochrome 1/2

CRYA/B/G . . . α-, β-, γ-crystallins

CT . . . . . circadian time

Cx36 . . . . . connexin 36

DAC . . . . . dopaminergic amacrine cell

DAG . . . . . diacylglycerol

DAPI . . . . . 4',6-diamidino-2-phenylindole

DBP . . . . . albumin D-site binding protein

DD . . . . . constant darkness (dark-dark, in reference to housing condition)

DIO2 . . . . . deiodinase 2

dLGN . . . . . dorsal lateral geniculate nucleus

DRD1/2/4 . . . . dopamine receptor D1/D2/D4

E-box . . . . . enhancer box

EGR1 . . . . . early growth response protein 1

ERG . . . . . electroretinogram

EYFP . . . . . enhanced yellow fluorescent protein

FACS . . . . . fluorescence-activated cell sorting

FCS . . . . . fetal calf serum

FDR . . . . . false discovery rate

FOS . . . . . Fos proto-oncogene

FWHM . . . . . full width at half maximum

GABA . . . . . gamma-aminobutyric acid

GCL . . . . . ganglion cell layer

GFAP . . . . . glial fibrillary acidic protein

GFP . . . . . green fluorescent protein

GPCR . . . . . G protein-coupled receptor

GRIK4 . . . . . glutamate receptor ionotropic, kainate 4

GRK . . . . . G protein-coupled receptor kinase

GSK-3β . . . . . glycogen synthase kinase-3β

GUCY . . . . . guanylate cyclase
GWAS . . . . . genome-wide association study
HCN channel . . hyperpolarisation-activated cyclic nucleotide-gated channel
HDAC . . . . . class IIa histone deacetylase
IDH1 . . . . . isocitrate dehydrogenase 1
IGL . . . . . intergeniculate leaflet
IL . . . . . interleukin
ILM . . . . . inner limiting membrane
INF . . . . . interferon
INL . . . . . inner nuclear layer
IP_3 . . . . . inositol 1,4,5-trisphosphate
IPL . . . . . inner plexiform layer
IPM . . . . . interphotoreceptor matrix
IRBP . . . . . interphotoreceptor retinoid-binding protein
IRC . . . . . irradiance response curve
IRD . . . . . inherited retinal degeneration
JUN . . . . . Jun proto-oncogene
K2P channel . . . two-pore-domain potassium channel
KI . . . . . knock-in
LCA . . . . . Leber congenital amaurosis
LD . . . . . light-dark (in reference to housing condition)
LED . . . . . light-emitting diode
LH . . . . . lateral habenula
LIRD . . . . . light-induced retinal damage
LP . . . . . light pulse
LPo . . . . . lateroposterior dorsal thalamic complex
LRAT . . . . . lecithin-retinol acyltransferase
Luc . . . . . luciferase
M . . . . . million
M1-M6 . . . . . pRGC subtypes
M-cone . . . . . middle-wavelength-sensitive cone
MEA . . . . . microelectrode array

MeA . . . . . medial amygdala

MS . . . . . mass spectrometry

MT1 . . . . . melatonin receptor 1

ND . . . . . neutral density

NFL . . . . . nerve fiber layer

NPAS2 . . . . . neuronal PAS domain protein 2, a CLOCK paralog

NPAS4 . . . . . neuronal PAS domain protein 4

NR4A1 . . . . . nuclear receptor subfamily 4 group A member 1

OCT . . . . . optimum cutting temperature

ONH . . . . . optic nerve head

ONL . . . . . outer nuclear layer

OPL . . . . . outer plexiform layer

OPN . . . . . olivary pretectal nucleus

OPN4 . . . . . melanopsin

OPN5 . . . . . neuropsin

P . . . . . postnatal day

PAC1 . . . . . PACAP receptor, type I

PACAP . . . . . pituitary adenylate cyclase-activating peptide

PBS . . . . . phosphate-buffered saline

PCA . . . . . principal component analysis

PCR . . . . . polymerase chain reaction

PDE . . . . . phosphodiesterase

PER1/2/3 . . . . period 1/2/3

PFA . . . . . paraformaldehyde

PIP_2 . . . . . phosphatidylinositol 4,5-bisphosphate

PLC . . . . . phospholipase C

POS . . . . . photoreceptor outer segments

pRGC . . . . . photosensitive retinal ganglion cell

PV . . . . . parvalbumin

RDH . . . . . retinol dehydrogenase

rd/rd . . . . . a transgenic mouse line carrying a mutation in *Pde6b* gene, which leads to rod degeneration

rdta	a transgenic mouse line expressing attenuated diphteria toxin under the control of the rhodopsin promoter, which leads to rod degeneration
RetNet	Retinal Information Network
REV-ERB	also known as NR1D, nuclear receptor subfamily 1, group D
RGC	retinal ganglion cell
RHO	rhodopsin
RHT	retino-hypothalamic tract
RIN	RNA integrity number
RNA-seq	RNA sequencing
ROR	retinoic acid-related orphan receptor
RORE	retinoic acid-related orphan receptor response element
RP	retinitis pigmentosa
RPE	retinal pigment epithelium
RPE65	retinal pigment epithelium-specific 65 kDa protein
RT-qPCR	quantitative reverse transcription polymerase chain reaction
S1P	sphingosine 1-phosphate
S1PR	sphingosine receptors
SC	superior colliculus
SCN	suprachiasmatic nucleus
S-cone	short-wavelength-sensitive cone
SD	standard deviation
SEM	standard error of the mean
SIK1	salt-inducible kinase 1
SPHK	sphingosine kinase
SRIF	somatostatin
STK11	serine/threonine kinase 11
TLR	toll-like receptor
TNF	tumour necrosis factor
TRPC channel	transient receptor potential canonical channel
TTFL	transcriptional-translational feedback loop
TUNEL	terminal deoxynucleotidyl transferase dUTP nick end labelling

V1 . . . . . the primary visual cortex
V2 . . . . . the secondary visual cortex
VIP . . . . . vasoactive intestinal peptide
VEGF . . . . . vascular endothelial growth factor
vLGN . . . . . ventral lateral geniculate nucleus
VLPO . . . . . ventrolateral preoptic area
VPAC1/2 . . . . VIP receptors 1/2
WT . . . . . wild-type
ZT . . . . . Zeitgeber time

1 Introduction

1.1 The structure and function of the mammalian retina

The mammalian eye is responsible for two entirely different sensory tasks. The more familiar of those is vision, the ability to process light information to create an image of the surroundings. In addition to the visual function, the eye also senses the overall brightness of the environment to mediate several non-visual or non-image-forming responses. Life on Earth has evolved in a regularly and predictably alternating 24-hour cycle of light and darkness. From wildflowers to whales, most organisms have developed circadian rhythms in multiple aspects of their physiology, which allow them to anticipate these rhythmic changes. Light encoding by the eye mediates the synchronisation of these circadian rhythms to the environmental light-dark cycle. It also adjusts the physiology in response to more short-term changes in light intensity [1].

In mammals, the visual and non-visual light responses are mediated by the retina, the light-sensitive neural tissue at the back of the eyeball. Light entering the eye passes through the cornea and the lens, which refract the light rays, then traverses the transparent vitreous body and comes into focus on the retina. Underneath the retina lies the retinal pigment epithelium (RPE), the choroid, and the sclera, which is the eye's fibrous outer layer [2].

The retina consists of five types of neurons: the photoreceptors, bipolar cells, retinal ganglion cells (RGCs), horizontal cells, and amacrine cells, which are organised into three layers of cell bodies and two layers of synapses (Fig. 1.1). The photoreceptors are located in the outermost part of the retina on top of the RPE, which provides metabolic support to the photoreceptor outer segments. The vertebrate retinas use two conventional photoreceptors, the rods and cones, which form distinct circuits in the retina. Both photoreceptor classes use multiple retinal pathways to relay light signals to higher-order neurons, and the pathways are incredibly complex [3]. To simplify, the rods synapse primarily with the rod and the cones with the cone bipolar cells in the outer plexiform layer. The cone bipolar cells, in turn, synapse with the third-order neurons, the retinal ganglion cells (RGCs), while the rod bipolar cells send their signals to the RGCs primarily through a subset of amacrine cells. These second-order synapses are localised to the inner plexiform layer. All light signals are ultimately transmitted to the RGCs [3]. The axons of the RGCs form the nerve fibre layer (NFL) in the innermost portion of the retina, converge and exit the eye as the optic nerve, which projects to various visual and non-visual subcortical areas. Signal transmission in the plexiform layers is modulated by retinal interneurons, the horizontal and amacrine cells. The photoreceptor nuclei constitute the outer nuclear layer (ONL), and the nuclei of bipolar, horizontal and amacrine cells are located in the inner nuclear layer (INL). The five main neuronal types have multiple subtypes, making the retinal structure and connectivity very intricate. Approximately 100 specific cell types have been identified in the mammalian retina, including 3-4 types of photoreceptors (1 rod and 2-3 cone subtypes, depending on the species), 50-70 types of interneurons (bipolar, horizontal and amacrine cells), and 20-30 distinct RGCs [2].

In addition to neurons, the retina contains three types of glial cells: Müller cells, astrocytes and microglia. Müller cells stretch radially across the retina from its inner border to the distal end of the ONL. They represent 90% of the retinal glia and provide structural and metabolic support to photoreceptors and other retinal neurons [4]. Astrocytes are mainly localised to the ganglion cell layer (GCL)

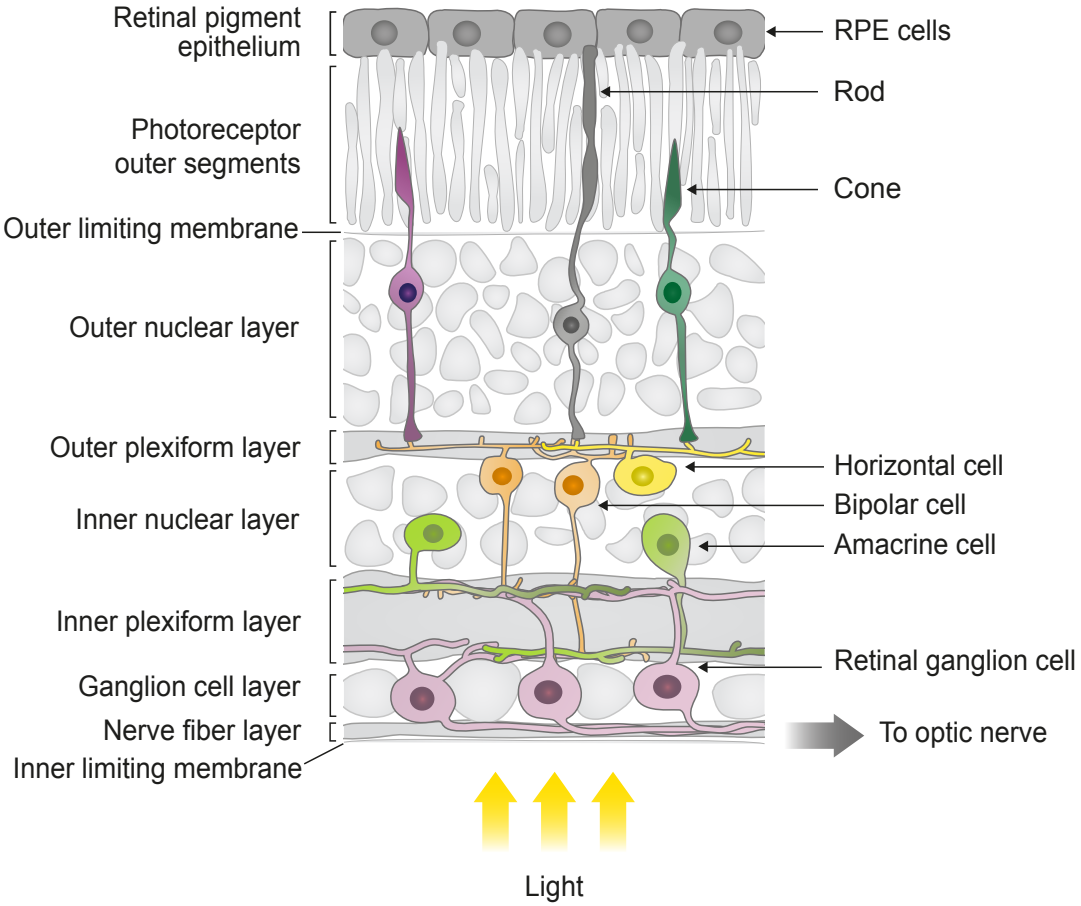


Figure 1.1: The general structure of the mammalian retina. The retina is composed of five neuronal cell types organised into three cellular layers. The outer segments of the visual photoreceptors, rods and cones, are situated in the outermost part of the retina, and their nuclei form the outer nuclear layer. The outer rod segments are embedded in the retinal pigment epithelium (RPE). Photoreceptors synapse onto bipolar cells in the outer plexiform layer. The signals from bipolar cells are ultimately relayed to the retinal ganglion cells in the inner plexiform layer. The horizontal and amacrine cells are interneurons modulating information flow in the two plexiform layers. Their cell bodies lie together with the bipolar cell nuclei in the inner nuclear layer. The axons of retinal ganglion cells constitute the nerve fibre layer and optic nerve, which projects to the brain. The retinal glial cells, primarily the Müller cells, form the outer and the inner limiting membranes. The mouse cone photoreceptors are depicted in this figure.

and NFL and similarly to Müller cells support the functioning of neurons. The astrocytes and the endfeet of Müller cells form the inner limiting membrane (ILM), the boundary between the retina and the vitreous (Fig. 1.1). In their outermost part, the Müller cells form adherens junctions with each other and with photoreceptors, creating the outer limiting membrane (OLM) (Fig. 1.1). Microglia are the resident tissue macrophages of the retina situated in the GCL, and the principal sources of pro-inflammatory mediators in response to pathogenic stimuli [4].

1.1.1 Visual responses

Visual processing begins in the photoreceptors, the rods and the cones. The photoreceptor outer segments are modified cilia filled with discs of folded double membranes and are densely packed with the photopigments, rhodopsin and cone opsins in rods and cones, respectively. A photopigment consists of an opsin protein and a light-sensitive chromophore 11-*cis*-retinal, a vitamin A derivative. Light reaching the outer segments is absorbed by the photopigments, resulting in the activation of the phototransduction cascade [5].

Phototransduction begins with the light-induced isomerisation of 11-*cis*-retinal to all-*trans*-retinal, which leads to a conformational change in the opsin molecule. The opsin molecules themselves are G protein-coupled receptors. When activated, they bind to and activate their partner G protein transducin, a heterotrimeric protein. When activated, transducin dissociates into α and $\beta\gamma$ subunits, initiating a further downstream signalling cascade, including the activation of cGMP phosphodiesterase (PDE), the drop in intracellular cGMP and the closure of cyclic nucleotide-gated channels (CNGCs). The influx of positive ions is thus reduced, leading to cellular hyperpolarisation, and a decrease in glutamate release from the photoreceptors. This, subsequently, results in the depolarisation of the bipolar cells. The drop in cytoplasmic Ca^{2+} concentration in the photoreceptors initiates the restoration of intracellular cGMP levels, thus opening CNGCs and restoring the initial membrane potential [5]. An overview of the phototransduction cascade is depicted in Figure 1.2.

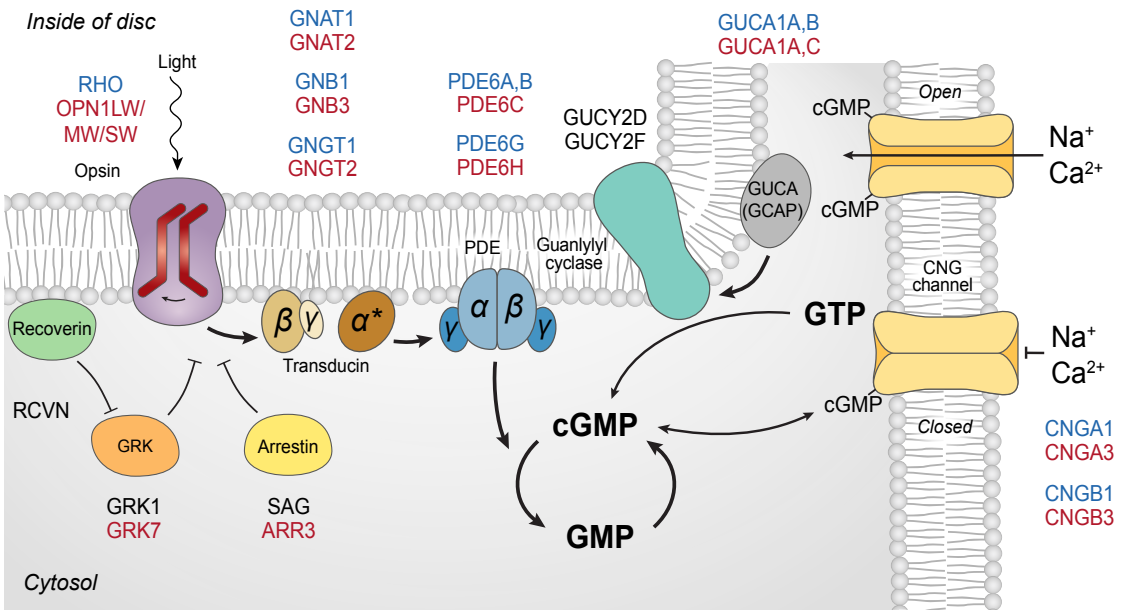


Figure 1.2: Phototransduction cascade of rods and cones. Rhodopsin and cone opsins are coupled to a G protein transducin. In the dark, the opsin is in its inactive conformation and attached to a chromophore 11-*cis*-retinal. Upon activation with light, 11-*cis*-retinal isomerises to all-*trans*-retinal, leading to a conformational change in the opsin and the activation of transducin. Its α subunit dissociates from its βγ subunits, binds to the cGMP phosphodiesterase (PDE) γ subunit, preventing it from inhibiting the catalytically active PDE βγ subunits. PDEβγ hydrolyses cGMP to GMP, resulting in a decline in cellular cGMP and the closure of cyclic nucleotide-gated cation channels (CNGCs) in the plasma membrane. The reduced influx of Na^+ and Ca^{2+} leads to the hyperpolarisation of the photoreceptor cell. Opsin signalling is rapidly inactivated. The opsin is first phosphorylated by the G protein-coupled receptor kinase (GRK) and then bound by arrestin (ARR), preventing the opsin from further activating transducin molecules. GRKs themselves are, in turn, inhibited by recoverin. The fall in intracellular Ca^{2+} allows the guanylyl cyclase-activating proteins (GCAP) to activate guanylate cyclase (GUCY), which converts GTP to cGMP and replenishes the intracellular cGMP levels. The membrane configuration of a rod is illustrated in this schematic. The proteins with expression restricted to rods or cones are blue and red, respectively; black indicates expression in both photoreceptors. Schematic is based on Larhammar et al. [6].

The visual system is very sensitive to light due to the high concentration of opsin molecules in the photoreceptors and the significant amplification in the photoreception process. One rhodopsin molecule can activate multiple transducin molecules, and each PDE molecule can convert hundreds of cGMP molecules per second. Remarkably, the response to a single photon leads to the hydrolysis of approximately 2000 cGMP molecules in a mouse rod cell [7]. Cone photoresponses are well adjusted to respond to a change in illumination very rapidly, and cones

thus mediate high acuity vision at higher light intensities [8].

The activated opsins are rapidly inactivated by phosphorylation and subsequent binding of arrestin (ARR) molecules, preventing the opsins from further activating transducin molecules. The opsin molecule must bind a new molecule of 11-*cis*-retinal to regain its sensitivity to light. Therefore, the all-*trans*-retinal must be converted back to 11-*cis*-retinal in a process called the visual cycle. The visual cycle involves the reduction of the all-*trans*-retinal molecule and its subsequent transport to the RPE, where a series of enzymatic conversions by lecithin retinol acyltransferase (LRAT), retinal pigment epithelium-specific 65 kDa protein (RPE65) and 11-*cis*-retinol dehydrogenase (11cRDH) results in the regeneration of 11-*cis*-retinal. The chromophore is then transported back to the photoreceptor cell. The rods are entirely dependent on the RPE for the visual cycle, whereas some cone chromophore is regenerated in the Müller cells [5]. An overview of the visual cycle is depicted in Figure 1.3.

The light signals from the rod and cone pathways converge ultimately on the RGCs, which project their axons as part of the optic nerve to the subcortical visual nuclei, which in turn are connected to cortical visual centres [9]. There are two main visual pathways in mammals: the retinogeniculate and the retinotectal pathway (Fig. 1.4). The majority of visual information in primates is transmitted in the retinogeniculate pathway, allowing advanced integration and interpretation of visual information. The primate visual information processing relies mainly on the information processing in the fovea, an area of the retina where the centre of the visual field comes into focus. The fovea is tightly packed with cones, supporting high spatial resolution vision. Non-primates, including mice, lack a fovea and thus their visual performance is significantly lower. The retinogeniculate pathway contains the RGCs projecting to the dorsal lateral geniculate nuclei (dLGN) in the thalamus, which send their axons mainly to the primary visual cortex (V1), also called the striate cortex because of its striped appearance. V1 provides input to the second visual area (V2). Both V1 and V2, in turn, send information to a

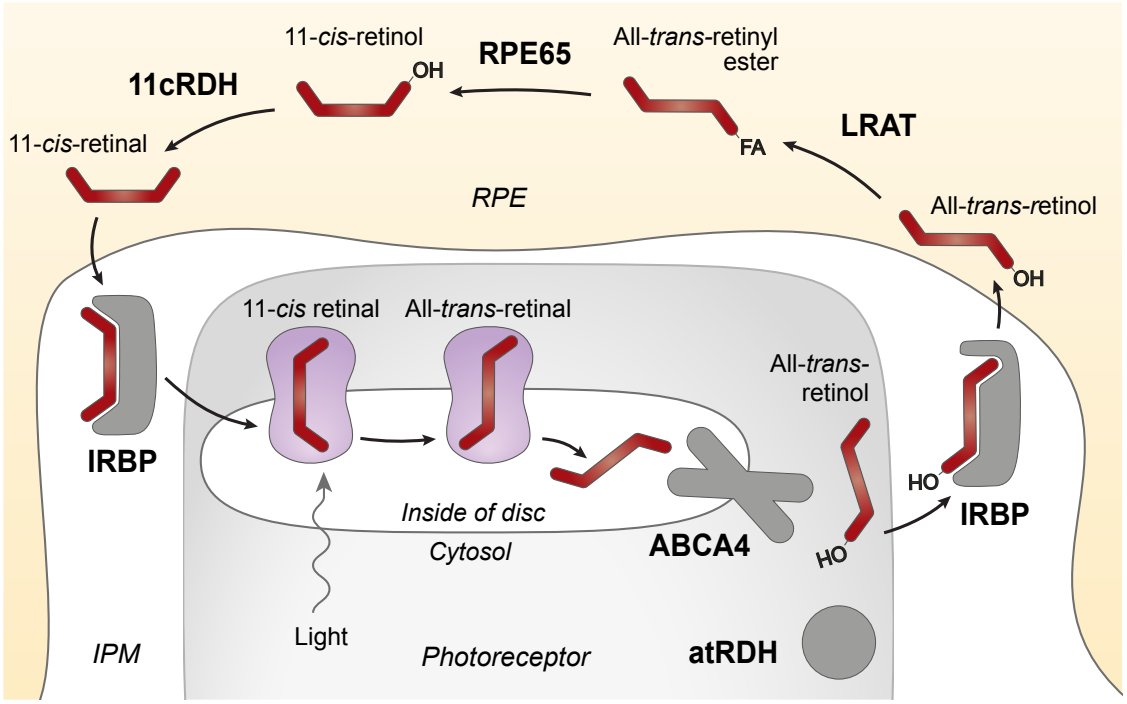


Figure 1.3: The visual cycle. Absorption of light leads to a conformational change in the chromophore attached to the opsin molecule: the 11-*cis*-retinal is converted to all-*trans*-retinal, which dissociates from the opsin molecule to the inside of the photoreceptor disc. From there, it is transported to the photoreceptor cytosol by the ATP-binding transporter 4 (ABCA4), reduced by all-*trans*-retinol dehydrogenase (atRDH) to retinol, which exits the photoreceptor, crosses the interphotoreceptor matrix (IPM) while bound to interphotoreceptor retinoid-binding protein (IRBP) and is taken up by the RPE cells. Sequential action of lecithin retinol acyltransferase (LRAT), retinal pigment epithelium-specific 65 kDa protein (RPE65) and 11-*cis*-retinol dehydrogenase (11cRDH) leads to the regeneration of 11-*cis*-retinal, which is then transported back to the photoreceptor molecule. FA, fatty acid; RPE, retinal pigment epithelium.

wide variety of extrastriate areas of the forebrain, where the complex interpretation of visual information takes place [9].

The second visual pathway, the retinotectal pathway, only receives input from approximately 10% of the RGCs in primates, whereas the proportion is approximately 50% in non-primate mammals. Its main subcortical relay centre is the superior colliculus (SC). In addition to the input from the RGCs, the SC also receives connections from descending pathways from V1 and extrastriate areas [9]. The retinotectal pathway is not essential for visual perception, but instead directs spatial attention [10]. The SC projects to the thalamus, which sends axons to extrastriate areas, primarily to the secondary visual cortex (V2) [9].

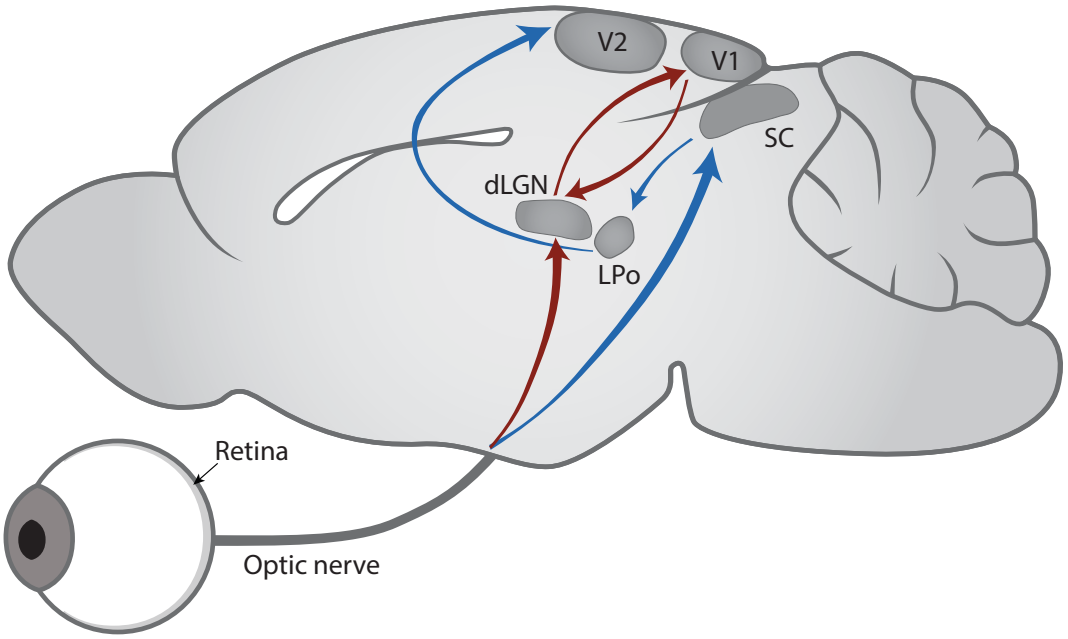


Figure 1.4: A simplified schematic of ascending visual pathways in rodents. The primary visual pathway or the retinogeniculate pathway (red) comprises the retinal ganglion cells (RGCs) targetting the dorsal lateral geniculate nuclei (dLGN), which in turn project to the primary visual cortex (V1) and further to an array of additional cortical visual centres. The retinotectal pathway (blue) is formed of the RGCs innervating the superior colliculus (SC), which sends its axons to the lateroposterior dorsal thalamic complex (LPo). LPo, in turn, is connected with the secondary visual cortex (V2). Schematic based on Mueller et al. [11].

1.1.2 Non-visual responses

Discovery of non-visual responses

The first evidence to suggest that the eye has other functions besides vision came almost a century ago from the observation that mice with no functional rods and no retinal electrical light responses were nevertheless able to constrict their pupils in response to light stimulation [12]. These mice were called *rodless* (*rd*, hereafter referred to as *rd/rd*) [12]. It was later identified that these animals carried an autosomal recessive mutation in a gene involved in phototransduction in rods, the beta subunit of rod cGMP-phosphodiesterase (*Pde6b*) [13]. Another physiological response found to rely on environmental light levels was the organism's ability to synchronise its activity pattern to the environmental light-dark (LD) cycle, termed circadian entrainment. Namely, rats whose LD cycle was reversed, re-entrained

their activity profile to the new schedule in approximately a week [14]. Therefore, it was clear that light regulates other aspects of mammalian physiology, but the mechanisms remained a mystery. Since many non-mammalian vertebrates have photoreceptors in the pineal gland, the deep-brain and the skin, the potential contribution of any other organ in addition to the eye could not be excluded [15].

Soon thereafter, it was discovered that the eye specifically mediates circadian entrainment as mice and squirrels whose eyes had been removed were unable to align their activity to the environmental LD cycle [16]. Interestingly, the circadian system seemed to be regulated independently of vision as the *rd/rd* mice showed no deficits in circadian entrainment [17]. Furthermore, the *rd/rd* mice were able to shift their activity rhythm in response to nocturnal light exposure, termed as the circadian phase-shifting response [17]. However, detailed immunohistochemical analysis determined that while the *rd/rd* animals had profoundly degenerate retinas, they retained some immunoreactivity for rod and cone opsins [17]. Therefore, it remained a possibility that the few remaining visual photoreceptors were mediating the circadian responses.

Discovery of pRGCs

A significant breakthrough in the field came with the development of a mouse model lacking all rods and cones. Freedman et al. [18] made use of another retinally degenerate mouse model, the *rdta cl* mice. These animals express an attenuated diphtheria toxin A chain under the control of the rhodopsin promoter (hence *rdta*), as well as under the cone opsin promoter (coneless, *cl*) and lose all their rods and cones early in development. Despite having no detectable rod and cone opsins in their retinas, the *rdta cl* were nevertheless able to shift their activity cycle in response to a nocturnal light pulse [18]. Furthermore, the *rd/rd cl* animals showed normal entrainment to a light-dark cycle [19], retained their pupil response at high irradiances [20], showed suppression of pineal melatonin in response to a light pulse [19], and suppressed their activity in response to a bright light pulse, a response

termed negative masking [21]. These studies provided powerful evidence that the mouse retina contained another yet uncharacterised photoreceptor.

One approach employed to uncover the identity of the novel photoreceptor was to analyse which wavelength of light the photoresponses were most sensitive to. The first characterisation of the spectral sensitivity of this photoreceptor was performed by Lucas et al. [20]. They showed that the pupil reflex in *rd/rd cl* animals was most sensitive to blue light with a peak sensitivity at 480 nm [20]. At the time of these discoveries, it was known that the behavioural rhythms in mammals were mediated by the suprachiasmatic nucleus (SCN) in the hypothalamus [22, 23], which laid the basis for another breakthrough. Berson et al. [24] injected fluorescent microspheres to the rat SCN region, which were transported retrogradely to the retina. The researchers subsequently examined these retinas and discovered fluorescent labelling in a subset of RGCs. Next, they performed intracellular recordings of the fluorescently labelled cells and demonstrated that they were activated by light even when rod and cone inputs were abolished. Furthermore, the action spectrum of light responses had a peak sensitivity to 484 nm blue light [24]. A parallel study on *rd/rd cl* retinas used calcium imaging and similarly identified a subset of light-sensitive RGCs with peak sensitivity to 470 nm light [25]. Collectively, these investigations led to the discovery of photosensitive retinal ganglion cells (pRGCs).

Discovery of melanopsin

Despite it being established that a subset of retinal ganglion cells displayed intrinsic photosensitivity, the blue light sensitive molecule responsible for mediating this photosensitivity remained elusive. It was suggested that the novel photoreceptor might be pinopsin, a recently characterised photoreceptor with maximum sensitivity to 470 nm light isolated from the chick pineal gland [26]; or cryptochromes, blue light sensitive flavin-containing molecules with a well-characterised role in plant seedling establishment [27]; or heme pigments [28]; or another blue light sensitive

vitamin A-based opsin discovered from frog skin melanophores and hence named "melanopsin" (OPN4) [29].

Notably, the action spectrum of the pupillary light reflex and pRGC light responses had a particular shape, characteristic of a vitamin A-based photopigment [20, 24, 25], thus increasing the possibility of the novel photopigment being melanopsin. The human and mouse melanopsin genes were cloned shortly after its discovery in frogs, and shown to be present in the human retina, specifically in the ganglion cell layer [30]. Further evidence for this hypothesis came from a study by Hattar et al. [31]. They injected fluorescent retrograde tracer into the rat SCNs and confirmed that the labelled retinal cells were intrinsically photosensitive [31]. Furthermore, the researchers used immunohistochemistry to demonstrate that these photosensitive cells expressed melanopsin [31]. They also found that the melanopsin-positive RGCs accounted for 2.5% and 1% of the total number of RGCs in the rat and the mouse retinas, respectively, and they innervated multiple brain areas, including the SCN [31]. Finally, triple-knock-out mice, who lacked rods, cones and melanopsin were developed, and these animals were unresponsive to light in any aspect studied: they did not have a pupil reflex, were unable to entrain to an LD cycle and did not exhibit a negative masking response [32, 33]. Together, these data opened a new exciting avenue of research to understand the cellular and molecular characteristics of melanopsin and the pRGCs, and their contributions to mammalian physiology.

1.2 The structure and function of melanopsin and pRGCs

Since their discovery 20 years ago, significant progress has been made in our understanding of the structure, function and properties of pRGCs and their photopigment melanopsin. The characteristics of melanopsin are distinct from other vertebrate opsins and in fact, resemble invertebrate opsins. The pRGCs, at first a seemingly homogeneous cell type, have since been shown to have at least six subtypes, differing in their morphology, brain projections and functions.

1.2.1 The properties of melanopsin

Similarly to rod and cone opsins, melanopsin is also a G protein-coupled receptor and uses 11-*cis*-retinal as its chromophore. In most other respects, however, the photoreceptors are quite distinct. Of note, the amino acid sequence of melanopsin is more similar to invertebrate than to vertebrate opsins as it shares 39% identity with octopus rhodopsin and only 30% with vertebrate rhodopsin [29]. This distinction is vital for understanding the signalling properties and physiology of melanopsin.

Melanopsin's phototransduction cascade involves very different mechanisms from rods and cones. Sequence analysis of melanopsin suggests that the molecule can interact with and thus activate various G proteins, unlike the classical photopigments that signal only through transducin [34]. The primary G proteins activated by melanopsin seem to belong to the $G_{q/11}$ family, leading subsequently to the activation of phospholipase C (PLC), which catalyses the breakdown of PIP_2 into DAG and IP_3 [34]. The IP_3 secondary messenger triggers the opening of the transient receptor potential canonical (TRPC) channels, which results in an influx of Na^+ and Ca^{2+} ions, and therefore cellular depolarisation [34]. This model is supported by research demonstrating a significant attenuation of melanopsin photoresponses by inhibiting PLC and by applying antibodies against $G_{q/11}$ proteins [35, 36]. Furthermore, co-expression of melanopsin and TRPC channels leads to cells being able to depolarise in response to light, thus confirming that melanopsin indeed forms a photopigment [33, 36].

In addition to the activation of TRPC channels, there is also evidence to suggest other melanopsin-mediated signalling cascades. Namely, melanopsin light responses have been shown to lead to the closure of two-pore domain (K2P) potassium channels, also through a G_q/PLC-based transduction cascade [37]. Another report suggests that pRGCs can also use a third signalling mechanism, one that is independent of $G_{q/11}$ and PLC. Instead, this resembles the phototransduction cascade present in classical photoreceptors in that it involves cyclic nucleotides: melanopsin activation leads to increased levels of cyclic nucleotides and the opening of non-selective

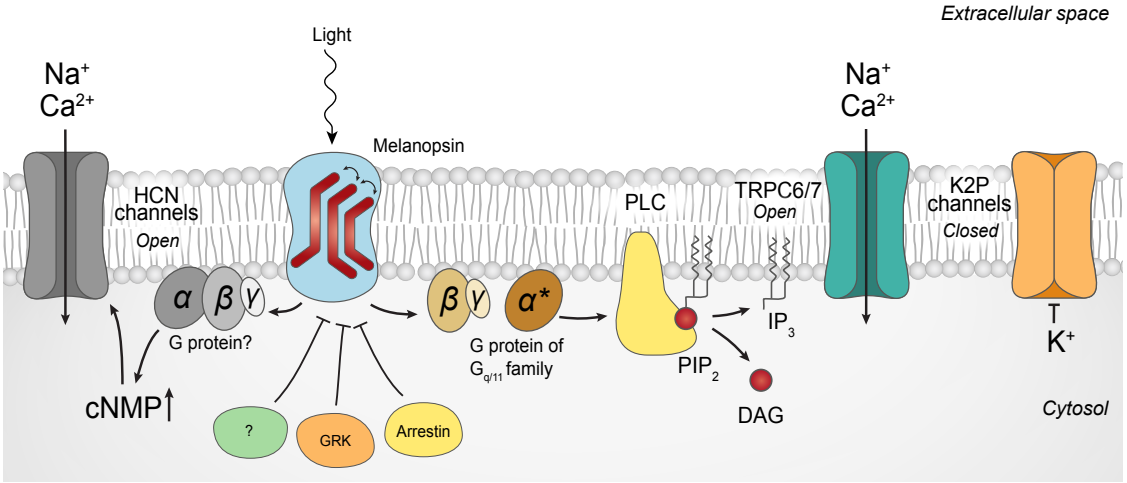


Figure 1.5: Phototransduction cascade of pRGCs. Melanopsin is coupled to a $G_{q/11}$ protein. Upon melanopsin activation, the associated G protein triggers the activation of phospholipase C (PLC), which catalyses the breakdown of phosphatidylinositol bisphosphate (PIP_2) to diacylglycerol (DAG) and inositol trisphosphate (IP_3). The latter mediates the opening of the non-selective cation channel of the canonical transient receptor potential (TRPC) family and the influx of Na^+ and Ca^{2+} ions. In addition, the actions of IP_3 result in the closure of two-pore domain (K2P) potassium channels. There is also evidence of melanopsin signalling leading to a rise in cyclic nucleotides (cNMP) and the opening of hyperpolarisation-activated cyclic nucleotide-gated (HCN) channels. These three events all lead to cellular depolarisation. Melanopsin molecule is tristable. After photoactivation, the 11-*cis*-retinal is isomerised and remains attached to the opsin. Further absorption of light leads to the regeneration of 11-*cis*-retinal. Schematic is based on Davies et al. [43].

cation channels, the HCN channels [38]. All three mechanisms result in overall depolarisation of the pRGCs. Together, these data provide evidence for three signal transduction cascades being present in pRGCs, distinguishing melanopsin activation from the visual opsins (simplified overview in Figure 1.5).

Melanopsin activation is limited by the phosphorylation of the opsin molecule, which is most likely mediated by GRKs [39, 40] and the subsequent binding of arrestins [40, 41], similarly to the visual opsins. Melanopsin has 38 potential phosphorylation sites, and multiple different phosphorylation combinations can lead to a similar overall deactivation [42]. It may be that the specific phosphorylation events are essential for melanopsin deactivation in different pRGC subtypes [42].

The phototransduction cascade kinetics of the melanopsin photoresponse is markedly different from that of visual opsins, owing to the $G_{q/11}$ signal transduction

cascade. When stimulated with light, the melanopsin response latency is several seconds to a minute [24]. Moreover, the response is sustained as the pRGCs continue to signal even after the light pulse ends [24]. This slow and sustained activation makes the melanopsin molecule and the pRGCs suitable for encoding environmental light levels and mediating circadian functions.

Another significant difference between melanopsin and classical visual opsins lies in how the photopigment regains its sensitivity to light. In contrast to visual opsins, melanopsin does not require the visual cycle to regenerate the photopigment but is instead bistable. Once melanopsin absorbs light, the 11-*cis*-retinal is isomerised to all-*trans*-retinal, which does not dissociate from the opsin, but remains attached to it. This leads to a change of melanopsin peak sensitivity from approximately 480 nm to a slightly longer wavelength, and in this state, the melanopsin molecule cannot be further activated. However, upon absorption of another photon of light, the all-*trans*-retinal is able to change its conformation back to 11-*cis*-retinal [44]. Another more recent study indicates that melanopsin is, in fact, tri-stable and has two inactive states: the photoactivated melanopsin can switch to a state with peak absorption shifted to a longer wavelength of light or to the violet spectrum (453 nm) [45].

1.2.2 The central projections of pRGCs

Since their discovery, the functions of pRGCs have been studied extensively. Detailed anatomical studies have investigated the projections of pRGCs, identifying a wide variety of brain targets responsible for various non-visual and visual responses, making the distinction between these two increasingly ambiguous.

The best-studied brain target of pRGCs mediating non-visual responses to light is the SCN, responsible for circadian entrainment and phase shifting. It has been shown in several studies that these nuclei receive input exclusively from the pRGCs via the retinohypothalamic tract [46–48]. In addition, pRGCs project to other regions implicated in circadian entrainment, including the ventral lateral geniculate nucleus (vLGN) and the intergeniculate leaflet (IGL). Furthermore, projections have been described to the olivary pretectal nucleus (OPN) controlling

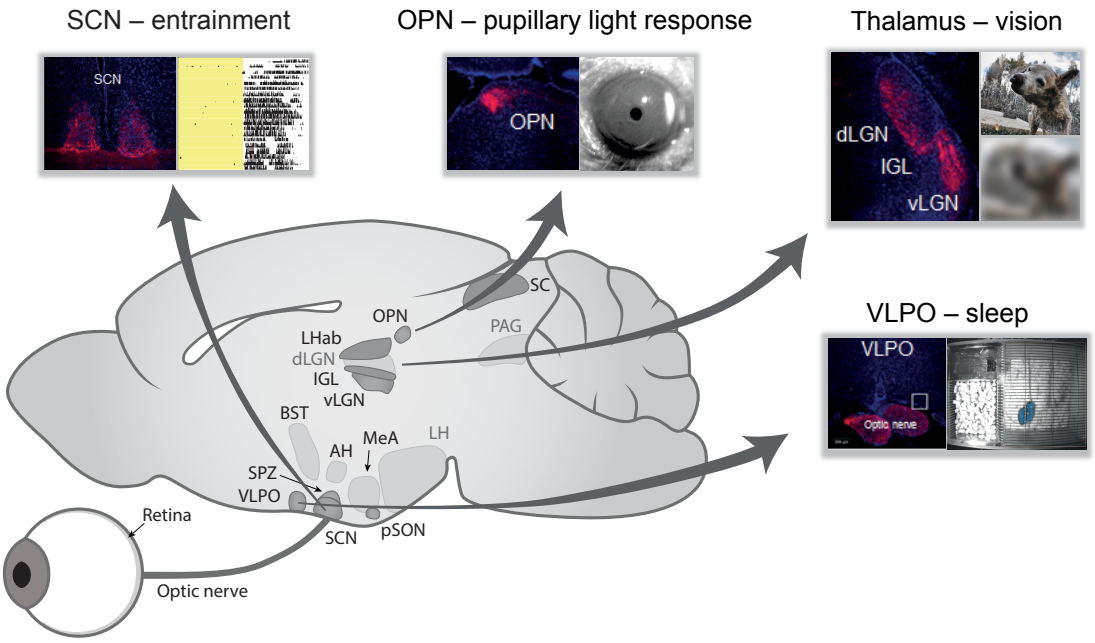


Figure 1.6: Projections of pRGCs and associated physiological processes. Projections of pRGCs are depicted on a sagittal section of the mouse brain. Primary brain targets are shown in dark grey, additional projections in light grey. The best-characterised projection of pRGCs is to the SCN, which mediates circadian entrainment. Among other projections are those to the OPN for pupillary light reflex, and to the thalamus for visual processing. AH, anterior hypothalamic nucleus; BST, bed nucleus of the stria terminalis; dLGN, dorsal lateral geniculate nucleus; IGL, intergeniculate leaflet; LH, lateral hypothalamus; LHab, lateral habenula; MeA, medial amygdala; OPN, olivary pretectal nucleus; PAG, periaqueductal grey; pSON, peri-supraoptic nucleus; SC, superior colliculus; SCN, suprachiasmatic nucleus; SPZ, subparaventricular zone; vLGN, ventral lateral geniculate nucleus; VLPO, ventrolateral preoptic area. Projection schematic based on Hattar et al. [49].

the pupillary light reflex [49–51], the ventrolateral preoptic area (VLPO) associated with sleep regulation [49–51], and the medial amygdala (MeA) and lateral habenula region (LH), brain areas involved in emotion processing [49]. In contrast to the SCN, the other non-visual brain targets of pRGCs receive input from both pRGCs and conventional RGCs, demonstrating the convergence between the visual and non-visual light responses [48, 52].

The pRGCs also project to brain areas responsible for visual processing, including the dLGN and SC, and play a role in visual responses [49–51]. Similarly to several pRGC brain targets, the dLGN and SC receive robust innervation from pRGCs, as well as conventional RGCs [48]. pRGC projections are summarised in Figure 1.6.

The pRGCs use the excitatory neurotransmitter glutamate as their primary neurotransmitter [53]. In addition, and unlike any other RGCs, the pRGCs release a peptide neurotransmitter PACAP (pituitary adenylate-cyclase-activating peptide) [54]. A recent report by Sonoda et al. [55] demonstrated that a subset of pRGCs also releases the inhibitory neurotransmitter gamma-aminobutyric acid (GABA). These GABAergic projections preferentially target the non-visual brain nuclei, e.g. the SCN and OPN, whereas visual areas, such as the dLGN and SC, receive fewer projections [55]. Surprisingly, 12% of the pRGC nerve fibres in the SCN stained positive for the rate-limiting enzyme in GABA synthesis, thus providing strong evidence of a substantial GABAergic inhibitory input to the SCN [55].

1.2.3 The diversity of pRGCs

Although the pRGCs account for only 2.5% and 1% of the total number of RGCs in the rat and mouse retinas, respectively [31], they are a very diverse group of cells. Differences in anatomical and physiological parameters have led to the identification of six distinct pRGC subtypes (M1-M6) in mice [49, 50, 52, 56, 57]. The main criteria for the classification of pRGCs have been the lamination of the pRGC dendrites in the IPL, their level of melanopsin expression, and the size of the cell bodies. It has become increasingly clear that the pRGC subtypes also exhibit different electrophysiological properties.

The various pRGC subtypes send their axons to distinct brain areas. The M1 cells form a large proportion of the pRGC projections to non-visual brain areas as they compose 80% of the pRGCs projecting to the SCN and approximately half of the pRGC projections to the OPN [52]. The M2 cells have been found to send their axons to the non-visual centres, e.g. the SCN and OPN [50, 52], as well as the visual centre dLGN [58]. The M3-M6 cells have been identified to innervate exclusively nuclei involved in visual responses, namely the dLGN and SC [57–60].

The M1 cells are the most well-studied of the subtypes, partly because of their high levels of melanopsin expression, which has made these cells easier to identify with immunohistochemical methods. Melanopsin levels are slightly lower in M2

and M3 cells, and significantly lower in M4-M6 cells. The M1 cell dendrites stratify in the distal half (OFF sublamina) of the IPL and their cell bodies are relatively small. The M2 cells laminate in the proximal half (ON sublamina) of the IPL, while the M3 cells are bistratified, sending their dendrites to both ON and OFF sublamina. The M2 and M3 have similar soma sizes and express lower levels of melanopsin than the M1 cells [61]. The M4-M6 pRGCs cells were discovered more recently [50, 56, 57], mainly due to their lower expression of melanopsin. M4 cells are synonymous with ON RGCs, which are crucial in pattern vision. They have the largest somas and laminate in the ON sublamina of the IPL [62]. The M5 cells stratify in the ON sublamina while the M6 cells have the smallest somas of the pRGC subtypes and are bistratified [61]. These differences in morphological characteristics between pRGC subtypes are displayed in Figure 1.7.

In addition to cellular diversity, pRGCs express different isoforms of melanopsin, the long and short isoforms (OPN4L and OPN4S, respectively), which result from alternative splicing [63]. The short isoform is 40 times more abundant in the retina than the long isoform [63]. The M1 and M3 cells express both isoforms while the M2 cells only the long [63]. Since the levels of melanopsin in M4-M6 cells are low, it is currently unclear whether these cell types also show isoform specificity. Notably, the two isoforms appear to mediate different melanopsin responses. Silencing the short melanopsin isoform disrupted primarily the pupillary light reflex, while silencing the long isoform led to an attenuated negative masking response [64]. However, the circadian phase-shifting response seems to be mediated by both isoforms [64].

The pRGC subtypes also differ in their electrophysiological properties. The melanopsin-mediated photoresponses have the lowest threshold and highest amplitude in M1 pRGCs and a lower amplitude in M2-M6 cells [50, 56, 57, 59]. The M2-M6 cells exhibit centre-surround antagonism, meaning that when they are stimulated over a large area in the retina, their photoresponses are dampened, indicating them encoding contrast [57, 59]. M1 cells, on the other hand, lack this property and the larger the area of an M1 cell that is activated, the more spikes

it fires [59]. This characteristic suggests that the M1 cells are better adjusted to encode overall environmental illuminance.

1.2.4 Intraretinal connections

The pRGCs are located downstream of the visual processing pathway and thus receive input from other retinal cell types. In addition to their intrinsic photosensitivity, all subtypes of pRGCs receive input from the rods and cones via bipolar and amacrine cells [57, 59]. The pRGCs also receive input from the dopaminergic amacrine cells (DACs), as the activation of DACs attenuates pRGC photocurrents through dopamine receptor 1a (DRD1a) signalling [65]. Another amacrine cell type, the somatostatin (SRIF) amacrine cell modulates the pRGC-DAC interaction by providing collateral inhibition to both cell types [66]. The M5 cells have been shown to be colour opponent. In the mouse retina, they are activated by UV light through signalling by cone bipolar cells and inhibited by green light via GABAergic amacrine cells [67]. Since the pRGC photocurrents are known to be modulated by adenosine [68], melatonin [69], opioids [70] and somatostatin [66], the pRGCs may receive additional inputs, which remain to be discovered.

Although the pRGCs lie downstream of the photoreceptors and the second-order neurons, it has become increasingly evident that the pRGCs constitute cellular mechanisms for retrograde signalling. The first evidence supporting this phenomenon came from a report demonstrating that retinas of mice with no rod and cone phototransduction displayed light-induced activation of cells in both the GCL and INL [71]. Further, by injecting pRGCs with a compound able to cross gap junctions, it was shown that M1-M3 pRGCs are coupled to displaced GABAergic amacrine cells, with each individual pRGC making approximately ten connections [72]. It was also demonstrated that the pRCGs mediated the light-induced sustained firing of ON amacrine cells, which was abolished when pRGC input was blocked [73]. Moreover, pRGCs have been demonstrated to drive sustained light responses in DACs through melanopsin activation [74, 75]. Intriguingly, a subset of pRGCs sends axon collaterals to the IPL, making connections to DACs to mediate this

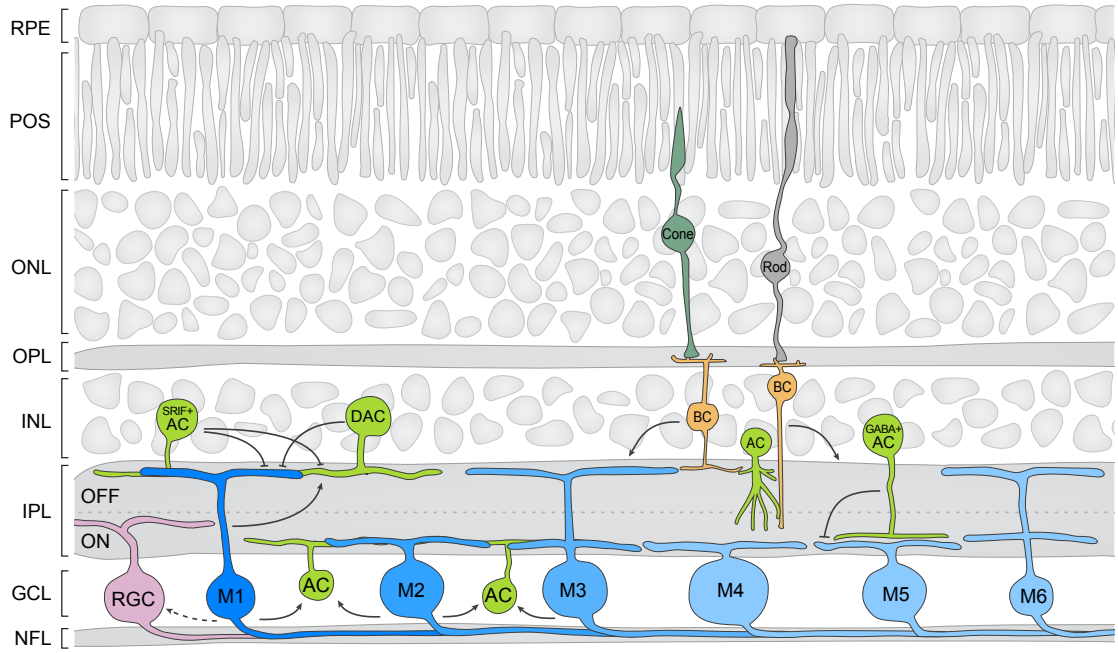


Figure 1.7: pRGC subtypes and intraretinal connections. There are six distinct pRGC subtypes (M1-M6), differing in their level of melanopsin expression (darker blue indicating more melanopsin), soma size and dendritic lamination among other characteristics. All pRGC subtypes receive input from rods and cones via bipolar (BP) and amacrine cells (AC). pRGCs themselves drive the sustained responses of dopaminergic amacrine cells (DACs), which in turn inhibit pRGC firing. The somatostatin (SRIF) amacrine cells inhibit both pRGCs and DACs. The M1-M3 cells activate displaced amacrine cells through gap junctions. There is also evidence of inhibitory GABAergic amacrine cell input to M5 pRGCs. RPE, retinal pigment epithelium; POS, photoreceptor outer segments; ONL, outer nuclear layer; OPL, outer plexiform layer; INL, inner nuclear layer; IPL, inner plexiform layer; GCL, ganglion cell layer; NFL, nerve fibre layer.

feedback [76, 77]. pRGCs signalling also modulates the firing rate of other RGCs in a melanopsin-dependent manner, although the exact mechanism of this phenomenon is yet to be characterised [78]. An overview of the inputs and outputs of pRGC signalling is depicted in Figure 1.7.

1.2.5 Role in non-visual responses

The pRGCs and melanopsin play a significant role in regulating various non-visual responses. As the pRGCs receive input from the rods and cones in addition to melanopsin photosensitivity, the lack of melanopsin often leads to relatively subtle impairments of non-visual functions. In contrast, the loss of pRGCs themselves, which project to the various non-visual centres, can have a much more dramatic impact.

Circadian entrainment and phase-shifting response

All three photoreceptor classes contribute to the circadian photoentrainment and phase-shifting responses. These circadian responses persist in animals lacking all functional rods and cones [19], as well as in animals lacking melanopsin [32, 33], indicating considerable redundancy in the circadian system. The circadian light responses are abolished in mice with no phototransduction from all three retinal photoreceptors [32, 33], and after the genetic ablation of M1 pRGCs [47, 79]. The lack of melanopsin leads only to a slight attenuation in phase-shifting response [80, 81], while the animals with only melanopsin phototransduction (the *rdta cl* animals) show, in fact, an exaggerated phase-shifting response at high irradiances [18]. Therefore, the circadian light responses are mediated by M1 pRGCs activated by the rods, cones, and melanopsin.

Pupillary light reflex

As with circadian entrainment, all three photoreceptors mediate the pupillary light reflex, and therefore, the reflex is retained in animals lacking rods and cones, although this response is much less sensitive than in wild-type animals [20]. Furthermore, the lack of melanopsin itself leads to a pupil constriction deficit only at higher light intensities [82], while the ablation of M1 pRGCs results in a more pronounced defect [47]. A more recent study investigated the effect of melanopsin on pupil response under continuous illumination and found that while the transient pupil constriction was largely mediated by rods and glutamate release, the sustained pupil constriction was mediated by melanopsin phototransduction and the release of PACAP [83]. Thus, the lack of melanopsin led to pupil redilation in response to a sustained light pulse [83].

In addition to retinal photoresponses, there is evidence of mouse pupil response being mediated through local photoreception in the iris. Wang et al. [84] demonstrated that the expression of melanopsin in the iris sphincter muscle is driving pupil constriction in an *ex vivo* iris explant and that removing melanopsin specifically from smooth muscle cells abolished pupil constriction. The light levels used in these

experiments were several log units higher than what is needed to achieve maximum pupil constriction in mice *in vivo*. However, the report opens an exciting avenue for the investigation of potential non-retinal functions of melanopsin.

Sleep regulation

Another physiological function modulated by melanopsin and the pRGCs is sleep. Direct light input modulates sleep behaviour and promotes sleep in nocturnal species. The main sleep-promoting centre in the brain is the VLPO, which receives direct input from the pRGCs [49]. Early studies demonstrated that unlike wild-type mice, animals lacking melanopsin did not display sleep behaviour or activation of VLPO in response to nocturnal light exposure, indicating that melanopsin activation was crucial for sleep induction [85]. However, another report showed that direct melanopsin activation leads to arousal and anxiety, not sleep [86]. In an attempt to reconcile these discrepant findings, Pilorz et al. [87] found that blue (470 nm) light induces arousal, whereas green (530 nm) light promotes sleep in mice, with concomitant activation of the SCN and VLPO, respectively [87]. Both of these effects were attenuated in mice lacking melanopsin [87].

Mood

The effect of light on mood is well known as a reduction in environmental light levels leads to seasonal affective disorder. Furthermore, light therapy is widely used for the treatment of seasonal and non-seasonal depression [88]. In mice, the pRGCs are known to project to brain areas involved in emotion processing, the MeA and LH [49]. These findings have led to the investigation of pRGCs in mood regulation. An experimental model where animals are raised in a light-dark cycle consisting of 3.5 hours of light and 3.5 hours of darkness, induces depression-like behaviour and cognitive deficits. However, these mood changes were not present in mice in which the pRGCs were ablated [89], revealing that pRGC projections are to some extent responsible for mediating this light-dependent effect.

1.2.6 Role in visual responses

The discovery of pRGCs led to the reframing of the physiological role of the eye, highlighting the importance of ocular photoreception in several non-visual responses. While the visual and non-visual responses seemed to be mediated preferentially by the classical photoreceptors and pRGCs, respectively, there is considerable evidence to show this distinction is not completely clear, and there is significant interplay between the two systems. The discoveries that the pRGCs project to visual nuclei the dLGN and SC [49, 50, 90], suggested that the pRGCs may have a role in vision. Indeed, it was shown that the *rd/rd cl* animals could learn to discriminate between an illuminated target in a visual water task [91]. Similarly, mice with no rod and cone phototransduction could discriminate gratings in the same task [50]. Furthermore, since the M4 cells are ON alpha RGCs, ablation of these cells specifically, leads to visual defects manifested as reduced contrast sensitivity [62]. Contrast sensitivity is also reduced in melanopsin-null mice [62].

Further evidence for the role of melanopsin in visual responses came from human studies. Research on visually blind subjects lacking most of their rods and cones and any conscious visual perception has shown that some of these subjects are nevertheless able to sense bright blue light. A study by Zaidi et al. [92] reported that a blind person could perceive "brightness" when presented with 481 nm light, but not any shorter nor longer wavelength, suggesting that melanopsin is mediating this effect. Also, when presented with light that illuminates all rod and cone photoreceptors to a similar extent, but only changes the amount of melanopsin activation, humans perceive higher melanopsin stimulation as brighter [91]. Together, these results provide substantial evidence for melanopsin and the pRGCs having a role in visual responses.

1.2.7 Role in retinal development

Early visual experiences shape the development of the retina and visual pathways. Melanopsin-containing pRGCs are the first functional photoreceptors in the retina as they display light-responses already at birth [93, 94] and start expressing melanopsin

in embryonic stages [95], while the rod and cone opsins are detectable only in postnatal retinas from postnatal day 1 and 5, respectively [95]. It has been revealed that melanopsin photoreception during development is crucial for regulating the number of RGCs and the maturation of retinal blood vessels in the retina [96]. Mice lacking melanopsin show an increased number of RGCs, increased levels of vascular endothelial growth factor (VEGF) and the overgrowth of retinal vasculature [96]. This phenotype can be replicated by rearing mice in constant darkness from embryonic stages [96], suggesting that melanopsin light responses and not any other potential function mediate this effect.

Throughout development, the cones are guided to their appropriate position in the outer retina through light signalling, and early in the development, some cones are displaced to inner retinal layers [97]. Interestingly, pRGCs of mainly the M1 subtype send their dendrites to the outer plexiform layer early in postnatal stages, and these pRGC connections seem to be critical for cone development. The ablation of pRGCs leads to an increased number of displaced cones in the inner retinal layers throughout adulthood. Importantly, it was shown that aberrant cone localisation was dependent on neurotransmitter release from pRGCs, and the number of displaced cones was reduced in retinal explants by the supplementation of a dopamine 4 receptor (DRD4) agonist [98]. Retinas lacking melanopsin also show an increased number of displaced cones in early postnatal stages, imitating the phenotype of dark-reared mice [98]. However, the number of displaced cones in melanopsin-null mice is reduced by P16 [98], suggesting that signalling from classical photoreceptors can rescue the phenotype. It was also recently shown that photoreceptor orientation in the mouse retina depends on light signalling and is independent of rod and cone photoreception [99], leading to the possibility of this effect being mediated by melanopsin.

Early postnatal retinas display spontaneous electrical activity sweeping across the entire retina, termed retinal waves, which are essential for the proper wiring of the RGCs to their brain targets [100]. These retinal waves are also known to be modulated by light, particularly melanopsin photoreception [100]. Subsequently,

melanopsin-null mice display abnormal segregation of retinal projections to the dLGN [100]. Ablation of pRGCs in early development results in an even more severe disruption of these projections, and these mice have a reduction in visual acuity [46]. Altogether, these data provide substantial evidence for the involvement of pRGCs and melanopsin in the development of the retina and its projections to the brain.

1.3 Circadian rhythms

1.3.1 The concepts and terminology of circadian rhythms

Earth's rotation around its axis results in day-night cycles of 24 hours and thus in very regular changes in environmental light levels and temperature. To better adapt to the rhythmically changing environment and anticipate the changes, most organisms on Earth have developed intrinsic 24-hour rhythms in much of their physiology. These rhythmic biological processes are synchronised or entrained to the external world by environmental cues or "Zeitgebers" (from German "time-givers"). The most potent Zeitgebers for mammals are environmental light levels and feeding pattern, while some non-mammalian species can also synchronise their behaviour to the rhythmic changes in temperature [101].

In the presence of environmental cues, a biological rhythm is said to have diurnal rhythmicity, and the time is expressed as Zeitgeber time (ZT). When the Zeitgeber is light, ZT0 marks the beginning of the light phase. Biological rhythms that persist in conditions where all environmental parameters are kept constant are called circadian rhythms, derived from the Latin words "circa dies", meaning "approximately a day". In these constant conditions the biological rhythm is self-sustaining, i.e. free-running and its period (*tau*), or time it takes to complete one cycle of rhythmicity, is close to, but not exactly 24 hours. The time in constant conditions is expressed as circadian time (CT) where CT0 marks the start of the subjective day and CT12 subjective night. Since there are no environmental cues to measure time, circadian time is

defined by the start of activity: in diurnal and nocturnal animals, the start of activity marks CT0 and CT12, respectively [101].

Besides period, the circadian rhythms are also characterised by other numeric parameters. The amplitude is defined as half of the difference between the peak and the trough of the rhythmic value. The phase of a rhythm is defined as the timing of a reference point, which can be the start of an event or the peak value, relative to a fixed point, which is often the beginning of the subjective day. The timing of the maximum value is called acrophase. The mean value of a rhythmic parameter is mesor, which is estimated by fitting a cosine function to the rhythmicity data [101] (Fig. 1.8A).

A biological rhythm can only be said to display circadian rhythmicity if it meets three fundamental criteria. First, the rhythm has to persist in constant conditions, i.e. without any rhythmic input from the environment, and to have a free-running period of approximately 24 hours. Second, the rhythm has to be entrainable to a Zeitgeber. And finally, the rhythm has to exhibit temperature compensation, meaning that the free-running period should vary minimally over a range of biological temperatures [102].

For the circadian rhythms to be beneficial to the organism, they must be appropriately aligned to the external world by sensing the environmental Zeitgebers. Since the free-running period of circadian rhythms is slightly different from 24 hours, the rhythm is reset to the external environment every day. The ability of an external stimulus to induce a shift in the phase of the rhythm is often studied in constant conditions. In the case of light, the circadian system is only sensitive to light during the relative night. Light exposure in the first half of the subjective night results in a phase delay and second half of the subjective night in a phase advance [101] (Fig. 1.8B, C).

1.3.2 The suprachiasmatic nucleus and central circadian rhythms

The most prominent circadian rhythm in mammals is the sleep-wake cycle, but circadian rhythms go well beyond that. Humans display circadian rhythms in body

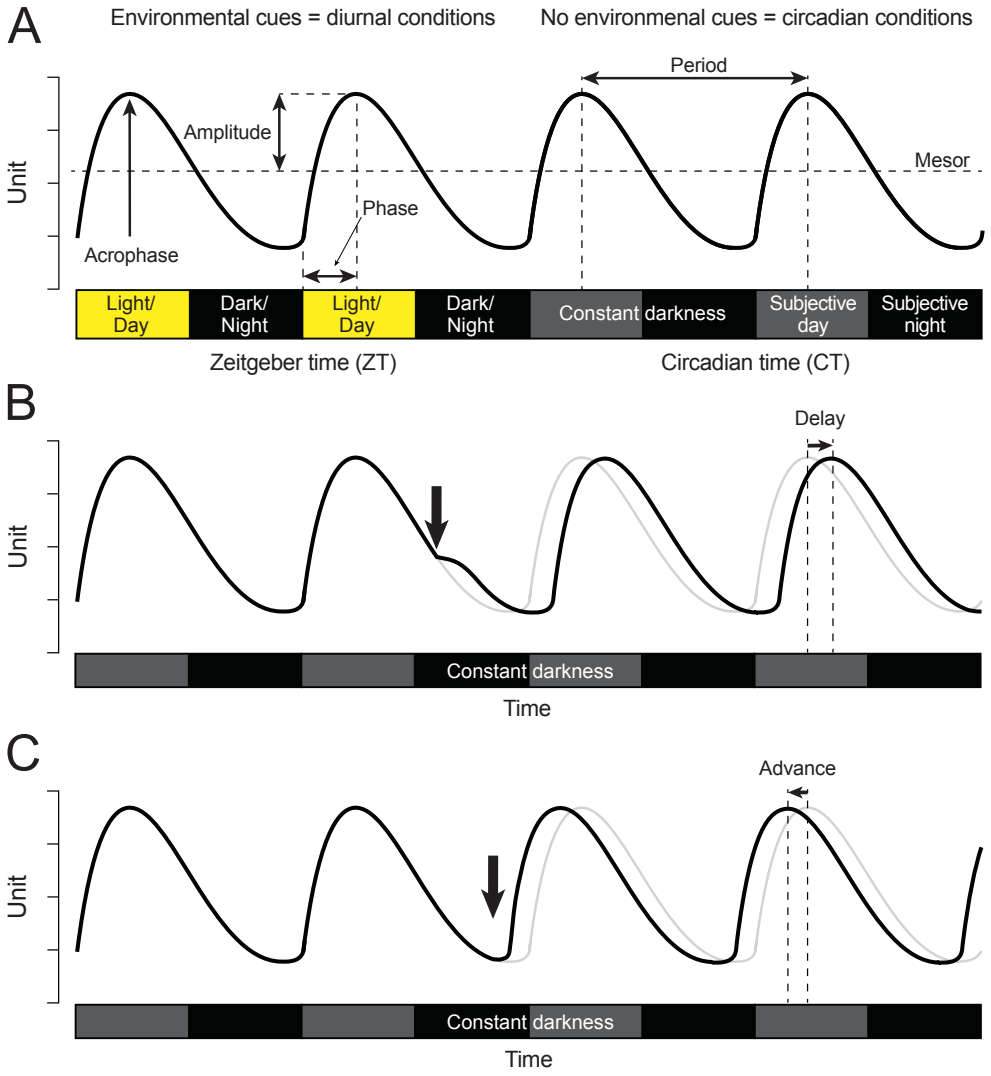


Figure 1.8: Terminology of circadian rhythms. (A) A biological process displaying rhythmicity over a 24-hour light-dark cycle is said to have diurnal rhythmicity. The environmental light schedule acts as a time cue or Zeitgeber, and the time is measured as Zeitgeber time (ZT) with ZT0 indicating the beginning of the light phase. The persistence of rhythmicity in the absence of any environmental cues in constant or circadian conditions means the process has circadian rhythmicity. In constant conditions, time is measured as circadian time (CT) consisting of subjective day and night, determined from the activity pattern. The time it takes to complete one cycle of the biological rhythm is termed period. Amplitude is defined as half the extent of rhythmic change in a cycle. Phase is the timing of a reference point in the cycle (e.g. the peak) relative to a fixed event, while the phase of the maximum value is termed acrophase. Mesor is the rhythm-adjusted mean estimated by fitting a cosine curve to the data. (B, C) The rhythm can be reset in constant conditions by exposure to a signal, e.g. exposure to a light pulse. Light exposure in the first half of the subjective night leads to a phase delay (B) while light exposure in the latter half of the subjective night to a phase advance (C). The grey line depicts an unchanged rhythm. Schematic is based on Vitaterna et al. [101].

temperature, blood pressure, alertness, metabolism and various hormone levels, e.g. melatonin, cortisol, and growth hormone [103–105]. In mammals, the master circadian clock is located in the SCN, a paired structure located on either side of the third ventricle directly above the optic chiasm in the hypothalamus. These paired nuclei, each consisting approximately of 10,000 cells in size in mice [106] and 50,000 cells in humans [107], are specialised for encoding the environmental luminance. In response to light stimulation, the SCNs display tonic activation in both diurnal and nocturnal organisms [108].

The discovery of the SCN as the central pacemaker dates back almost 50 years when it was shown that the ablation of SCN in rats led to the loss of diurnal rhythmicity in blood corticosterone levels [22]. Surprisingly, rats that had been blinded by enucleation retained their corticosterone rhythm, but it started to drift over time [22]. Similar observations were made by lesioning the SCNs in rats and investigating their rhythms in activity pattern and the timing of drinking behaviour [109]. These results established that an intrinsic clock in the SCN drives the rhythmicity of corticosterone and activity pattern. The absence of light input to the central clock does not abolish the biological rhythms but results in their misalignment with the environment.

Further evidence of the SCN as a pacemaker came when it was demonstrated that the electrical activity of the SCN is rhythmic *in vitro*, with higher activity during the day [110]. In fact, each SCN neuron was shown to act as a circadian oscillator as dissociated SCN neurons retained the intrinsic ability to fire action potentials, although their phases drifted apart over time [111]. Moreover, it was shown that hamsters, whose SCNs had been destroyed, lost their circadian rhythm of activity [23]. However, this rhythm could be restored by transplanting the SCN tissue harvested from another hamster into the arrhythmic animal's third ventricle [23]. This finding indicated that it is indeed the SCN that drives the circadian rhythms. At a similar time, it was noted that one particular hamster strain displayed a shortened period of approximately 20 hours, and these animals were called the *tau* mutants [112]. Similarly, it was shown that transplanting the SCN from the

tau mutant hamster to an arrhythmic animal with an ablated SCN restored the host's activity rhythms [113]. Amazingly, the host animal's circadian period was determined by the donor SCN's intrinsic period [113]. Collectively, these data provided indisputable evidence for the role of the SCN as the master circadian clock that is entrained to the environmental light-dark cycle by light input from the eye.

1.3.3 Molecular mechanisms of circadian rhythms

Once the SCN was identified as the master circadian pacemaker, research focussed on investigating the molecular mechanisms of SCN oscillations. Studies in *Drosophila melanogaster* pioneered the identification of the molecular clockwork. By employing a forward genetics approach of mutagenesis and subsequent screening of progeny, it was demonstrated that three different mutations in a particular gene, the *period* (*per*) gene, led to aberrations in circadian locomotor behaviour; one mutant was arrhythmic, while the other two retained rhythmicity but with an altered period, one with 19 hours and the other 28 hours [114]. Furthermore, transducing the *per* gene to arrhythmic flies with *per* mutations restored the wild-type rhythmicity of locomotor behaviour [115]. The *per* gene was thus the first core clock gene identified.

A similar forward genetics approach was employed in mice. The first mouse circadian mutant identified displayed a lengthened circadian period, and after about two weeks in constant conditions, they became arrhythmic [116]. The gene was called "circadian locomotor output cycles kaput" or *Clock* [116]. Subsequently, mouse homologs of previously identified fly core circadian clock genes were discovered, and this founded the basis for our understanding of the molecular clockwork in mammals.

The molecular clock is characterised by a transcriptional-translational feedback loop (TTFL) consisting of a positive and a negative arm. The positive arm of the TTFL is formed by the transcription factors CLOCK and BMAL1, which form heterodimers and bind to specific DNA sequences, E-boxes (enhancer boxes), and drive the transcription of their target genes. Among these transcripts are the *Period* genes (*Per1-3*) and the *Cryptochrome* genes (*Cry1-2*), which form the negative arm of the TTFL [117]. The resulting PER and CRY proteins dimerise and inhibit

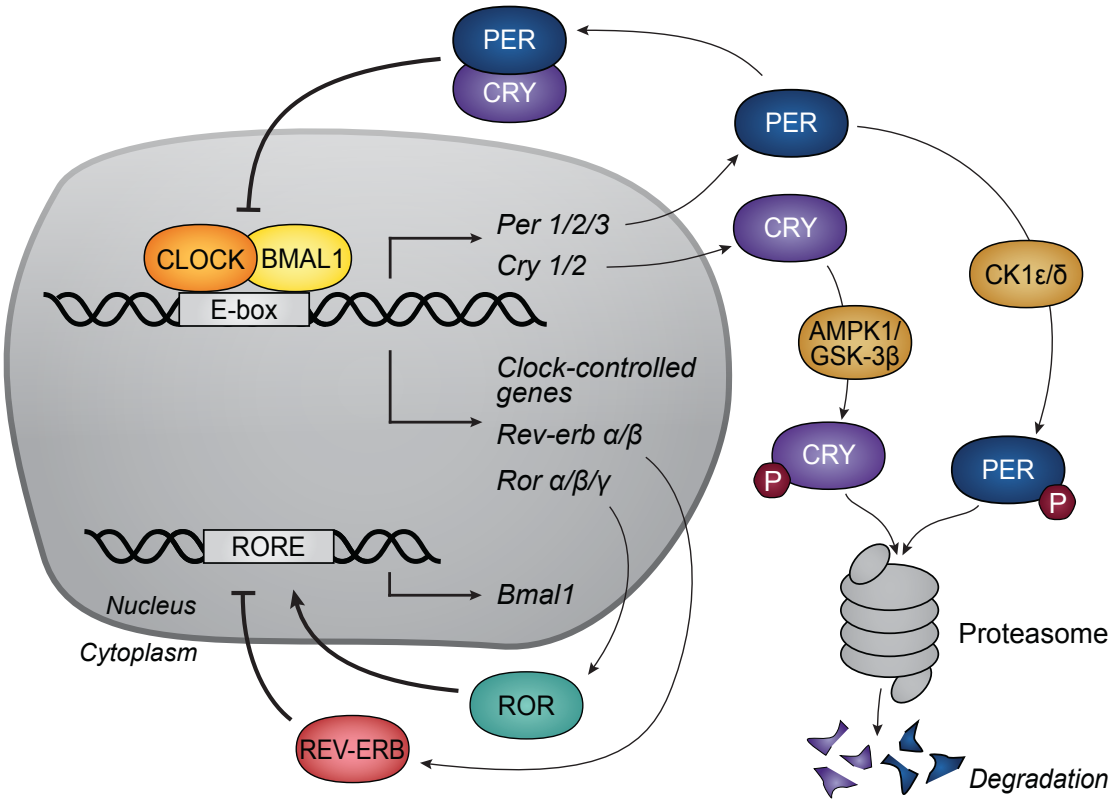


Figure 1.9: The molecular mechanism of the mammalian core circadian clock. The circadian transcriptional-translational feedback loop contains CLOCK-BMAL1 heterodimers that bind to the E-boxes of their target genes in the cell nucleus. This leads to the transcription of *Per* and *Cry*, which are transported to the cytoplasm and translated into proteins. The PER and CRY proteins form heterodimers and repress the CLOCK/BMAL1 complex's transcriptional activity, thereby repressing their own expression. In parallel, the CLOCK/BMAL1 heterodimers induce several clock-controlled genes, regulating various aspects of cellular physiology. Two of those genes are *Rev-erb* and *Ror*, which form the secondary loop regulating the transcription of BMAL1. Upon translation, REV-ERB represses while ROR activates the transcription of *Bmal1* by acting on the RORE binding sites within its promoter. Proteasomal degradation of PER and CRY proteins is mediated by their phosphorylation by CK1ε/δ, AMPK or GSK3β, respectively. E-box, enhancer box; RORE, retinoic acid-related orphan receptor response element.

the CLOCK/BMAL1 heterodimers' activity, therefore leading to the inhibition of their own synthesis. One cycle of this process takes approximately 24 hours and controls the period of a circadian clock [105] (Fig. 1.9).

However, this primary TTFL is modified on multiple levels by several other processes. One of them is the secondary feedback loop generated by REV-ERBs (also known as NR1D, nuclear receptor subfamily 1, group D) and RORs (retinoic acid-

related orphan receptors). The CLOCK/BMAL1 heterodimers induce the expression of *Rev-erb α/β* and *ROR α/β* and once translated, these proteins repress and activate, respectively, the transcription of *Bmal1* by acting on the retinoic acid-related orphan receptor response element (RORE) present in the *Bmal1* promoter [105]. Another layer of clock regulation is controlled by the degradation of PER and CRY proteins, an event critical for removing the suppression on the positive limb of the TTFL. Both PER and CRY proteins have to be phosphorylated in order to be targetted to the proteasome for degradation. Phosphorylation of PER proteins is mediated by casein kinase 1 ε/δ (CK1ε/δ) and CRY proteins by adenosine monophosphate activated protein kinase 1 (AMPK1) and glycogen synthase kinase-3β (GSK-3β), and mutations in these kinases have been associated with abnormal circadian periods. The *tau* mutation is, in fact, a point mutation in the CK1ε gene, which leads to a deficiency in the kinase's ability to phosphorylate its targets [105] (Fig. 1.9).

1.3.4 Peripheral circadian rhythms

Understanding the molecular mechanisms of the circadian clockwork laid the foundation for research into peripheral tissues' circadian rhythms. Soon after the discovery of the master circadian pacemaker in the SCN, it was observed that several peripheral tissues and cells also exhibit circadian rhythms in their physiology and retain these rhythms when isolated from the SCN [118]. Much of the circadian rhythmicity in peripheral organs is governed by rhythmic clock gene expression, and peripheral tissues exhibit distinct periods, which are not always the same as the period of the SCN [119]. In addition, the phases of the peripheral clocks are not the same, although they maintain distinct phase relations to the SCN [119]. The circadian rhythms of peripheral organs are regulated intrinsically and thus retained in mice with lesioned SCNs [119]. Importantly however, the rhythms lose their phase coordination over time [119]. Therefore, although the SCN itself is responsible for driving several aspects of circadian physiology, e.g. the rest-activity cycle and cortisol secretion, in the context of peripheral tissues, the SCN can be thought of as a master synchroniser of circadian clocks [118] (Fig. 1.10).

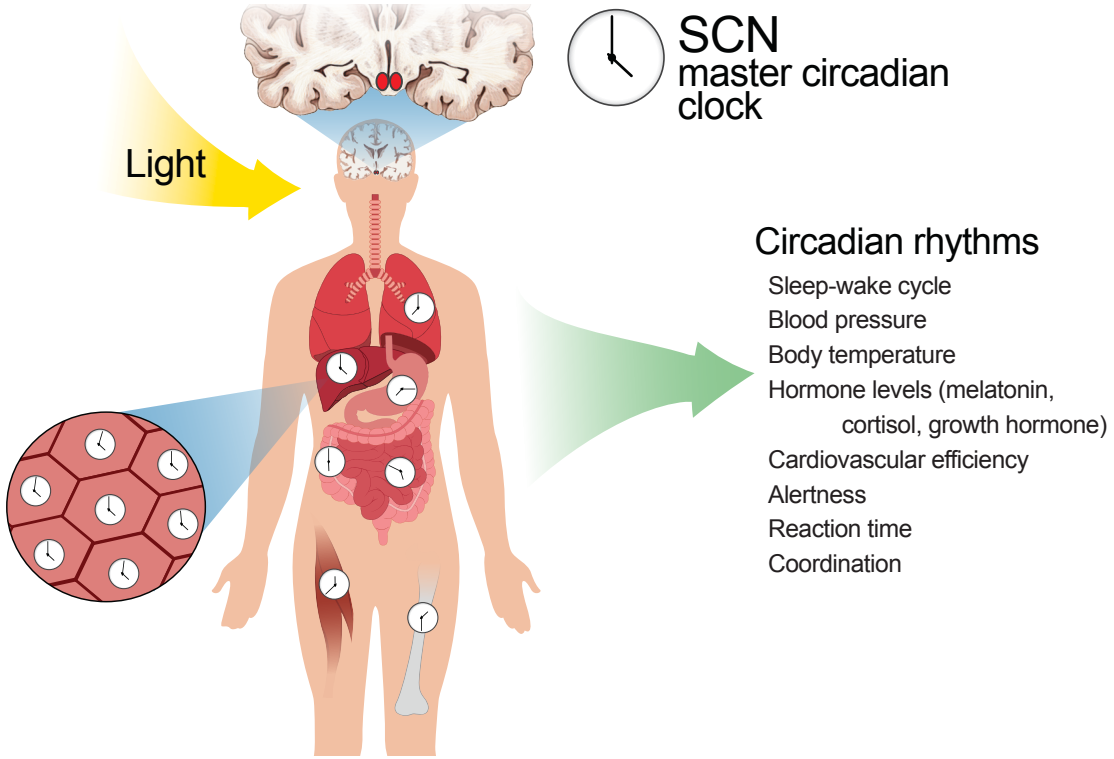


Figure 1.10: The hierarchical organisation of circadian clocks. The SCN located in the hypothalamus acts as a master circadian clock, receiving information about the environmental light levels through the eyes, which resets the central circadian clock. Each tissue in the body displays a circadian rhythm, and notably, these rhythms exhibit distinct phase relations, which is maintained by the SCN. Each cell in an organ also has an internal circadian clock. The central and peripheral clocks drive the circadian rhythmicity in multiple aspects of mammalian physiology.

1.4 Retinal circadian rhythms

One of the first tissues shown to retain intact circadian rhythms when removed from the organism and thus from the control of the SCN, was the retina. Besharse and Iuvone [120] demonstrated almost 40 years ago that frog retinas maintained the circadian rhythmicity of melatonin synthesis pathway and could reverse this rhythm when exposed to a reversed LD cycle *in vitro*. Another retinal circadian rhythm involves the rod outer segments. Rod photoreceptors constantly renew their outer segments by shedding their outer discs, which are phagocytosed by the RPE. Terman et al. [121] showed that this rhythm was retained in rats whose SCNs has been lesioned. Evidence for similar regulation of retinal and central circadian rhythms on a molecular level came from research by Tosini et al. [122].

They demonstrated that the circadian rhythm of retinal melatonin release free-ran in constant conditions *in vitro* and the rhythmicity followed that of the SCN: the retinas of *tau* mutant hamsters with a shorter free-running activity period also showed shorter periods of retinal circadian rhythms [122]. The retinal circadian rhythms govern multiple aspects of retinal physiology. On a molecular level, these rhythms seem to be regulated primarily by the core molecular TTFL.

1.4.1 Physiological significance of retinal circadian rhythms

The visual system operates over a wide range of light intensities from starlight to a sunny day, across approximately 11 log units [3]. The retina has developed complex mechanisms to adapt to the changes in illuminance [3]. Visual function is regulated by retinal circadian rhythms, which controls, in broad terms, the connectivity between the rod and cone pathways. This circadian regulation allows the retina to be very sensitive to light at night, while adjusts the retina to high spatial resolution vision during daytime [123, 124].

Vision at night relies primarily on rods, while cones play a more significant role at day. However, recent evidence suggests that rods can adapt to higher light levels and thus contribute to vision at higher irradiances [125]. Therefore, the dichotomy between rod-dominated vision at night and cone-dominated vision at daytime is not as straightforward as previously thought, although we are still missing a complete mechanistic understanding of the entire process.

1.4.2 Retinal connectivity and retinal circadian rhythms: rod-cone coupling

Although the exact cellular events controlling information flow in the rod and cone pathways are not fully known, the connectivity between the rod and cone pathways has been proven to be regulated by the retinal circadian clock. One of the mechanisms underlying the connectivity involves direct electrical coupling between the rods and cones [124]. The photoreceptors are connected via gap junctions, and their major component is connexin 36 (Cx36). Cx36 is phosphorylated at night,

resulting in increased conductance of the gap junctions and photoreceptor electrical coupling [126]. Higher dopamine levels at daytime and their action on the dopamine receptor 4 (DRD4) result in Cx36 dephosphorylation, decreased conductance of the gap junctions and thus weaker rod-cone coupling [124]. A recent report demonstrated that this circadian rhythm is also regulated by retinal adenosine independent of dopamine [127]. Overall, increased coupling enhances the reliability of rod responses at night and increases the retinal sensitivity to very dim light stimuli.

1.4.3 Outputs of retinal circadian rhythms

Cone electroretinogram

Photoreceptor coupling can be investigated by measuring the circadian regulation of retinal electrical signals in response to light flashes, termed the electroretinogram (ERG). By modifying the parameters of light flashes, it is possible to isolate cone and rod responses. Upon light stimulation, the photoreceptor hyperpolarisation is manifested as a negative deflection on the ERG (a-wave) [128]. Subsequent depolarisation of second-order neurons, the bipolar cells, results in a positive deflection on the ERG (b-wave) [129].

As the mouse retina contains very few cones, they are incapable of driving a measurable a-wave. The cone ERG b-wave, however, is known to have circadian rhythmicity in its parameters. The b-wave amplitude is larger at daytime and the time to the b-wave peak is short [130, 131]. The reverse is true at night: the b-wave amplitude is lower and the implicit time longer [130, 131], indicating the rhythmicity in retinal connectivity.

Contrast sensitivity

One of the circadian visual functions is contrast sensitivity as mice can detect contrast better at day than at night [132]. In practice, contrast sensitivity in mice is measured as a reflex elicited by moving gratings: having moving stimuli in the visual field triggers reflexive eye and head movements in the direction of the moving gratings, serving to keep the image on the retina stable. The eye

movements (optokinetic response) or head movement (optomotor response) are measured in response to stimuli of different spatial frequencies. The lowest contrast able to induce the reflex at each spatial frequency is determined, and their inverse is reported as contrast sensitivity function [133].

Pupillary light reflex

Another retinal function with a circadian rhythm is pupil response. Namely, the maximum pupil constriction at daytime is greater than at night [134]. This rhythm may also serve as an adaptation to high-sensitivity vision at night as it leads to an increased amount of light reaching the peripheral retina. As with contrast sensitivity, pupil constriction in response to light is a reflex [135]. Its afferent limb involves pRGC and RGC projections to the OPN [48, 52], while the efferent limb consists of parasympathetic nerve fibres innervating the iris sphincter muscle. Importantly, light stimulation of one retina results in the constriction of both ipsilateral and contralateral pupils [135].

1.4.4 Mechanisms of retinal circadian rhythms

Location of the retinal circadian clock

Where precisely the retinal clock is, has remained a mystery. Ruan et al. [136] isolated gene transcripts from single cells at a single time point and showed that horizontal and bipolar cells, several subtypes of amacrine and ganglion cells express the six primary clock genes *Clock*, *Bmal1*, *Per1/2* and *Cry1/2*. However, these genes were undetectable in rods [136], indicating that cells other than rods have the prerequisites of containing a molecular circadian clock. In another study, Liu et al. [137] used immunohistochemistry to investigate the levels of retinal clock proteins CLOCK, BMAL1, NPAS2 (a CLOCK paralog), PER1/2 and CRY2. When sampled at a single time point, all cell types studied, except rods, showed clock protein expression above background levels. They also quantified the clock protein levels with immunohistochemistry and showed that the levels of all clock proteins were rhythmic in cones in both LD and DD [137]. Intriguingly however, all clock

proteins were in the same phase with their acrophase in the middle of the subjective day [137]. This finding is surprising because in the SCN, the circadian rhythms of PER and CRY are antiphasic to the rhythm of BMAL1 [117]. In addition, the SCN levels of CLOCK do not show a rhythmic expression pattern [117]. Therefore, the potential cone circadian clock may be regulated differently from the SCN clock.

In another attempt to shed light on the localisation of retinal clock, Dkhissi-Benyahya et al. [138] used laser microdissection to separate the inner and outer retinas and quantified the levels of clock transcripts. They saw that most clock genes studied (*Per1/2*, *Clock*, *Bmal1*, *Cry1/2*, *Reverba* and *Rorβ*) were rhythmically expressed in the outer retina, but not in the inner retina under constant conditions. In addition, of the clock transcripts that showed rhythmicity in the inner retina, *Clock* was in the same phase as in the outer retina, but *Per1/2* and *Rorβ* were antiphasic to the outer retinal rhythms [138]. These results indicate that the inner and outer retina may have independent clocks, which are in opposite phases.

Neurotransmitters of the retinal circadian clock

In the retina, the actions of melatonin and dopamine are mutually inhibitory, and their circadian rhythms in antiphase [122, 139]. Melatonin, which originates from the photoreceptors, acts as the dark-adaptive signal and its levels peak in the middle of the subjective night [122, 140]. On the other hand, dopamine mediates light adaptation and its levels peak in the middle of the subjective day [139]. Although animals that do not produce melatonin show rhythmic dopamine levels in diurnal conditions, they lose this rhythm in constant darkness [139]. Interestingly, it is possible to restore the circadian rhythm of retinal dopamine release by injecting mice daily with melatonin over ten days [139]. Therefore, the rhythmic levels of dopamine depend on a rhythmic LD cycle or the presence of melatonin. However, melatonin rhythm is independent of dopamine rhythm as the ablation of inner retinal neurons, where dopamine originates from, does not influence the rhythmicity of melatonin synthesis [141]. These results suggest that retina contains multiple circadian oscillators.

In addition to melatonin and dopamine, other potential neurotransmitters could also drive retinal circadian rhythms. For example, retinal adenosine [127] and GABA levels [142] show a circadian rhythm. By studying the retinal rhythms of mice expressing PER2 protein fused to firefly luciferase (PER2::Luc), researchers have been able to use bioluminescence to visualise the rhythmic expression of PER2 protein *in vitro* [119]. Ruan et al. [143] demonstrated that the retinal circadian rhythms of PER2::Luc remained intact when melatonin, acetylcholine, glutamate, dopamine, or glycine signalling was disrupted. Only the application of GABA dampened the amplitude of PER2::Luc expression [143].

It is important to note that several mouse strains, including the commonly used C57/BL6, do not have melatonin in the retina and elsewhere in the body, because of mutations in enzymes catalysing melatonin synthesis [144]. However, the melatonin-deficient C57/BL6 animals retain their circadian rhythms of ERG [130] and contrast sensitivity [132], as well as the rhythmic levels of retinal PER2 [119, 136, 145, 146], suggesting that the lack of melatonin does not abolish retinal circadian rhythms. Therefore, a lot remains to be studied about how exactly the retinal circadian rhythms are regulated.

Entrainment of the retinal circadian clock

Another study made use of melanopsin-null *rd/rd* animals that cannot entrain their activity to the external LD cycle, but instead, display a free-running rhythm. Buhr er al. [145] were able to show that in these animals the circadian rhythms of clock gene expression in the SCN and liver were in entrained to the animal's activity pattern, but that the retinal circadian rhythm did not free-run, and was instead entrained to the LD cycle. These retinas also showed robust PER2::Luc oscillations *in vitro* and were able to shift this rhythmicity in response to a change in the LD cycle [145]. Since these animals were retinally degenerate and did not express melanopsin, the entrainment of retinal circadian clock did not seem to be dependent on any known photoreceptor. However, these animals may have retained some residual rods and cones.

Further evidence for a novel clock mechanism in the retina came from a study demonstrating that the phase-shifting response of *ex vivo* retinas was abolished in mice lacking neuropsin (*Opn5*) [146]. The expression of neuropsin was localised to a subset of retinal ganglion cells [146]. Similarly to the retina, neuropsin was also responsible for entraining the circadian clock of outer ear skin to the external LD cycle [147]. Furthermore, this function seemed to be dependent on the supply of 9-cis-retinal *in vitro* [147]. The exact mechanisms for neuropsin-mediated retinal circadian rhythm entrainment, however, remain to be investigated.

1.4.5 Circadian rhythms and retinal degenerative diseases

Several lines of evidence suggest there may be an interaction between circadian rhythms and retinal degenerative diseases. One of these potential mechanisms involves melatonin. Research has shown that melatonin has neuroprotective properties, increasing the survival of cultured RPE cells in response to oxidative stress [148]. Also, mice lacking melatonin receptor 1 (MT1) show a loss of photoreceptors by one year of age [149]. The effect of melatonin on the function of the retina has also been studied in humans. In one study, the administration of melatonin to age-related macular degeneration (AMD) patients resulted in a stabilisation of visual acuity after a 6-month follow-up period [150]. Unfortunately, this study did not include a control group and did not report the long-term impact of melatonin administration [150]. Another study looked at the primary melatonin metabolite levels in AMD patients and reported lower metabolite levels in AMD patients compared to age-matched controls [151]. Furthermore, retinal melatonin synthesis decreases during ageing [152] as does the retinal responsiveness to exogenous melatonin [153].

There is also evidence that retinal degenerations are associated with poorer sleep quality. In particular, blind subjects with various retinal degenerations have been demonstrated to have disrupted sleep in comparison to normally sighted individuals [154]. The effect of retinal degenerations on sleep may be mediated by a deficient light input to the SCN or perhaps additionally by a disrupted retinal circadian clock.

An aberrant core molecular clock also affects the retinal function. The absence of *Bmal1* specifically in the retina leads to a reduced rod and cone function in aged mice [155]. Furthermore, these mice show a reduction of retinal thickness and reduced viability of retinal cones [155]. The simultaneous lack of *Clock* and *Npas2* also leads to retinal abnormalities in ageing, particularly the thinning of the ONL [156]. Furthermore, the clock component *RORA* has been implicated in AMD [157]. This evidence suggests that an aberrant function of the retinal clock could regulate photoreceptor survival in ageing.

Additional evidence for an interaction between retinal clock and degeneration comes from studies on a rat model of retinal damage. It was shown that while exposure to a bright light pulse induced retinal damage, the extent of damage was dependent on the time the light pulse is administered. Exposure to a light pulse at night resulted in more significant damage than exposure to the same intensity light pulse at day. This study suggests that the retinal clock controls the regulation of retinoprotective factors [158].

In conclusion, the retinal circadian clock influences retinal health through several mechanisms. First, melatonin, a key circadian neurotransmitter in the retina, seems to have retinoprotective properties. Furthermore, the loss of core clock genes leads to reduced photoreceptor function and viability in ageing, and finally, the clock phase controls retinal susceptibility to light damage.

1.5 Thesis aims

Retinal light responses, particularly those mediated by melanopsin signalling, affect retinal and central circadian rhythms. Furthermore, as melanopsin functions as an irradiance detector in the circadian system, its signalling may have broader implications on retinal function, particularly in retinoprotection. In addition, the current understanding of the similarities and differences in the regulation of retinal and central light responses remains unclear.

Therefore, the aims of this thesis are to:

1. Investigate how melanopsin affects the retinal circadian clock, and the retinal and SCN light responses.

2. Examine whether melanopsin mediates retinoprotection in a mouse model of light-induced retinal degeneration, and study how well the mouse model replicates human retinal degenerations.

3. Determine to what extent the retinal and SCN light responses are regulated similarly by investigating retinal light responses in another mouse model, who contrary to melanopsin-null animals, display enhanced central circadian light responses.

2
Methods

2.1 Animals

All animal work was carried out in accordance with the Home Office Animals (Scientific Procedures) Act 1986 under Home Office personal licence I883EFC39 and project licences I9A85BA93 (Assoc. Prof. Aarti Jagannath) and 30/3371 (Assoc. Prof. Stuart N. Peirson). All wild-type (WT) animals used in this thesis were age-matched littermate controls. Mixed cohorts of male and female animals were used unless stated otherwise.

2.1.1 Animal housing

Mice were group-housed under a 12:12 hour light-dark (LD) cycle and their cages illuminated from above with white light-emitting diode (LED) lights at an intensity of 100 lux, unless stated otherwise (for light spectrum, see Fig. A.1B). Water and standard rodent diet were provided *ad libitum*.

2.1.2 Breeding

Melanopsin knock-out mice

In the melanopsin (*Opn4*) knock-out mice (officially designated $Opn4^{tm1.1Yau}$ and hereafter referred to as $Opn4^{-/-}$ mice [31]), the *Opn4* gene sequence between exons

1 and 9 has been replaced by tau-LacZ. The colony was maintained on a mixed C57BL/6J x 129 genetic background and kept as an inbred colony by crossing two hemizygous animals.

Salt-inducible kinase knock-in mice

In the salt-inducible kinase (SIK1) knock-in mice (officially designated $Sik1^{tm1.1Arte}$ and hereafter referred to as SIK1 KI mice [159]), the endogenous *Sik1* gene has been replaced with a version carrying a point mutation, which renders the protein kinase-dead. By changing the amino acid at position 182 of SIK1 from threonine to alanine, the serine/threonine kinase 11 (STK11), also known as liver kinase B1 (LKB1), is unable to activate the SIK1 protein. The SIK1 KI animals were on a C57BL/6J genetic background and maintained as an inbred colony by crossing two hemizygous animals. The SIK1 KI colony was genotyped and managed by Dr Lewis Taylor.

2.1.3 Genotyping

Genomic DNA was extracted from an ear punch by incubating the tissue in 100 µl 50 mM sodium hydroxide solution at 95°C for one hour. After brief vortexing, tubes were centrifuged at 10,000 xg for 15 seconds and 10 µl of 1 M Tris hydrochloride (pH 5.0) was added. Tubes were briefly vortexed and centrifuged again at 10,000 xg for 15 seconds. 500 µl of molecular grade water was added and 1 µl of the final solution was used for subsequent polymerase chain reactions (PCR).

Wild-type *Opn4* gene was detected with 5' - AGAAGTGGCTCTTTGGGGAGAC - 3' (in exon 3 of *Opn4*) and 5' - GCAGAAGGCATAGAACTCGCAAC - 3' (in exon 4 of *Opn4*) primers, which amplify a 200 bp product with a melting temperature of 82°C. *LacZ* transgene was determined with 5' - AAGCAGTCAGCAGCCCAAAG - 3' and 5' - TGTCACCCTCCTGGTCTTGC - 3' primers, which yield a 300 bp product with a melting temperature of 86°C.

The *Opn4* colony was also genotyped for the *Rpe65* gene at codon 450 by sequencing the product amplified with 5' - ACCAGAAATTTGGAGGGAAAC - 3' and 5' - CCCTTCCATTCAGAGCTTCA - 3' primers. All animals in this colony

were homozygous for the WT *Rpe65* variant as they had a CTG sequence at codon 450, which codes for Leu. Some pigmented mouse strains are known to have ATG sequence in that position, resulting in the expression of the *Rpe65* Leu450Met variant, which confers resistance to light damage [160].

Knock-in mutation of *Sik1* was detected using primers 5' - CTTGCTCTTAAG-GTGTTCTTAAGG - 3' and 5' - ACAGAGCCACTAACAAGACTGC - 3'. The wild-type allele gives rise to a 307 bp and the mutant allele to a 368 bp product.

The $Opn4^{-/-}$ colony was genotyped using quantitative polymerase chain reaction (qPCR) and SYBR Green PCR Master Mix (Applied Biosystems). The SIK1 KI colony was genotyped using Platinum Hot Start PCR Master Mix (Thermo Fisher Scientific) and PCR products separated on a 1.5% agarose gel. The manufacturers' protocols were followed in both cases.

2.2 *In vivo* assessment of circadian and visual function

2.2.1 Circadian activity monitoring

Animals were housed individually under a 12:12 hour LD cycle in cages fitted with running wheels. Multiple cages were kept in light-tight chambers with adjustable LD schedules. Light intensity in the cage was 100 lux unless stated otherwise. Activity data (number of wheel revolutions in one minute bin) was recorded and analysed with ClockLab software (Actimetrics, Wilmette, IL, USA). Circadian period τ was calculated from a chi-square periodogram.

2.2.2 Phase-shifting protocols

Animals were housed individually under a 12:12 hour LD cycle in cages fitted with running wheels. Multiple cages were kept in light-tight chambers with adjustable LD schedules. Upon reaching stable behavioural entrainment, animals were released into constant darkness (DD). On day 5 of DD, animals were exposed to a 15-minute light pulse at circadian time (CT) 16, which was calculated from the CT12 of the previous day, defined by the onset of activity in DD. Where indicated, pupil dilation

was applied before the onset of activity at CT11-12 by applying a drop of 1% tropicamide and 2.5% phenylephrine (Bausch & Lomb) to both eyes under dim red light (0.1 lux, for spectrum, see Fig. A.3D). Animals were further left under constant conditions (DD) for 5-7 days. The phase angles of activity before and after the light pulse were determined and used for calculating the phase shifts. As per convention, phase delays were defined as positive and phase advances as negative shifts.

Two dim red light sources were used for experiments performed in the dark. One of those was fitted to the ceiling of some rooms (for spectrum, see Fig. A.3C) and the other was a portable red light source (for spectrum, see Fig. A.3D). Depending on the experiment, one or the other was used, and the exact light is specified in each methods section.

2.2.3 Bright light exposure

Only male mice were used for retinal light damage experiments. In the first subset of light experiments, animals were exposed to a 3-hour 10,000 lux white light pulse using a custom-built panel fitted with two 100 W LED chips (for spectrum, see Fig. A.2A). The light panel was placed above a 20 x 20 x 20 cm white box. Bedding was removed, and animals were provided with food and water for the duration of the light pulse. Animals were pulsed in their respective cage groups. In these experiments, pupils were not dilated during light exposure.

In the second subset of experiments, animals were exposed to a 20,000 lux white light pulse from 90 minutes to 6 hours with an LED light panel (NL660, Neewer, for spectrum, see Fig. A.2B) placed on top of a 20 x 20 x 20 cm white box. Bedding was removed and animals were provided with food and water. The box was divided into four areas, and all animals were pulsed individually. During those experiments, pupils were dilated with 1% tropicamide and 2.5% phenylephrine (Bausch & Lomb). For light pulses lasting longer than 3 hours, the abovementioned mydriatics were reapplied 3 hours into the light pulse.

All bright light pulses were administered during the dark phase. In the first set of experiments, animals were exposed to light between Zeitgeber time (ZT) 15-18,

and in the second set of experiments, the midpoint of pulses was at ZT18. In both experiments, control animals were not exposed to light.

2.2.4 Pupillometry

Pupil response was assessed as described previously [161]. All animals were dark-adapted for at least 1 hour before testing, and their left pupils were dilated with 1% tropicamide (Bausch & Lomb) 30 minutes before the first recording. For the recordings, unanaesthetised animals were restrained using conventional husbandry techniques and positioned on the pupillometry setup with their dilated left eye facing the light source and the right eye facing the camera. 10-second light stimuli were presented to the left eye from an LED projecting to a 2-inch integrated sphere (Pro-Lite Technology) to ensure uniform illumination of the entire pupil area. The light pulse was controlled by custom-built software, which regulated the opening of a mechanical shutter in the light path. The experimental area was illuminated by an infrared LED (for spectrum, see Fig. A.2F) and the consensual pupil response was recorded with a Prosilica near infrared-sensitive video camera (Brian Reece Scientific Limited), positioned in front of the right eye. Each recording consisted of a 2-second baseline recording, a 10-second light pulse and a 17-second recovery phase and was captured at a rate of 5 frames per second. Recordings were performed in a room illuminated by dim red light (0.1 lux, for spectrum, see Fig. A.3C).

All animals were habituated on at least two occasions before undergoing experimental measurements. Unless stated otherwise, pupillometry was performed during the diurnal light phase between ZT 4 and 8. In instances where an animal underwent multiple pupillometry measurements during a session, one hour was left between recordings and pupils were dilated every two hours.

Three LED light sources were used in this thesis: a blue, a yellow and a UV LED (for light spectra, see Fig. A.2C-E). Unless explicitly stated otherwise, the blue LED was used for pupillometry recordings. The intensity of light stimuli was adjusted with neutral density (ND) filters (Lee Filters) placed in front of the light source.

Images were analysed in ImageJ/FIJI [162] by drawing an ellipse around the pupil and measuring its area. Data are presented as the pupil area relative to baseline fully dilated pupil area before administering the light pulse.

2.2.5 Optomotor response

A physical optokinetic drum, consisting of a turntable and Perspex drum with an internal diameter of 30 cm and height of 55 cm, was used to measure optomotor responses (Fig. 2.1A). Paper sheets with gratings of various parameters were fitted to the inside of the drum. Visual acuity measurements were performed using square-wave gratings of 0.03, 0.1, 0.4 and 0.6 cycles per degree (cpd), designed in Adobe Illustrator (Adobe Inc.) (Fig. 2.1B, C). The drum was illuminated from above with a lamp fitted with an incandescent light bulb (for spectrum, see Fig. A.1C). Illuminance in the centre of the arena was 250 lux and corneal illuminance 50 lux, which ensured that both rod and cone pathways contributed to the optomotor response [133]. A camera (ePathChina 6 mm Lens 600TVL HD 1280 x 960P 1/3 inch CMOS, Amazon) was attached to the lamp and connected to a computer via a video capture adapter (A07JR, Maplin). For the recordings, mice were placed on a 10 cm diameter Petri dish attached to a 20 cm high platform in the middle of the drum.

For experimental recordings, the animal was placed onto the platform with a blank white sheet fitted to the drum. After a 3-minute acclimatisation period, the drum was rotated for 2 minutes at a speed of 12 degrees per second, which corresponds to the optimal visual acuity in mice [133]. The drum was controlled by AutoStep Software (PC Control Ltd), and the direction of rotation was changed every 30 seconds. The paper sheet was then replaced, and animals allowed to acclimatise for 30 seconds before running the same 2-minute protocol. This procedure was repeated with all gratings tested. The Petri dish was cleaned thoroughly with 70% ethanol between animals. Each animal was habituated on two occasions before experimental recordings. Habituation entailed placing the animal onto the platform with the drum fitted with 0.6 cpd 100% contrast square-wave gratings. The drum was kept stationary for 3 minutes, followed by running the 2-minute protocol.

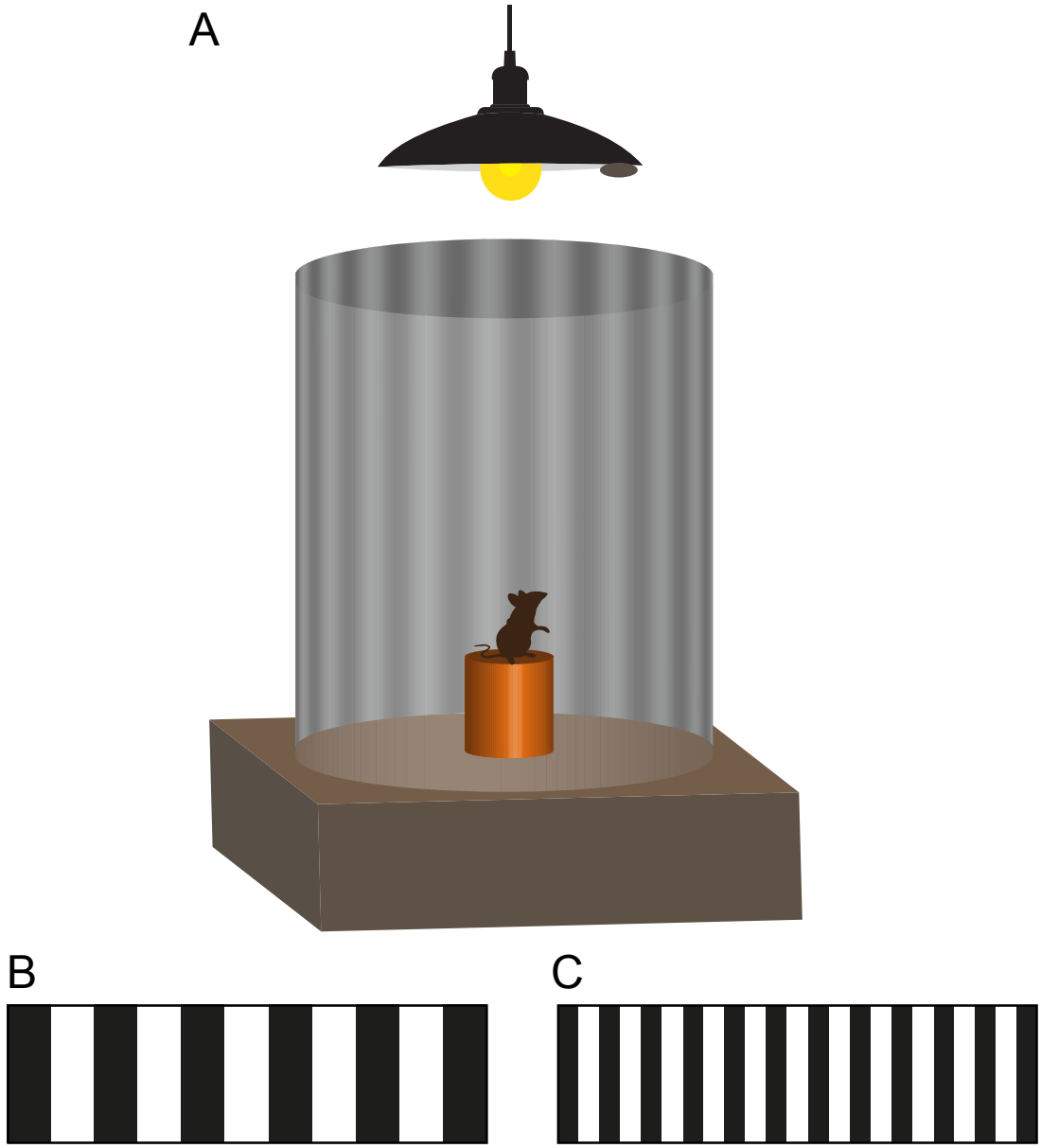


Figure 2.1: Schematic of the optomotor system. (A) The setup consisted of a Plexiglas drum and a turntable, which was controlled with a custom-built software. A lamp, with a camera attached to it, was illuminating the drum from above. The animal was placed on a platform in the middle of the drum, and the inside of the drum was fitted with gratings of different parameters. The drum was rotated for 2 minutes per grating, and the number of head tracking episodes was later quantified from the captured videos. Square wave gratings of 100% contrast with a lower (B) and higher (C) spatial frequency.

The testing sessions were recorded and video files coded by another scientist. The videos were scored by counting the number of times the animal's head travelled in the direction of the gratings for >15°. An episode was considered complete when the mouse looked in any other direction. Data are presented as the number of tracking episodes per minute.

2.2.6 Novel visuospatial context recognition task

A modified version of the novel object recognition task was carried out as described by Tam et al. [163]. Walls of a white 20 x 20 x 20 cm arena were decorated with various visual stimuli (a star, chequerboard and chevron, Fig. 2.2). The arena was illuminated from above with a white LED light (for spectrum, see Fig. A.1B), and illuminance in the arena was kept at 50 lux. A camera (ePathChina 6 mm Lens 600TVL HD 1280 x 960P 1/3 inch CMOS, Amazon; video capture adapter A07JR, Maplin) was positioned 40 cm above the arena. Animals were habituated in the arena one day before testing by allowing them to explore the empty arena for 10 minutes. On the day of testing, two identical neutral objects (e.g. candle holders, small toy houses or pyramids, neutrality determined by Tam et al. [163]) were placed in two corners of the arena, and the animal was allowed to explore the arena for 10 minutes during the sample phase. The animal was then removed from the arena and placed back into its home cage for 5 minutes. During this time, the arena and the objects were cleaned thoroughly with 70% ethanol. One of the objects was then placed in a different corner (Fig. 2.2) and the animal put back into the arena for another 3 minutes for the test phase.

Both the sample and the test phase were recorded, and the 3-minute test phase was further analysed in ANY-maze software (version 4.5, Stoelting, Wood Dale, IL, USA). The regions of objects were marked on the video and the amount of time the animal spent in those regions was determined with automated head tracking. Results are presented as the amount of time the animal spent exploring the object in the novel location over time spent exploring either object. An index of >0.5

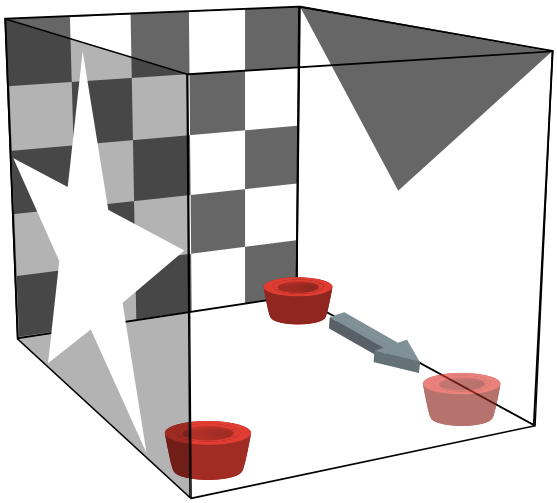


Figure 2.2: Novel visuospatial context recognition task. The animal was placed in a box with decorated walls and allowed to explore the arena with two identical objects placed in two corners. The animal was then removed from the arena for 5 minutes, and the box and the objects were thoroughly cleaned. One of the objects was moved to a novel location, and the animal was allowed to explore the arena for an additional 3 minutes. A preference for the object in novel visuospatial context indicates preserved visual and cognitive functions.

suggested a preference for the item in the novel visuospatial context and the ability to recognise and memorise environmental visual cues [163].

All visuospatial context recognition experiments were carried out during the light phase between ZT4 and ZT8, and animals were handled with cardboard tubes, which causes less anxiety than the traditional tail handling [164]. The positioning of objects was counterbalanced within the experimental groups. To eliminate the possibility that animals used other cues, such as a smell gradient in the room, the box was rotated for the test phase in one experiment. The analysis showed that these results did not differ from those obtained by not rotating the box. Another scientist coded the captured videos, and video analysis was conducted masked to animals' genotypes and experimental conditions. Each set of objects was only used once for each animal to retain the novelty of the objects.

2.2.7 Electroretinography

Experiment setup

The electroretinography (ERG) setup was built in-house by Dr Moritz Lindner and me with advice and help from Prof. Mark Hankins, Prof. Machelle Pardue and Dr Morven Cameron. A white LED light source (Thorlabs; for spectrum, see Fig. A.3B) was used to administer light flashes. The LED was controlled by a six-position motorised filter wheel (Thorlabs) fitted with 1, 2, 3, 4 and 5 ND filters (Thorlabs), allowing the modulation of flash intensity. Another white LED light (Thorlabs; for spectrum, see Fig. A.3A) was mounted to the same light path with a 400-700 nm beam splitter (Thorlabs) for the delivery of background light for light-adapted protocols, none of which were analysed in this thesis. The light path was elongated with 1-inch diameter lens tubes (Thorlabs) and light diffused with a ground glass diffuser (Thorlabs).

A multi-strand 8-denier nylon silver-impregnated ERG thread (Unimed Electrode Supplies), attached to a 3 mm diameter mini contact lens (OcuScience) through slits cut on opposite sides of the lens, was used as the recording contact lens electrode (CLE). A Mini-Grabber composed of a small grabber with 100 cm cable (Unimed Electrode Supplies) was used to connect the ERG thread to a BioAmp 100 preamplifier (Axon Instruments) and an amplifier (Molecular Devices / Axon Instruments). The analogue signal was converted to digital with Digidata 1440A (Molecular Devices), low-pass filtered at 300 Hz and sampled at 20 kHz. The digitiser, amplifier, motorised filter wheel and shutter were controlled with Clampex 10.7 software (Molecular Devices / Axon Instruments), running on a 32-bit Windows 7 computer. Animals' core body temperature was maintained with a silicone heat mat (RS Components) insulated with copper mesh (0.567 mm aperture, The Mesh Company Ltd) and controlled by a dual-channel temperature controller (Warner Instruments).

To minimise electromagnetic noise, a Faraday cage was constructed around the recording area with woven copper mesh (0.567 mm aperture, The Mesh Company

Ltd). The room was illuminated with dim red light (for spectrum, see Fig. A.3D) and the inside of the cage was lined with blackout fabric to reduce the impact of any environmental light on the recordings.

Experiment procedure

Animals were dark-adapted overnight before recordings. Anaesthesia was initiated with 5% isoflurane in an induction chamber (O_2 flow rate 3 l/min). Paw withdrawal reflex was used to assess the depth of anaesthesia, and when the reflex was lost, the animal was transferred into the ERG recording chamber and placed onto the heat mat to maintain core body temperature (set to 37°C). Inhalational anaesthesia was maintained with 2% isoflurane (O_2 flow 2 l/min), delivered using a mouse face mask (World Precision Instruments). The right pupil was dilated by applying a drop of 1% tropicamide and 2.5% phenylephrine (Bausch & Lomb), and the left eye protected from corneal dehydration by applying a drop of 2 mg/g carbomer (Novartis). Paw withdrawal reflex was tested before inserting the reference and ground needle electrodes (Unimed Electrode Supplies) subcutaneously to the forehead and tail, respectively. Care was taken to place the reference electrode in a similar position between the animals. A drop of artificial tears containing 2% methylcellulose (OmniVision) was placed in the concavity of the contact lens electrode (CLE), which was then positioned on the right eye. Electrode placement was conducted under dim red light (for spectrum, see Fig. A.3D). The recording chamber was then closed and the animal left in complete darkness for an additional 10 minutes before any recordings.

On some occasions, the CLE would spontaneously pull away from the eye during the recording session. In these instances, the recording chamber was opened under dim red light and the position of the CLE restored. When this occurred while recording the dark-adapted ERG protocols, the recording chamber was closed, and the animal left to dark-adapt for 10 minutes before resuming with the recordings.

Dark-adapted irradiance responses were elicited with white 10 ms flashes attenuated with ND filters to achieve corneal irradiances from –3 to 2.5 log cd $\cdot$ s/m^2

(roughly –3.5 to 2 log µW/cm^2 and 0.0014 to 455 lux). For detailed protocols, see Table 2.1. ERG was recorded at subjective day (CT4-8).

Data analysis

Data were imported to R and analysed with the ERGTools package, developed specifically to analyse these data by Dr Moritz Lindner and me. The a-wave, which is a result of photoreceptor hyperpolarisation [128], was detected as the first negative deflection of the ERG trace and its amplitude measured from the baseline to its trough. The b-wave, originating from ON bipolar cell depolarisation [129], was defined as the first positive deflection and its amplitude measured from the trough of the a-wave to the peak of the b-wave. In cases where no a-wave was present, the b-wave amplitude was measured from the baseline to the peak of the b-wave.

Table 2.1: ERG protocols used

Step	**Flash intensity, log cd · s/m^2**	**Number of trials**	**Interstimulus interval, s**
	First experiment		
	Dark adaptation >16 hours		
1	–3	10	20
2	–2	10	20
3	–1	10	20
4	0	4	60
5	1	3	120
	Second experiment		
	Dark adaptation >16 hours		
1	–2.5	50	3
2	–1.5	30	5
3	–0.5	12	20
4	0.5	8	30
5	1.5	5	60
6	2.5	4	90

2.3 RNA expression analysis

2.3.1 Tissue collection for RNA analysis

Animals were housed under a 12:12 hour LD cycle, and unless stated otherwise, tissue was collected during the light phase (ZT2-10). In experiments studying the effect of light on gene expression, animals were exposed to a white light pulse at CT16 during the first day in DD using the LED lights fitted in the LTCs (for spectrum, see Fig. A.1B). Animals were pulsed in their home cages with food removed from the food hopper and food pellets placed in the cage floor to prevent the animals from hiding under the food hopper during the light pulse. Animals were sacrificed by cervical dislocation either immediately after the light pulse or left in the darkness for an additional 30 minutes. Tissue from sham-treated control animals not exposed to light was collected at the same time point. A dim red light (for spectrum, see Fig. A.3C, D) was used to illuminate the room while sacrificing animals in the dark. Where explicitly stated, pupils were dilated before the light pulse under dim red light with 1% tropicamide and 2.5% phenylephrine (Bausch & Lomb).

Eyes were enucleated, flash-frozen immediately on dry ice and stored at -80°C until further processing. For the suprachiasmatic nucleus (SCN) samples, brains were dissected and stored briefly in ice-cold phosphate-buffered saline (PBS). The brain was then placed in a mouse stainless steel 1 mm cut coronal brain matrix with the ventral side facing up. Two razor blades were placed just rostrally and caudally of the optic chiasm and a 1 mm slice cut. SCN samples were obtained by punching the coronal brain slice just above the optic chiasm with a biopsy punch (1 mm internal diameter, Integra Miltex). SCN samples were flash-frozen on dry ice and stored at -80°C until RNA extraction.

2.3.2 RNA extraction

Total RNA was extracted using QIAzol and RNeasy Micro kit RNA extraction methods (both from QIAGEN). Retinas were dissected from the eyes stored at -80°C in ice-cold PBS and homogenised with a tissue homogeniser (Argos Technologies)

in 100 µl QIAzol. In the case of SCNs, 100 µl of QIAzol was added directly to the tube containing the tissue punch and the tissue was immediately homogenised. An additional 400 µl of QIAzol was added, the tubes were kept at room temperature for 5 minutes and then placed on ice. 100 µl of chloroform (Sigma-Aldrich) was added to the homogenates, the tubes shaken vigorously for 15 seconds, placed at room temperature for 3 minutes and then kept on ice. Samples were centrifuged at 12,000 xg for 15 minutes at 4°C, and the upper colourless aqueous phase was transferred to a new nuclease-free microcentrifuge tube (approximately 200 µl). An equal volume of 70% ethanol was added and mixed well by pipetting. Samples were then transferred onto RNeasy MiniElute spin columns, and the RNeasy Micro kit protocol was followed with two minor modifications: the RPE buffer wash was repeated twice, and RNA was eluted in 30 µl, not 14 µl of RNase-free water.

2.3.3 RNA quantity and quality analysis

RNA quantity was routinely measured with a NanoDrop 1000 (Thermo Fisher Scientific). Samples used for RNA sequencing (RNA-seq) underwent RNA quality analysis with the Agilent 2100 Bioanalyzer (Agilent Technologies) using an RNA 6000 Pico Kit (Agilent Technologies) or with the Agilent 4200 TapeStation system using the High Sensitivity RNA ScreenTapes (Agilent Technologies). For analysis with the Bioanalyzer system, the manufacturer's protocol was followed with a minor modification: RNase Zap was not used to clean the electrodes before running the assay. Only non-filter tips were used when loading the chip, and the introduction of any air bubbles was carefully avoided. Analysis with the Agilent 4200 TapeStation system was carried out at the University of Oxford Department of Zoology Sequencing Facility.

2.3.4 Reverse transcription and quantitative reverse transcription PCR

For quantitative analysis of gene expression, 100-300 ng of RNA was reverse transcribed to cDNA using the qScript cDNA Synthesis Kit (Quantabio). Quantitative reverse transcription PCR (RT-qPCR) reactions were set up using QuantiFast SYBR

Green PCR Kit (QIAGEN) following the manufacturer's protocol, and reactions run on the StepOnePlus Real-Time PCR System (Applied Biosystems). Gene expression was analysed using the relative standard curve method. Expression of the genes of interest was normalised to the expression of three housekeeping genes (HKGs). The HKGs used for retinal samples were *Gapdh*, *Gusb* and *Rplp0*, which I determined to be the most stably expressed housekeeping genes in the mouse retina (data not shown). For the SCN samples, *Gapdh*, *Rps9* and *B2m* HKGs were used, previously established to be stably expressed by the Jagannath Lab. For primer sequences, please refer to Appendix B.

2.3.5 RNA sequencing

RNA-seq experiments were performed using the Ion Torrent sequencing platform. Samples with an RNA integrity number (RIN) >7.0 were considered suitable for subsequent RNA-seq analysis. Only male mice were used for the retinal light damage and retinal circadian time-course RNA-seq experiments.

Library preparation

Sequencing libraries were prepared with the QuantSeq 3' mRNA-Seq Library Prep Kit for Ion Torrent (Lexogen). 250 µg of RNA was used as input material for each library, and the manufacturer's protocol was followed without modifications. The optimal number of library amplification cycles was determined to prevent under- or overcycling the library. A modified protocol of the manufacturer's PCR Add-on Kit for Ion Torrent (Lexogen) was used to set up an RT-qPCR assay. Briefly, 2 µl of nuclease-free water was added to the 17 µl of each non-amplified purified library. The RT-qPCR reaction was set up as instructed in the add-on kit, using the PCR master mix and DNA polymerase provided. Additionally, 0.1X SYBR Green I dye (Sigma Aldrich) was added to the reaction to quantify the amplification of the library. 1.7 µl of the diluted library was used for each reaction, and a total of 40 RT-qPCR cycles were run. Since the amount of library used for this reaction was ten times smaller than the remaining library to be amplified, the optimal

number of cycles was approximated by subtracting three from the number of cycles needed to reach 50% of maximum fluorescence.

The size distribution and concentration of amplified libraries were analysed with the Agilent 2200 TapeStation system using the High Sensitivity D1000 ScreenTape. The TapeStation analysis was performed at the University of Oxford Department of Zoology Sequencing Facility. Libraries were diluted to 300 pM, pooled and sequenced with the Ion Proton System (Thermo Fisher Scientific) following the manufacturer's instructions. Sequencing runs were set up with the kind assistance of Mr Cillian Brophy from the Furger Lab at the University of Oxford Department of Biochemistry.

Data analysis

Raw reads from the Ion Torrent platform were converted to FASTQ files and data uploaded to the Galaxy web platform for read quality, alignment and count analysis [165]. Read quality was analysed with FastQC [166] and reads were aligned to the mm10 mouse genome assembly with the STAR alignment algorithm [167]. The resulting BAM files were filtered for duplicate and low-quality reads and counted with featureCounts [168]. Count normalisation and differential analysis between groups were carried out with DESeq2 [169] in R. Circadian rhythmicity parameters were determined with MetaCycle [170]. Differentially expressed pathways and cellular functions were further analysed using the KEGG database [171] and g:Profiler [172].

2.4 Mass spectrometry

Retinas were dissected in ice-cold PBS from eyes kept at -80°C. Dissected retinas were suspended in 200 µL buffer containing 8 M urea (Sigma Aldrich), 100 mM ammonium bicarbonate (Sigma Aldrich), 10 mM TCEP (Thermo Scientific), 50 mM chloroacetamide (Sigma Aldrich) with 2 µL of protease inhibitor cocktail (Sigma Aldrich) and 1 µL of phosphatase inhibitor cocktail (Sigma Aldrich). Cell suspensions were kept on ice and sonicated for 20 seconds (VibraCell, VCX 500, Sonics). The samples were submitted to Oxford Advanced Proteomics Facility for further sample preparation and analysis. Briefly, proteins were digested with LysC

and trypsin and analysed with high-performance liquid chromatography-tandem mass spectrometry (HPLC-MS/MS).

2.5 Cell culture and plasmid transfection

Mouse embryonic fibroblast NIH/3T3 cells were cultured in a cell culture incubator at 37°C with 5% CO_2 in Dulbecco's Modified Eagle's Medium (DMEM) containing 10% fetal bovine serum, 100 I.U./ml penicillin and 100 µg/ml streptomycin (all from Thermo Fisher Scientific). Cells were transfected with SIK1 or SIK1-GFP (green fluorescent protein) overexpression vectors using Lipofectamine 3000 reagent (Thermo Fisher Scientific). The overexpression vectors were constructed by Dr Lewis Taylor by cloning the mouse *Sik1* coding sequence (NCBI ID CCDS37552.1) into pcDNA3.1 or pcDNA3.1/CT-GFP Fusion vectors (Addgene), respectively. Transfection was carried out following the manufacturer's protocol. Briefly, 7.5 µl Lipofectamine and 2.5 µg DNA with 5 µl P3000 Reagent were diluted separately in 125 µl Opti-MEM Medium (Thermo Fisher Scientific) for each well of a 6-well cell culture plate. Diluted DNA was added to Lipofectamine and incubated at room temperature for 5 minutes. DNA-lipid complexes were added to cells at ~80% confluency, and cells were harvested 24 hours after transfection.

2.6 Immunostaining

2.6.1 Immunocytochemistry

Before transfection and immunostaining, NIH/3T3 cells were grown on 22 mm x 22 mm glass coverslips in 6-well cell culture plates. Cells were rinsed briefly in PBS and fixed for 10 minutes at room temperature using 4% paraformaldehyde (PFA) in PBS. Samples were then washed three times for 5 minutes, permeabilised in 0.2% Triton X-100 for 5 minutes, blocked in 10% donkey serum for 30 minutes, and incubated with rabbit anti-SIK1 primary antibody (1:100 or 1:300 dilution, 51045-1-AP, Proteintech) overnight at 4°C. Samples were then washed three times for 5 minutes and incubated with donkey anti-rabbit Alexa Fluor 568 secondary antibody

(1:200 dilution, Invitrogen) for 1 hour at room temperature. Samples were washed another three times for 5 minutes, incubated with DAPI (500 ng/ml) for 10 minutes at room temperature, washed once more and mounted with ProLong Gold antifade mountant (Invitrogen). All washes were performed in PBS at room temperature and antibodies diluted in PBS with 2.5% donkey serum and 0.1% Triton-X.

2.6.2 Frozen tissue sections

Animals were sacrificed by cervical dislocation and the superior part of the cornea marked with a marker pen. Eyes were removed, the corneas punctured with a needle and eyes placed in 4% PFA for an overnight fixation at 4°C. Eyes were cryoprotected with an overnight incubation with 30% sucrose (Sigma-Aldrich) at 4°C, mounted in Tissue-Tek OCT compound (Sakura Finetek) and stored at -80°C. 20 µm thick sections were cut with a Leica CM1850 cryostat (Leica Microsystems), keeping the cryostat chamber at -22°C and the sample at -20°C. Sections were collected on poly-L-lysine coated glass slides (Thermo Scientific) and kept at -20°C until further processing. For immunohistochemical analysis, sections were permeabilised in 0.2% Triton-X in PBS for 20 minutes at room temperature, blocked in 10% donkey serum for 1 hour at room temperature and incubated with primary antibodies overnight at 4°C (for a list of primary antibodies, see Table 2.2). Tissue sections were then washed three times for 10 minutes and incubated with the respective Alexa Fluor dye conjugated secondary antibodies (1:200 dilution, Invitrogen) for 2 hours at room temperature (for a list of secondary antibodies, see Table 2.3). Sections were washed three times for 10 minutes, incubated with DAPI (500 ng/ml) for 10 minutes at room temperature, washed once more and mounted with ProLong Gold antifade mountant (Invitrogen). All washes were performed in PBS with 0.1% Tween-20 at room temperature and antibodies diluted in PBS with 2.5% donkey serum and 0.2% Triton-X.

SCN sections were obtained by removing the mouse brain after sacrification by cervical dislocation. The brain was fixed, cryoprotected, mounted in OCT compound (Sakura Finetek) and sectioned as described above for the eyes, and this

tissue processing was performed by Dr Jovi Wong. Sections containing the SCN were identified by investigating the coronal brain sections under a light microscope. The SCNs are located in the ventral hypothalamus above the optic chiasm, and the two nuclei are separated in the midline by the third ventricle. These sections were immunostained using the same procedure as for the retinal sections.

Table 2.2: Primary antibodies used

Target	Host	Supplier	Product code	Clonality	Dilution
BRN3A	Goat	Santa Cruz	sc-31984	Polyclonal	1:1000
CALB	Rabbit	Abcam	ab108404	Monoclonal	1:1000
GAD67	Mouse	Millipore	MAB5406	Monoclonal	1:500
GFAP	Rabbit	Abcam	ab7260	Polyclonal	1:1000
GLUL	Mouse	Abcam	ab64613	Monoclonal	1:1000
HCN4	Rabbit	Abcam	ab69054	Polyclonal	1:1000
M-opsin	Rabbit	Chemicon	AB5405	Polyclonal	1:1000
OPN4	Rabbit	Advanced Targeting Systems	AB-N38	Polyclonal	1:2500
PCP-2	Mouse	Santa Cruz	sc-13706	Monoclonal	1:1000
PKCα	Rabbit	Abcam	ab32376	Monoclonal	1:1000
Rhodopsin (1D4)	Mouse	Abcam	ab5417	Monoclonal	1:1000
S-opsin	Goat	Santa Cruz	sc-14363	Polyclonal	1:1000
SIK1	Rabbit	Proteintech	51045-1-AP	Polyclonal	1:100, 1:300

2.6.3 Retinal flat-mounts

Eyes with the superior part of the cornea marked with a marker pen were fixed in 4% PFA overnight at 4°C. Retinas were dissected, noting the orientation of the retina, and permeabilised in 1% Triton-X in PBS for 20 minutes at room temperature. Retinas were then blocked in 10% donkey serum for 1 hour at room temperature and incubated with primary antibodies for 72 hours at 4°C. The incubation was followed by three 10-minute washes and incubation with the respective Alexa Fluor dye conjugated secondary antibodies (1:200 dilution, Invitrogen) overnight at 4°C. Retinas were then washed another three times for 10 minutes and mounted with ProLong Gold antifade mountant (Invitrogen). All washes were performed in PBS with 0.2% Triton-X at room temperature and antibodies diluted in PBS with 2.5% donkey serum and 1% Triton-X.

Table 2.3: Secondary antibodies used

Name	Supplier	Product code	Dilution
Alexa Fluor 488 donkey anti-rabbit IgG	Invitrogen	A21206	1:200
Alexa Fluor 568 donkey anti-rabbit IgG	Invitrogen	A10042	1:200
Alexa Fluor 633 donkey anti-rabbit IgG	Invitrogen	A31573	1:200
Alexa Fluor 488 donkey anti-goat IgG	Invitrogen	A11055	1:200
Alexa Fluor 568 donkey anti-goat IgG	Invitrogen	A11057	1:200
Alexa Fluor 633 donkey anti-goat IgG	Invitrogen	A21082	1:200
Alexa Fluor 488 donkey anti-mouse IgG	Invitrogen	A21202	1:200
Alexa Fluor 568 donkey anti-mouse IgG	Invitrogen	A10037	1:200
Alexa Fluor 488 donkey anti-sheep IgG	Invitrogen	A11015	1:200

2.6.4 Confocal microscopy image aquisition

Confocal images were acquired with an inverted Fluoview FV1000 confocal microscope (Olympus, Tokyo, Japan). Individual channels were collected sequentially. Laser lines for excitation were 405 nm, 488 nm, 559 nm and 635 nm, with emissions collected between 440–480 nm, 505–550 nm, 580–625 nm and 650-700 nm for blue, green, red and far-red fluorescence, respectively. Whole retinal flat-mounts and sagittal retinal cross-sections were imaged using the tiling functionality of the microscope. For tiling, the overlap of individual images was calculated and set to $objective\ magnification * zoom/8 + 3$. Image post-processing, restricted to global enhancement of brightness, cropping and sub-selecting fluorescent channels, was performed in ImageJ/FIJI [162]. In experiments where the fluorescence intensity was compared between individual samples, no post-processing was performed.

2.6.5 Retinal thickness measurements

Retinal cross-sections were immunostained and imaged as described above. Images were imported into ImageJ/FIJI [162], and the thickness of the outer nuclear layer (ONL) and inner nuclear layer (INL) were measured from the DAPI-stained images every 400 µm from the optic nerve head (ONH). In experiments where the dorsoventral position of the ONL and INL measurements is not reported, the INL and ONL thicknesses were measured from images across one retina, and the

averaged results are reported. The superior and inferior sections were determined by staining the sections for S-opsin, which is known to exhibit a dorsoventral expression gradient [173, 174]. Sections with high S-opsin staining were classified as ventral and those with low staining as dorsal.

2.6.6 Determining retinal cone distribution

The strategy for determining retinal cone distribution was similar to that described by Sawant et al. [174]. Images of S- and M-opsin immunolabelled retinal flat-mounts were acquired as described above, and the density of cone subtypes was quantified in six regions along the dorsoventral axis, termed mid-dorsal (MD), far-dorsal (FD), far-far-dorsal (FFD), mid-ventral (MV), far-ventral (FV) and far-far-ventral (FFV). Images from the specified regions were imported into ImageJ/FIJI [162], a merged fluorescence image of the two layers was created to enable the detection of dual cones expressing both S- and M-opsin, and cells were manually counted with the Cell Counter plugin. Results are expressed as the number of S-, M- and dual cones per mm^2.

2.7 Multielectrode array recordings

Animals were dark-adapted for >1 hour and sacrificed in a dim red light illuminated room (for spectrum, see Fig. A.3D) by cervical dislocation at ZT 4–8. Eyes were immediately enucleated and retinas dissected under dim red light (for spectrum, see Fig. A.3D) in oxygenated (95% O_2, 5% CO_2) AMES medium (pH 7.4, Sigma-Aldrich). The retinas were then moved onto glass-coated metal harps (ALA Scientific Instruments) with the GCL facing up, and the harps were carefully lifted from the medium. The harps were then placed upside down onto glass-bottomed multielectrode array (MEA) chambers with the GCL now in contact with the electrodes. The MEA chambers, containing 60 electrodes, each 30 µm in diameter and spaced 200 µm apart (Multi Channel Systems), were placed into an MEA recording device (MEA1060-Inv, Multi Channel Systems) mounted onto the stage of an inverted Olympus IX71 microscope, and fitted with gas permeable

perfusion manifolds (ALA Scientific Instruments). The recording electrodes were thus positioned in the microscope light path. Retinas were perfused continuously at 2 ml/minute with oxygenated (95% O_2, 5% CO_2) AMES medium (pH 7.4), which was maintained at 34°C using a bead bath (36°C), an in-line perfusion heater (35°C), and a base plate heater incorporated into the MEA system (34°C).

Retinas were perfused in the dark for 60 minutes before recording light responses. Pulses of white light from an X-cite 120 W metal halide light source (Thorlabs) were delivered to the retina through a 10X microscope objective beneath the MEA chamber. The duration of light pulses was controlled with Metafluor software (Molecular Devices). Retinas were dark-adapted for 10 minutes between pulses. AA92593 (Sigma-Aldrich) was used to block melanopsin light-responses.

Recorded signals were collected, amplified and digitised at 25 kHz using MC Rack software (Multi Channel Systems). Spikes were extracted with the Spike Sorter feature of the software by defining the threshold for each channel as 4 standard deviations from the baseline firing rate. The baseline firing rate was determined from the recording before the administration of the first light pulse. The extracted spikes from all electrodes were summarised in Microsoft Excel with a data analysis template developed by Dr Steven Hughes, and plotted with Prism (versions 8 and 9, GraphPad).

2.8 Light measurements

Spectral irradiance was measured with a radiometrically calibrated spectrophotometer (Ocean Optics). The power of light stimuli was measured with an in-line power meter (PM160T, Thorlabs). Illuminance was measured with a calibrated ILM1335 light meter (RS Components). The irradiance conversion toolbox [175] was used to convert the measurements between units. The spectral irradiances of all light sources used in this thesis are listed in Appendix A.

2.9 Meta-analysis of acute gene expression changes in light-induced retinal damage

2.9.1 Identifying studies

A PubMed search was conducted using the following search statement:

> *retina AND (light OR photooxidative) AND (damage OR degeneration) AND (microarray OR RNA-seq OR RNA seq)*

The Gene Expression Omnibus (GEO) database was queried with the following statement:

> *retina AND (light OR photooxidative) AND (damage OR degeneration)*

An ArrayExpress search was performed with the search term "retina". All three searches were conducted on August 23, 2020. The results were screened for studies that met the following inclusion criteria:

1. Using mice (*Mus musculus*) as experimental animals
2. Exposing them to a single high-intensity light pulse (>1,000 lux)
3. Subjecting the retinas to transcriptome profiling analysis

2.9.2 Data extraction and analysis

Only data from WT retinal samples were included in the meta-analysis. The CEL files of microarray datasets were downloaded and analysed locally in Bioconductor. Raw data was background corrected and normalised with Robust Multichip Averaging (RMA) in the oligo package [176], followed by the extraction of $\log_2$ expression values with the Biobase package [177]. For RNA-seq datasets, the count matrices of mapped reads were downloaded and used for further analysis.

Normalised microarray expression values and counts of mapped reads of RNA-seq datasets were imported to NetworkAnalyst [178] where the further analysis was carried out. RNA-seq read counts were $\log_2$ transformed and normalised, and study batch effects were corrected for with robust empirical Bayes regression

(ComBat) [179], which standardises gene expression values such that each gene has a similar overall mean and variance. Differentially expressed genes were identified by combining effect sizes of individual experiments using a random-effects model with a p value cut-off of 0.05. The effect size was defined as the difference between the mean expression values of the control and light damage groups divided by the standard deviation. Gene network analysis was performed with the International Molecular Exchange (IMEx) consortium Interactome tool [180], pathway analysis of differentially expressed genes was carried out using Gene Set Enrichment Analysis (GSEA) [181] and KEGG database [171] and visualised with inbuilt functions of NetworkAnalyst [178].

Homologous genes between human, mouse and baboon genomes were identified with biomaRt package in Bioconductor [182]. Those genes which were not found to have a homolog were also queried in the Mouse Genome Database [183].

Only data from WT retinal samples were included in the meta-analysis. The CEL files of microarray datasets were downloaded and analysed locally in Bioconductor. Raw data was

2.10 Defining retinal cell-specific gene enrichment

Throughout my thesis I infer which retinal cell types may contribute to the changes seen in bulk retinal transcriptome by using a dataset by Siegert et al. [184]. They isolated distinct retinal cell populations from 22 transgenic mouse lines, each expressing a fluorescent marker under a specific promoter, and subjected these subpopulations to microarray analysis. The cell types in their dataset include all the major retinal cell classes, the rods and cones, horizontal cells, various bipolar and amacrine cells and RGCs.

The raw data matrix containing the normalised expression values of each gene in each of the 22 retinal cell types was accessed. The analysis of "enrichment" in a particular cell type was carried out as follows:

1. The average expression value of each gene across all the cell populations included in the dataset was calculated

2. The subset of genes of interest was extracted from the entire dataset (e.g. all circadian genes or all genes expressed differentially between two conditions)

3. For each gene of interest, it was calculated in which cell populations its level was >2 standard deviations (SD) higher than the average value for that gene in the dataset.

4. For each subset of genes of interest, the number of genes expressed >2 SD higher than the average value was counted for each cell type.

5. As some cell populations are more similar to the average cell in the dataset, each cell type is enriched for several genes purely by chance. Therefore, the number of genes across the entire transcriptome that would be expected to be expressed in each cell type >2 SD higher than the average value was calculated.

6. The values calculated from 4. were normalised to the values calculated from 5. Therefore, an enrichment value of 1.0 indicates that the number of genes expressed in the particular cell population >2 SD higher than the average expression value for the genes across the dataset can be expected by chance, i.e. there is no enrichment.

2.11 Statistical analysis

All data, except the transcriptome profiling and ERG data, were analysed using Prism (versions 8 and 9, GraphPad). Data on graphs are presented as mean + or ± SEM, as detailed in each figure legend. For comparisons between two experimental groups, two-tailed paired or unpaired t-tests were used for normally distributed data, and Wilcoxon rank-sum tests or Wilcoxon signed-rank tests for non-normally distributed data. To analyse three or more groups for a single variable, one-way analysis of variance (ANOVA) with Dunnett's correction for multiple comparisons

was applied. Two-way ANOVA with Šidák's correction for multiple comparisons was used to compare multiple groups for two variables. The particular statistical tests are specified in figure legends. A p value of < 0.05 was considered statistically significant.

3

The role of melanopsin in retinal and central circadian rhythms

3.1 Introduction

Multiple aspects of the visual function display circadian rhythms, and mice lacking melanopsin display defects in some of those retinal rhythms [185]. However, the precise molecular mechanisms of how melanopsin regulates the retinal functions are not known. The circadian clocks of the retina and the SCN entrain constantly their rhythms to the surrounding light environment and the light sensitivity of the central circadian clock is reduced in the absence of melanopsin [32, 33, 186]. Whether the lack of melanopsin results similarly in a dampened light sensitivity of the retina is unclear as there are conflicting reports in the literature [138, 187, 188].

In this chapter, I am addressing the first aim of my thesis. The purpose of this chapter is to explore the mechanisms whereby melanopsin affects the local retinal circadian rhythms, and study the effect of melanopsin signalling on retinal and SCN light responses.

3.1.1 Retinal circadian rhythms in *Opn4*$^{-/-}$ animals

Circadian rhythms are well documented in multiple retinal functions, including contrast sensitivity, pupillary light response and cone ERG. These rhythms aid with

the visual system's ability to switch between high-sensitivity vision during the day to high-specificity vision at night, enabling the detection of stimuli over a wide range of light intensities. The cellular basis for at least some aspects of the retinal circadian rhythms is the coupling between rods and cones. At night, the photoreceptors are connected via gap junctions, which allows rods to signal through cone pathways and increases the sensitivity of the visual circuits. At daytime, the gap junctions are closed, and the rod and cone pathways remain separated to allow high specificity in the retinal circuits [124] (discussed in section 1.4). Interestingly, *Opn4*$^{-/-}$ animals lose the rhythmicity in some, but not all retinal functions, suggesting that the mechanisms governing the various retinal rhythms are distinct.

Pupillary light reflex

The maximum pupil constriction varies between day and night in both circadian and diurnal conditions [134]. In wild-type (WT) animals, the pupils constrict to approximately 5% of the initial dark-adapted pupil area at day and only 15% at night (Fig. 3.1A, B, E). While the maximum pupil constriction at day is attenuated in *Opn4*$^{-/-}$ mice, a finding that has been well established in the literature [82], these animals nevertheless retain diurnal rhythmicity of this response. The pupils of *Opn4*$^{-/-}$ animals constrict to 9% and 18% at day and night, respectively (Fig. 3.1C-E). Similar results were also obtained previously in our lab by Dr Jovi Wong, who tested animals in both diurnal and circadian conditions (unpublished data). It is of note that the pupillary light response seems to be regulated by the core molecular clock as the circadian rhythmicity is lost in animals lacking cryptochrome 1 (*Cry1*) [134]. However, it seems that the clock responsible for mediating this rhythm is unaffected by the lack of melanopsin.

Contrast sensitivity

Previous work in our lab by Dr Jovi Wong demonstrated that *Opn4*$^{-/-}$ animals lose the circadian rhythmicity of contrast sensitivity [189]. While in WT animals the contrast sensitivity was better at day and worse at subjective night (Fig. 3.2A),

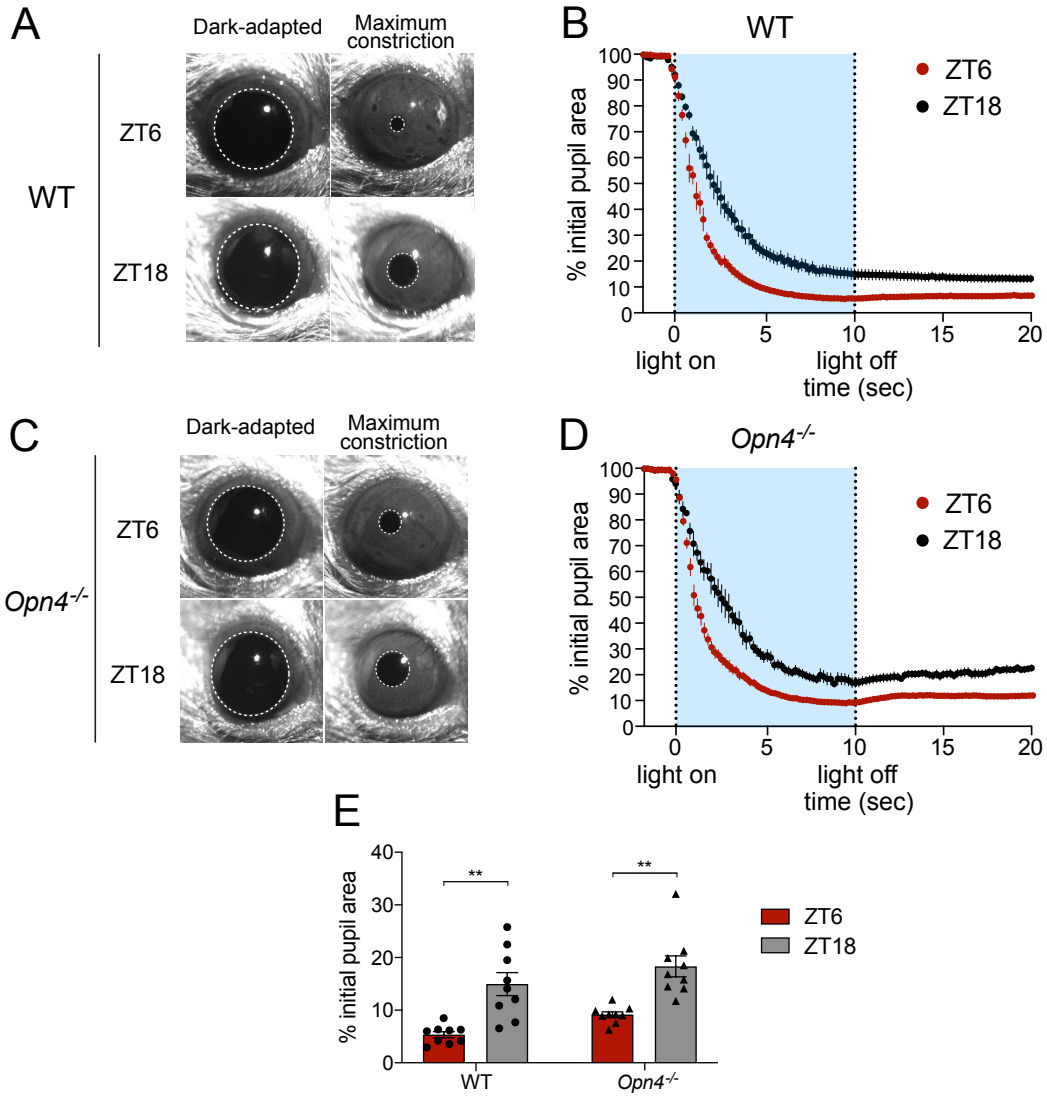


Figure 3.1: Diurnal rhythmicity of pupillary light response in WT and *Opn4*$^{-/-}$ animals. The pupillary light response recording consisted of a 2-second baseline recording followed by a 10-second blue light pulse and a post-illumination recording. Representative images of the pupils before and after the 10-second blue light pulse in WT (A) and *Opn4*$^{-/-}$ animals (C). Pupil constriction dynamics in WT (B) and *Opn4*$^{-/-}$ mice (D). (E) The maximum pupil response is expressed as the pupil area normalised to the dark-adapted pupil area. Data are mean ± SEM, n = 9. Statistical analysis was performed using two-way ANOVA with Šidák's correction for multiple comparisons. ** $p < 0.01$.

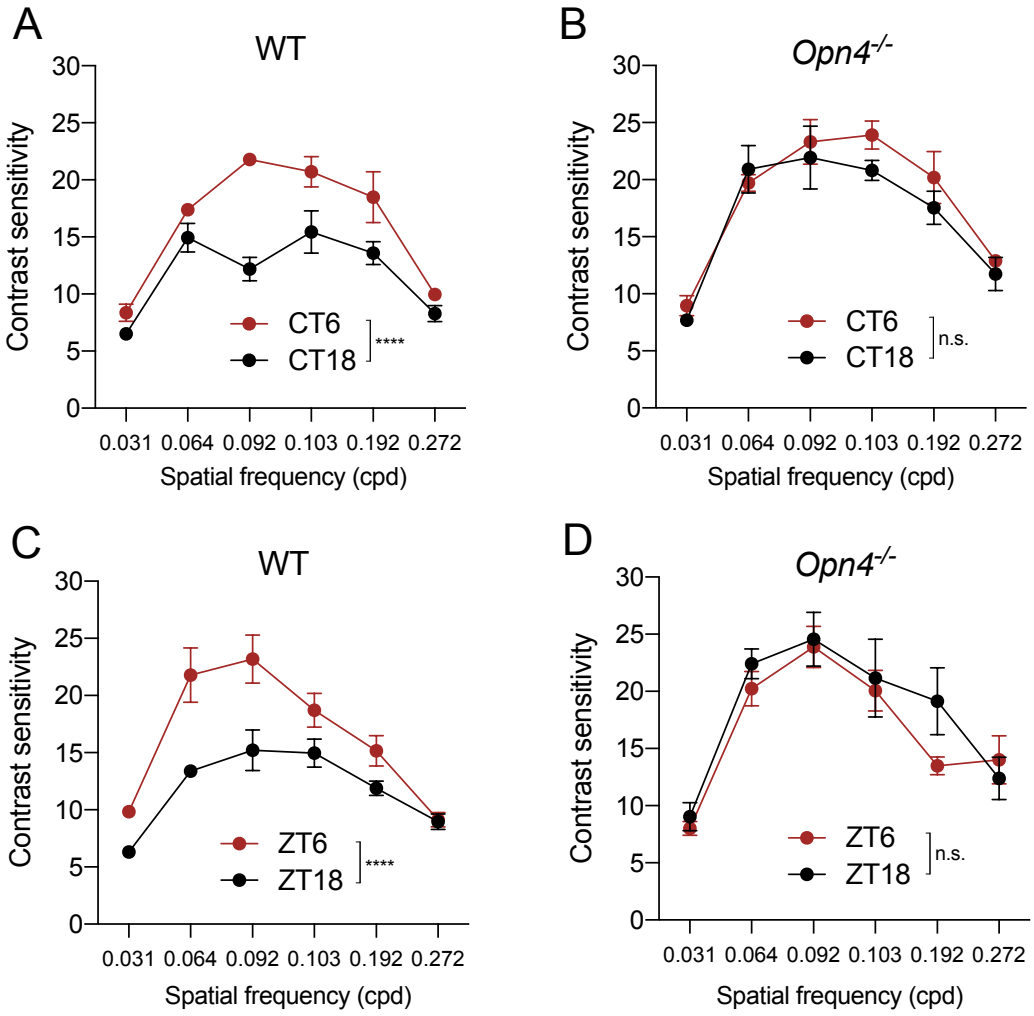


Figure 3.2: Circadian and diurnal rhythmicity of contrast sensitivity in WT and *Opn4*$^{-/-}$ animals. This experiment was performed by Dr Jovi Wong. Contrast sensitivity function in constant conditions in WT (A) and *Opn4*$^{-/-}$ animals (B), and in diurnal conditions in WT (C) and *Opn4*$^{-/-}$ animals (D). Data are mean ± SEM, n = 5-6. Statistical analysis was performed using two-way repeated-measures ANOVA, and the main effect of time of day is reported. n.s., not significant, **** $p < 0.0001$.

Opn4$^{-/-}$ animals show no reduction in their contrast sensitivity at night and their contrast-detection does not vary between day and night (Fig. 3.2B). This effect was present also in diurnal conditions (Fig. 3.2C, D). Therefore, *Opn4*$^{-/-}$ animals seem to retain their "day-like" contrast sensitivity function at night.

The detection of contrast is also modulated by the core molecular clock components. Similarly to *Opn4*$^{-/-}$ animals, *Cry1*$^{-/-}$ animals also show an enhanced contrast sensitivity at night and lose the circadian rhythm of this function [134]. Contrast sensitivity is also influenced by retinal dopamine. Reduced dopamine levels and the

lack of signalling through dopamine receptor 4 (DRD4) result in a diminished ability to detect contrast day [190]. However, the circadian rhythmicity of the function is retained [190]. Therefore, the loss of contrast sensitivity rhythm in *Opn4*$^{-/-}$ animals may have to do with the aberrant regulation of the core molecular clock or involve increased dopamine signalling. Interestingly, *Opn4*$^{-/-}$ animals mimic the contrast sensitivity phenotype of *Cry1*$^{-/-}$ animals, but not their maximum pupil response, suggesting that the mechanisms regulating these two circadian rhythms are different.

Cone ERG

Another rhythmic retinal readout influenced by melanopsin is the cone electroretinogram (ERG). As discussed in section 1.4, the cone ERG b-wave amplitude is higher during the day compared to night. Furthermore, the time to the b-wave peak (implicit time) is shorter at day than at night [130, 131, 185].

Similarly to the circadian rhythms of pupil response and contrast sensitivity, the rhythmicity of cone ERG is also influenced by the core molecular clock. Mice lacking the core clock genes *Bmal1* and *Cry1*$^{-/-}$*Cry2*$^{-/-}$ lose their cone ERG rhythmicity and display opposite phenotypes. The cone ERG of *Bmal1*$^{-/-}$ animals is in a constant "night-like" state. Their cone b-wave amplitude at day is lower, and its implicit time longer compared to WT animals [130]. The phenotype of the *Cry1*$^{-/-}$*Cry2*$^{-/-}$ mice is the opposite, their cone ERG is constantly in a "day-like" state, the b-wave amplitude at night higher and implicit time shorter compared to WT littermates [131]. These results suggest that the retinal clock controlling the cone ERG rhythm in those two animal models is fixed in the opposite phases. Furthermore, the cone ERG is also affected by dopamine and melatonin signalling, illustrated by the findings that the retinas lacking melatonin receptor 1 and dopamine result in a loss of cone ERG rhythmicity and a constant "night-like" state [132, 191].

Barnard et al. [185] studied the cone ERG in *Opn4*$^{-/-}$ mice. They found that the lack of melanopsin led to an aberrant cone ERG (Fig. 3.3A). Their cone b-wave amplitude was lower compared to WT animals at day, while the amplitudes were

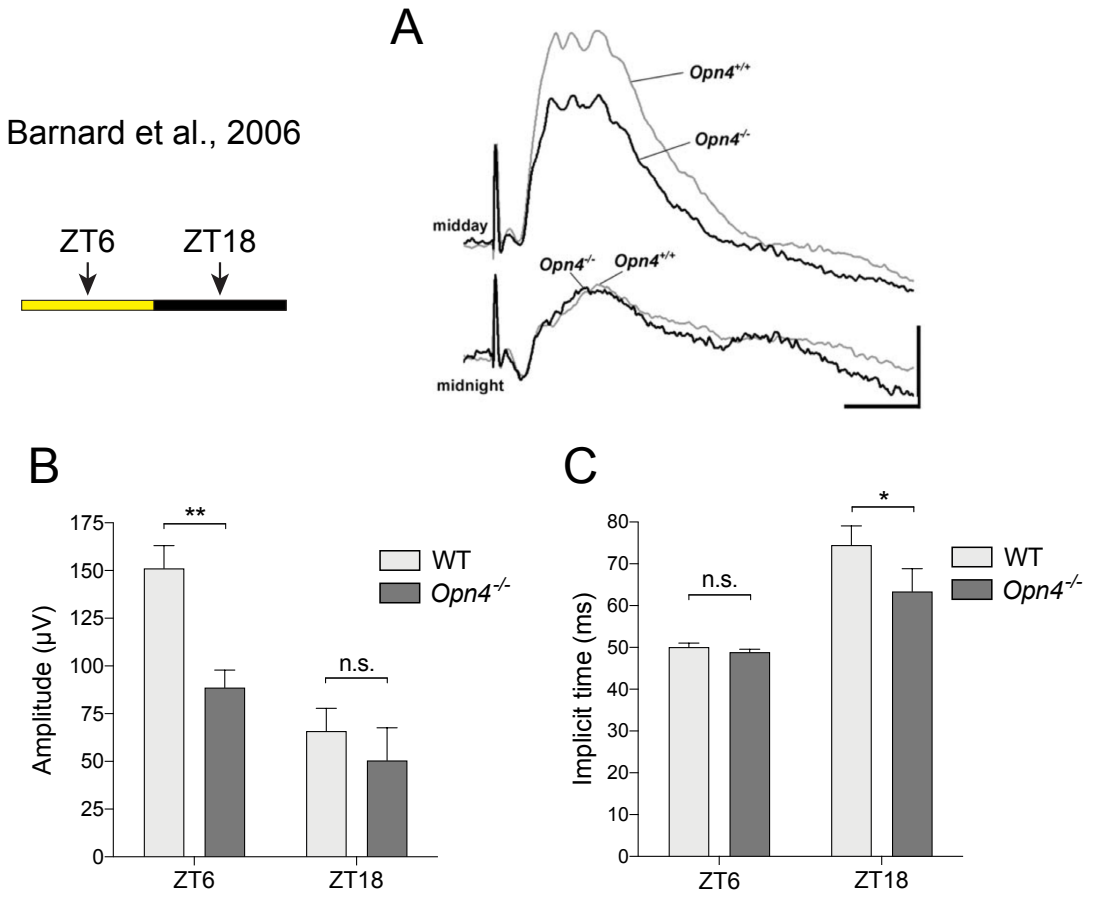


Figure 3.3: Diurnal rhythmicity of cone ERG in WT and *Opn4*$^{-/-}$ animals. All data presented on this figure are reproduced from Barnard et al. 2006 [185], who investigated cone ERG in WT and *Opn4*$^{-/-}$ mice. (A) Representative cone ERG traces of WT and *Opn4*$^{-/-}$ mice at midday (ZT6) and midnight (ZT18). Cone ERG b-wave amplitude (B) and implicit time (C) in diurnal conditions at ZT6 and ZT18. Data are mean + SEM, n = 5-9. Statistical analysis was performed using the mean, SEM and group sizes reported by the authors. Two-way ANOVA with Šidák's correction for multiple comparisons was utilised. n.s., not significant, * $p < 0.05$, ** $p < 0.01$.

the same between the genotypes at night (Fig. 3.3B). It was suggested that *Opn4*$^{-/-}$ mice thus lose the diurnal rhythmicity of the cone ERG.

Re-analysis of their original data showed that in addition to the differences in cone b-wave amplitude, there were also slight changes in cone ERG b-wave implicit time. Should a lower b-wave indicate increased photoreceptor coupling, it would be complemented by a lengthening in the b-wave implicit time. Surprisingly, the b-wave implicit time of *Opn4*$^{-/-}$ animals at night was instead slightly *shorter* compared to WT animals. This finding instead indicates a faster signal transmission and could

be interpreted as a "day-like" cone ERG (Fig. 3.3). Therefore, although the cone ERG of *Opn4*$^{-/-}$ mice is abnormal, the data can be interpreted in two different ways. On the one hand, the reduced b-wave amplitude at day points towards *Opn4*$^{-/-}$ retinas being in a constant "night-like" state. On the other hand, the shorter b-wave implicit time at night could mean that there is less coupling between the photoreceptors at night, suggesting that *Opn4*$^{-/-}$ retinas are instead in a "day-like" state at night. The latter interpretation also implies that *Opn4*$^{-/-}$ retinas have an additional defect in their b-wave amplitude at day, resulting from other factors, such as the properties of cones or their connectivity. In conclusion, the cone ERG of *Opn4*$^{-/-}$ animals is abnormal, and the results could be interpreted in different ways.

Circadian rhythmicity in retinal gene expression

The retinal circadian rhythms are regulated by the core molecular clock proteins. There is evidence that the absence of melanopsin disrupts the circadian rhythms of retinal core clock gene expression. Dkhissi-Benyahya et al. [138] microdissected retinal cross-sections to separate the inner and outer retinas, and subjected these to RT-qPCR analysis. Notably, the outer retinas of WT animals showed circadian rhythmicity in most core clock genes, but most transcripts, except for *Clock* and *Per1*, lost rhythmicity in *Opn4*$^{-/-}$ outer retinas. However, in the inner retina, the genes that exhibited rhythmic expression were different between WT and *Opn4*$^{-/-}$ animals. Although the lack of melanopsin led to the loss of rhythmicity in some clock genes, it also resulted in the rhythmic expression of some clock genes that were not rhythmic in WT inner retinas. Furthermore, the phases of *Per2* and *Clock* peak expression were directly opposite between WT and *Opn4*$^{-/-}$ inner retinas [138]. These data indicate that melanopsin regulates retinal clock gene expression in the inner as well as outer retinas.

In conclusion, *Opn4*$^{-/-}$ animals retain the rhythmicity in pupil response but lose the rhythmicity in contrast sensitivity and cone ERG. Since the cone ERG and contrast sensitivity rhythms are both in a "day-like" state in *Cry1*$^{-/-}$ animals [134], these processes could be regulated by the same retinal clock. If the cone ERG

and contrast sensitivity are indeed regulated by similar mechanisms, it would be highly unlikely that the contrast sensitivity of *Opn4*$^{-/-}$ animals is in a constant "day-like" state and their cone ERG in a "night-like" state. Therefore, I hypothesise that *Opn4*$^{-/-}$ animals instead have an isolated defect in their cone ERG amplitude and their retinal clock is fixed in a "day-like" state. The mechanisms may involve dopamine and melatonin signalling, or the loss of rhythmic expression of the core molecular clock components, which are known to be affected by the lack melanopsin. However, the understanding of the molecular mechanisms driving the retinal circadian rhythms are largely unexplored, as is the role of melanopsin in modulating these rhythms. To understand the mechanisms underpinning the phenotype in *Opn4*$^{-/-}$ retinas, I aim to investigate the retinal circadian transcriptome in the absence of melanopsin.

3.1.2 Light-induced phase shifts in *Opn4*$^{-/-}$ animals

An essential characteristic of the circadian clocks is their sensitivity to environmental cues that enable the clocks to adjust their timings. As the intrinsic period of any circadian clock is close to, but not exactly 24 hours, this plasticity ensures the proper entrainment of the circadian rhythms to the environment. The retinal and central circadian clock are both sensitive to light. When exposed to a light stimulus at an unusual time, i.e. during the dark phase, the retinal and SCN tissues trigger mechanisms to shift their circadian clocks [138, 186]. The circadian phase-shifting process is coupled with the induction of the core clock genes *Per1/2* in the retina [138] and the SCN [186], which feed into the core molecular circadian clock.

Melanopsin light activation results in a slow and sustained signalling response by the pRGCs [24], making the molecule suitable for encoding environmental light levels and mediating light responses in the central and retinal circadian clocks. It has been shown that the absence of melanopsin leads to a reduced sensitivity of the central circadian clock to light. Namely, in response to a nocturnal light pulse, *Opn4*$^{-/-}$ animals display a slightly attenuated phase shift in their activity [33]. This finding is complemented by a study by Jagannath et al. [186] who demonstrated

that the SCN light responses of *Opn4*$^{-/-}$ animals are also impaired on the molecular level. They found that a 30-minute nocturnal light pulse led to the upregulation of 100 genes in the SCNs of WT mice, and 92 of those genes were induced to a lower extent in the SCNs of *Opn4*$^{-/-}$ mice.

Melanopsin's role in retinal light responses mirrors in some respects its function in the SCN. A nocturnal light pulse induces retinal dopamine release, which is essential for light adaptation [132]. However, the data on melanopsin's role in mediating retinal dopamine release are conflicting. One report demonstrated that dopamine release was reduced in *Opn4*$^{-/-}$ retinas compared to controls, but concurrently, *Opn4*$^{-/-}$ retinas had significantly higher dopamine levels before the light pulse [138]. Yet two studies with a similar experimental design found no differences in nocturnal light-induced dopamine turnover in *Opn4*$^{-/-}$ retinas [187, 188]. Therefore, there is no consensus in the field as to what extent melanopsin activation influences retinal light responses and hence, how melanopsin's role in retinal light responses compares to its function in mediating the SCN light responses.

One possible confounding factor in the experiments researching retinal light responses in *Opn4*$^{-/-}$ animals is the pupil size. *Opn4*$^{-/-}$ animals display a maximum pupil constriction deficit at day, with their pupil area almost two times larger than WT pupils [82] (Fig. 3.1). This would lead to significant differences in the light dose reaching WT and *Opn4*$^{-/-}$ retinas. Furthermore, a report by Keenan et al. suggests that melanopsin phototransduction is also essential for keeping the pupil constriction sustained [83], further increasing the differences in the amount of light received by *Opn4*$^{-/-}$ mice. However, the lack of a sustained pupil response was only investigated at daytime, not at night, and it is therefore difficult to estimate whether the differences in pupil response could be a confounding factor in the experiments published to date.

Therefore, I aim to investigate the light responses of *Opn4*$^{-/-}$ animals in the retina and the SCN to study whether melanopsin's role in the retinal light responses is similar to its role in the SCN light responses. In formulating my methodology, I will investigate the extent to which the retinal light doses differ between WT and

Opn4$^{-/-}$ animals. If necessary, I will control for the potential confounder of pupil size by dilating the animals' pupils before light exposure.

3.1.3 Retinal development of *Opn4*$^{-/-}$ animals

An additional factor that could account for some of the differences in retinal circadian rhythms and light responses in *Opn4*$^{-/-}$ animals is the development of retinal cones. As discussed, the *Opn4*$^{-/-}$ animals have lower cone ERG b-wave amplitude at day [185]. Another study simulated the lack of melanopsin signalling using a light source that allowed the researchers to modulate the stimulation of individual photoreceptors. They used two background lights, both activated the rods and the cones to the same extent but differed substantially in melanopsin activation. With this paradigm, these researchers were able to study the effect of melanopsin activation on cone ERG in a WT retina. As the cone ERG b-wave amplitude in *Opn4*$^{-/-}$ animals at daytime is lower than in WT animals, one would expect that the lack of melanopsin stimulation would also lead to a lower cone ERG b-wave amplitude. Instead, the researchers found that the lack of melanopsin stimulation led to a higher cone ERG b-wave amplitude in WT animals [192]. Therefore, the lower b-wave amplitude in *Opn4*$^{-/-}$ animals might not have to do with melanopsin signalling itself but reflect a more global cone connectivity deficit.

Another line of evidence suggesting that *Opn4*$^{-/-}$ animals might have developmental deficits in their cones comes from the studies on the role of *Bmal1* in the retina as the *Bmal1*$^{-/-}$ animals, who lose their cone ERG circadian rhythmicity [130], have severe defects in their retinal cones. The mouse retina expresses two cone opsins, the S- and M-opsins, with peak sensitivities in the UV and green range, respectively. The expression of S-opsin increases dorsoventrally while M-opsin is expressed throughout the retina [173, 193]. The expression of opsins in cones determines three cone subtypes: the S-cones express only S-opsin, the M-cones only M-opsin and dual cones simultaneously both opsins [173, 193].

Sawant et al. [193] discovered that the lack of *Bmal1* specifically in cones resulted in an abolished dorsoventral gradient of S-opsin expression, with its levels

high throughout the retina. Interestingly, these animals had a shift in their ERG spectral sensitivity as their cone ERG b-wave amplitude in response to UV light was higher than in WT animals, but lower in response to longer wavelength light [193]. Additionally, the loss of *Per2* led to the opposite defect, a reduction in S-opsin expression [193]. Whether or not the deficit in the cone ERG circadian rhythmicity in *Bmal1*$^{-/-}$ animals [130] can be explained by the aberrant cone development, is unclear and should be studied further. Nevertheless, since there are indications that *Opn4*$^{-/-}$ retinas show abnormalities in the rhythmicity of core clock transcripts, this defect in the core molecular clock could lead to abnormal development of cone subtypes, which could result in lower cone ERG b-wave amplitude. Similarly to *Bmal1*$^{-/-}$ animals, these potential developmental changes could also influence retinal spectral sensitivity.

Melanopsin has been researched in the context of cone development in the early postnatal period. In early postnatal retinas, some cones are displaced to the inner retinal layers and guided to the outer retina through light signalling. It is known that *Opn4*$^{-/-}$ animals have more displaced cones in their retinas than WT mice at postnatal day 7 (P7) [98]. This defect is rescued by P16 and is linked to retinal DRD4 signalling [98]. Apart from this study on the development of cones, the overall number and subtype distribution of cones in adult *Opn4*$^{-/-}$ animals has not been studied to date. Therefore, to get an overview of the potential mechanisms leading to some of the aberrations in retinal circadian rhythms in *Opn4*$^{-/-}$ animals, I will analyse the distribution of retinal cones in adult *Opn4*$^{-/-}$ mice.

3.2 Aims of this chapter

There is evidence to suggest that melanopsin modulates the retinal circadian clock as *Opn4*$^{-/-}$ animals lose rhythmicity in contrast sensitivity and have an abnormal cone ERG. However, the mechanisms leading to these phenomena are unclear. In addition, melanopsin affects the extent to which light is able to shift the circadian clock in the SCN, but the data on melanopsin's role in retinal light responses is less conclusive. Furthermore, there seems to be an interplay between the core

clock components, retinal cone development and spectral sensitivity of the retina. Therefore, abnormal development of retinal cones could explain some of the retinal function defects in *Opn4*$^{-/-}$ animals, particularly their abnormal cone ERG. The overarching aim of this entire chapter is to investigate the mechanisms of how melanopsin affects the retinal circadian clock, and its ability to respond to light, drawing parallels to the light responses of the SCN.

The experimental aims of this chapter are to:

1. Analyse the circadian retinal transcriptome in the absence of melanopsin to uncover the molecular mechanisms of how melanopsin regulates the retinal circadian rhythms
2. Investigate and compare the role of melanopsin in retinal and SCN light responses, controlling for the pupil size
3. Describe the effect of melanopsin on the distribution of cone subtypes and cone signalling in the retina

3.3 Results

3.3.1 Circadian rhythmicity of the retinal transcriptome is not abolished but altered in *Opn4*$^{-/-}$ animals

To understand the molecular mechanisms that could explain the deficits in the retinal rhythms in *Opn4*$^{-/-}$ animals, I performed RNA sequencing (RNA-seq) on WT and *Opn4*$^{-/-}$ retinas collected every 6 hours over a circadian day (CT4-CT28). I used 3'-sequencing, which meant I could analyse all transcripts coding for proteins. The overall quality of the sequencing was good. I obtained an average of 8.1 million (M) reads per sample and an average of 6.5 million (M) reads (80%) mapped uniquely to the mouse genome (Fig. 3.4A, B). Out of those, an average of 4.1 M reads per sample mapped to unique exons, and these counts were used for downstream analysis (Fig. 3.4C, D).

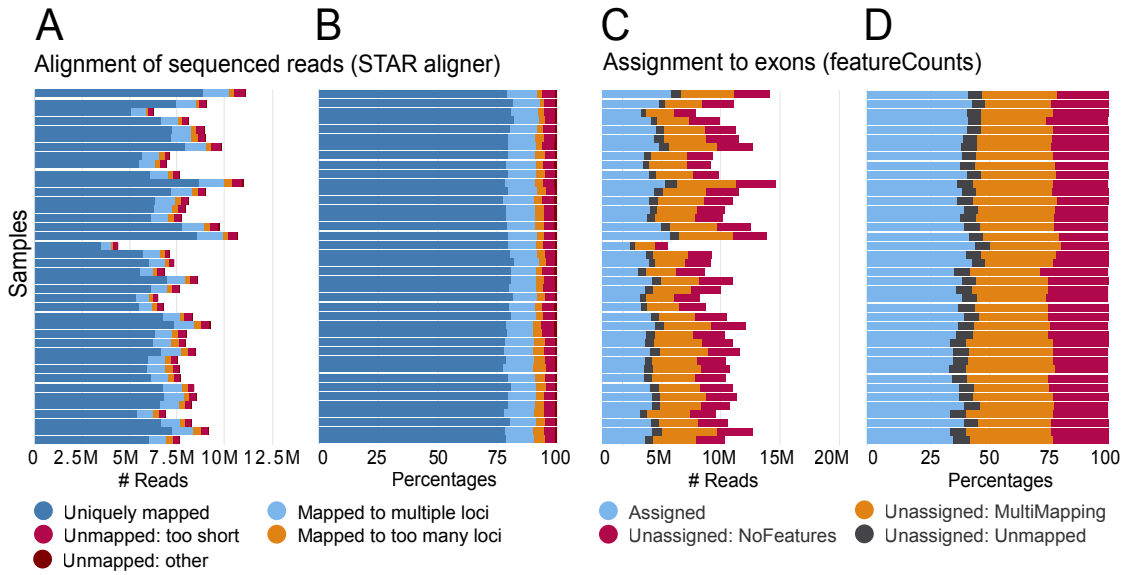


Figure 3.4: Quality control metrics of the retinal circadian time course RNA-seq samples. (A, B) The sequenced reads were aligned to the mouse genome using the STAR alignment tool and an average of 6.5 M (80%) reads were uniquely mapped to the mouse genome. (C, D) Reads mapping to exons were counted with featureCounts, yielding an average of 4.1 M reads per sample, which were used for downstream analysis. Data were summarised with MultiQC [194].

To determine any apparent clustering of the samples, which could cause a bias in downstream analysis, I carried out a principal component analysis of the samples based on the gene counts. Since I had many samples, 40 altogether, I had prepared the sequencing libraries in two batches to adhere to the protocol as precisely as possible. Although the libraries were prepared on the same day, visual inspection of the principal component analysis (PCA) plot revealed that the library preparation procedure had introduced a batch effect in the dataset (Fig. 3.5A). However, the filtering and normalisation procedure in DESeq2 [169], removed this batch effect (Fig. 3.5B).

To determine the genes that displayed a circadian rhythm in their expression pattern, I used the R package MetaCycle [170]. This method combines two algorithms, the Lomb-Scargle periodogram [195] and JTK_CYCLE [196]. I decided to use a p value cutoff of 0.05 to define the genes that were expressed in a rhythmic manner. Therefore, the genes that did not meet this criterion were not necessarily arrhythmic but could have retained some level of rhythmicity, potentially with a

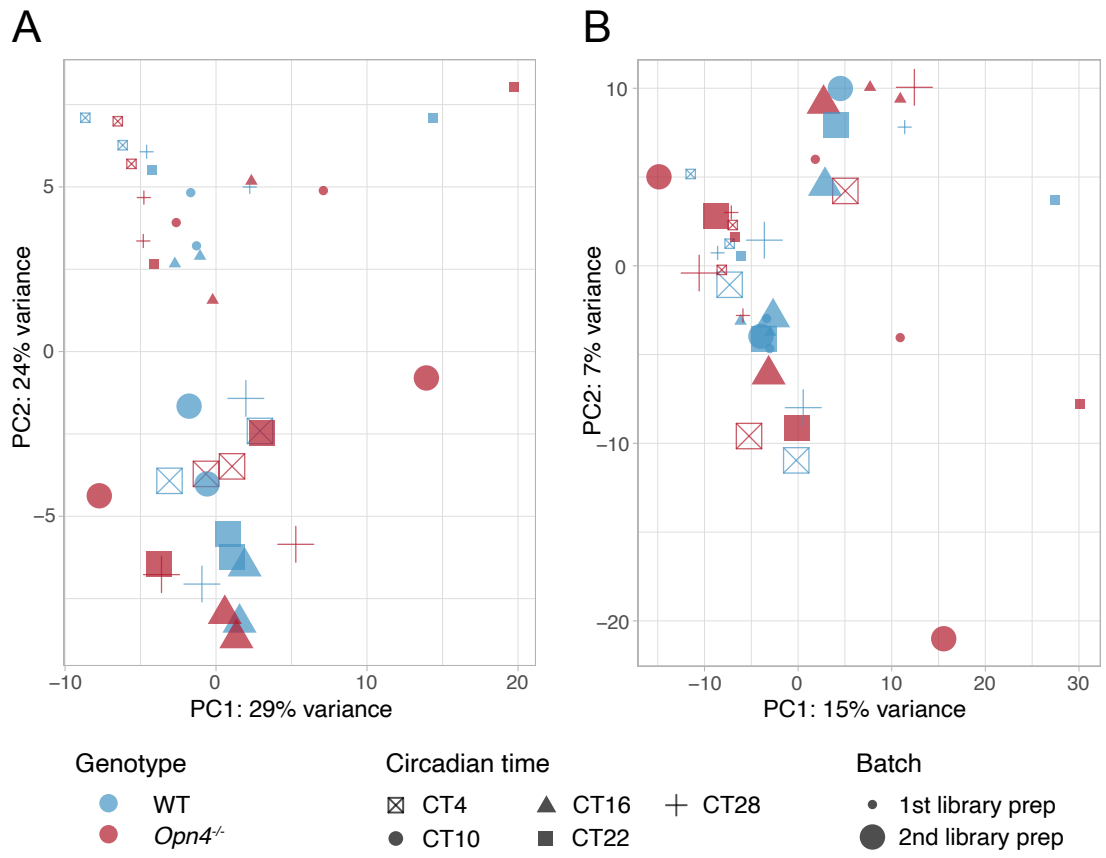


Figure 3.5: Principal component analysis of WT and *Opn4*$^{-/-}$ retinal circadian time course RNA-seq samples. Due to the large number of samples, the RNA-seq libraries were prepared in two batches. It was evident that this induced a batch effect as samples prepared together clustered distinctly before normalisation (A). This clustering was lost after the dataset was normalised (B).

lower amplitude or less robustness. With this cutoff, the analysis identified 647 circadian genes in WT and 691 in *Opn4*$^{-/-}$ retinas. Surprisingly, only 178 genes were rhythmic in both genotypes (Fig. 3.6A, B).

The 20 genes that showed the most significant rhythmicity are illustrated in Figure 3.7, and interestingly, there was no overlap between WT and *Opn4*$^{-/-}$ retinas. Therefore, the circadian rhythmicity of gene expression was not abolished in retinas lacking melanopsin. On the contrary, *Opn4*$^{-/-}$ retinas had a higher number of circadian genes. However, the rhythmic gene populations were distinct between the two genotypes.

I was then interested in seeing how the rhythms of circadian genes compared

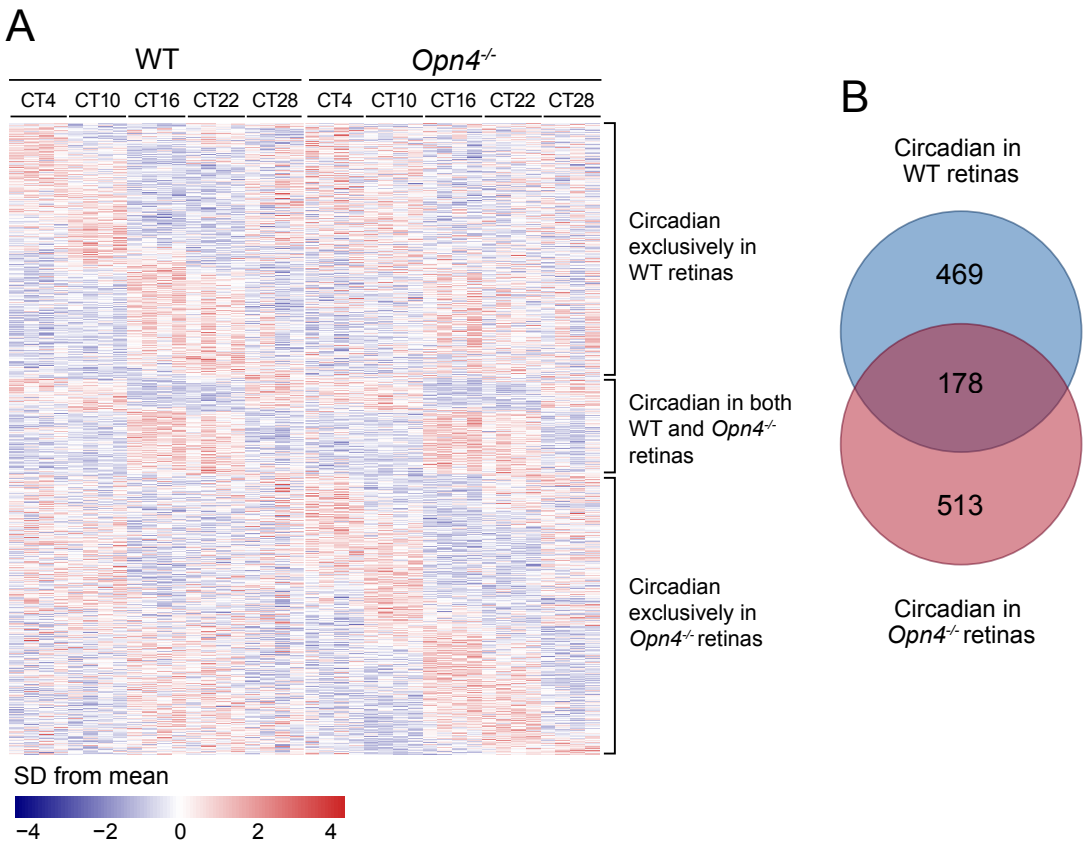


Figure 3.6: An overview of the circadian transcriptomes of WT and *Opn4*$^{-/-}$ retinas. (A) The expression profile of all circadian genes in WT and *Opn4*$^{-/-}$ retinas. Each row represents an individual gene and rows are ordered by the peak phase of expression. (B) A corresponding Venn diagram demonstrating the overlap in the circadian gene populations.

between WT and *Opn4*$^{-/-}$ retinas, which could shed light on deficits seen in *Opn4*$^{-/-}$ mice. Therefore, I analysed the phase of each circadian gene, which is defined as the time in the circadian day when the transcript is expressed at its highest level. Interestingly, despite the small overlap in the circadian genes, the phase distributions of the circadian transcripts were remarkably similar between WT and *Opn4*$^{-/-}$ retinas, with a large proportion of genes peaking around CT18 (Fig. 3.8A, B). Additionally, the 178 genes circadian in both genotypes showed similar phases, especially the genes peaking in the second half of the circadian day, while there was more variability in the genes peaking between CT0 and CT12. Overall, the phases were close to being significantly different between the genotypes ($p = 0.0502$, Wilcoxon matched-pairs signed-rank test, Fig. 3.8C). As can be seen, despite the

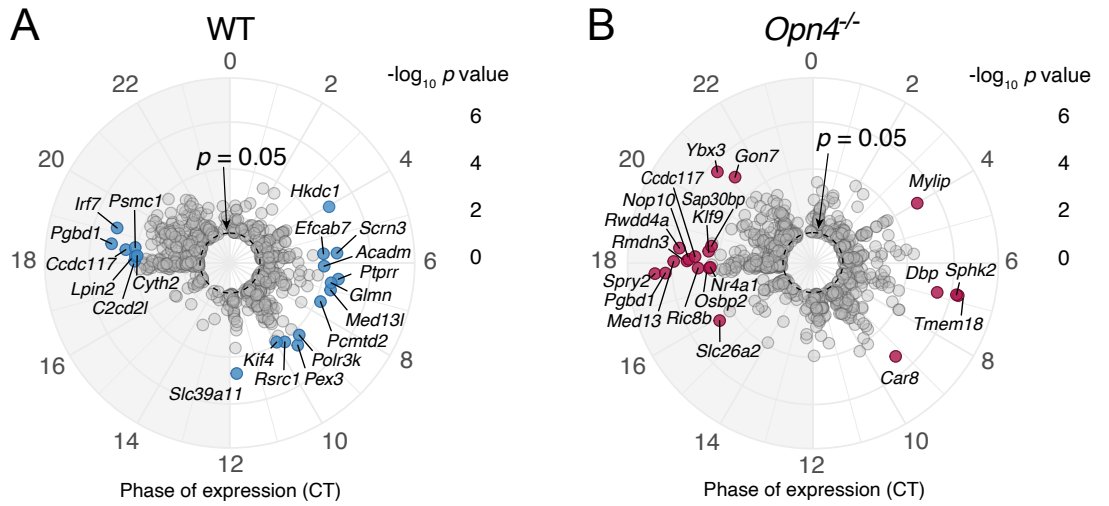


Figure 3.7: Genes showing circadian rhythmicity in WT and *Opn4*$^{-/-}$ retinas. Radial plots of all circadian genes in WT (A) and *Opn4*$^{-/-}$ (B) retinas, with the 20 most significantly rhythmic genes highlighted. The position on the angular axis indicates the peak phase of expression from CT0 to CT24. The radial axis denotes the -$\log_{10}$ p value of circadian rhythmicity and increased distance from the plot centre indicates, therefore, a higher significance. Both parameters were calculated with MetaCycle. The dashed line corresponds to a p value of 0.05 (-$\log_{10}$ p value of 1.3).

circadian genes themselves having little overlap between WT and *Opn4*$^{-/-}$ retinas, the peak phases of the gene populations were very similar.

The retina is a complex tissue composed of approximately 100 different cell types [2]. The global analysis of the retinal circadian transcriptome makes it challenging to predict which cell types contribute to the molecular circadian rhythms. One way of examining the cells involved in driving the retinal circadian transcriptome is to compare the expression levels of the circadian genes in different retinal cell types. A higher expression level of a transcript in a particular cell indicates a more significant functional importance of a transcript in that cell type. Furthermore, the cells with a higher expression level are also more likely to drive the global differences in the retinal transcriptome.

Therefore, I analysed which retinal cell types were enriched for the retinal circadian genes of WT and *Opn4*$^{-/-}$ retinas. I made use of a dataset created by Siegert et al. [184] who isolated distinct retinal cell populations from 22 transgenic mouse lines, each expressing a fluorescent marker under a specific promoter, and

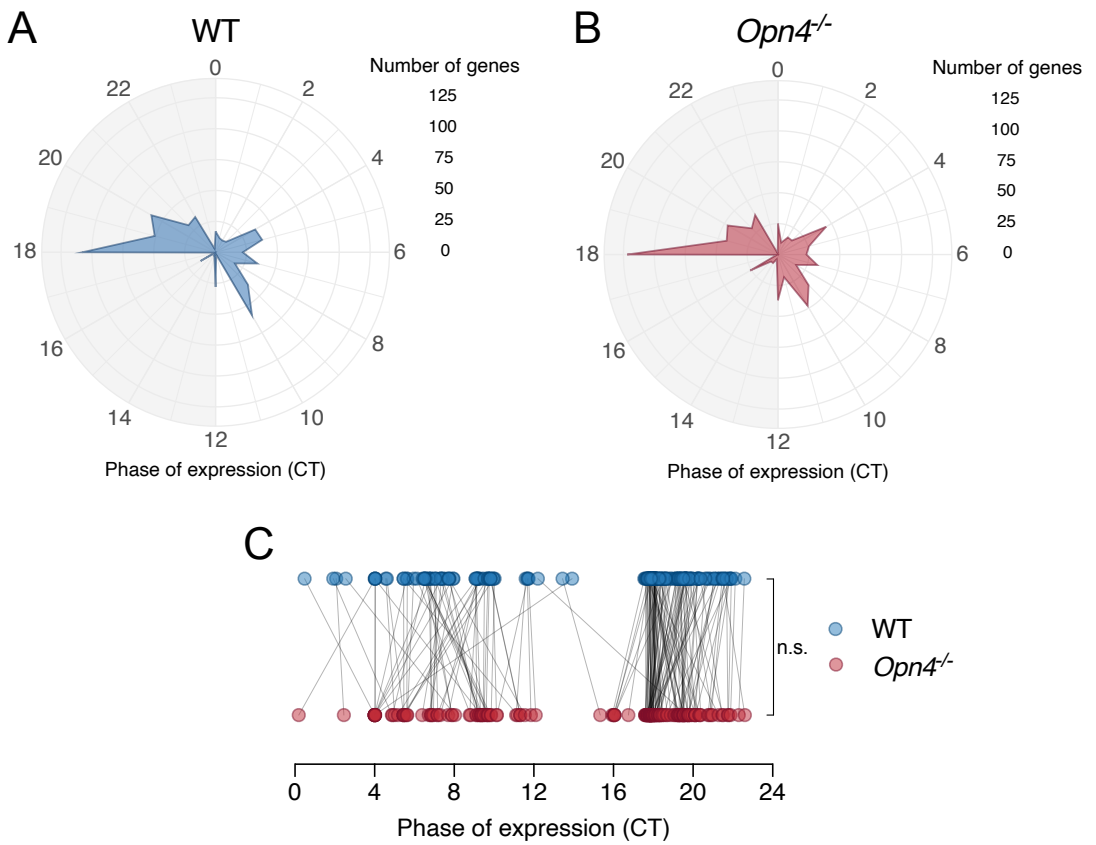


Figure 3.8: The distribution in peak phases of circadian transcripts in WT and *Opn4*$^{-/-}$ retinas. Radar plots of the number of genes peaking at distinct circadian times in WT (A) and *Opn4*$^{-/-}$ (B) retinas, summarised in one hour bins. (C) The phases of the 178 genes that were rhythmic in both genotypes are not significantly different between genotypes ($p = 0.0502$, Wilcoxon matched-pairs signed rank test). n.s., not significant.

subjected these subpopulations to microarray analysis. In their article, the authors provide extensive validation of the markers they used for cell sorting. Nevertheless, to confirm that the gene expression was as expected in the dataset, I analysed whether the markers used for cell selection were highly expressed in the respective cell types. In the case of the photoreceptors, I studied the levels of the opsins.

I found that the population of rods was indeed enriched for rhodopsin and the two populations of cones for cone opsins and the expression of opsins was approximately four SD higher in the respective photoreceptors than on average across the dataset (Fig. 3.9). Additionally, most of the remaining 19 cell populations showed high expression of the respective marker. However, there were two exceptions, the DRD4

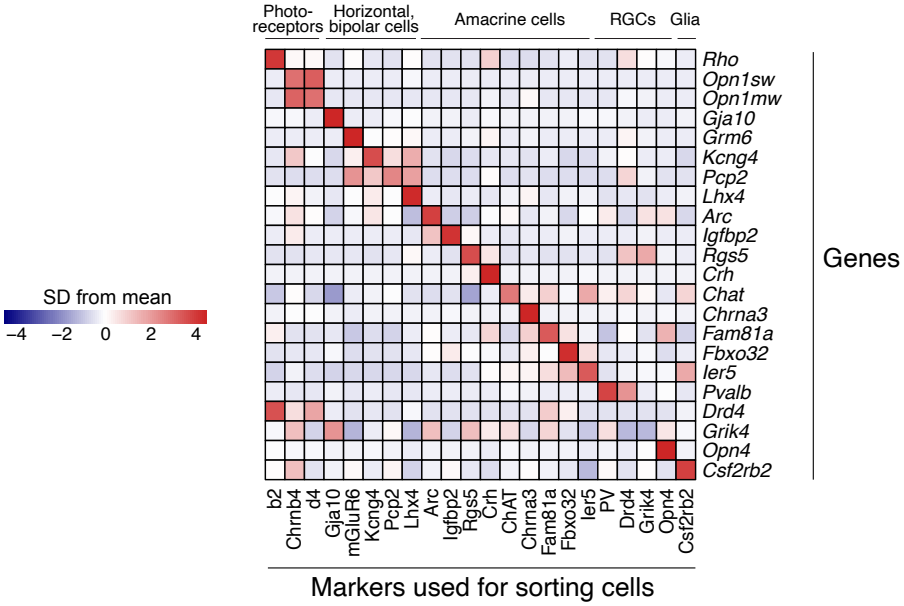


Figure 3.9: Cell-specific gene expression of the markers used for cell sorting by Siegert et al. Cells were sorted based on the expression of fluorescent markers. The expression of rhodopsin and cone opsins is enriched in photoreceptors, and the majority of markers used for cell sorting are enriched in respective cell subpopulations. Each row represents one gene and each column a subpopulation of retinal cells. Gene expression values are normalised across rows.

and GRIK4-sorted (glutamate receptor ionotropic, kainate 4) cell populations, which did not express high levels of *Drd4* and *Grik4*, respectively. This discrepancy could be caused by the fact that gene and protein expression do not always correlate as the transcripts' turnover might be considerably faster than the turnover of the resulting protein. In addition, *Drd4* is known to be expressed in photoreceptors [197], as can also be seen in Figure 3.9, and the DRD4-sorted cell population might include some photoreceptors in addition to the RGCs. Overall, however, this analysis validates that most cell populations in the dataset were indeed enriched for the transcript of the marker they were sorted by.

Next, I went on to determine which retinal cell types were enriched for the circadian genes. I defined "enrichment" as outlined in section 2.10 and the value of 1.0 indicates that the number of genes expressed more than 2 SD higher than the average expression of the genes can be expected by chance, i.e. there is no enrichment.

I was curious to see how cell-type enrichment compared between WT and

Opn4$^{-/-}$ retinas, as the involvement of different cells could to some extent explain the circadian deficits of *Opn4*$^{-/-}$ retinas. I conducted the enrichment analysis on three subsets of genes: those circadian in both WT and *Opn4*$^{-/-}$ retinas and those circadian exclusively in either genotype. Interestingly, the genes that were circadian in both genotypes showed 3.7x enrichment in cones, which were sorted by the marker d4. Other cell types included parvalbumin-expressing RGCs, ON bipolar cells and also pRGCs (Fig. 3.10A). The genes circadian exclusively in WT retinas showed the highest enrichment in a subset of GABAergic amacrine cells and the genes circadian exclusively in *Opn4*$^{-/-}$ retinas in ON bipolar cells and also pRGCs (Fig. 3.10B, C). These results show that the cones are enriched for genes that exhibit circadian rhythmicity in their expression pattern, suggesting that cones might possess a circadian clock. Intriguingly, this clock seems to be intact in *Opn4*$^{-/-}$ retinas. The differences in the retinal circadian function between WT and *Opn4*$^{-/-}$ retinas might instead result from an aberrant function of bipolar or amacrine cells.

To gain insight into the cellular and molecular pathways the circadian genes are involved in, and to determine the processes abnormally regulated in the absence of melanopsin, I studied pathway enrichment using the KEGG database [171]. Most genes have functions in multiple tissues and disease processes, and heavily annotated genes can lead to the discovery of pathways that are not biologically relevant for the study [198]. Therefore, I focussed on exploring the significantly enriched pathways with potential biological relevance to the retina. While I have depicted all significant pathways on the subsequent figures, I have only provided the pathway name for the more relevant ones. It undoubtedly leads to bias in the analyses but simultaneously aids with interpreting the results.

The genes circadian in both WT and *Opn4*$^{-/-}$ retinas were most significantly enriched for dopaminergic synapse and gap junction pathways, other synaptic pathways and circadian entrainment. The genes only circadian in WT animals showed enrichment for RNA transport, phototransduction and sphingolipid signalling pathways, while the genes exclusively circadian in *Opn4*$^{-/-}$ retinas were enriched for different pathways related to carbon metabolism (Fig. 3.11A). These

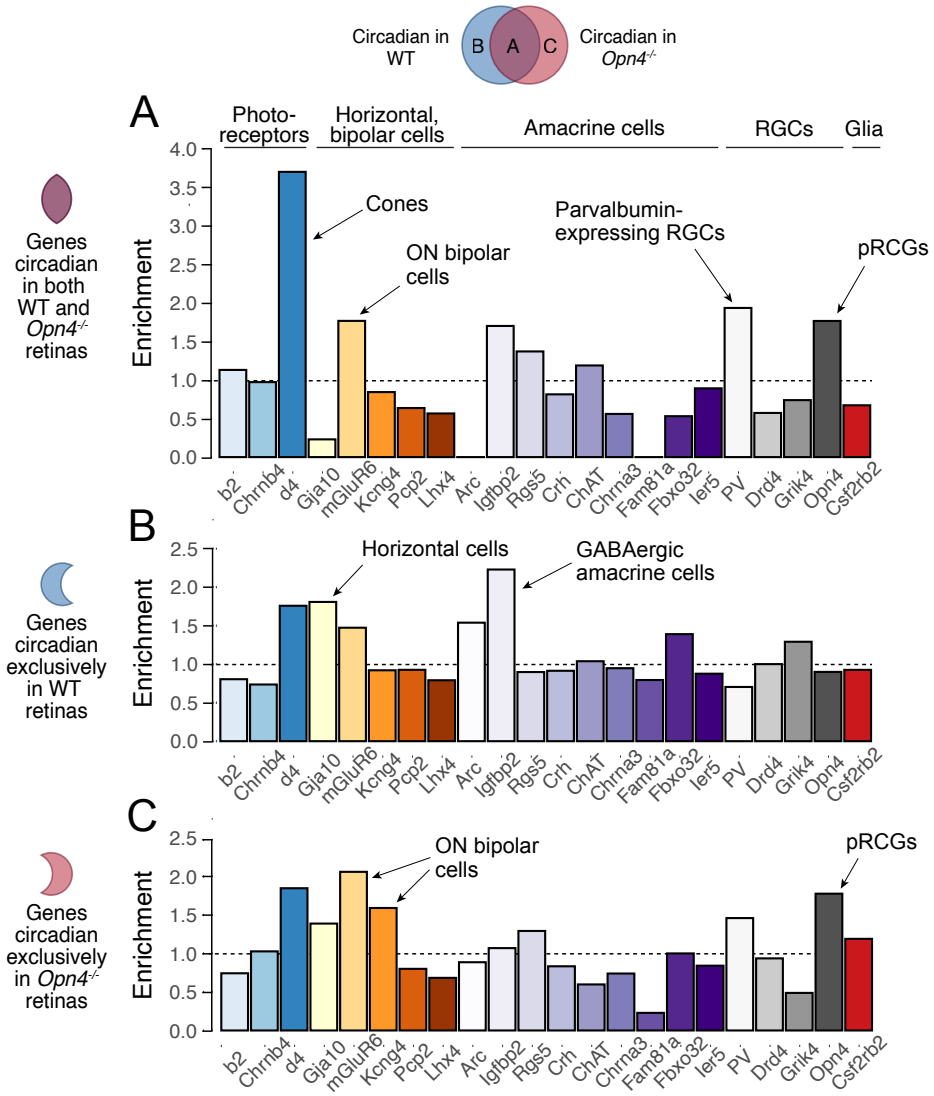


Figure 3.10: Enrichment of circadian genes in retinal cell subpopulations. Enrichment of genes in each retinal cell subpopulation was calculated as the number of genes expressed more than 2 SD higher than the mean expression of that gene across all subpopulations normalised to the number of genes enriched in each subpopulation across the entire transcriptome. Data are displayed for genes rhythmic simultaneously in both WT and *Opn4*$^{-/-}$ retinas (A) and exclusively in WT (B) or *Opn4*$^{-/-}$ (C) retinas.

results agree with published literature, indicating that the retinal circadian rhythms are influenced by dopamine signalling and the circadian regulation of gap junctions [124]. However, these results also suggest that these two processes do not underlie the retinal circadian rhythm defects of *Opn4*$^{-/-}$ mice, which might instead result from abnormal rhythms in phototransduction or sphingolipid signalling pathways.

Next, I was curious to see what were the exact genes and their circadian rhythmicity parameters contributing to the pathways that were enriched for circadian genes. Although the genes rhythmic simultaneously in WT and *Opn4*$^{-/-}$ retinas were enriched for several processes, this does not necessarily indicate that the circadian rhythmicity parameters of the genes were similar. Should one gene be rhythmic in WT and *Opn4*$^{-/-}$ retinas, but the phase of expression opposite, the resulting functional outcome of the circadian process would be very different.

Among the circadian genes associated with the term "dopaminergic synapse" were transcripts of dopamine receptors D1 and D4 (*Drd1* and *Drd4*) and several protein phosphatase 2A subunits (*Ppp2r1b*, *Ppp2r2b* and *Ppp2r5d*) (Fig. 3.11B). The phases of gene expression were very similar between WT and *Opn4*$^{-/-}$ retinas. The genes associated with gap junctions and circadian entrainment both included two adenylate cyclases (*Adcy1* and *Adcy6*) and again, the phases were similar in the two genotypes (Fig. 3.11B). The transcripts belonging to the phototransduction cascade that were circadian in WT, but not in *Opn4*$^{-/-}$ retinas, included *Pde6a* and *Gucy1b*, the genes in the sphingolipid signalling pathway included the sphingosine receptor *S1pr1* (Fig. 3.11C). Among the carbon metabolism pathway, enriched for genes solely circadian in *Opn4*$^{-/-}$ retinas, were genes belonging to the citrate cycle, e.g. aconitase 1 (*Aco1*) and isocitrate dehydrogenase 1 (*Idh1*) (Fig. 3.11D). In conclusion, the genes of the pathways enriched for circadian transcripts in both genotypes have very similar phases, and the pathways are thus similarly regulated on a transcript level.

The pathway enrichment analysis gave valuable information on the processes involved in the circadian rhythms of WT and *Opn4*$^{-/-}$ retinas. However, the entire retinal transcriptome was treated as that of a homogeneous tissue, not taking into

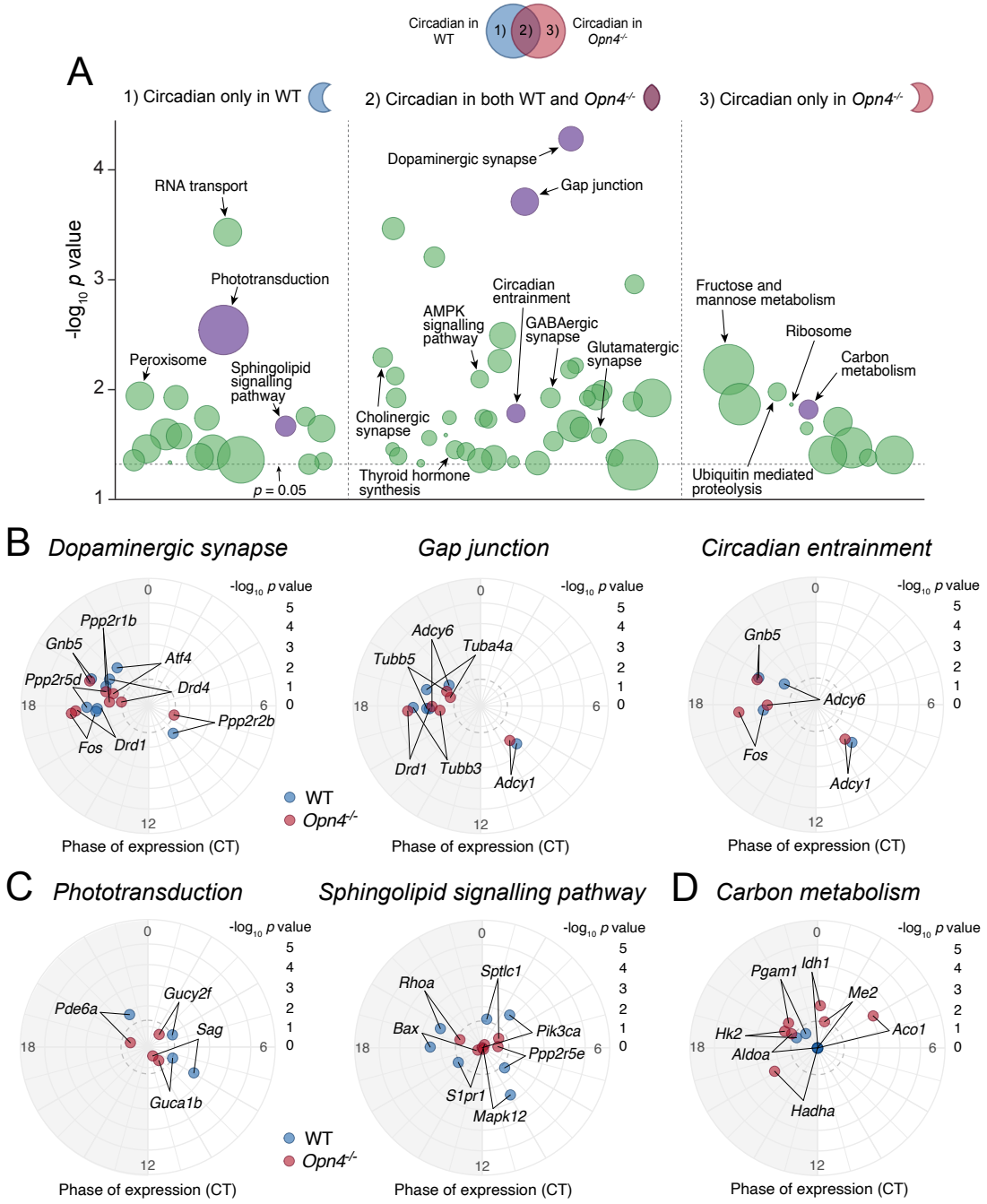


Figure 3.11: Analysis of overrepresented pathways in the circadian genes. (A) KEGG pathways enriched for genes that are circadian simultaneously in WT and *Opn4*$^{-/-}$ retinas (2) or exclusively in WT (1) or *Opn4*$^{-/-}$ (3) retinas. The y-axis indicates the significance of pathway overrepresentation and the dashed line a p value of 0.05. The size of each pathway is proportional to the fraction of the pathway genes present in the subset of circadian genes. A selection of pathways are marked in violet and analysed further in (B-D). (B-D) Radial plots of genes that constitute the overrepresented genes in the selected pathways. (B) Dopaminergic synapse, gap junction and circadian entrainment pathways are enriched for genes circadian in both genotypes. (C) Genes exclusively rhythmic in WT retinas are overrepresented for phototransduction and sphingolipid signalling pathways. (D) Genes exclusively rhythmic in *Opn4*$^{-/-}$ retinas show an overrepresentation for carbon metabolism pathway.

account the various retinal cell types. Therefore, to get a more granular view of the cells potentially involved in the circadian pathways, I next studied the expression of the pathway genes across the retinal cell types using the dataset by Siegert et al. [184].

The genes belonging to the dopaminergic synapse pathway showed higher expression in photoreceptors and RGCs (Fig. 3.12A), similarly to the genes involved in gap junction pathway (Fig. 3.12B). There was no obvious enrichment pattern for genes involved in circadian entrainment (Fig. 3.12C). The phototransduction genes were most highly expressed in rod photoreceptors (Fig. 3.12D). The sphingolipid signalling genes were expressed across the retina, although there was a cluster of genes with higher expression in retinal microglia and photoreceptors (Fig. 3.12E). The carbon metabolism genes did not show an apparent cell-specific expression pattern and were expressed across the cell types (Fig. 3.12F). Overall, these results demonstrate that the genes of the circadian pathways are expressed throughout the retina. Intriguingly, the genes in pathways that are circadian in WT and not *Opn4*$^{-/-}$ retinas, namely phototransduction and sphingolipid signalling, show enrichment in rods and microglia, indicating that melanopsin might affect the circadian function of these cell types.

3.3.2 *Opn4*$^{-/-}$ retinas display dampened circadian rhythmicity of core clock genes

Much of the cellular physiology, including circadian gene expression, is governed by the core molecular circadian clock. To understand whether the differences in the circadian transcriptome of WT and *Opn4*$^{-/-}$ retinas could be explained by the regulation of the molecular clock, I analysed the expression of the core clock genes in the RNA-seq dataset. Additionally, I validated the RNA-seq results by analysing the expression of these genes in the same samples with RT-qPCR.

The results demonstrated that the clock genes of the positive arm of the TTFL, *Clock* and *Bmal1* were not rhythmic in the RNA-seq dataset (Fig. 3.13A, B). Interestingly, the *Bmal1* transcript showed rhythmicity in WT retinas with RT-qPCR analysis, but the rhythm was non-significant in *Opn4*$^{-/-}$ retinas (Fig.

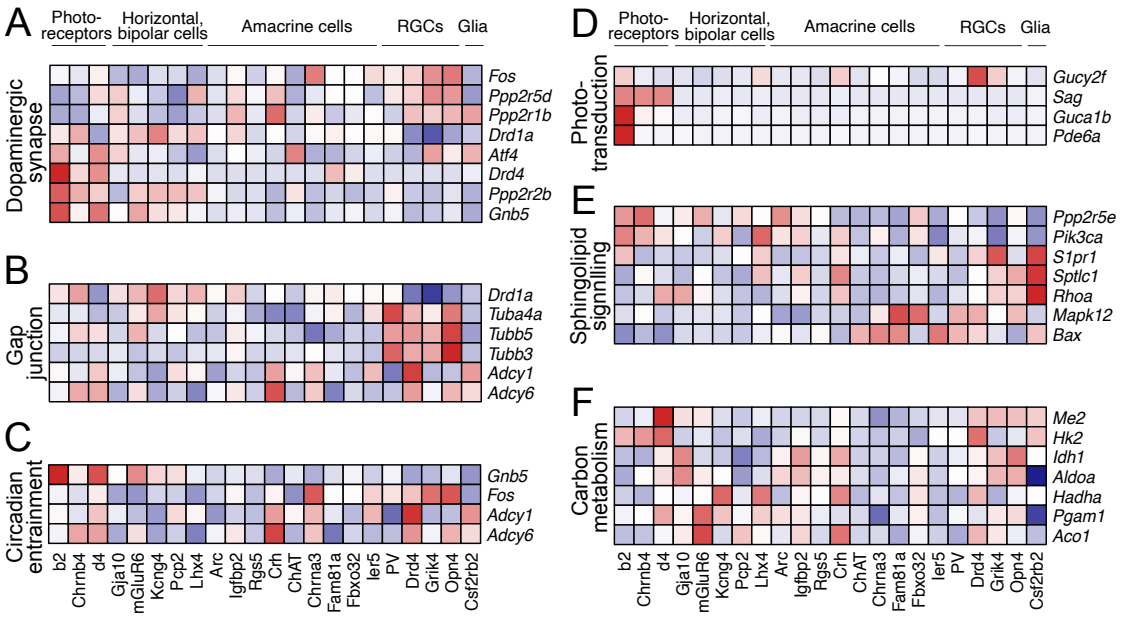


Figure 3.12: Cell-specific expression of the circadian genes belonging to differentially regulated pathways. Pathways enriched for genes circadian in both WT and *Opn4*$^{-/-}$ retinas: dopaminergic synapse (A), gap junction (B), and circadian entrainment (C). Pathways enriched for genes circadian exclusively in WT retinas: phototransduction (D), and sphingolipid signalling pathway (E). The only pathway enriched for genes circadian in exclusively *Opn4*$^{-/-}$ retinas was carbon metabolism (F). Each row represents one gene and each column a subpopulation of retinal cells. Gene expression values are normalised across rows.

3.13C, D). Albumin D-site binding protein (*Dbp*), a clock-controlled gene highly rhythmic in many mammalian tissues [199], showed similar expression patterns in both analysis methods and was rhythmic in both WT and *Opn4*$^{-/-}$ retinas (Fig. 3.13E, F). I also quantified the expression of *Opn4* and the transcript showed no detectable rhythmicity in WT, and the levels were, as expected, low in *Opn4*$^{-/-}$ retinas (Fig. 3.13G, H). The core clock transcripts of the negative arm of the TTFL, *Per1/2* and *Cry1/2*, showed a similar expression pattern when analysed with RNA-seq and RT-qPCR, although the expression values determined with RT-qPCR analysis had lower variance. Two transcripts, *Per2* and *Cry1* showed circadian rhythmicity in WT retinas, but there was no significant rhythmicity in *Opn4*$^{-/-}$ retinas (Fig. 3.14). An overview of the molecular clock circadian rhythmicity analysis is presented in Figure 3.15.

In conclusion, while *Opn4*$^{-/-}$ retinas retain the circadian expression pattern of

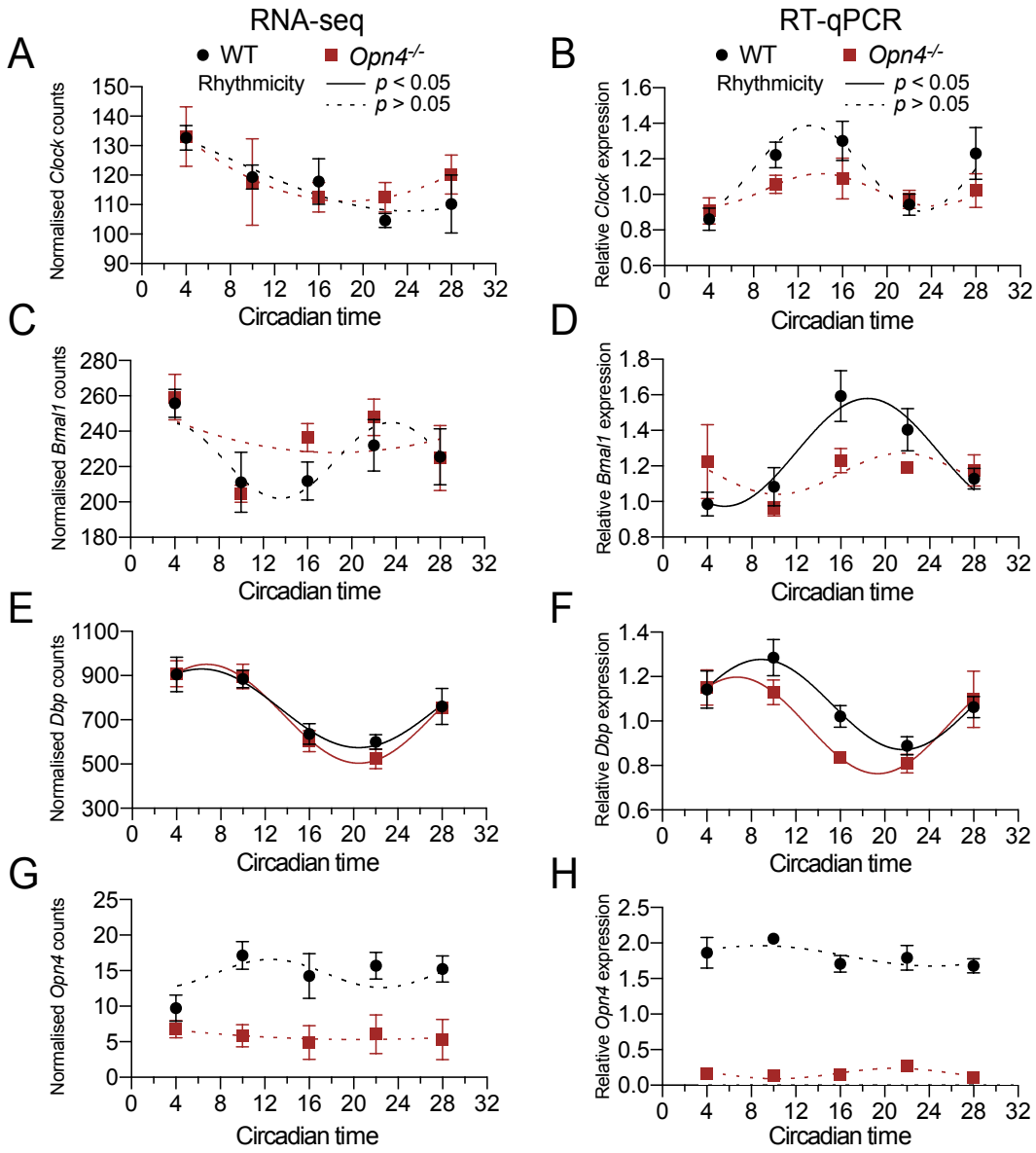


Figure 3.13: Circadian expression of core clock and related genes in WT and *Opn4*$^{-/-}$ retinas. Expression of core clock genes *Clock* (A, B) and *Bmal1* (C, D), a clock output gene *Dbp* (E, F) and the *Opn4* gene (G, H) in WT and *Opn4*$^{-/-}$ retinas. The same RNA samples were analysed with RNA-seq (A, C, E, G) and RT-qPCR (B, D, F, H). Expression values are fitted with a sine wave and rhythmic expression patterns, defined as MetaCycle p value < 0.05, are illustrated with solid lines, non-significant rhythmicity with dashed lines.

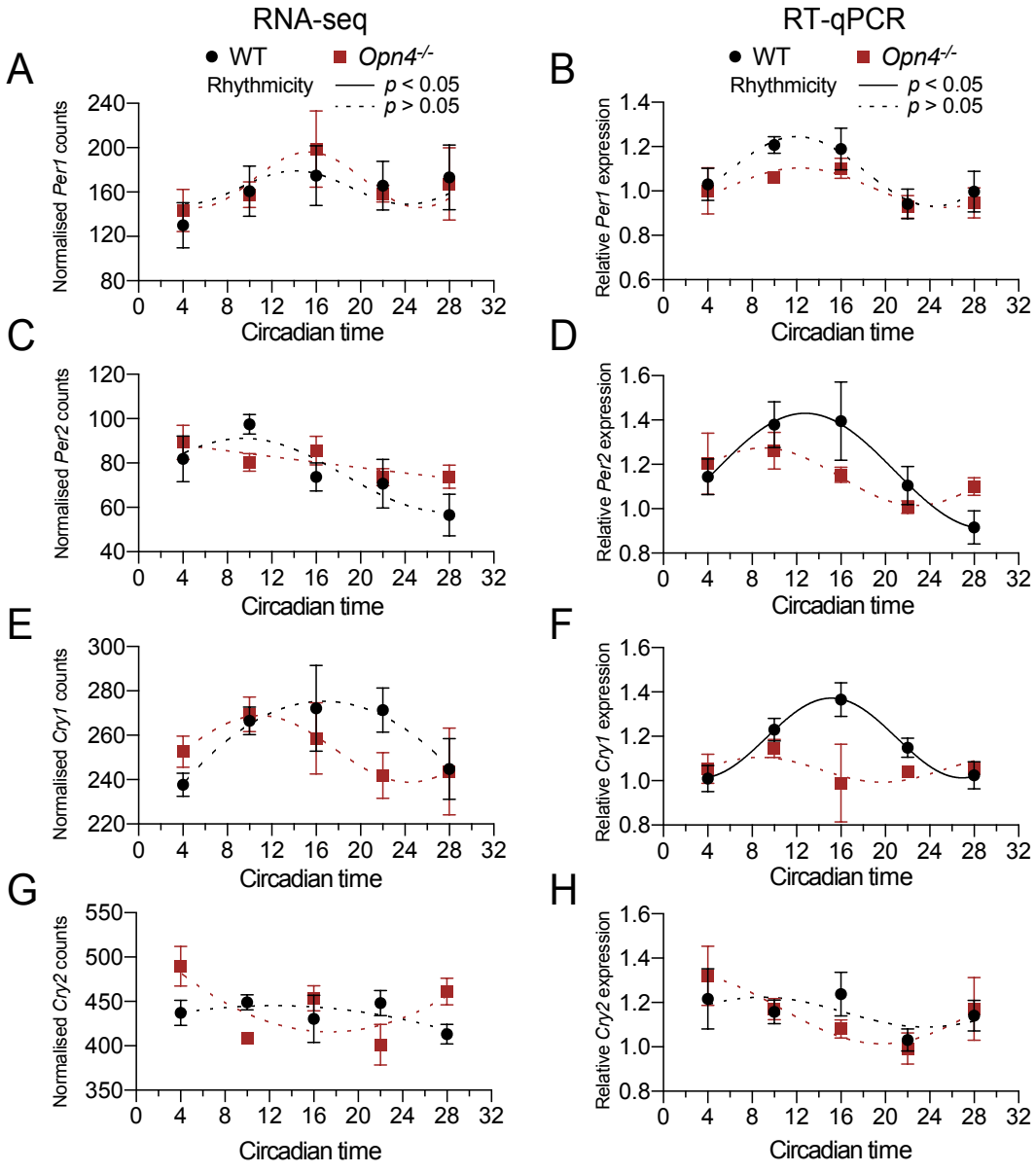
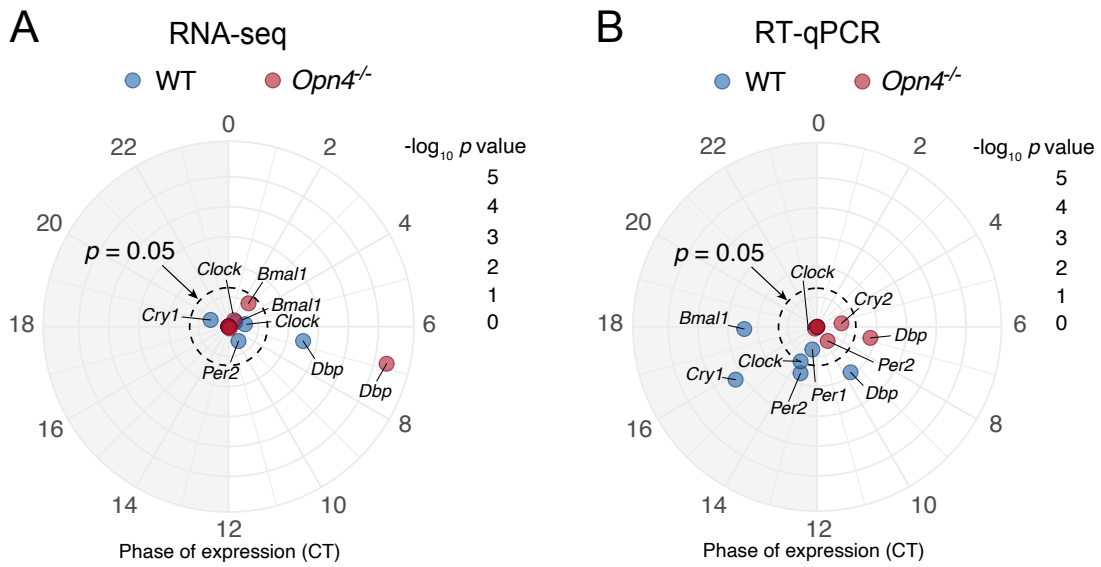


Figure 3.14: Circadian expression of core clock genes in WT and *Opn4*$^{-/-}$ retinas. Expression of core clock genes *Per1* (A, B), *Per2* (C, D), *Cry1* (E, F) and *Cry2* (G, H) in WT and *Opn4*$^{-/-}$ retinas. The same RNA samples were analysed with RNA-seq (A, C, E, G) and RT-qPCR (B, D, F, H). Expression values are fitted with a sine wave and rhythmic expression patterns, defined as MetaCycle p value < 0.05, are illustrated with solid lines, non-significant rhythmicity with dashed lines.



RNA-seq

WT

Gene	*p* value	Phase	Relative amplitude
Clock	0.28	5.5	0.04
Bmal1	0.52	3.8	0.09
Per1	1.0	15.0	0.08
Per2	0.26	9.7	0.16
Cry1	0.23	19.4	0.07
Cry2	1.0	18.9	0.02
Dbp	**0.0029**	6.7	0.26

Opn4$^{-/-}$

Gene	*p* value	Phase	Relative amplitude
Clock	0.52	2.8	0.07
Bmal1	0.095	2.7	0.10
Per1	1.0	16.1	0.15
Per2	1.0	12.9	0.00
Cry1	1.0	11.7	0.05
Cry2	1.0	10.2	0.05
Dbp	**0.000004**	6.9	0.35

RT-qPCR

WT

Gene	*p* value	Phase	Relative amplitude
Clock	0.052	13.7	0.21
Bmal1	**0.0036**	17.9	0.23
Per1	0.17	12.8	0.13
Per2	**0.022**	13.3	0.19
Cry1	**0.0005**	15.8	0.15
Cry2	1.0	12.8	0.02
Dbp	**0.013**	9.6	0.18

Opn4$^{-/-}$

Gene	*p* value	Phase	Relative amplitude
Clock	1.0	13.7	0.09
Bmal1	1.0	18.5	0.08
Per1	0.80	15.5	0.06
Per2	0.26	9.6	0.11
Cry1	1.0	9.8	0.05
Cry2	0.15	5.5	0.12
Dbp	**0.015**	6.8	0.26

Figure 3.15: Circadian rhythmicity parameters of clock genes in WT and *Opn4*$^{-/-}$ retinas. Radial plots of the circadian parameters of core clock genes and the clock output gene *Dbp* in WT and *Opn4*$^{-/-}$ retinas analysed with RNA-seq (A) and RT-PCR (B). The dashed line indicates a p value of 0.05. The calculated circadian parameters are displayed below. The relative amplitude is defined as the absolute amplitude divided by mesor.

the clock-controlled gene *Dbp*, they show a dampened circadian rhythmicity of the core clock transcripts *Bmal1*, *Per2* and *Cry1*, which may underlie the differences in the circadian transcriptome between WT and *Opn4*$^{-/-}$ retinas, and contribute to the retinal clock defects of *Opn4*$^{-/-}$ mice.

As the circadian rhythmicity of core clock genes was dampened in *Opn4*$^{-/-}$ retinas, I was curious to see which cell types show higher expression of these transcripts.

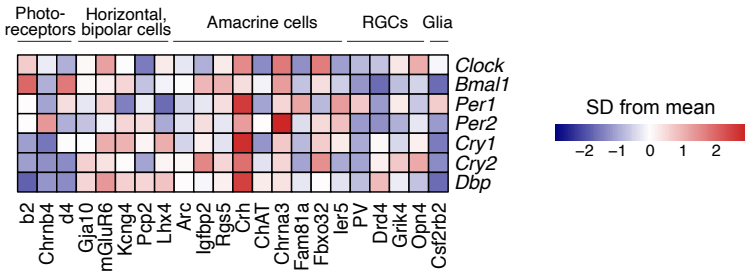


Figure 3.16: Expression of core clock genes in different retinal cell populations. Each row represents one gene and each column a subpopulation of retinal cells. Gene expression values are normalised across rows.

Intriguingly, one particular cell type, the corticotropin-releasing hormone (Crh) positive amacrine cells, showed remarkably high levels of all the core clock transcripts, including *Clock*, *Bmal1*, *Per1/2*, *Cry1/2* and *Dbp* (Fig. 3.16). Although it is difficult to estimate to what extent the transcriptome changes in these cells would contribute to the total retinal transcriptome, the high expression of core clock components compared to other retinal cells raises the possibility that the Crh-positive cells might be driving some aspects of the retinal circadian rhythms.

3.3.3 There are global differences in retinal gene expression between WT and *Opn4*$^{-/-}$ animals

In addition to the differences in the circadian transcriptome, WT and *Opn4*$^{-/-}$ retinas may show global differences in gene expression, which could contribute to the retinal phenotype of the *Opn4*$^{-/-}$ animals. Indeed, by analysing the dataset with DESeq2 [169], I identified 550 retinal genes that were differentially expressed between the two genotypes, with 224 and 226 genes showing higher levels in WT or *Opn4*$^{-/-}$ retinas, respectively (Fig. 3.17A). Interestingly, the expression of the most differential or most significant genes was not confined to any particular cell type (Fig. 3.17B).

Again, to gain insight into the cellular processes the differentially expressed genes participate in, I made use of the KEGG database [171]. The genes with higher levels in WT retinas were enriched for glycan degradation and RNA transport pathways, while those more highly expressed in *Opn4*$^{-/-}$ retinas showed enrichment for pathways such as prolactin, Wnt and FoxO signalling. Surprisingly, the sphingolipid signalling

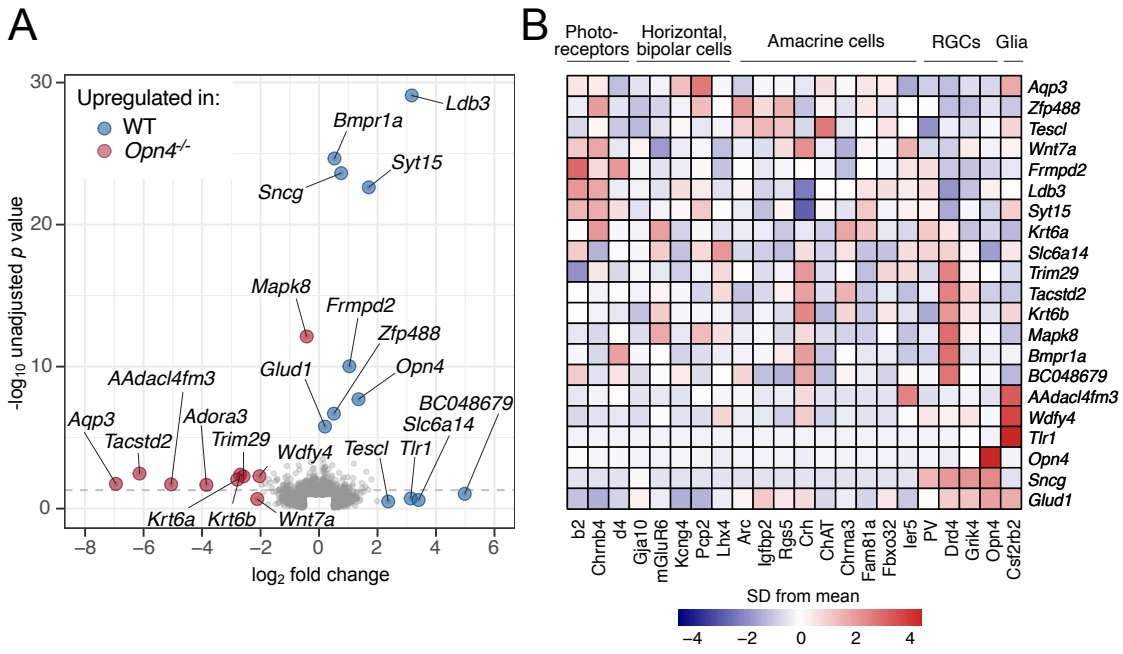


Figure 3.17: Global gene expression differences between WT and *Opn4*$^{-/-}$ retinas. (A) The genes differentially expressed between WT and *Opn4*$^{-/-}$ retinas, with the most significantly and highly differentially expressed genes highlighted. The dashed line indicates a p value of 0.05. (B) The expression of genes highlighted in (A) in subpopulations of retinal cells. Each row represents one gene and each column a subpopulation of retinal cells. Gene expression values are normalised across rows.

pathway, which was enriched for WT circadian genes, was also enriched for genes more highly expressed in *Opn4*$^{-/-}$ retinas (Fig. 3.18A). I further analysed this pathway and saw that the genes with overall higher levels in *Opn4*$^{-/-}$ retinas, were not the same genes that were rhythmic in WT retinas (Fig. 3.18B). The appearance of this pathway in both circadian and global gene expression analysis suggests that sphingolipid signalling could also play a role in global deficits in *Opn4*$^{-/-}$ retinas.

3.3.4 Mouse and baboon rhythmic retinal transcriptomes show little overlap

The circadian rhythms of nocturnal and diurnal animals are differentially regulated in multiple tissues, and the clock gene expression phases are often opposite [200]. However, such comparisons are lacking for the retinas. Therefore, I decided to use the publicly available dataset by Mure et al. [200] who performed RNA-seq analysis on several baboon tissues collected over a diurnal day, including the retina.

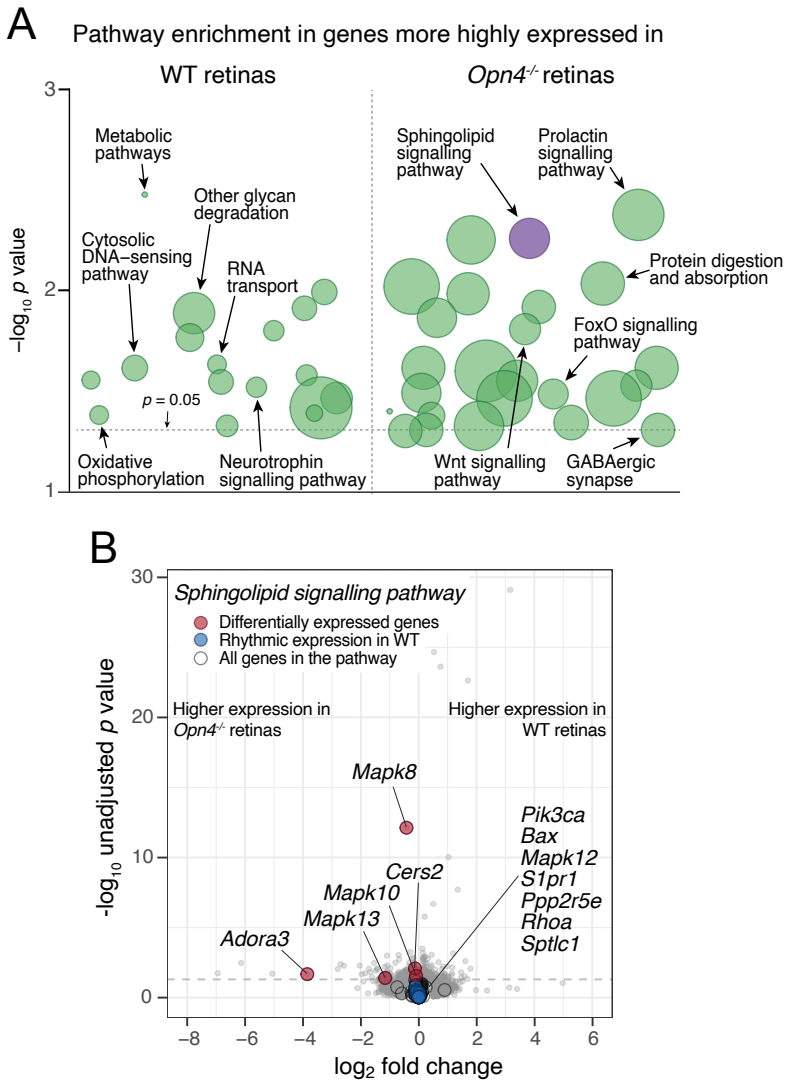


Figure 3.18: Analysis of overrepresented pathways in genes differentially expressed between WT and *Opn4*$^{-/-}$ retinas. (A) KEGG pathways enriched for genes upregulated in WT or *Opn4*$^{-/-}$ retinas. The y-axis indicates the significance of pathway overrepresentation and the dashed line a p value of 0.05. The size of each pathway is proportional to the fraction of the pathway genes present in the differentially regulated genes. (B) Differential expression of genes belonging to the sphingolipid signalling pathway. All genes that showed a rhythmic expression pattern in WT, but not *Opn4*$^{-/-}$ retinas are also highlighted.

Interestingly, only 33 mouse retinal circadian genes (approximately 5%) showed diurnal rhythmicity in baboon retinas (Fig. 3.19A). This is very similar to the fraction of overlapping rhythmic genes between the baboon and mouse SCN, liver and several other tissues [200]. Furthermore, none of the core molecular clock genes showed significant diurnal rhythmicity in baboon retinas (Fig. 3.19B), which might have to do with the lower power of that dataset. The overall distribution of peak expression phases of rhythmic genes also showed very distinct patterns in the two species as the largest fractions of baboon genes peaked around ZT1-2 and ZT13 compared to CT18 and CT10 in mouse (Fig. 3.19C, D). Likewise, the 33 genes that were rhythmic in both species did not show similar phases, although the difference in phases was not statistically significant ($p = 0.39$, Wilcoxon matched-pairs signed-rank test, Fig. 3.19E).

In conclusion, in this part of the chapter, I investigated the genes and pathways rhythmic in WT and *Opn4*$^{-/-}$ retinas. Interestingly, the *Opn4*$^{-/-}$ retinas retained circadian rhythmicity in gene expression and had a similar number of circadian genes as WT retinas. Surprisingly, the circadian genes themselves were significantly different between the two genotypes. The pathways shared by genes that were circadian in both genotypes included those related to dopamine signalling and gap junctions, indicating that these rhythms are intact in the absence of melanopsin. However, the pathways exclusively rhythmic in WT retinas were related to phototransduction and sphingolipid signalling, which might be regulating the aberrant retinal circadian function of *Opn4*$^{-/-}$ animals. Further, I showed that the circadian rhythmicity of core clock components is dampened in *Opn4*$^{-/-}$ retinas. The retinal cell showing very high expression of molecular clock transcripts was the Crh-positive amacrine cell, which might be the source of retinal circadian rhythms. Additionally, I demonstrated that the lack of melanopsin led to overall differential regulation of approximately 500 retinal genes, and those more highly expressed in *Opn4*$^{-/-}$ retinas showed enrichment for sphingolipid signalling pathway. Lastly, I found that the mouse circadian transcriptome had limited overlap with the diurnal baboon transcriptome. Overall,

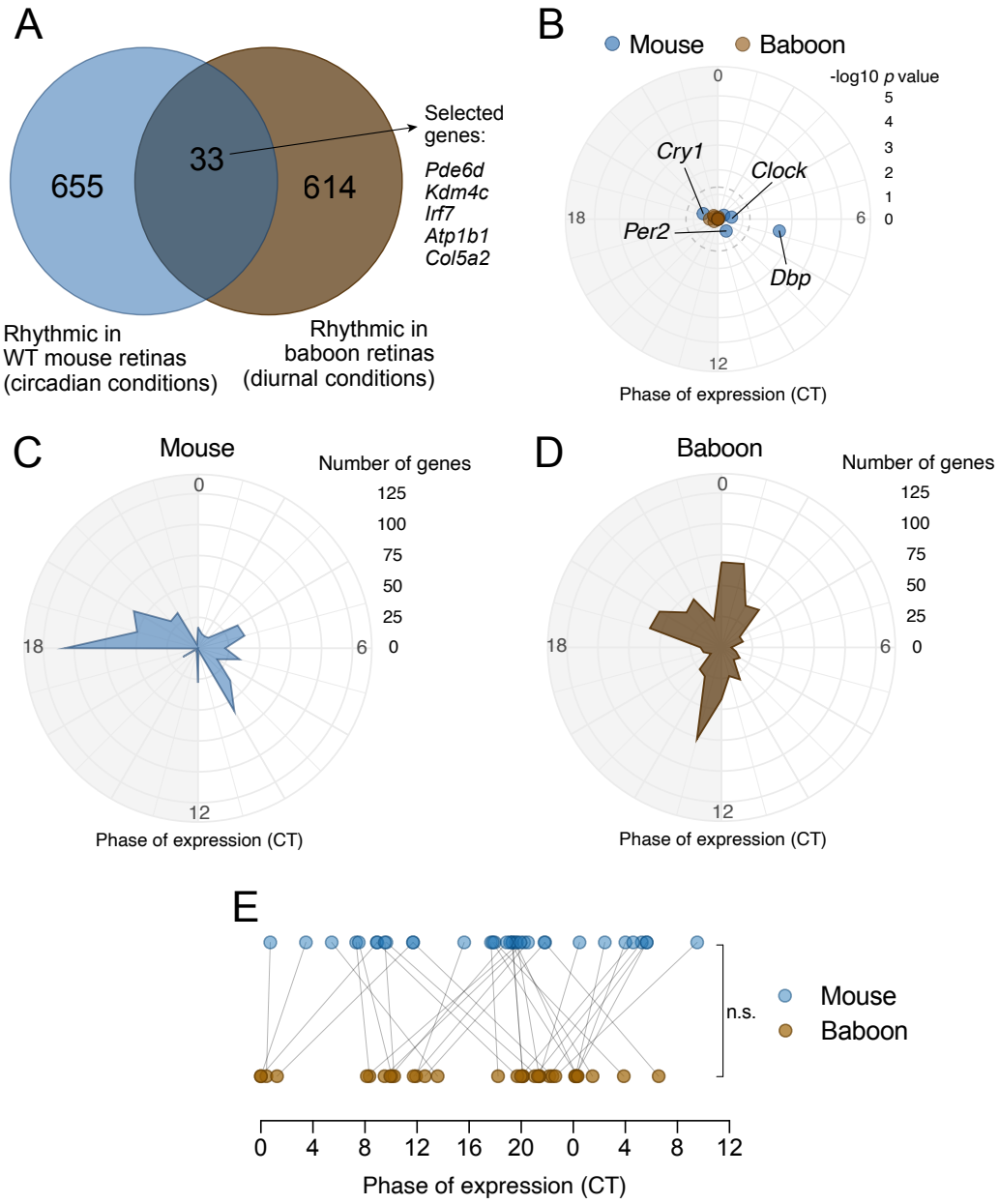


Figure 3.19: Comparison of mouse retinal circadian genes and baboon retinal diurnal genes. (A) The overlap of genes rhythmic in mouse and baboon retinas. (B) The rhythmicity parameters of core clock genes in mouse and baboon retinas. (C, D) The distributions of peak phases of mouse circadian genes (C) and baboon diurnal genes (D). (E) The peak expression phases of the overlapping 33 genes ($p > 0.05$, Wilcoxon matched-pairs signed-rank test). n.s., not significant.

these results provide a thorough analysis of the circadian genes and pathways of a WT mouse retina and how it compares to a retina lacking melanopsin.

3.3.5 The light responses of the retina, but not the SCN, are affected by the light dose reaching the retinas of WT and *Opn4*$^{-/-}$ animals

Another essential characteristic of the circadian clock is its ability to adjust in response to environmental factors. The most potent Zeitgeber for the retina and the central circadian pacemaker in the SCN is light, and as mentioned previously, *Opn4*$^{-/-}$ animals display reduced phase shifting response and a dampened SCN gene induction to a nocturnal light pulse. However, there is inconclusive evidence on whether melanopsin's role in the retina is similar to its role in the SCN. In this part of the chapter, I address my second aim and investigate the retinal light responses in conjunction with the SCN light responses, a process crucial for mediating the plasticity of the circadian clocks.

The sustained pupil response at CT16

The central circadian clock of nocturnal animals is most responsive to light at CT16 as a light pulse administered at CT16 causes the largest phase shifts in activity [201]. The retina is also most sensitive to light around CT16, measured by a shift in the circadian oscillations in bioluminescence of PER2::Luc retinas *in vitro* and complemented by an increase in *Per1* and *Per2* transcripts [145]. Therefore, I also decided to use a CT16 light pulse to study the light responses of the retina and the SCN.

First, to ensure that I would be delivering an equal dose of light to WT and *Opn4*$^{-/-}$ retinas and thus the SCNs, I investigated the pupil constriction of these mice in response to a sustained CT16 white light pulse. I chose two commonly used light intensities for my experiments: 100 lux and 400 lux. Throughout the 30-minute light exposure, the pupils of WT animals remained fully constricted at around 20% and 5% of the dark-adapted pupil area for the 100 lux and 400 lux light pulse, respectively (Fig. 3.20A, B). On the contrary, the pupil constriction

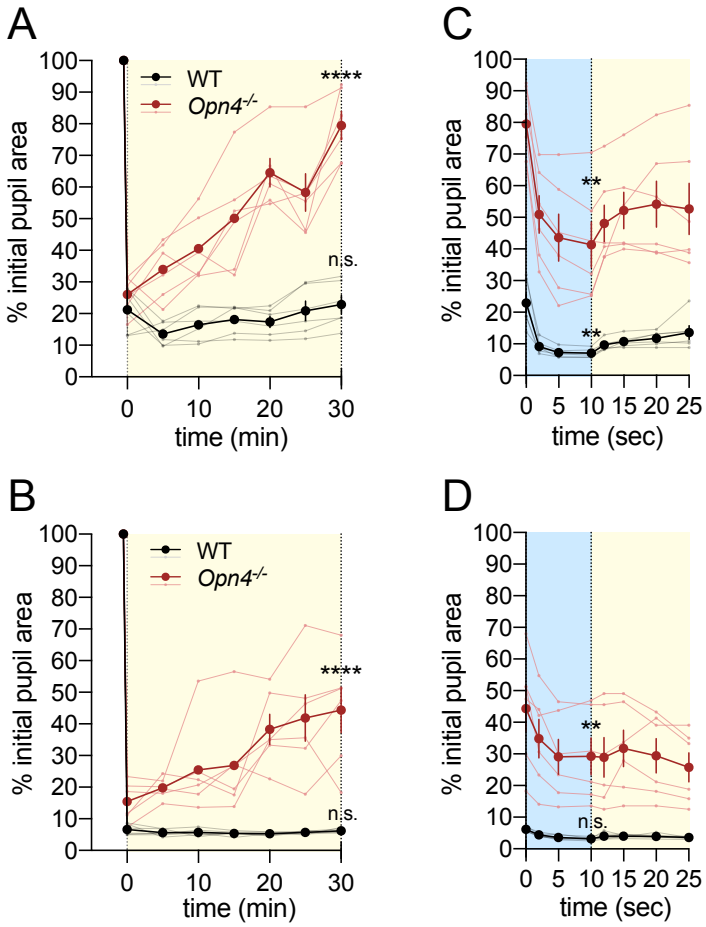


Figure 3.20: Pupil constriction of WT and *Opn4*$^{-/-}$ mice in response to a sustained white light pulse. Pupil constriction dynamics of WT and *Opn4*$^{-/-}$ animals in response to a 30-minute 100 lux (A) and 400 lux (B) white light pulse. (C, D) At 30 minutes, an additional 10-second 14.8 log photons/cm^2/sec blue light pulse, superimposed on the background light pulse, was administered. Data are mean ± SEM, n = 6 (A, B), n = 4 (C). Statistical analysis was performed using two-way ANOVA with Šidák's correction for multiple comparisons, comparing pupil area at 30 minutes and after the superimposed light pulse to the initial maximum pupil constriction. n.s., not significant, **** $p < 0.0001$.

of *Opn4*$^{-/-}$ animals was not sustained. Their pupils dilated from approximately 15% to 75% of dark-adapted pupil area over the 30-minute pulse at 100 lux; and from 15% to 45% at 400 lux (Fig. 3.20A, B).

Furthermore, I was interested in analysing how the retinas of *Opn4*$^{-/-}$ animals would encode a superimposed bright light pulse once their pupils had dilated. Therefore, I administered a 10-second blue light pulse at the end of the 30-minute white light pulse. The pupils of WT animals constricted to or remained constricted

Table 3.1: Differences in light doses between WT and *Opn4*$^{-/-}$ animals at commonly used light pulses

		WT	***Opn4*$^{-/-}$**	**Difference (x)**	***p* value**
100 lux	15 min	249	563	2.3	0.00140
	30 min	595	1612	2.7	0.00001
400 lux	15 min	87	332	3.8	0.00430
	30 min	197	940	4.8	0.00008

Note:
Area under curve (AUC) calculations of the light dose reaching the retinas of WT and *Opn*4$^{-/-}$ animals were performed and the fold difference between the doses calculated.

at approximately 5% of dark-adapted pupil area (Fig. 3.20C, D). However, the pupils of *Opn4*$^{-/-}$ animals did not reach the maximum pupil constriction values (Fig. 3.20B, D), indicating that the rods and cones were unable to signal the further change in retinal illuminance in the absence of melanopsin.

Circadian experiments are often performed by administering a 15- or 30-minute light pulse. To understand the difference in light doses the WT and *Opn4*$^{-/-}$ retinas will receive, I calculated the areas under the pupil constriction functions. The overall light dose the *Opn4*$^{-/-}$ retinas received was significantly higher after both 15-minute and 30-minute light pulses at either light intensity (Table 3.1). One commonly used light pulse in circadian experiments is a 30-minute 400 lux light pulse, and under these conditions, *Opn4*$^{-/-}$ retinas receive 4.8 times more light than WT animals. In conclusion, *Opn4*$^{-/-}$ animals receive a much larger light dose upon stimulation with a sustained 100 lux or 400 lux light pulse.

Retinal light responses with and without pupil dilation

I then went on to study the retinal light responses of WT and *Opn4*$^{-/-}$ mice. Since the pupils of *Opn4*$^{-/-}$ animals redilated when exposed to a sustained light pulse, I decided to dilate the pupils of WT and *Opn4*$^{-/-}$ animals pharmacologically before light exposure to keep the effective light doses equal between the two genotypes. To my knowledge, the effect of pupil constriction and the subsequent light-induced gene expression has not been studied before, and I was curious to see how substantial

the effect of pupil constriction dynamics on the light-induced gene expression was. I exposed the one group of animals to a CT16 30-minute 100 lux light pulse, which would result in *Opn4*$^{-/-}$ animals receiving 2.7x higher light dose than WT animals. To another group of animals, I applied mydriatics at CT11-12 and pulsed them at CT16 with a 20 lux light pulse. I chose this light intensity as the pupils of WT animals constrict to approximately 20% of the dark-adapted pupil area in response to a 100 lux light pulse, and therefore, the effective light dose in WT animals between the two experiments was the same.

To assess the retinal responsiveness to light, I analysed the induction of immediate early genes Fos proto-oncogene (*Fos*) and early growth response protein 1 (*Egr1*), markers of neuronal activation whose retinal levels increase in response to a light stimulus [202]; and deiodinase 2 (*Dio2*), a light-induced gene mediating light adaptation in the retina [203]. All of these genes were induced in WT and *Opn4*$^{-/-}$ retinas in response to a 100 lux light pulse (Fig. 3.21A, C, E). When the pupils were pharmacologically dilated before light exposure, and thus the light dose between the two genotypes kept the same, *Fos* and *Egr1* were light-induced in both WT and *Opn4*$^{-/-}$ retinas (Fig. 3.21B, D), but the levels of *Dio2* changed significantly only in WT retinas (Fig. 3.21F). The core clock genes, including *Per1/2*, were not induced in response to these light pulses (data not shown), most likely because the light dose was not sufficient. In conclusion, keeping the light doses the same between WT and *Opn4*$^{-/-}$ animals had a subtle effect on the light-induced retinal gene expression of WT and *Opn4*$^{-/-}$ animals.

Circadian phase shifting with and without pupil dilation

One of the circadian deficits of *Opn4*$^{-/-}$ animals is their reduced phase-shifting response and all studies demonstrating this defect have been conducted without dilating animals' pupils [32, 33, 64]. *Opn4*$^{-/-}$ animals have thus received a significantly greater light dose. However, should the light dose be kept equal, the phase-shifting deficit of *Opn4*$^{-/-}$ animals could be much larger. Therefore, I attempted to measure the circadian phase-shifting response by first dilating the animals' pupils.

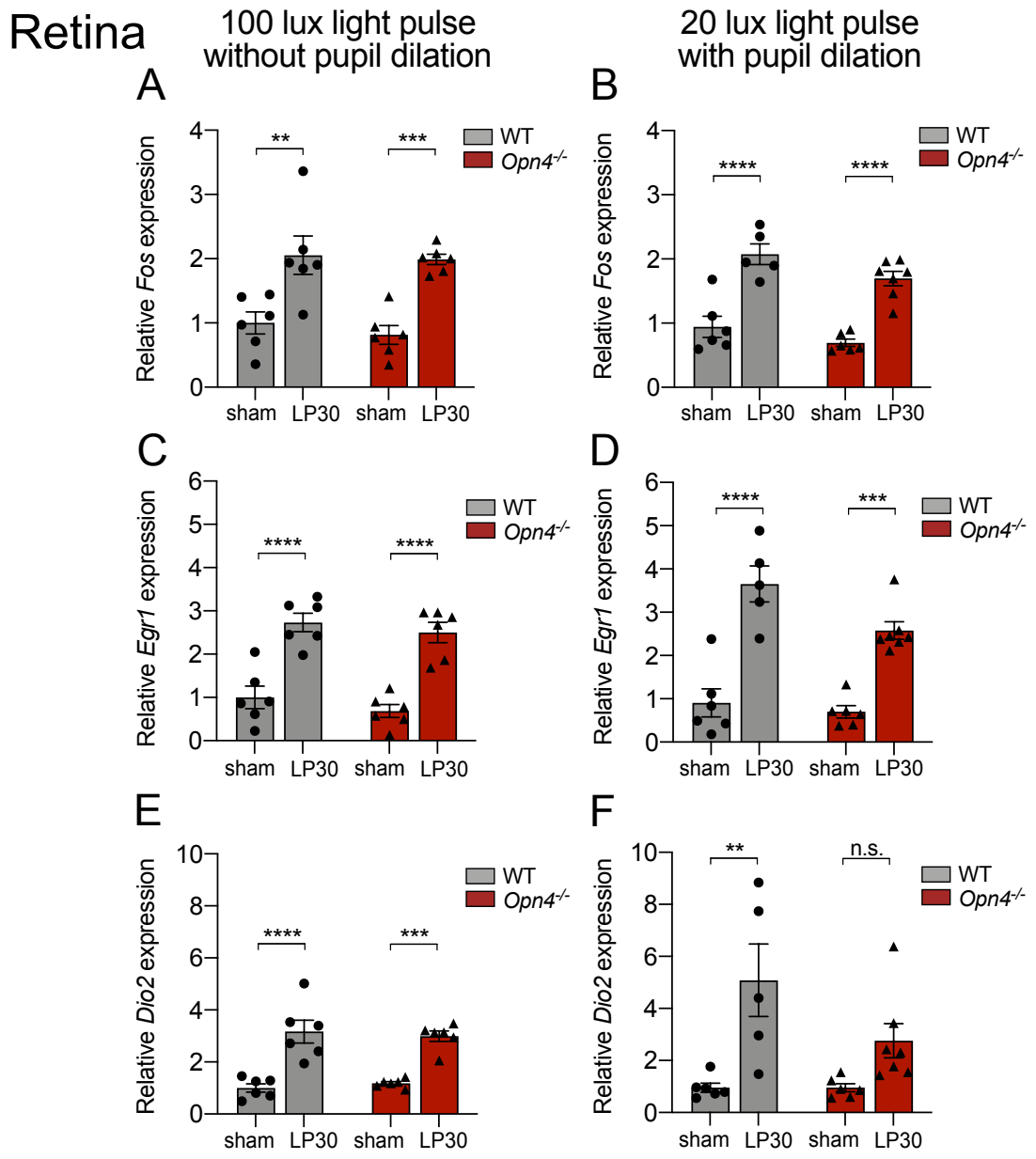


Figure 3.21: Expression and light regulation of immediate early genes genes in WT and *Opn4*$^{-/-}$ retinas upon an equal light dose. Expression of *Fos* (A, B), *Egr1* (C, D) and *Dio2* (E-F) retinal transcripts at CT16 (sham) and upon exposure to a 30-minute white light pulse (LP30) of 100 lux (A, C, E) or 20 lux (B, D, F) with pupils dilated. Data are mean ± SEM, n = 5-7. Statistical analysis was performed using two-way ANOVA with Šidák's correction for multiple comparisons. n.s., not significant, ** $p < 0.01$, *** $p < 0.001$, **** $p < 0.0001$.

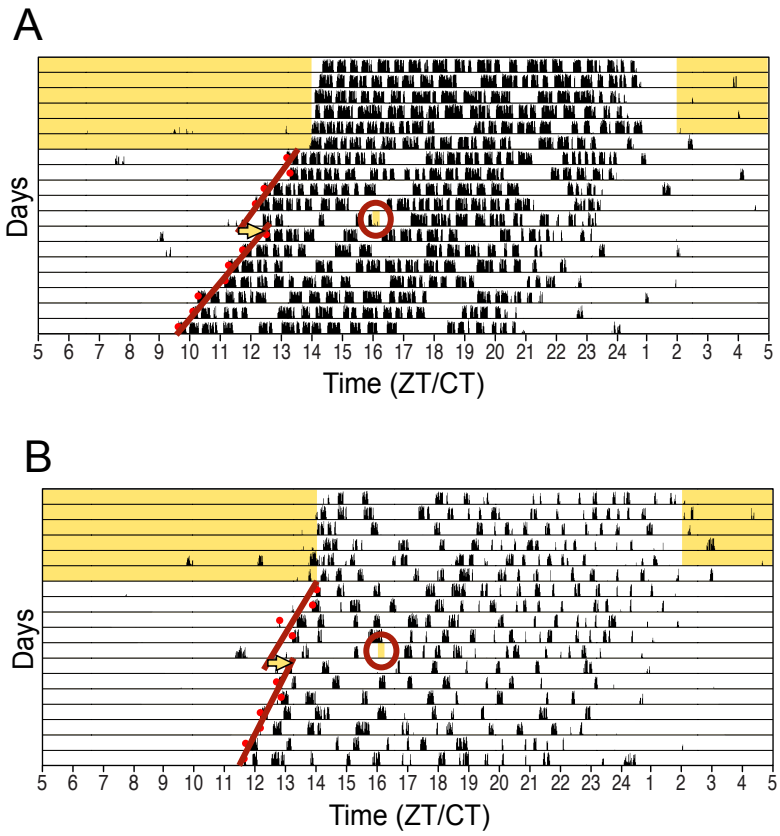


Figure 3.22: Representative actograms of mice in diurnal and circadian conditions. In diurnal conditions, the activity is entrained to the light-dark cycle. When released to constant darkness, the activity rhythm starts to free-run. Exposure to a CT16 light pulse delays the start of activity and is used to calculate the circadian phase-shifting response.

Two example actograms, showing the wheel-running activity of individual mice over several days, are shown in Figure 3.22. The yellow areas indicate when the lights are on, each row marks one day and time is displayed on the x-axis. Mice are entrained to the light-dark cycle as their activity starts when the lights are turned off. Once they are released into constant darkness, their circadian rhythms start to free-run. Upon exposure to a light pulse in the first half of their circadian night, at CT16, their activity is delayed, and the extent of delay marks the phase shift (small yellow arrow).

In response to a 15-minute 100 lux white light pulse without dilating the pupils, the phase-shifting response of *Opn4*$^{-/-}$ animals was smaller than the phase shifts of WT animals (Fig. 3.23A). The phase-shifting response of *Opn4*$^{-/-}$ animals is

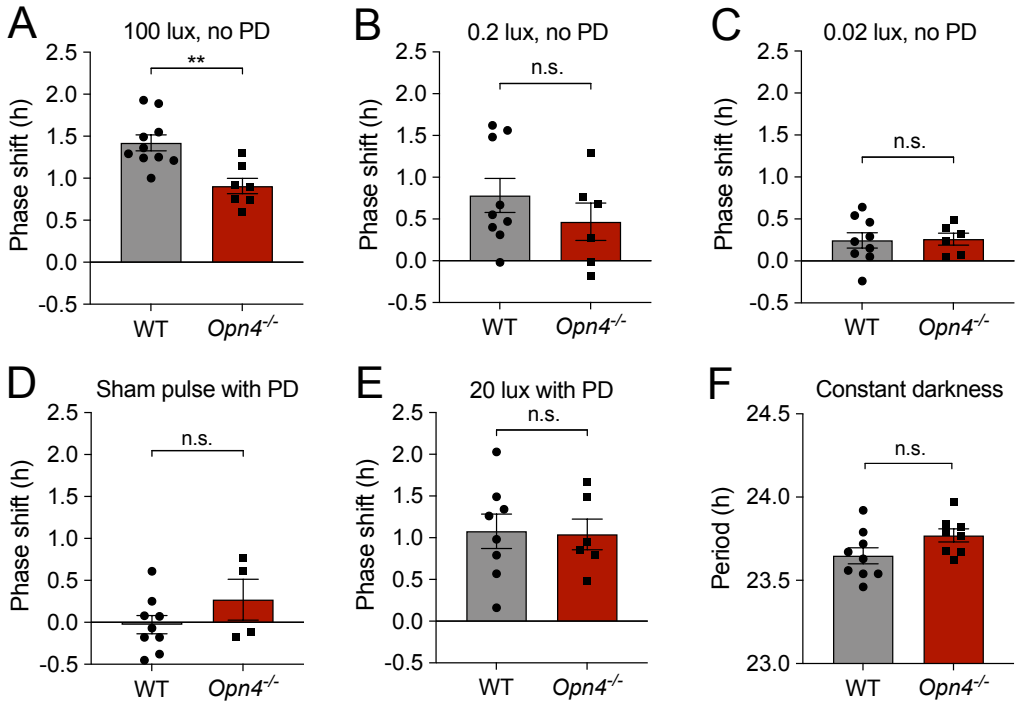


Figure 3.23: Circadian phase shifting of WT and *Opn4*$^{-/-}$ animals in response to CT16 light pulses. (A-C) Circadian phase shifting in response to 100 lux (A), 0.2 lux (B) and 0.02 lux (C) light pulse without applying pupil dilation. (D) Sham pulse with pupils dilated. (E) Phase shifting response to a 20 lux light pulse with animals' pupils dilated at CT11-12. (F) Free-running period in constant darkness. All light pulses were administered at CT16. Data are mean ± SEM, n = 4-10. Statistical analysis was performed using unpaired t-tests. PD, pupil dilation, n.s., not significant, ** $p < 0.01$.

also reduced at much lower light intensities [81]. Unexpectedly, however, the phase shifts did not differ between WT and *Opn4*$^{-/-}$ animals in response to 0.2 lux nor 0.02 lux light pulses (Fig. 3.23B, C).

I then went on to explore the phase-shifting response while also dilating animals' pupils. First, I determined whether pupil dilation itself could affect phase-shifting. I dilated the animals' pupils at CT11-12 and did not expose them to any additional light. Although there was variability in the data, I did not see a phase-shifting response to the pupil dilation procedure itself (Fig. 3.23D). I then applied mydriatics and recorded phase shifting in response to a 20 lux light pulse. Contrary to the expected, I did not see a difference between the genotypes (Fig. 3.23E). To ascertain that there were no overall circadian deficits in *Opn4*$^{-/-}$ animals that could explain the unexpected results, I also measured their period in constant darkness, which

was not different from WT animals (Fig. 3.23F), as expected [33].

A complicating factor to these experiments was that approximately half of the animals, both WT and *Opn4*$^{-/-}$ did not run on the running wheels, although the wheels were in working order and checked regularly. It was a very unusual behaviour that was not displayed by any other mouse colony in our facility. As illustrated in Figure 3.22B, some mice showed very low activity, which made the phase shift calculations more variable. Since the colony had been inbred, there might have been a drift in their genetic background that could have accounted for their low activity profile.

SCN light responses with and without pupil dilation

The shift in activity profile results from light-induced activation of the SCN and the subsequent induction of clock genes *Per1/2* among others. Despite the animals of the *Opn4*$^{-/-}$ colony showing low activity profiles, there were no indications of their light signalling from the retina to the SCN being dysfunctional. Therefore, I used the same paradigm to investigate light-induced SCN gene expression in WT and *Opn4*$^{-/-}$ animals to a 100 lux light pulse, and a 20 lux light pulse with prior pupil dilation.

I detected an increase in immediate early genes *Fos* and *Egr1* in the SCNs of WT and *Opn4*$^{-/-}$ mice after a 30-minute 100 lux light pulse (Fig. 3.24A, C). Unexpectedly and contrary to what has been shown before in response to a 400 lux light pulse [186], I did not see any significant differences in immediate early gene induction between WT and *Opn4*$^{-/-}$ SCNs, although *Opn4*$^{-/-}$ animals received a much higher light dose. Neither *Fos* nor *Egr1* was induced in response to a 20 lux light pulse with prior pupil dilation in either genotype (Fig. 3.24B, D). There was significant variability in the data, and the experiment might not have been adequately powered. Nevertheless, unlike in the retina where pupil dilation resulted in subtle differences in gene induction, this was not the case for the SCN.

I then went on to study the expression of core clock genes *Per1* and *Per2*. Interestingly, these genes were not induced by light in either genotype in response to a 100 lux (Fig. 3.25A, C, E) or a 20 lux light pulse (Fig. 3.25B, D, F).

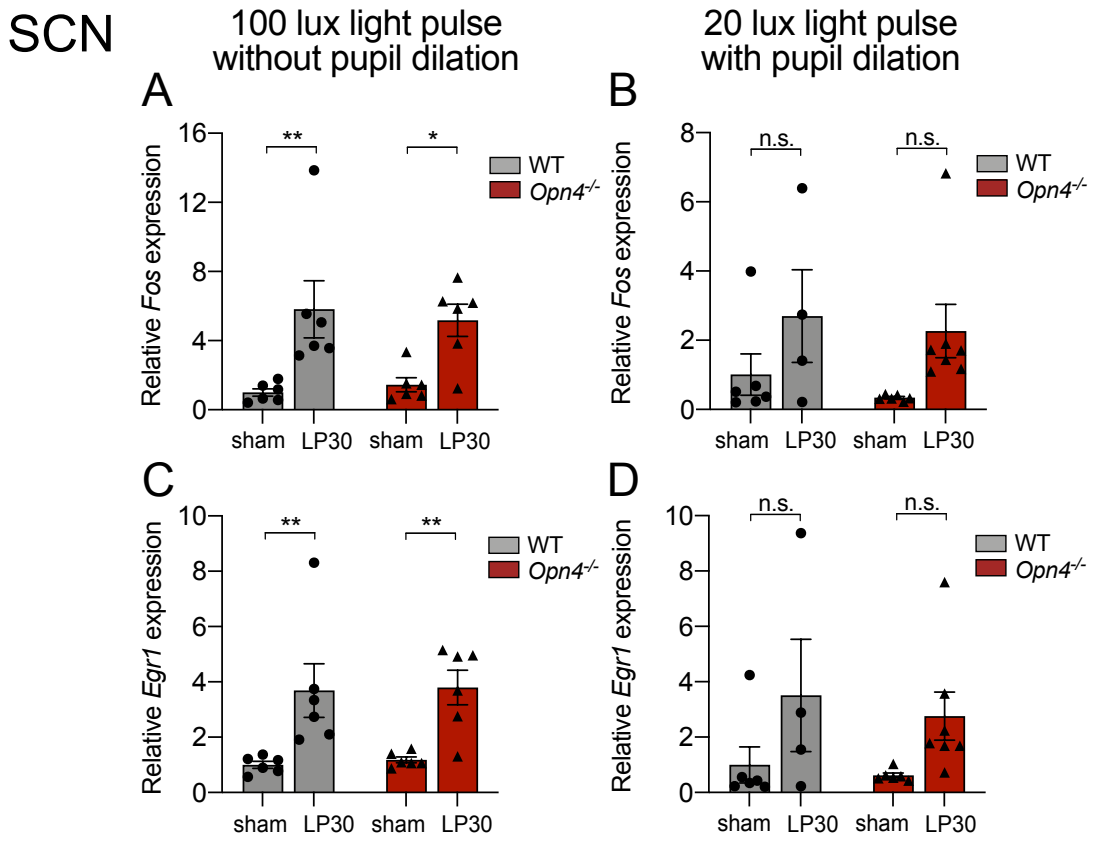


Figure 3.24: Expression and light regulation of immediate early genes genes in WT and *Opn4*$^{-/-}$ SCNs upon an equal light dose. Expression of *Fos* (A, B) and *Egr1* (C, D) SCN transcripts at CT16 (sham) and upon exposure to a 30-minute white light pulse (LP30) of 100 lux (A, C) or 20 lux (B, D) with pupils dilated. Data are mean ± SEM, n = 4-7 and normalised to WT sham values, which is set to equal 1. Statistical analysis was performed using two-way ANOVA with Šidák's correction for multiple comparisons. n.s., not significant, * $p < 0.05$, ** $p < 0.01$.

Similarly to what I saw in the retina, the light dose might not have been substantial for inducing the transcripts.

In conclusion, in this part of the chapter, I addressed my second aim and investigated the retinal and central light responses in the absence of melanopsin. First, I determined that *Opn4*$^{-/-}$ animals receive a significantly higher light dose than WT animals when exposed to a standard CT16 light pulse. Therefore, I analysed the retinal and SCN light responses with prior pharmacological dilation of animals' pupils. I saw that when the mydriatics were not applied, the induction of light-responsive genes was similar in WT and *Opn4*$^{-/-}$ retinas. However, when the light doses were kept equal, there were subtle differences as WT, but not

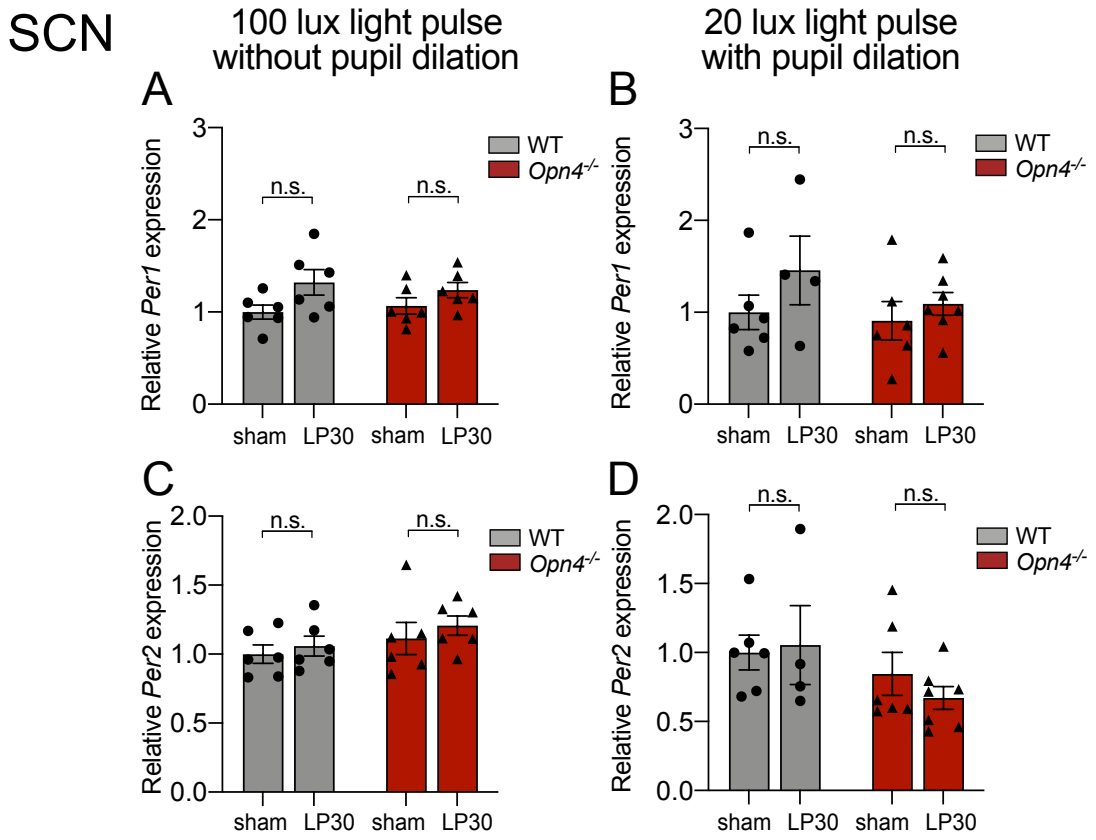


Figure 3.25: Expression and light regulation of clock genes genes in WT and *Opn4*$^{-/-}$ SCNs upon an equal light dose. Expression of *Per1* (A, B) and *Per2* (C, D) SCN transcripts at CT16 (sham) and upon exposure to a 30-minute white light pulse (LP30) of 100 lux (A, C) or 20 lux (B, D) with pupils dilated. Data are mean ± SEM, n = 4-7 and normalised to WT sham values, which is set to equal 1. Statistical analysis was performed using two-way ANOVA with Šidák's correction for multiple comparisons. n.s., not significant.

Opn4$^{-/-}$ retinas upregulated the gene *Dio2*, indicating a slightly dampened light response in the absence of melanopsin.

Further, I studied the SCN light responses to draw parallels between melanopsin's role in the retinal and central circadian clock. Contrary to what I expected, I did not see a more pronounced deficit in the phase-shifting response of *Opn4*$^{-/-}$ animals when prior pupil dilation was applied. The light-induced gene expression in the SCN was not different between WT and *Opn4*$^{-/-}$ animals whether or not the light dose was kept equal. My results indicate that the lack of melanopsin leads to a lightly dampened retinal light response, but I was unable to replicate findings that are well established in the literature, such as the attenuated phase-shifting response

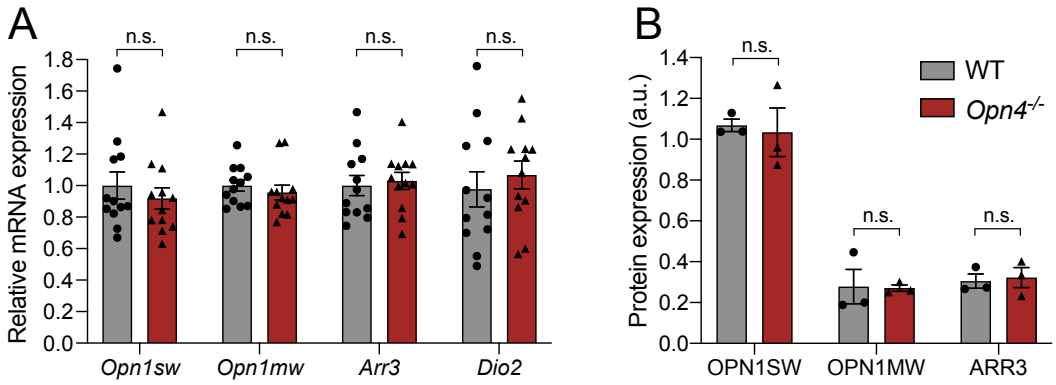


Figure 3.26: Expression of cone genes and proteins in WT and *Opn4*$^{-/-}$ retinas. (A) Transcript levels of S-opsin (*Opn1sw*), M-opsin (*Opn1mw*), cone arrestin (*Arr3*), and diodonase 2 (*Dio2*). (B) Protein levels of the OPN1SW, OPN1MW and ARR3. (A) Data are normalised to WT values, which are set to equal 1, n = 12. (B) No normalisation conducted between the different proteins, n = 3. Data are mean ± SEM. Statistical analysis was performed using multiple unpaired t-tests with Holm-Šidák's correction for multiple comparisons. n.s., not significant.

of *Opn4*$^{-/-}$ animals, nor the reduced SCN light responses.

3.3.6 There are no discernible cone abnormalities in *Opn4*$^{-/-}$ retinas

As discussed in my introduction, one of the reasons for an abnormal cone ERG in *Opn4*$^{-/-}$ animals could be related to cone development. Therefore, to study the retinal cones of *Opn4*$^{-/-}$ animals, I first looked at the expression of cone genes, S-opsin, M-opsin and cone arrestin (*Arr3*), and *Dio2*, which is known to regulate cone development [174]. I did not detect any differences in the transcript levels between WT and *Opn4*$^{-/-}$ retinas (Fig. 3.26A). Since the transcripts do not always reflect the protein abundance, I also studied the cone proteins levels with mass-spectrometry. Similarly to the transcript levels, there were also no significant differences between the genotypes (Fig. 3.26B). Therefore, the retinal levels of cone-related genes and proteins were not affected by the absence of melanopsin.

Despite there being no differences in the levels of cone-related transcripts and proteins, there might be more subtle changes in retinal cones in *Opn4*$^{-/-}$ animals, for example, their retinal distribution. As mentioned in my introduction, the mouse retina has a distinct dorsoventral gradient in cone distribution, which several clock mutants lose. To get an overview of the cone distribution of WT and *Opn4*$^{-/-}$

retinas, I immunostained the retinas for S- and M-opsins and measured the retinal areas with high expression of either cone opsin. The retinas with abnormal cone development, such as *Bmal1*$^{-/-}$, show a larger retinal proportion with high expression of S-opsin [193]. However, WT and *Opn4*$^{-/-}$ retinas had a similar proportion of area with high S-opsin expression (Fig. 3.27). Therefore, the lack of melanopsin did not lead to extensive defects in retinal cones.

Although there were no abnormalities in the gross cone distribution in the *Opn4*$^{-/-}$ retinas, there might be defects on a more granular level. As per the analysis performed on *Bmal1*$^{-/-}$ retinas, I next counted the number of cones in six different regions along the dorsoventral retinal axis as illustrated in Figure 3.28A. The analysis showed that the overall number of cones across the entire retina was the same in WT and *Opn4*$^{-/-}$ retinas (Fig. 3.28C). Approximately 63% of the cones in WT retinas were dual cones, 25% S-cones and 12% M-cones, which is very similar to the cone subtype distribution reported for albino, but not pigmented C57/BL6 mice [173]. Our *Opn4*$^{-/-}$ colony was pigmented but maintained on a mixed 129 C57/BL6 background, which might explain this finding. The analysis revealed slight differences in the number of specific cone subtypes between WT and *Opn4*$^{-/-}$ retinas ($p < 0.0001$, two-way ANOVA interaction between cone type and genotype). However, the pairwise comparisons of cone types between the genotypes did not show any significant differences (Fig. 3.28D). The overall density of cones increased dorsoventrally ($p < 0.0001$, two-way ANOVA main effect of retinal region), similar to what was reported before [173], but the total number of cones in the six regions did not differ between WT and *Opn4*$^{-/-}$ retinas (Fig. 3.28E). Therefore, the overall numbers of cone subtypes in *Opn4*$^{-/-}$ retinas were very similar to WT retinas.

Next, I was interested to see whether the cone distribution in any retinal region differed between WT and *Opn4*$^{-/-}$ retinas. As expected and reported previously, the dual cones were present throughout the retina, the dorsal retina had a higher number of M-cones, and the ventral retina more S-cones [173, 174] (Fig. 3.29A-F). There were minor differences in the cone subtype distribution in the far-dorsal (FD) and mid-dorsal (MD) retinas ($p < 0.05$, two-way ANOVA interaction between cone

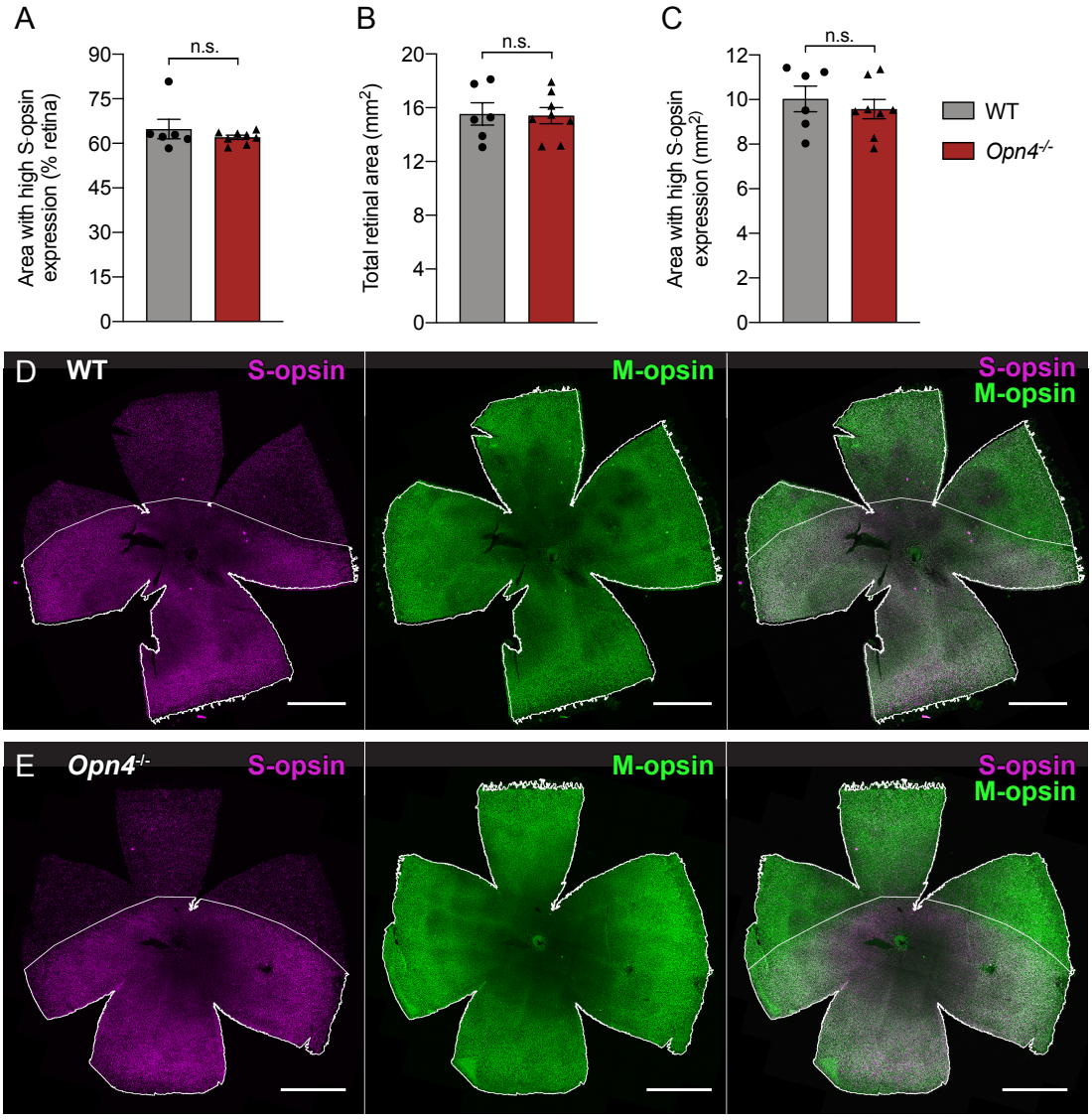


Figure 3.27: Cone distribution in WT and *Opn4*$^{-/-}$ retinas. Proportion of the retina expressing high levels of S-opsin (A), total retinal area (B) and total area with high S-opsin expression (C) are not altered in *Opn4*$^{-/-}$ retinas. Representative immunohistochemistry images of S- and M-opsin expression in a WT (D) and *Opn4*$^{-/-}$ (E) retinas. Outlines surrounding the areas of high S-opsin expression and the entire retina were used for quantification. Scale bars 1 mm. n.s., not significant. Data are mean ± SEM, n = 6-8. Statistical analysis was performed using Student's t-tests. n.s., not significant.

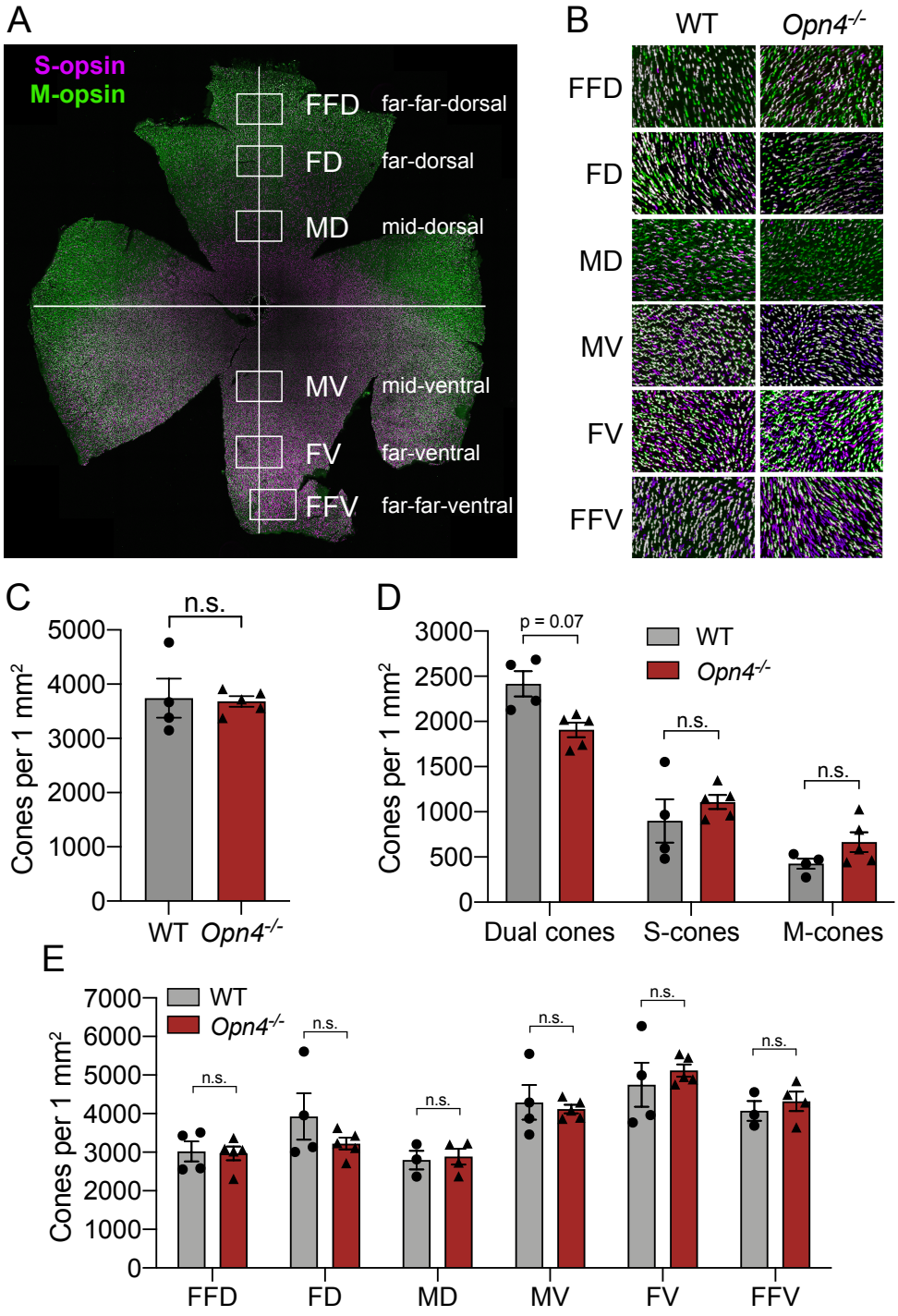


Figure 3.28: Number of cones along the dorsoventral axis in WT and *Opn4*$^{-/-}$ retinas. (A) Representative image of a retina and the regions used for cone number analysis, these were kept the same across all retinas. (B) Representative images of WT and *Opn4*$^{-/-}$ retinas in those retinal regions. (C) Average density of all cones and (D) different cone subtypes. (E) Average density of all cones along the dorsoventral axis. Data are mean ± SEM, n = 3-5. Statistical analysis was performed using two-tailed t-test (C) or two-way ANOVA with Šidák's correction for multiple comparisons (D-E). FFD, far-far-dorsal; FD, far-dorsal; MD, mid-dorsal; MV, mid-ventral; FV, far-ventral; FFV, far-far-ventral. n.s., not significant.

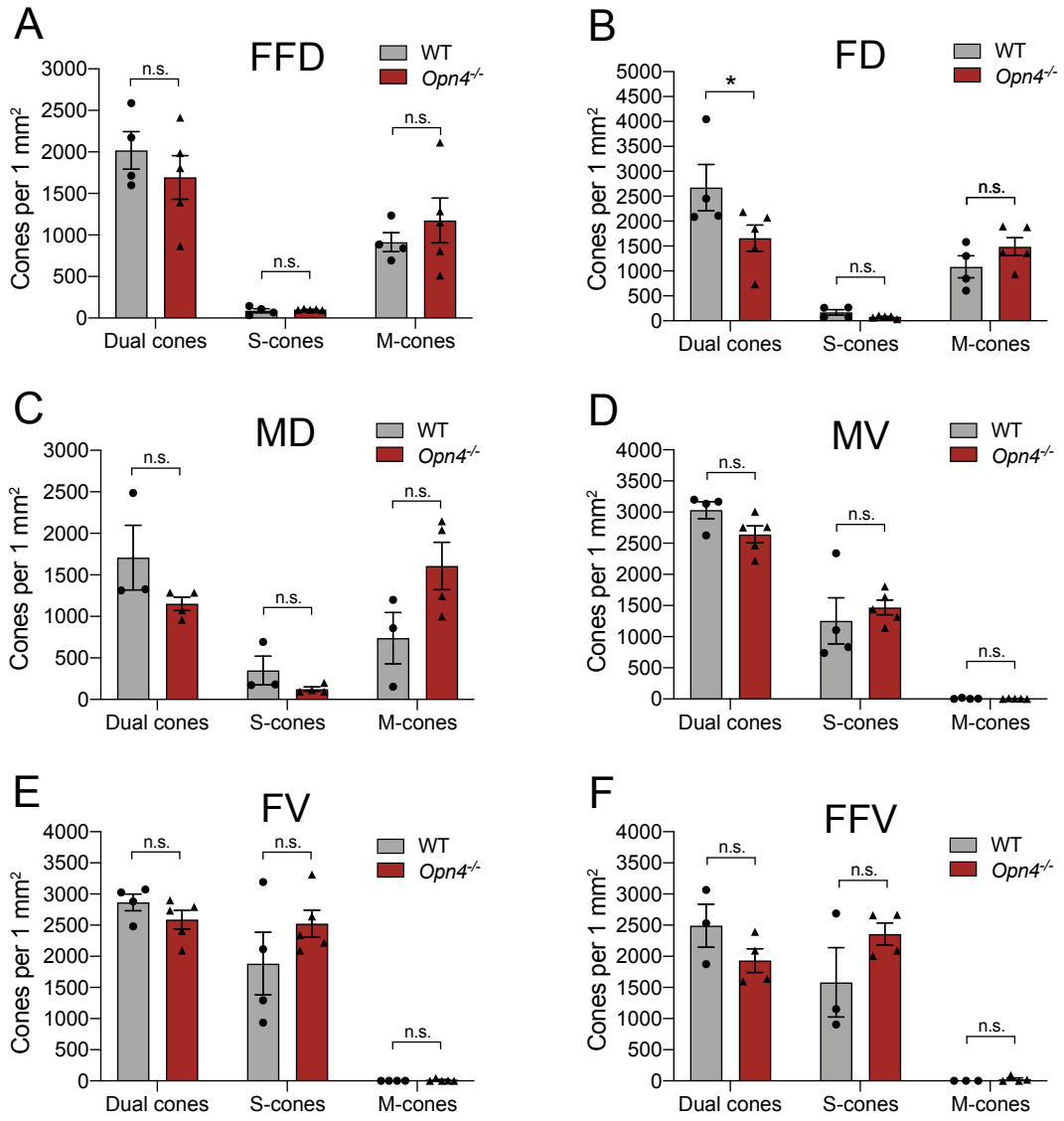


Figure 3.29: Density of cone subtypes along the dorsoventral axis in WT and *Opn4*$^{-/-}$ retinas. The number of dual, S- and M-cones in far-far-dorsal (FFD, A), far-dorsal (FD, B), mid-dorsal (MD, C), mid-ventral (MV, D), far-ventral (FV, E), far-far-ventral (FFV, F) areas of the retina. Data are mean ± SEM, n = 3-5. Statistical analysis was performed using two-way ANOVA with Šidák's correction for multiple comparisons. n.s., not significant, * $p < 0.05$.

type and genotype), as WT retinas showed higher numbers of dual cones on the expense of the single cones (Fig. 3.29B, C). The number of individual cone types was not different in five of the regions between WT and *Opn4*$^{-/-}$ retinas (Fig. 3.29A, C-F). Only in FD retina were there significantly less dual cones in *Opn4*$^{-/-}$ retinas (Fig. 3.29A). In conclusion, the cone distribution in *Opn4*$^{-/-}$ retinas is very similar to WT retinas with minor differences in the dorsal retina.

I was then interested in seeing whether the slight difference in cone distribution resulted in a change in their retinal function of *Opn4*$^{-/-}$ animals. For example, *Bmal1*$^{-/-}$ retinas that express increased amounts of S-opsin are subsequently more sensitive to UV light compared to WT retinas [174]. The reduced cone ERG b-wave amplitude in *Opn4*$^{-/-}$ animals was detected in response to a white light pulse [185], which preferentially activates M-opsin. Therefore, since *Opn4*$^{-/-}$ retinas have marginally higher numbers of S-cones, one could hypothesise that the slight cone ERG defect may be the result of an altered retinal spectral sensitivity. To test this hypothesis, I measured the retinal function with pupillometry and quantified the maximum pupil constriction of WT and *Opn4*$^{-/-}$ animals in response to three wavelengths of light: UV, blue and yellow. These light sources stimulated the retinal photoreceptors to a different extent and enabled me to analyse the contribution of each of the four photoreceptors to the maximum pupil response. The UV light stimulated mainly S-cones, the blue light activates melanopsin, rhodopsin and M-opsin. The yellow light is absorbed primarily by M-opsin and rhodopsin but has minimal effect on S-opsin and melanopsin (Fig. 3.30).

I recorded pupil constriction in response to a 10-second light pulse over a range of light intensities. The maximum pupil constriction was very similar between WT and *Opn4*$^{-/-}$ animals in response to UV light (Fig. 3.31A, B) and yellow light (Fig. 3.31E, F). As expected, *Opn4*$^{-/-}$ animals showed a pupil constriction deficit in response to blue light stimulation at the higher light intensities (Fig. 3.31C, D). With all wavelengths of light, there was considerable variability in the maximum constriction at lower light intensities, which could be caused by the slight inaccuracies in positioning of the animal in front of the light source. Overall, however, I did not see any apparent spectral shift in *Opn4*$^{-/-}$ retinas compared to WT, but detected, as expected, an attenuated pupil constriction response to bright blue light.

In conclusion, in this part of the chapter, I found that the overall transcript and protein levels of cone opsins and cone-associated proteins did not differ between WT and *Opn4*$^{-/-}$ animals, and there were no significant changes in the overall retinal cone distribution. A more detailed analysis showed that *Opn4*$^{-/-}$ retinas

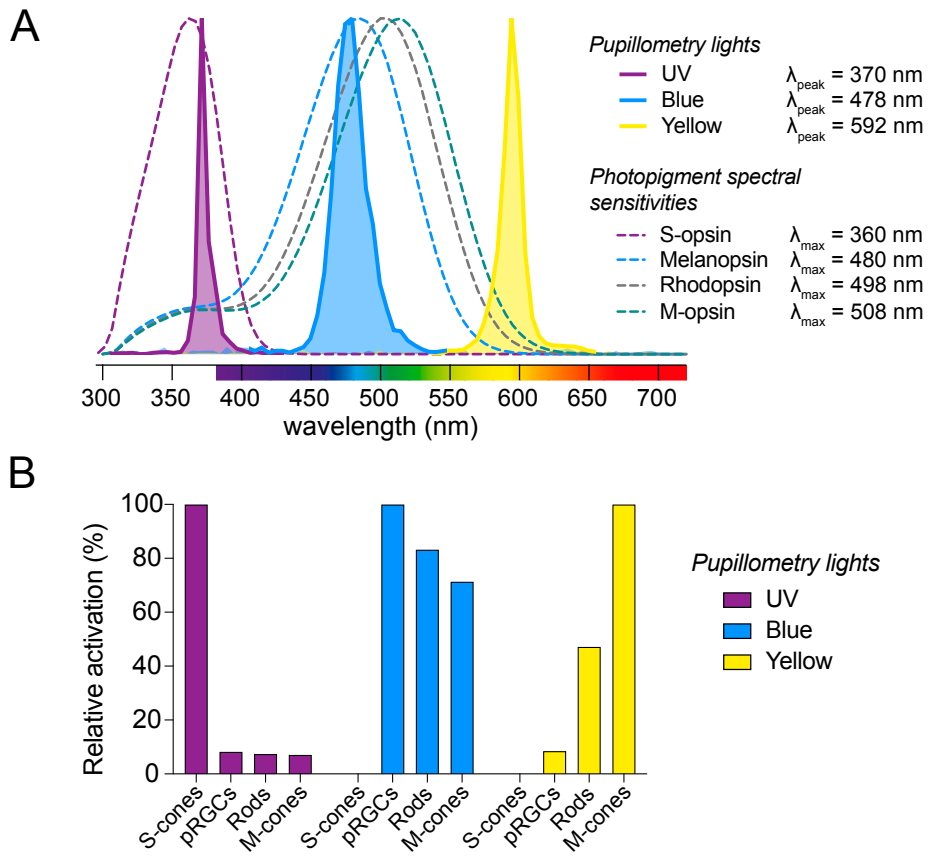


Figure 3.30: Schematic of chromatic pupillometry experiment setup. (A) Spectral sensitivity of mouse photoreceptors and the LED lights used in the chromatic pupillometry experiment. (B) Relative activation of mouse photoreceptors by the three LED lights. The activation of the photoreceptor stimulated the most is scaled to 100%.

had minor differences in overall cone distribution compared to WT retinas, which originated from the dorsal retina. However, these changes did not impact the maximum pupil constriction of *Opn4*$^{-/-}$ mice to chromatic stimuli, indicating that the spectral sensitivity of *Opn4*$^{-/-}$ retinas was not shifted. In conclusion, the absence of melanopsin does not seem to lead to aberrant cone distribution and function in adult mouse retinas.

Another possible explanation for the lower cone ERG b-wave amplitude of *Opn4*$^{-/-}$ animals is that the activation of melanopsin in response to a flash of light changes cone signalling in the retina. If true, blocking melanopsin phototransduction in an intact WT retina would dampen the retinal light responses to cone-activating stimuli. One way of blocking melanopsin is by applying the melanopsin antagonist opsinamide, which competes reversibly with 11-*cis*-retinal for the chromophore

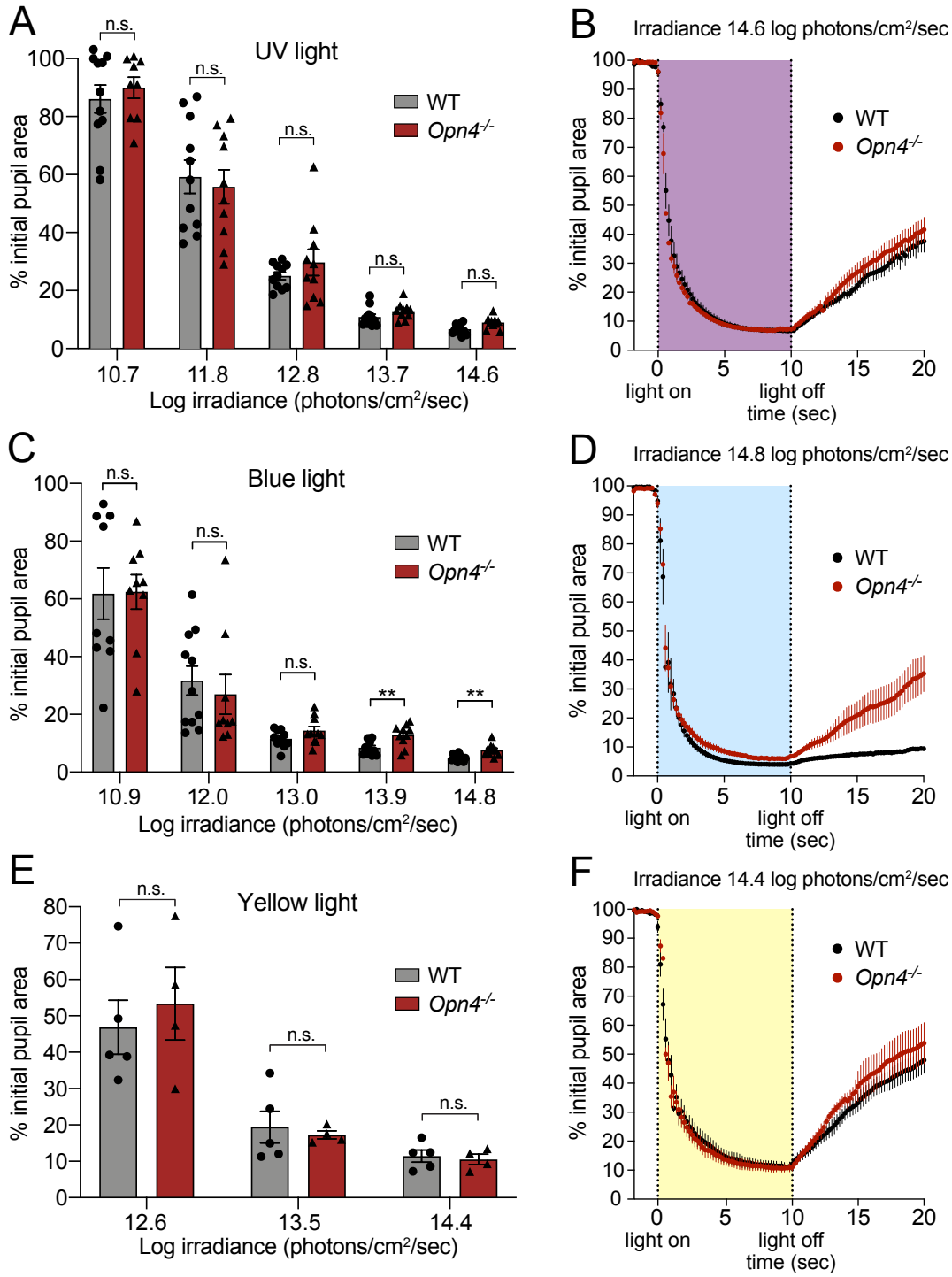


Figure 3.31: Maximum pupil constriction of WT and *Opn4*$^{-/-}$ animals in response to different wavelengths of light. Maximum pupil constriction in response to UV (A), blue (C), and yellow (E) light of different intensities, and the pupil constriction dynamics in response to the highest intensity light pulse (B, D, and E, respectively). Data are mean ± SEM, n = 10-11 (A, C, E), n = 4 (B, D, F). Statistical analysis was performed using multiple unpaired t-tests with Holm-Šidák's correction for multiple comparisons. ** $p < 0.01$.

binding site in the melanopsin molecule [204]. To test whether blocking melanopsin leads to the suppression of cone responses, I designed an experiment to stimulate a WT retina with different wavelengths of light to preferentially activate cone subtypes, both in the presence and absence of opsinamide. The electrical output of the retinas was measured using a multielectrode array by quantifying the changes in spike firing rate recorded from the ganglion cell layer in response to 10-second light pulses.

First, I studied the effect of opsinamide on melanopsin, rod and cone photoresponses, to ensure that the drug blocks melanopsin phototransduction specifically. Therefore, I first applied opsinamide to a retina from an aged *rd/rd* animal, which only retains melanopsin photoresponses. I saw that after the application of opsinamide, the melanopsin photoresponses were still present in the retinas for two light pulses, but were abolished by the third light pulse (Fig. 3.32A).

Next, I determined whether opsinamide had any off-target effects on the rods and cones, which would complicate the study of opsinamide in a WT retina. I investigated the effect of opsinamide in an *Opn4*$^{-/-}$ retina whose light responses originate from rods and cones only. I saw that opsinamide did not affect the retinal spike firing rate, indicating that the drug did not impact the overall retinal photoresponses of rods and cones (Fig. 3.32B). In conclusion, opsinamide blocked melanopsin photoresponses and had no detectable off-target effects on the retinal spike firing rate in response to rod and cone activation.

Further experiments recording the light responses of a WT retina, followed by the application of opsinamide to block melanopsin phototransduction, would clarify the effect of melanopsin phototransduction on cone responses. By stimulating the retina with different wavelengths of light, it would be possible to study the effect of melanopsin phototransduction on different retinal photoreceptors. Should the retinal light responses change upon opsinamide application, it would indicate feedback from melanopsin to rod and cone phototransduction. If the light responses in the presence of opsinamide were dampened, it would provide evidence for melanopsin activation inhibiting cone responses and would suggest that the deficits in cone ERG b-wave amplitude in *Opn4*$^{-/-}$ mice could be explained by the effect of melanopsin

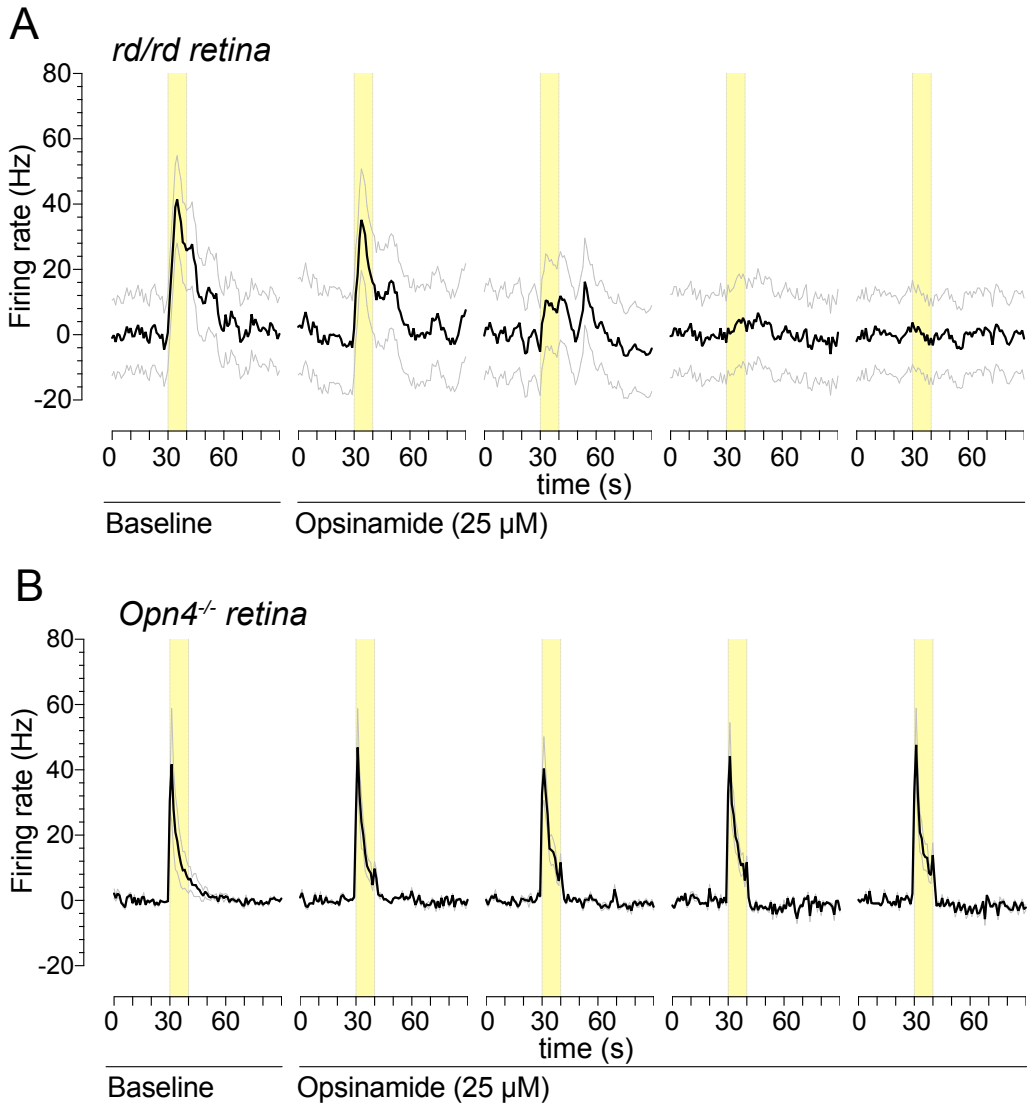


Figure 3.32: Effect of opsinamide on melanopsin, and rod and cone photoreception. Each individual recording consisted of a 30-second recording in the dark, a 10-second light pulse, marked by yellow bars, and an 80-second recovery recording. A 10-minute interval was left between the individual recordings. (A) RGC firing rate in *rd/rd* retinas at baseline and upon application of opsinamide. (B) RGC firing rate of *Opn4*$^{-/-}$ retinas at baseline and upon application of opsinamide. Data are mean ± SEM, n = 38 electrodes (A), n = 9 electrodes (B).

activation on cone signalling. In addition to the spike firing rate, it would also be interesting to analyse more subtle changes in retinal electrical potentials, such as cone ON and OFF responses.

3.4 Discussion

In this chapter, I investigated how melanopsin affects the retinal circadian clock and its light responses, aiming to compare melanopsin's role in the light responses of the retina and the SCN. As some of the retinal deficits of *Opn4*$^{-/-}$ mice could be explained by aberrant cone development, I also studied the distribution and spectral sensitivity of *Opn4*$^{-/-}$ retinas.

3.4.1 Retinal circadian rhythms and the role of melanopsin

To my knowledge, this is the first analysis of the retinal circadian transcriptome in mammals. While Mure et al. [199] analysed the diurnal retinal transcriptome of baboons and Storch et al. [130] analysed the circadian transcriptome of the mouse eye, the retinal circadian transcriptome has not been studied to date. I found that the circadian genes were enriched for dopamine signalling and gap junction pathways. This result aligns well with the literature on retinal circadian rhythms as one of the mechanisms behind retinal circadian rhythms is known to be the dopamine-mediated regulation of rod-cone coupling [124].

The circadian rhythms of retinal dopamine are driven by retinal melatonin, and the melatonin-deficient mice do not show a circadian rhythm in dopamine turnover [139]. The mice used in this study are devoid of melatonin but exhibit a circadian rhythm in the transcripts related to dopamine signalling. Even if their dopamine levels are not rhythmic, the dopamine receptor transcripts *Drd1* and *Drd4* were circadian in WT and also in *Opn4*$^{-/-}$ mice, indicating that the circadian rhythmicity of dopamine signalling may be regulated on a receptor level. This finding suggests some redundancy in the mechanisms setting the retinal rhythms. It has been shown that in addition to melatonin [122, 140] and dopamine [139], the retina also displays

circadian rhythmicity in GABA turnover [142] and adenosine levels [127], yet the hierarchy and interactions of the circadian neurotransmitters are not known.

The retinal circadian rhythms of core clock transcripts *Bmal1*, *Per2* and *Cry1* were dampened in *Opn4*$^{-/-}$ retinas. Nevertheless, *Opn4*$^{-/-}$ retinas showed a rhythmic expression of the clock-controlled gene *Dbp*. As several lines of evidence suggest, the retina might possess multiple circadian clocks [139, 141], which might not be in similar phases. Therefore, analysing the global retinal levels of core clock transcripts will only provide limited information about the different tissue clocks. The lower circadian rhythmicity of clock genes may be caused by a reduced amplitude of the most highly expressed retinal clock, or the shift in the phase relations of the individual clocks. Whatever the exact mechanism, the retinal molecular clock regulation is aberrant in the absence of melanopsin.

By analysing the cell-type-specific expression of core clock transcripts, one particular cell type, the Crh-positive amacrine cell, showed very high levels of clock transcripts (Fig. 3.16). These cells are GABAergic inhibitory interneurons, and their primary role involves exerting tonic inhibition on ON alpha RGCs [205]. In their report, Ruan et al. [143] demonstrated that the rhythmicity of PER2 expression of *rd/rd* retinas in vitro remained intact when melatonin, acetylcholine, glutamate, dopamine, or glycine signalling was disrupted. Only the application of GABA dampened the amplitude of PER2::Luc bioluminescence [143]. Coupled with the evidence that GABA turnover has a circadian rhythm in the retina [142], these results suggest that the Crh-positive amacrine cells could be a source of retinal circadian rhythms and mediate it in a GABAergic mechanism. The M1-M3 pRGCs make extensive connections to GABAergic amacrine cells, each pRGC forms gap junctions with approximately ten GABAergic amacrine cells [72], and might therefore provide input to the Crh-positive amacrine cells.

There are several mechanisms whereby melanopsin, a light-sensitive molecule, could influence retinal circadian rhythms in complete darkness. Since melanopsin affects the development of retinal vasculature [96] and the cones in early postnatal stages [98], melanopsin might have an impact on the development of the retinal

clock. Furthermore, melanopsin could mediate the entrainment of the clock(s) to the light cycle, or set the phase relations of the different retinal clocks.

These results show that *Opn4*$^{-/-}$ retinas retain the rhythmicity in dopamine signalling and gap junction pathways, and suggest that these pathways are not the reasons behind the retinal clock disruptions in the absence of melanopsin. Instead, the circadian rhythmicity of phototransduction or sphingolipid signalling might play a role as genes in these pathways were circadian in WT, but not in *Opn4*$^{-/-}$ retinas. The rods are unlikely sources of the retinal circadian clock as core clock transcripts or proteins have not been found in rods [136, 137]. Instead, the circadian clock in cones might be affected. One candidate pathway that could influence the retinal clock in the absence of melanopsin is sphingolipid signalling.

The most critical bioactive sphingolipid is sphingosine 1-phosphate (S1P). S1P is generated by the phosphorylation of sphingosine, a cell membrane phospholipid, by sphingosine kinases (SPHK1/2) and it acts on G protein-coupled sphingosine receptors (S1PR1-5). The pathway regulates multiple processes, including angiogenesis, apoptosis, cell growth and motility [206]. There are several reports on the role of sphingolipids in the retina, but limited information on their role in retinal circadian rhythms. The sphingosine receptors S1PR1/3 are present on photoreceptors [207] although their function has not been studied.

Since the genes related to sphingolipid signalling showed overall higher levels in *Opn4*$^{-/-}$ retinas, the pathway might also have a more global effect on their retinas. *Opn4*$^{-/-}$ show abnormalities in the retinal vasculature, attributed to an increased number of RGCs, increased levels of vascular endothelial growth factor (VEGF), leading to an overgrowth of retinal capillaries [96]. Interestingly, sphingolipids are known to influence retinal vascular development. In particular, tissue hypoxia leads to the upregulation of S1PR2, which induces the formation of retinal blood vessels [208]. Since the sphingolipid pathway genes show higher expression levels, it is a potential candidate mediating the overgrowth of vasculature in *Opn4*$^{-/-}$ retinas.

These findings raise several exciting avenues for further research. In particular, it would be interesting to further study the impact of the circadian regulation of

phototransduction genes. The loss of these rhythms could mediate the "day-like" state of retinas lacking melanopsin. Additionally, the sphingolipid signalling could be another potential mediator of retinal circadian rhythms. Whether the effect of melanopsin on these pathways and the retinal rhythms in general, is a result of a defective maturation of retinal circadian clock(s), or is related to melanopsin signalling in the retina, remains to be determined.

3.4.2 Retinal and SCN light responses in the absence of melanopsin

In the second part of this chapter, I investigated the light-induced gene expression, which underlies the ability of light to shift the circadian clock, thus reflecting clock plasticity. Interestingly, I found that the pupils of *Opn4*$^{-/-}$ animals redilated at 100 and 400 lux light levels, resulting in significantly higher retinal light doses. This finding highlighted the importance of studying pupil constriction before investigating retinal or SCN light responses. One of the light responses that is of interest with regard to retinal circadian rhythms is the release of dopamine. There are several conflicting reports on light-induced dopamine release in the *Opn4*$^{-/-}$ retinas [138, 187, 188], and none of the studies stated they applied pupil dilation prior to light exposure. It would be interesting to study dopamine release in *Opn4*$^{-/-}$ animals while assuring the light dose received by the retinas is equal to that of WT retinas. This experiment could potentially reconcile the discrepant findings.

I then went on to study the light-induced gene expression in the retinas and detected a dampened induction of *Dio2* when I dilated the animals' pupils and thus kept the light dose reaching WT and *Opn4*$^{-/-}$ retinas equal. The phase-shifting response of *Opn4*$^{-/-}$ animals is attenuated [33] and their SCN light responses reduced even when their pupils are not dilated before the light pulse [186]. I was surprised not to see a defect in phase-shifting at most light intensities I studied. This result may have to do with the unusually low activity profile of these animals. Unfortunately, I was also unable to detect differential SCN gene induction between WT and *Opn4*$^{-/-}$ animals, a finding that has been published [186]. This might have to do with the slight differences in the light intensities, as in the published work, mice were exposed

to a 400 lux light pulse. Nevertheless, the lack of melanopsin in my experiment led to a slightly lower retinal light response. As *Opn4*$^{-/-}$ animals have also been shown to have a reduced SCN light response, it indicates that melanopsin signals light information similarly in the retina and the SCN.

3.4.3 Melanopsin and retinal cones

I did not detect any substantial deficits in the distribution of retinal cone subtypes in *Opn4*$^{-/-}$ retinas. On a general level, there was an interaction between the genotype and cone subtypes, as WT retinas contained more dual cones and less single cones compared to *Opn4*$^{-/-}$ retinas. However, there were no widespread differences when comparing the cone subtypes in different retinal areas. The number of retinas I analysed may have been too low to see any differences, but it seems that should there be an effect on the distribution of cones, it is subtle compared to the cone development phenotype of mice whose cones lack *Bmal1* or *Per2* [174].

3.4.4 Limitations of this study and future work

To gain an insight into which cell types could be involved in the retinal circadian rhythms, I used the dataset by Siegert et al. [184]. I analysed which retinal cell type the transcripts were enriched in. This analysis assumes that if a cell shows high expression of a transcript compared to other cells, the transcript codes for a protein important for the function of the particular cell. However, it is impossible to say whether any particular cell type drives the global retinal rhythmicity of a specific transcript since the dataset nor my analysis of it considers the abundance of any particular cell type in the retina. Furthermore, as the dataset is a snapshot in time, it is impossible to predict whether any transcript is rhythmic in any cell type. Nevertheless, it provides some indication as to what cells may be involved in the various processes analysed in this thesis. A single-cell RNA-seq of the retinal tissue at the exact time points the other experiments were conducted would provide very thorough overview of the cellular contributions to the retinal clock.

The cell type specificity calculated in this manner can further be validated by assessing the expression of the subset of genes of interest in the particular cell types by immunohistochemistry or fluorescent in situ hybridisation. Furthermore, should a cell type, e.g. the Crh-positive amacrine cells or cones, be a source of retinal circadian rhythms, ablating these cells in the retina would abolish the retinal circadian rhythms.

A limitation in studying the retinal cones is that the pupillary light response is not a very accurate method for detecting retinal spectral sensitivity, and more subtle defects could be detected with cone ERG. Another aspect of retinal cone function that I did not study, but that could affect the cone ERG b-wave amplitude is aberrant photoreceptor-bipolar cell connectivity, which would be interesting to examine.

4

The role of melanopsin in light-induced retinal damage

4.1 Introduction

The processes of encoding prior light history and light intensity of the environment are essential for allowing the visual system to function from starlight to bright sunshine [3]. Overstimulation of the phototransduction cascade and the visual cycle has the potential to damage the retinal tissue [209]. Therefore, detecting light history also serves to prevent any light-induced damage by upregulating retinoprotective mechanisms [210]. However, the exact cellular and molecular mechanisms governing retinoprotection are unknown. One candidate for encoding light history in the retina is melanopsin, and this is for three reasons. First, melanopsin signalling is sustained [24, 45], making it suitable for brightness detection [78, 192]. Furthermore, the pRGCs are the only retinal cells that contain PACAP, a neuropeptide with retinoprotective properties whose release from the pRGCs in the brain is mediated solely by melanopsin activation [83]. Third, data collected previously in the Jagannath Lab showed that melanopsin might be involved in regulating the expression of several transcripts with anti-apoptotic properties. These data collectively suggest that melanopsin may play a role in protecting the retina from potentially damaging light stimuli.

In this chapter, I am addressing the second aim of my thesis and explore whether melanopsin light responses mediate retinoprotection in the context of retinal light damage.

4.1.1 The damaging effect of light on the retina

Light encoding by the retina underlies our visual perception by activating the phototransduction cascade in rods and cones. However, exposure to high light doses leads to irreversible retinal damage. It has been known for centuries that looking at the Sun damages the retina, and the prevailing explanation was that the absorption of light leads to a rise in retinal temperature and subsequent tissue disruption [211]. However, a landmark paper by Noell et al. [209] brought about a shift in this hypothesis. They determined that retinal damage occurred at light levels unable to induce a significant change in the retinal temperature, therefore providing the basis for research into other mechanisms [209]. Subsequent studies led ultimately to the discovery that the primary factor initiating retinal damage upon exposure to light within the intensity range of natural light, is the activation of photoreceptors themselves, through a process termed photochemical damage [211].

The mechanisms of retinal light damage have been studied by investigating the spectral sensitivity of this phenomenon. Noell et al. [209] found that the rat retina was more susceptible to green than blue or red light. As the rods are most sensitive to green light with peak absorption at 498 nm [212], this report suggested that rhodopsin plays an essential role in mediating damage induction [209]. However, there have been a limited number of studies confirming this hypothesis [213]. Instead, subsequent work has suggested that short wavelength light in the UV and violet spectrum causes more damage in various animal species, including primates [214] and rodents [215]. A review of all retinal light damage action spectra identified only one other report confirming the action spectrum hypothesised by Noell et al., yet 16 studies demonstrating that the extent of retinal damage was inversely correlated with the wavelength of light, with UV and blue light causing the most severe retinal

damage [213]. The phenomenon of short wavelength light mediating most severe retinal damage is often referred to as the "blue light hazard" [213].

Blue light is also known to be the most damaging spectrum of visible light to the RPE due to the accumulation of the metabolite lipofuscin in the RPE cells [216]. This phenomenon has been studied in the context of cataract surgery, which involves replacing the opacified natural lens of the eye with an artificial one. For example, it has been shown that artificial lenses that block blue light decrease the light-induced apoptosis of RPE cells in response to blue [217] and white light [218]. In addition, the levels of VEGF, which are detrimental to the progression of AMD, were reduced with a blue light blocking lens [218]. These results highlight some of the potential benefits of reducing blue light exposure to the RPE.

Although the short wavelength light is most damaging to the retina, the process is nevertheless mediated largely by the stimulation of rod phototransduction and the visual cycle. Evidence supporting this comes from studies demonstrating that slowing the visual cycle reduces retinal susceptibility to light damage. For instance, mice under halothane anaesthesia are resistant to light damage as halothane competes with 11-*cis*-retinal for its binding site in the rhodopsin molecule, preventing the regeneration of rhodopsin [219, 220]. Additionally, damage cannot be induced in mice without functional visual cycle components, e.g. RPE65 or LRAT [220]. The overstimulation of the phototransduction cascade also exacerbates retinal damage. For example, it has been shown that the knock-out of arrestins and rhodopsin kinases, which result in the photoreceptors being constantly hyperpolarised, lead to an increased susceptibility to light damage [221, 222].

It may seem controversial how rhodopsin with peak sensitivity at 498 nm could mediate light damage with peak spectral sensitivity in the UV light spectrum. Two mechanisms can explain this phenomenon; the first involves the properties of all-*trans*-retinal [223]. Upon absorption of light and the isomerisation of 11-*cis*-retinal to all-*trans*-retinal, the all-*trans*-retinal molecule remains attached to the photoactivated opsin. All-*trans*-retinal is an aldehyde, and therefore, it has to be reduced to prevent it from damaging the surrounding molecules. However, if the

opsin molecule binds a new molecule of 11-*cis*-retinal before the reduction event occurs, all-*trans*-retinal is released to the photoreceptor disk membrane. The faster the visual cycle and the regeneration of 11-*cis*-retinal, the more readily this event occurs. Free all-*trans*-retinal is damaging because of its properties as an aldehyde and also because it can be further photoactivated by short wavelength light. In its photoactivated state, the all-*trans*-retinal molecule reacts readily with oxygen and mediates the production of singlet oxygen, superoxide radicals and other reactive oxygen species (ROS), which cause oxidative damage [223]. The photoreceptor outer segments contain a large amount of cell membranes, making them particularly susceptible to oxidative damage. The impact of free radicals on polyunsaturated fatty acids induces a chain reaction of lipid peroxidation, ultimately leading to the breakdown of cell membranes [223].

The second mechanism behind the increased retinal damage susceptibility to shorter wavelength light involves the regeneration of rhodopsin. When rhodopsin is activated, it undergoes a conformational change, shifting its spectral sensitivity to a peak sensitivity in the blue light range. This form of rhodopsin can be converted back to the active conformation by binding a molecule of 11-*cis*-retinal, but also by absorbing blue, but not green light in a process termed photoreversal [224]. Evidence supporting this mechanism came from studies showing that when the rodents were under halothane anaesthesia, and thus the regeneration of rhodopsin through the visual cycle was blocked, blue light was still able to damage the retina [220]. However, the extent of damage was smaller when anaesthesia was induced with halothane than with ketamine/xylazine [220]. When animals anaesthetised with halothane were exposed to a low-level green light for one hour before exposure to blue light, there was no resulting light damage [220]. Prior green light exposure under halothane anaesthesia bleached the rhodopsin molecule such that it was no longer able to undergo photoreversal by blue light [220]. Therefore, light in the short wavelength spectrum is most damaging to the retina, and this phenomenon is mediated at least in part by rhodopsin activation and subsequent regeneration.

4.1.2 The protective effect of light on the retina

Retinas are protected from light-induced damage by inherent adaptive mechanisms. For example, animals exposed to a bright light pulse, which itself was unable to cause damage, were more resistant to a damaging light pulse administered two days later [210]. This protective effect was characterised by an induction of the retinoprotective factors basic fibroblast growth factor (bFGF) and ciliary neurotrophic factor (CNTF) [210]. These results suggest that exposure to bright light induces parallel retinoprotective mechanisms, which counteract its potential harmful effect.

In addition to a prior bright light exposure, light damage susceptibility is also affected by the light environment where animals are reared. The retinas of rats raised at higher light levels were more resistant to damaging light pulses than rats raised at lower ambient light levels [225]. Furthermore, higher environmental light levels led to an increase in retinal antioxidative enzymes and antioxidants [225], reduced levels of rhodopsin, and a decreased number of photoreceptors [226]. In addition to preconditioning the retina to the potentially damaging effect of bright light, this adaptation allows the retinas of animals raised in different conditions to capture a similar number of photons over a day and is termed photostasis [226].

In conclusion, light absorption by the photoreceptors leads to the activation of phototransduction and the visual cycle, which are inherently damaging to the retina, but also to the induction of retinoprotective mechanisms. The balance between these two processes determines whether light exposure results in retinal damage.

4.1.3 The potential role for melanopsin in retinal protection

Retinal light adaptation

The exact mechanisms leading to the adaptive changes in the retina remain unknown. The slow activation and deactivation kinetics of melanopsin make it well-adjusted to encoding light levels over a wide range of irradiances [24, 45] (discussed previously in section 1.2.1), and melanopsin phototransduction is responsible for signalling the environmental light levels to the central circadian clock [32, 33].

In line with melanopsin's role as a circadian regulator, the molecule has also been shown to adapt local retinal light responses to environmental illumination. In particular, the lack of melanopsin stimulation results in the loss of cone ERG light adaptation in WT animals [192]. Another light-adaptation phenomenon regulated by melanopsin is the information flow rate in the RGCs of the optic nerve. Namely, higher retinal illumination leads to an increased firing rate of the RGCs, corresponding to the higher amount of light information processed by the retina. However, this increase is absent in *Opn4*$^{-/-}$ animals but can be induced by chemogenetic activation of pRGCs [78]. Together, these data indicate that the presence of melanopsin in the retina is crucial for encoding the environmental light intensity. Since encoding light history underlies the regulation of retinoprotective mechanisms, the induction of retinoprotective factors may be aberrant in the absence of melanopsin and may increase the susceptibility to retinal light damage.

Retinal PACAP

The potential retinoprotective role of melanopsin may be related to the neuropeptide PACAP, as its retinal expression is confined to the pRGCs [54]. PACAP is released together with glutamate from the pRGC axon terminals, and its release is dependent on melanopsin signalling. This finding is supported by work investigating the pupillary light reflex as the activation of rods and cones leads preferentially to the release of glutamate, whereas melanopsin signalling results in the release of PACAP [83]. Little is known about the release of PACAP locally in the retina. However, PACAP is protective in various models of retinal diseases, e.g. optic nerve injury and UV-A induced retinal damage [227]. Therefore, it is possible that PACAP release can occur locally in the retina, and the local control of PACAP release in the retina may be controlled similarly to its release in the central nervous system and provide a protective mechanism against retinal damage.

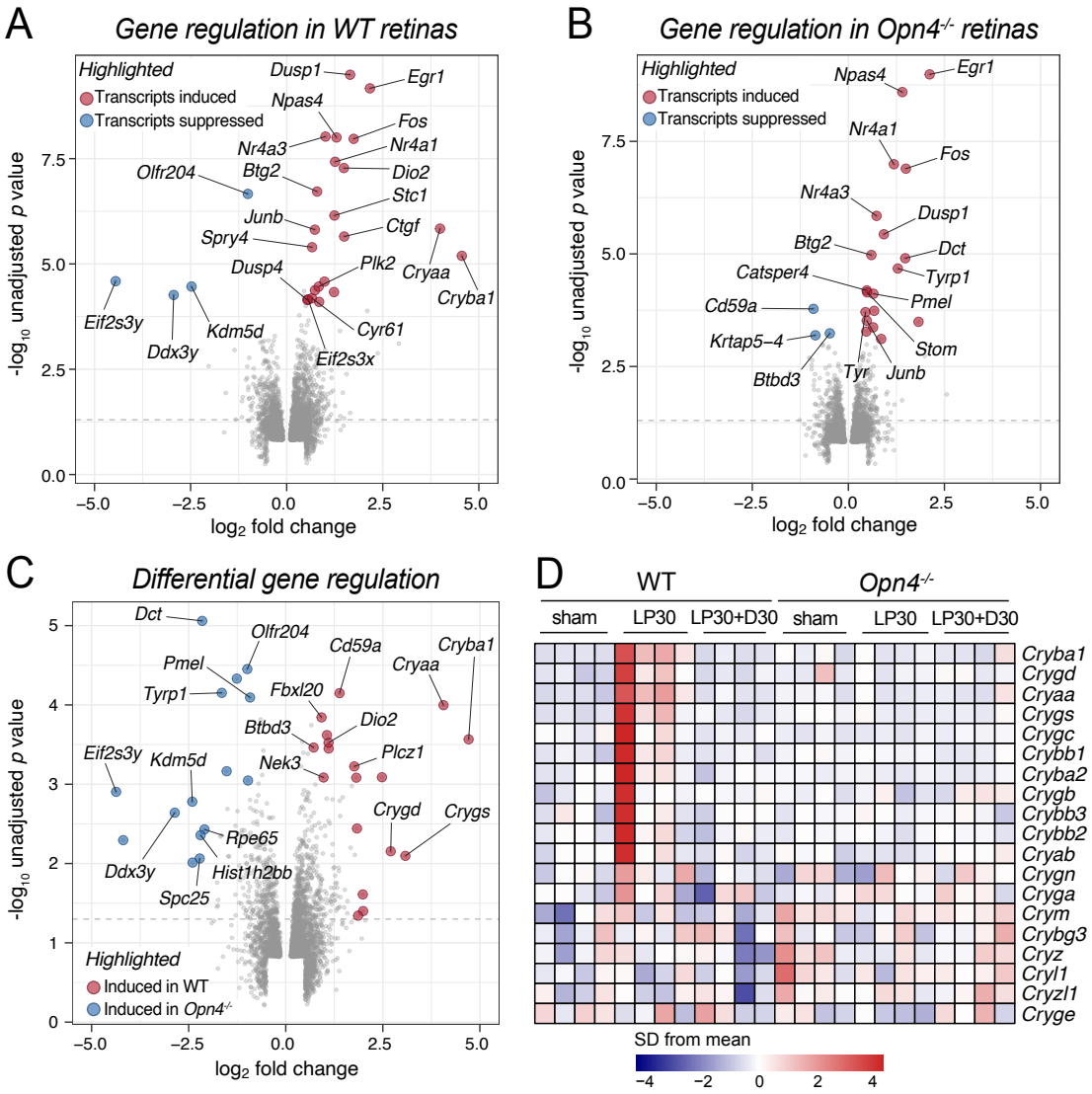


Figure 4.1: Light-induced transcriptome changes in WT and *Opn4*$^{-/-}$ retinas. All these data were acquired by Assoc. Prof. Aarti Jagannath. Gene regulation in response to a CT16 30-minute 400 lux white light pulse in WT (A) and *Opn4*$^{-/-}$ retinas (B) measured with microarrays. (C) The genes differentially regulated between the genotypes. (D) The expression of crystallins in individual samples of the microarray experiment. Transcript levels in WT and *Opn4*$^{-/-}$ retinas after the 30-minute light pulse (LP30) and after an additional 30 minutes in the darkness (LP30+D30). The gene expression values in (D) are normalised across rows.

Retinal crystallins

Another suggestion of a potential retinoprotective role of melanopsin came from a microarray study conducted by my supervisor Assoc. Prof. Aarti Jagannath before I joined her research group. WT and *Opn4*$^{-/-}$ animals were exposed to a 30-minute 400

lux white light pulse at their relative night at CT16, and their retinal gene expression dynamics were examined using microarrays. She found that the light pulse led to the induction of several transcripts in both genotypes, alongside the expected light-induced genes, e.g. *Fos*, *Egr1*, neuronal PAS domain-containing protein 4 (*Npas4*), nuclear receptor 4A1 (*Nr4a1*) and *Dio2* (Fig. 4.1A, B). Differential gene expression analysis found that the most significantly differentially regulated genes were several crystallins, which were upregulated in response to light exposure in WT, but not in *Opn4*$^{-/-}$ retinas (Fig. 4.1C). The finding was even more significant given that the light dose received by *Opn4*$^{-/-}$ retinas was almost five times higher as their pupil constriction was not sustained (see Table 3.1 in chapter 3). Indeed, analysing the individual gene expression values of each retinal sample showed that the crystallins as a gene family were upregulated in WT retinas after a 30-minute light pulse and their levels dropped after keeping the animals in the darkness for an additional 30 minutes (Fig. 4.1D). This upregulation was absent in *Opn4*$^{-/-}$ retinas.

Retinal crystallins are exciting candidates for mediating melanopsin's role in retinoprotection. Structurally, crystallins can be divided into two families. The α-crystallins are small heat shock proteins, induced by cellular stress and act to prevent the aggregation of damaged proteins [228]. The β- and γ-crystallins belong to a superfamily of structural proteins with a yet unknown function [228]. The α-, β- and γ-crystallins are all induced in the photoreceptors and the GCL in response to a bright light pulse (1000-1500 lux) [229, 230]. In addition, it has been shown that the absence of α-crystallins leads to increased retinal susceptibility to chemically induced hypoxia in mice [231]. There is also evidence of crystallins playing a role in human retinal degenerations, particularly in AMD as the levels of α-crystallins are elevated in AMD retinas [232]. In conclusion, crystallins are upregulated in human and murine retinas undergoing degenerative changes, and their absence leads to a higher susceptibility to retinal damage, suggestive of their neuroprotective properties.

At the start of my DPhil, I aimed to validate the finding that melanopsin controls the induction of retinal crystallins. Similarly to the microarray experiment, I exposed WT and *Opn4*$^{-/-}$ mice to a 30-minute 400 lux white light pulse at CT16 and

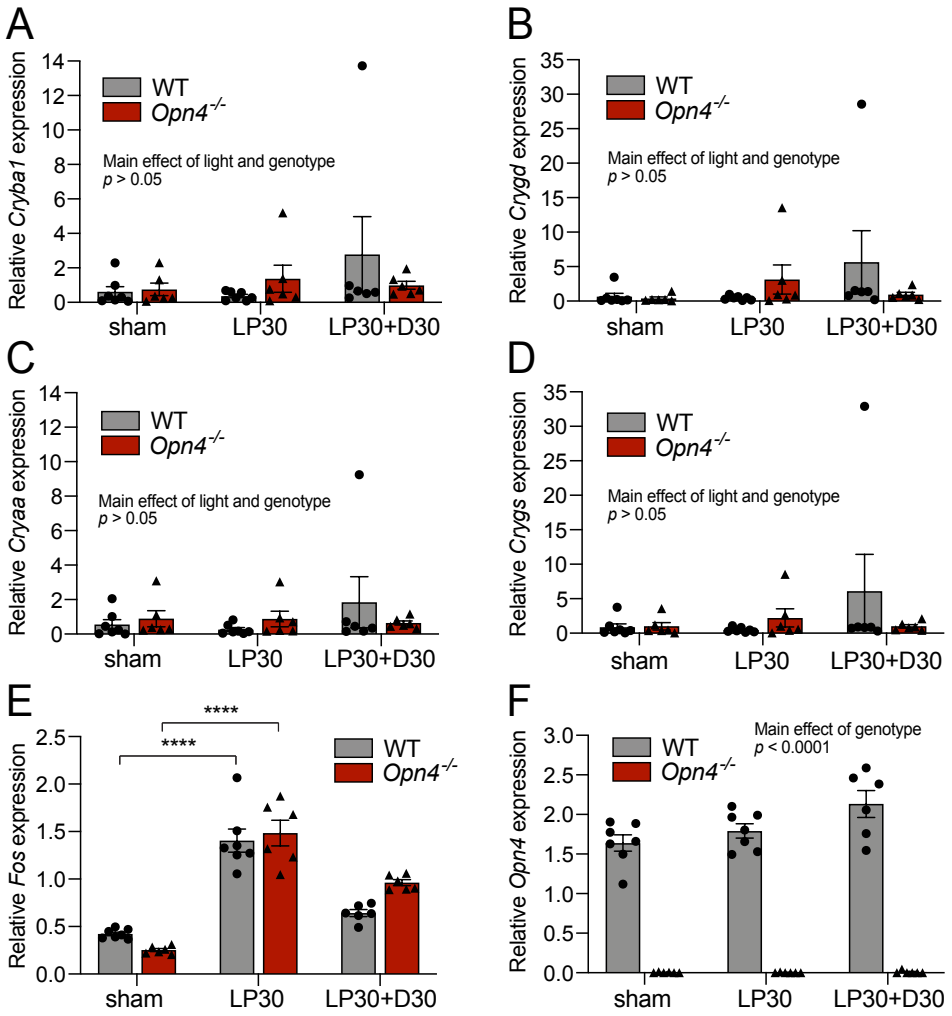


Figure 4.2: Light-induced expression of retinal crystallin genes. Expression of *Cryba1* (A), *Crygd* (B), *Cryaa* (C), *Crygs* (D) measured with RT-qPCR in WT and *Opn4*$^{-/-}$ retinas after a 30-minute light pulse (LP30) and after an additional 30 minutes in the darkness (LP30+D30). The expression of *Fos* (E) and *Opn4* (F). Data are mean ± SEM, n = 6-7. Statistical analysis was performed using two-way ANOVA with Šidák's correction for multiple comparisons. n.s., not significant, **** $p < 0.0001$.

measured the levels of crystallin transcripts with RT-qPCR. Intriguingly, however, I did not see an increase in retinal crystallin expression in WT nor *Opn4*$^{-/-}$ retinas (Fig. 4.2A-D). I also quantified the induction of *Fos*, and saw an increase in its expression in the retinas of both genotypes (Fig. 4.2E), assuring that these animals did receive a light pulse. Additionally, I quantified the levels of *Opn4* transcript and confirmed that the mice were of the correct genotypes (Fig. 4.2F). There was marked variability in crystallin expression levels, and other authors have also noted

that the crystallin levels show considerable variability in individual retinas [230, 233]. This inherent variability may be one reason my results were not in agreement with the results of Assoc. Prof. Jagannath. However, the 400 lux light pulse is multiple times lower than a light pulse able to induce retinal damage, and a brighter light pulse may thus result in a more significant upregulation of these transcripts.

4.2 Aims of this chapter

Retinal light exposure leads to an induction of factors that protect the tissue from the damaging effect of bright light stimuli. Several lines of evidence suggest that this effect could be mediated by melanopsin since it is suited for irradiance encoding and mediates several processes of retinal light adaptation. Additionally, as the release of PACAP in pRGC brain targets is mediated by melanopsin activation, melanopsin signalling could similarly control the local release of PACAP. There is also conflicting evidence of melanopsin-regulated induction of retinal crystallins. However, should melanopsin indeed regulate light-induced crystallin upregulation and the release of PACAP, retinas lacking melanopsin would be less able to upregulate protective factors in response to a bright light pulse and would thus be more susceptible to retinal light damage. Therefore, to resolve whether melanopsin signalling is responsible for the activation of retinoprotective mechanisms, I decided to examine the susceptibility of WT and *Opn4*$^{-/-}$ retinas to light-induced damage.

With this in mind, the experimental aims of this chapter are to:

1) Characterise the visual and retinal function of WT and *Opn4*$^{-/-}$ animals after bright light exposure

2) Characterise the retinal morphology of WT and *Opn4*$^{-/-}$ animals after bright light exposure

3) Characterise the melanopsin-mediated induction of retinal genes and pathways in response to bright light exposure

4.3 Results

4.3.1 The retinal and visual functions of *Opn4*$^{-/-}$ mice show a transient decline after exposure to a 10,000 lux light pulse

To evaluate the contribution of melanopsin to retinal light damage susceptibility, I first had to consider what light pulse intensity and duration would be the most optimal for these experiments. *Opn4*$^{-/-}$ animals are pigmented mice maintained as an inbred colony on a mixed C57BL/6J x 129 genetic background. The light damage protocols vary vastly between albino and pigmented mice as the latter are significantly more resistant to light damage [160]. One factor conferring retinoprotection is a mutation in the *Rpe65* gene. Some pigmented strains, particularly the C57BL/6J mice, express the RPE65 Leu450Met variant, which leads to reduced levels of RPE65 and slower isomerase activity, ultimately resulting in a slower regeneration of 11-*cis*-retinal in the visual cycle and lower susceptibility to light damage [160]. Surprisingly, mice in our *Opn4*$^{-/-}$ colony were homozygous for the normal *Rpe65* variant native to the 129 genetic background, suggesting they would be more susceptible to light damage than animals on a pure C57BL/6J genetic background.

Pathological variants of RPE65 are known to cause inherited retinal degenerations, including Leber congenital amaurosis (LCA) and retinitis pigmentosa (RP). Several disease-causing RPE65 variants show a reduced isomerase activity [234], which may seem to conflict the finding that the RPE65 Leu450Met variant with a lower isomerase activity, is conferring protection from light damage. The human disease develops under light levels that are physiological to the human retina, while in the mouse model of light damage, the light intensity the animals are exposed to is much higher than the physiological light levels for the nocturnal mice. A slower visual cycle may perhaps only be beneficial at light levels substantially higher than physiological for the species. Furthermore, the retinal morphology of mice carrying the RPE65 Leu450Met variant is not compromised [160], but to my knowledge, the effect of this variant has not been studied in aged mice.

While in albino mice, retinas are damaged already by a 20-minute 5,000 lux light pulse [160], the light doses used for pigmented mice range between an 18,000 lux pulse for 6 hours [235] up to a 70,000 lux pulse for 50 hours [236], which made it difficult to predict the most suitable light dose. In addition, the document governing animal procedures in our research group dictated that the maximum light exposure we could use was a 3-hour 10,000 lux pulse. As this is considerably lower than the protocols used by many other groups, it seemed unlikely to cause retinal damage. Furthermore, bright light pulses are usually administered after dilating animals' pupils, which was unfortunately not allowed under our animal licence. Nevertheless, I decided to explore the light damage susceptibility of WT and *Opn4*$^{-/-}$ mice.

I first tested the susceptibility of WT and *Opn4*$^{-/-}$ retinas to light damage by exposing the mice to a 10,000 lux light pulse for 3 hours at night between ZT15-18. The rationale for selecting this time point was threefold. First, the experiment showing upregulation of crystallins in WT, but not *Opn4*$^{-/-}$ retinas was done at night. Therefore, to look for a potential functional outcome of this finding, I decided to use similar timing for the light damage experiments. Second, the retina is more susceptible to damage at night [158]. Since the light dose was relatively low, performing the experiment at night increased the possibility of inducing retinal distress. Third, the maximum short-term pupil constriction differs between WT and *Opn4*$^{-/-}$ animals at day, but not at night (Fig. 3.1). Since I could not apply mydriatics before the bright light exposure, the pupil constriction dynamics would potentially minimise differences in the light doses. Crucially, however, I had not studied the sustained pupil response to a bright light pulse before conducting these experiments.

I used a within-subjects experimental design where I assessed the retinal and visual functions at baseline, i.e. before bright light exposure, and at several time points after the light pulse. I used pupillary light response as a measure of retinal function, and two behavioural tasks, the optomotor response and a novel visuospatial context recognition task, to measure visual function. All testing was done during the light phase between ZT4-ZT8, and I was masked to animals' genotypes when conducting the experiments and at data analysis. After completing the retinal and

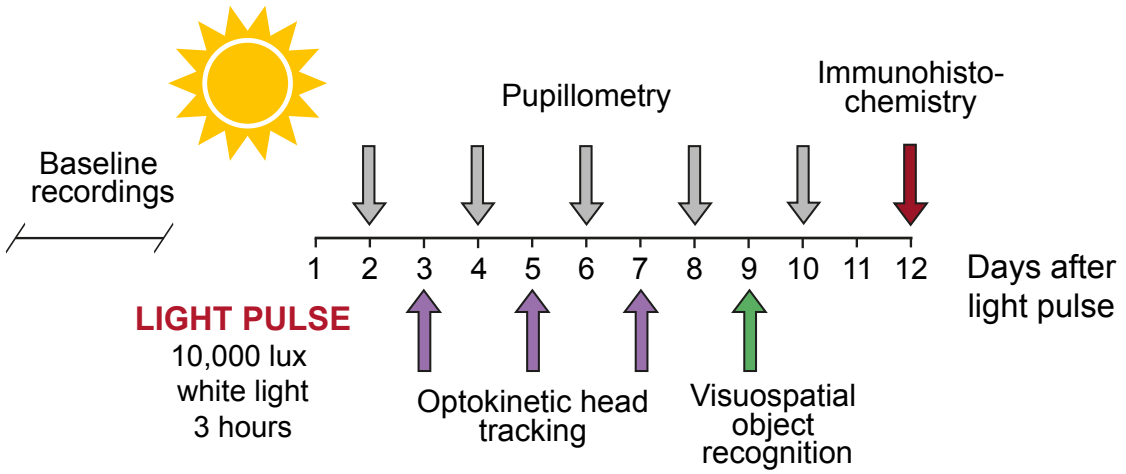


Figure 4.3: Timeline of the retinal light damage experiment. After baseline recordings of pupillometry, optomotor response and the visuospatial context recognition task, mice were exposed to a 3-hour 10,000 lux white light pulse at ZT15-18. Visual and retinal function was followed up with the same three tests over 10 days, and retinas were harvested for immunohistochemical analysis 12 days after bright light exposure.

visual assessments, the retinas were collected for immunohistochemical analysis 12 days after bright light exposure (see Fig. 4.3 for the timeline of the experiment).

At baseline, the maximum pupil constriction of WT and *Opn4*$^{-/-}$ animals differed significantly, as expected [82]. The pupils of WT animals constricted to 5.4% of the initial dark-adapted pupil area, while the pupils of *Opn4*$^{-/-}$ animals to only 8.5% ($p < 0.0001$, two-tailed t-test, Fig. 4.4). After bright light exposure, there were no changes in the maximum pupil constriction of WT animals on any of the days tested (Fig. 4.4B). However, *Opn4*$^{-/-}$ mice developed an additional pupil constriction deficit, and their maximum pupil constriction reached around 12% of initial pupil area after bright light exposure (Fig. 4.4B). This deficit was not statistically significant 10 days after bright light exposure, potentially because not all mice were followed up for the full 10 days, resulting in fewer replicates. This finding could also indicate a slight recovery of retinal function. The additional attenuation of maximum pupil constriction in *Opn4*$^{-/-}$ mice suggested that bright light exposure resulted in retinal deficits in these animals, which were potentially transient.

I also assessed whether bright light exposure affected the visual function of WT and *Opn4*$^{-/-}$ mice. To this end, I measured their optomotor response to square-wave

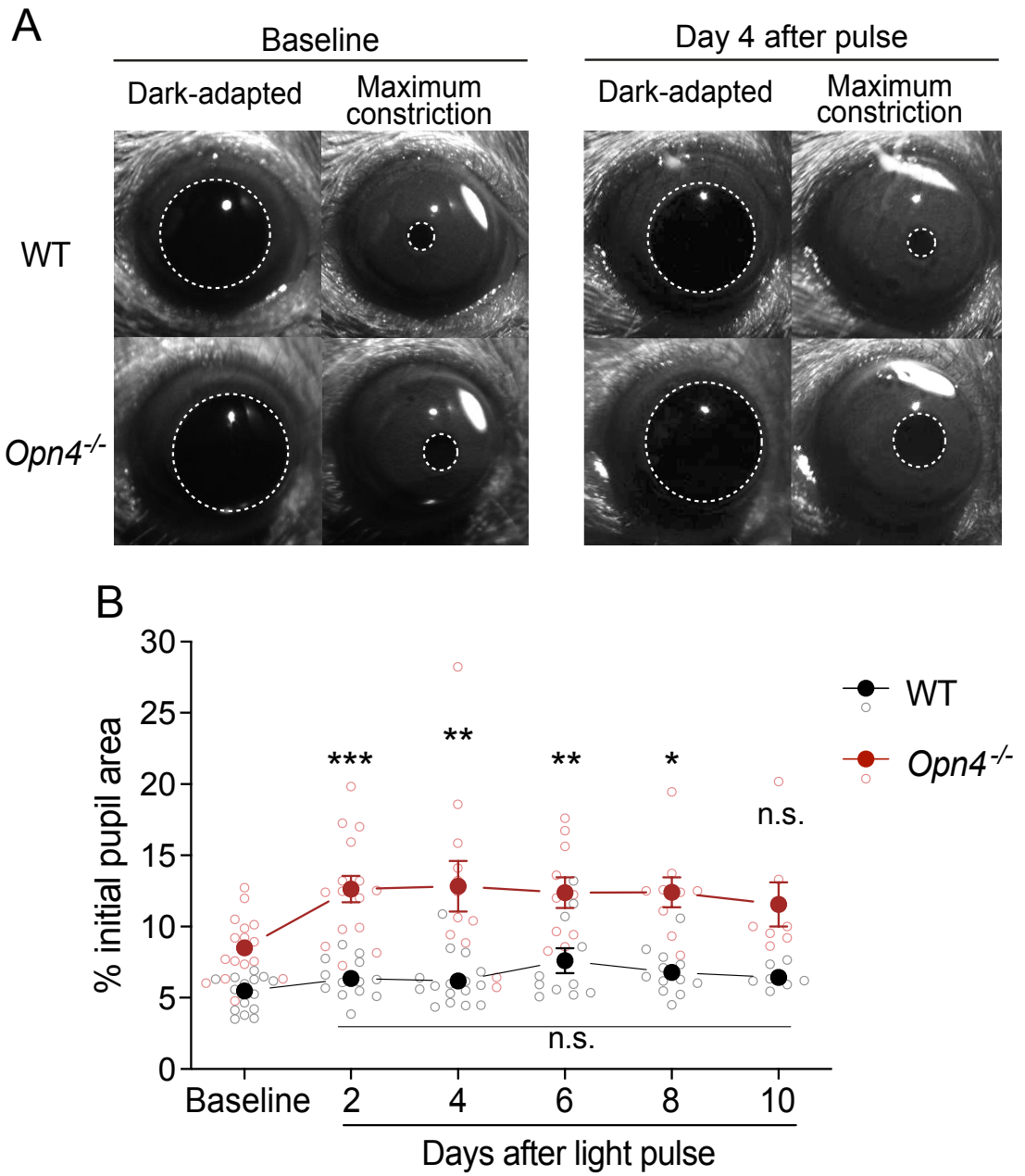


Figure 4.4: Maximum pupil constriction before and after bright light exposure. (A) Representative images of pupils before (dark-adapted) and at the end of a 10-second light pulse (maximum constriction) at baseline and 4 days after bright light exposure. Dotted lines mark the pupil edge and were used to calculate pupil constriction, which is expressed as the pupil area percentage of the initial dark-adapted pupil area. (B) Maximum pupil constriction at baseline and after bright light exposure in WT and *Opn4*$^{-/-}$ mice. Data are mean ± SEM, n = 7-16. Statistical analysis was performed using two-way ANOVA with Šidák's correction for multiple comparisons, pupil constriction after bright light exposure was compared to baseline values. * $p < 0.05$, ** $p < 0.01$, *** $p < 0.001$.

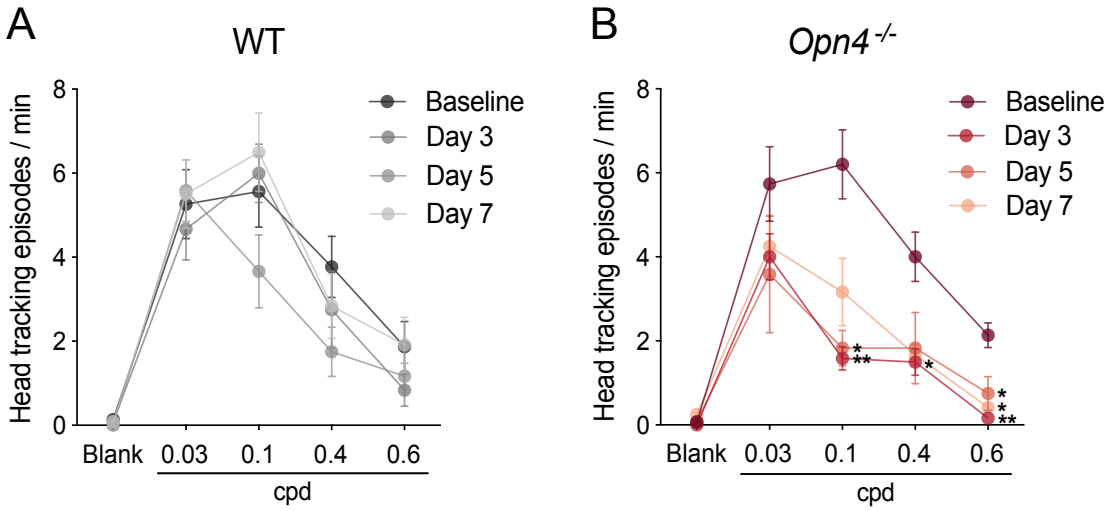


Figure 4.5: Optomotor response before and after bright light exposure. The number of head tracking episodes induced by moving gratings of different spatial frequencies in WT (A) and *Opn4*$^{-/-}$ animals (B) before and after bright light exposure. Data are mean ± SEM, n = 6. Statistical analysis was performed using two-way ANOVA with Šidák's correction for multiple comparisons, number of head tracking episodes are compared to baseline values. cpd, cycles per degree. * $p < 0.05$, ** $p < 0.01$.

gratings of different spatial frequencies (0.03, 0.1, 0.4, and 0.6 cycles per degree, cpd) by counting how many times the mice tracked the rotating stimuli. Before bright light exposure, both WT and *Opn4*$^{-/-}$ animals followed the gratings to a similar extent (Fig. 4.5). This result agrees with previously published data showing that the visual acuity of *Opn4*$^{-/-}$ animals does not differ from WT controls [237]. Both genotypes followed the 0.03 and 0.1 cpd gratings the most, aligning roughly with other reports demonstrating that the peak visual acuity in mice is 0.17 cpd [238] or 0.128 cpd [133]. Consistent with the pupillary light response results, WT animals displayed no deficits in the optomotor task after bright light exposure as the number of times they followed the gratings was not different from baseline (Fig. 4.5A). However, *Opn4*$^{-/-}$ animals tracked the gratings less after bright light exposure (Fig. 4.5B). In particular, the number of times they tracked the 0.1 cpd gratings, corresponding to the peak visual acuity, was reduced. Interestingly, the number of head tracking episodes at this spatial frequency showed a slight recovery by day 7. These results suggested that the visual function of *Opn4*$^{-/-}$, but not WT animals was reduced after bright light exposure, and this reduction may have been transient.

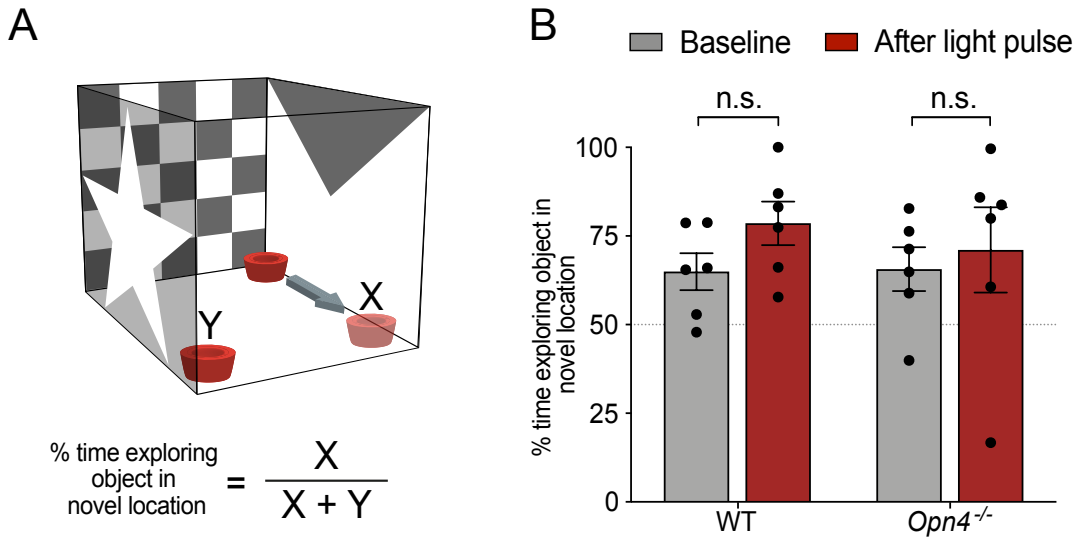


Figure 4.6: Novel visuospatial context recognition task performance before and after bright light exposure. (A) A schematic of the modified novel object recognition task. The time spent exploring the object in the novel location over the time spent exploring either object was determined. (B) The proportion of time animals spent exploring the object in the novel location before and after bright light exposure. Data are mean ± SEM, n = 6. Statistical analysis was performed using two-way ANOVA with Šidák's correction for multiple comparisons. n.s., not significant.

To further analyse the visual function of these animals, I used another behavioural test, the novel visuospatial context recognition task. It is a modified version of the novel object recognition task where the walls of a test arena are decorated, and the mouse is allowed to explore the arena with two identical objects placed in two corners. The mouse is removed from the arena, and the location of one of the objects is changed. The animal is then placed back into the arena and the proportion of time it spends exploring the object in the novel location is determined (Fig. 4.6A, [163]). Animals with an intact visual and cognitive function prefer to explore the object in the novel location [163].

At baseline, the WT animals spent more time exploring the object in novel visuospatial context than the object in the old context ($p < 0.05$, one sample t-test testing whether the novel location exploration rate is different from 50%, Fig. 4.6B). There was a strong trend in the same direction for *Opn4*$^{-/-}$ animals ($p = 0.0521$). Nine days after bright light exposure, mice from both genotypes displayed similar behaviour, having a preference for the object in the novel context (WT, $p < 0.05$;

Opn4$^{-/-}$, $p = 0.0514$; one-sample t-tests). There were no statistically significant differences in the exploration rate between WT and *Opn4*$^{-/-}$ mice at baseline or 9 days after bright light exposure (Fig. 4.6B). In conclusion, the performance of both WT and *Opn4*$^{-/-}$ animals in the novel visuospatial context recognition task was not affected by bright light exposure in the time frame tested, indicating their visual function and memory were sufficiently intact to recognise and remember the visual context of the objects.

4.3.2 Retinal morphology of WT and *Opn4*$^{-/-}$ mice is not affected by a 10,000 lux light pulse

The pupillometry and optomotor task results suggested that *Opn4*$^{-/-}$ mice may have developed photoreceptor stress and degeneration, which could have accounted for the deficits they exhibited after bright light exposure. To see whether the retinal and visual function changes were reflected in the retinal structure, I immunostained retinas harvested 12 days after bright light exposure for S-opsin and glial fibrillary acidic protein (GFAP), a protein upregulated in the Müller cells and astrocytes in response to retinal stress [239]. I imaged sections throughout the retinas and measured the ONL and INL thicknesses. The acute phase of retinal degeneration is characterised by the apoptosis of photoreceptors, manifested in the thinning of the ONL. Since the thickness of the retina varies across the tissue, but the ratio of different layers is similar, I normalised the ONL thickness to INL thickness as the second-order neurons are spared in the early stages of light damage. This method has also been used by other researchers [240, 241].

The analysis showed no statistically significant differences in the ONL/INL ratio between the control and light-damaged WT and *Opn4*$^{-/-}$ retinas (Fig. 4.7A, B). Some reports have shown that the superior retina is more susceptible to light damage than the inferior retina [242] and averaging the ONL/INL ratios across the entire retina may have diluted this effect. To get an approximate measure of whether there were dorsoventral differences in retinal morphology, I used the well-characterised expression gradient of S-opsin [173, 174] to classify the images of

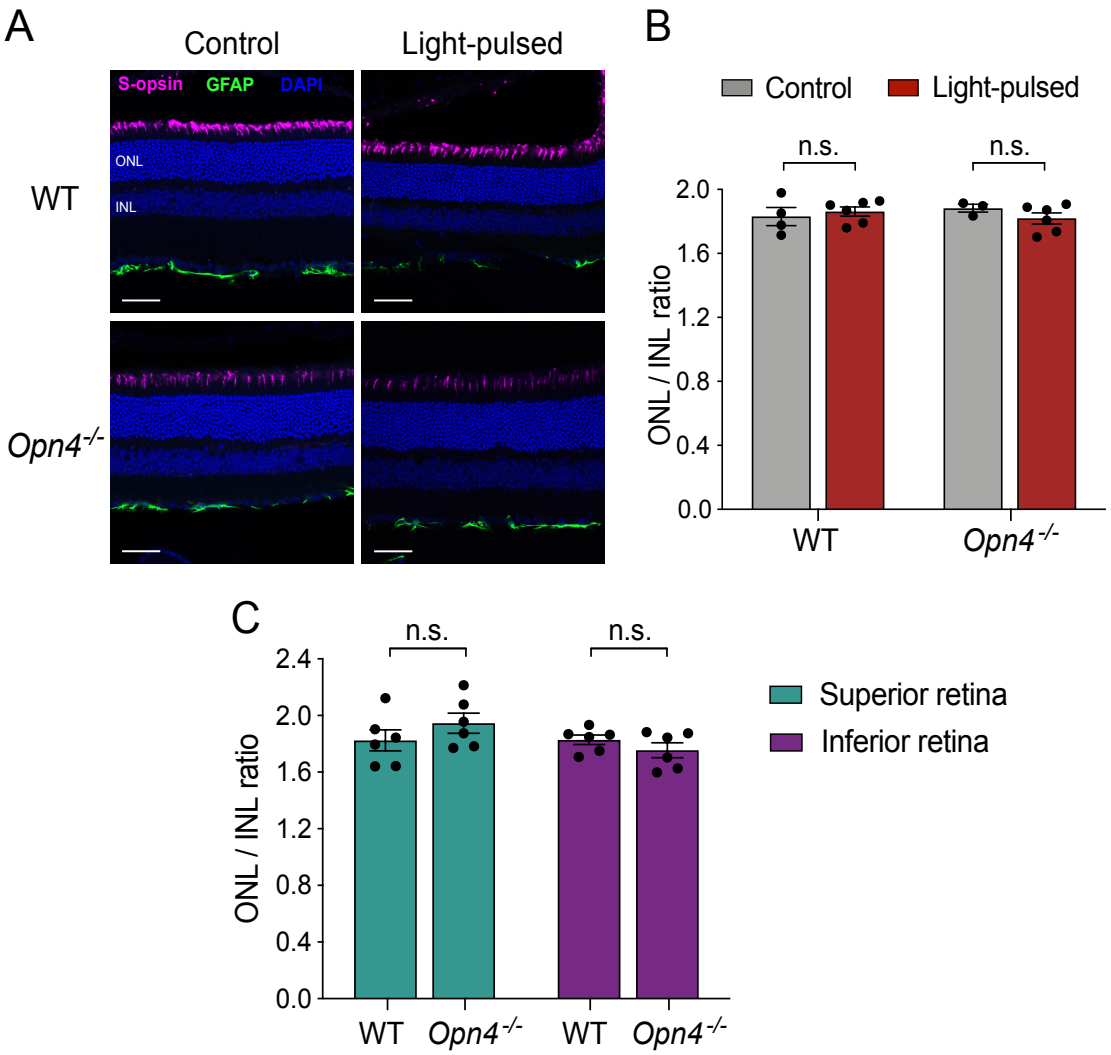


Figure 4.7: Immunohistochemical analysis of retinal morphology after a bright light exposure. (A) Representative images of WT and *Opn4*$^{-/-}$ retinas stained for GFAP, S-opsin and DAPI. (B) The ONL/INL thickness ratio across retinal sections (n = 3-6 retinas with 10-16 sections). (C) Quantification of the ONL/INL ratio in light-pulsed retinas from sections belonging to the superior and inferior retinas, determined by the expression of S-opsin (n = 6 retinas with 4-10 sections). Data are mean ± SEM. Statistical analysis was performed using two-way ANOVA with Šidák's correction for multiple comparisons. ONL, outer nuclear layer; INL, inner nuclear layer; n.s., not significant. Scale bars 50 μm.

all retinal cross-sections as superior or inferior, depending on whether the expression of S-opsin was low or high, respectively. I found no differences in the ONL/INL ratios of superior and inferior retinas between the two genotypes (Fig. 4.7C). In addition, the levels of GFAP immunostaining were not noticeably different between WT and *Opn4*$^{-/-}$ retinas, and the signal was restricted to the innermost portions of the Müller cells, or their endfeet (Fig. 4.7A), which does not suggest Müller cell activation. Therefore, I did not see any retinal degeneration, but I may have missed subtle focal damage since I averaged the measurements across multiple sections.

In conclusion, *Opn4*$^{-/-}$, but not WT animals developed a deficit in maximum pupil constriction and optomotor response after exposure to a bright light pulse, both of which showed a trend toward recovery between 7-10 days after the pulse. There were no defects in the novel visuospatial context recognition task. Additionally, there were no indications of ONL thinning, and therefore, retinal degeneration, in WT or *Opn4*$^{-/-}$ retinas 12 days after the bright light exposure. Overall, these results suggest *Opn4*$^{-/-}$ mice developed a transient functional deficit of the retina rather than permanent damage.

4.3.3 The pupils of *Opn4*$^{-/-}$ mice redilate when exposed to a 10,000 lux light pulse

For the experiments presented above, I did not dilate the animals' pupils before bright light exposure. However, there are indications in the literature [83] as well as in the previous chapter of my thesis (Fig. 3.20) that pupil constriction of *Opn4*$^{-/-}$ animals is not always sustained. Since the pupil constriction dynamics of *Opn4*$^{-/-}$ mice to a bright nocturnal light pulse had not been studied, I exposed another cohort of WT and *Opn4*$^{-/-}$ animals to the same 10,000 lux light pulse at ZT15 and measured the size of their pupils over three hours.

The pupils of WT animals constricted to approximately 5% of the initial pupil area and remained constricted for the entire 3-hour period (Fig. 4.8). Remarkably, the pupils of *Opn4*$^{-/-}$ mice, which constricted initially to approximately 12% of dark-adapted pupil area, exhibited a rapid re-dilation. After 5 minutes, their pupils

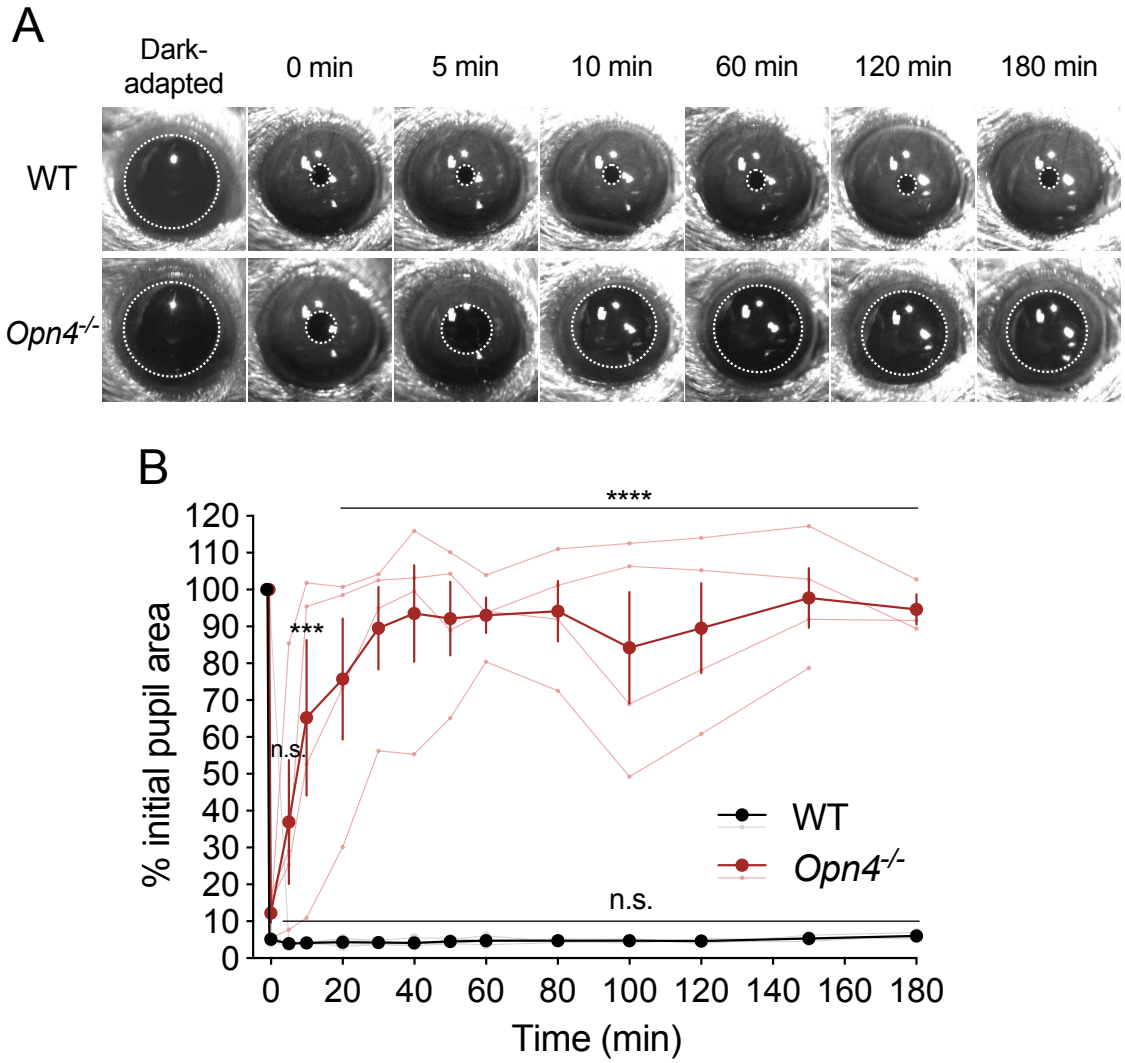


Figure 4.8: Pupil constriction dynamics in response to a sustained 10,000 lux light pulse. (A) Representative images of WT and *Opn4*$^{-/-}$ pupils during a 3-hour 10,000 lux light pulse. (B) Pupil constriction dynamics of WT and *Opn4*$^{-/-}$ animals. Data are mean ± SEM with individual values depicted by pale lines, n = 4. Statistical analysis was performed using two-way ANOVA with Šidák's correction for multiple comparisons, comparing pupil area to the initial maximum pupil constriction. n.s., not significant, *** $p < 0.001$, **** $p < 0.0001$.

were constricted to only approximately 35% of the dark-adapted pupil area, and by 30 minutes their pupils were almost fully dilated. The pupil dilation would have resulted in significant differences in the retinal light doses WT and *Opn4*$^{-/-}$ animals received in the previous experiment. To determine the light dose difference, I calculated the area under the pupil constriction function curves (Fig. 4.8) and determined that the light dose received by *Opn4*$^{-/-}$ retinas was approximately 18 times higher (total area under curve WT 865, *Opn4*$^{-/-}$ 15,768). Therefore, the results of the previous experiment comparing the retinal and visual function of WT and *Opn4*$^{-/-}$ animals after a bright light pulse, are difficult to interpret.

4.3.4 WT mice develop retinal degeneration upon exposure to a 3-hour light pulse of 20,000 lux

The results presented above highlighted the need to dilate the animals' pupils for the duration of the light pulse to deliver an equal light dose to WT and *Opn4*$^{-/-}$ retinas. Therefore, we amended the animal licence to allow the administration of mydriatics. In addition, the highest light dose we could use was increased to a 6-hour 20,000 lux light pulse. However, it was still unclear what the optimal light dose was, especially as the 10,000 lux light pulse did not cause any detectable long-term damage in *Opn4*$^{-/-}$ retinas despite their pupils being almost fully dilated throughout the light pulse.

Therefore, to determine the most suitable light pulse parameters, I exposed WT animals from the same mouse colony to a 20,000 lux light pulse of different durations ranging from 90 minutes to 6 hours with pupil dilation applied. As in the previous experiments, I administered the light pulse at night and kept the mid-point of the pulse at midnight at ZT18. To quantify any potential retinal damage, I harvested the eyes 7 days later and analysed them for photoreceptor and pro-inflammatory gene expression and retinal thickness. Should the retinal photoreceptors degenerate, the levels of visual opsins would decrease, retinas would become thinner, and the degeneration would be complemented by an inflammatory response.

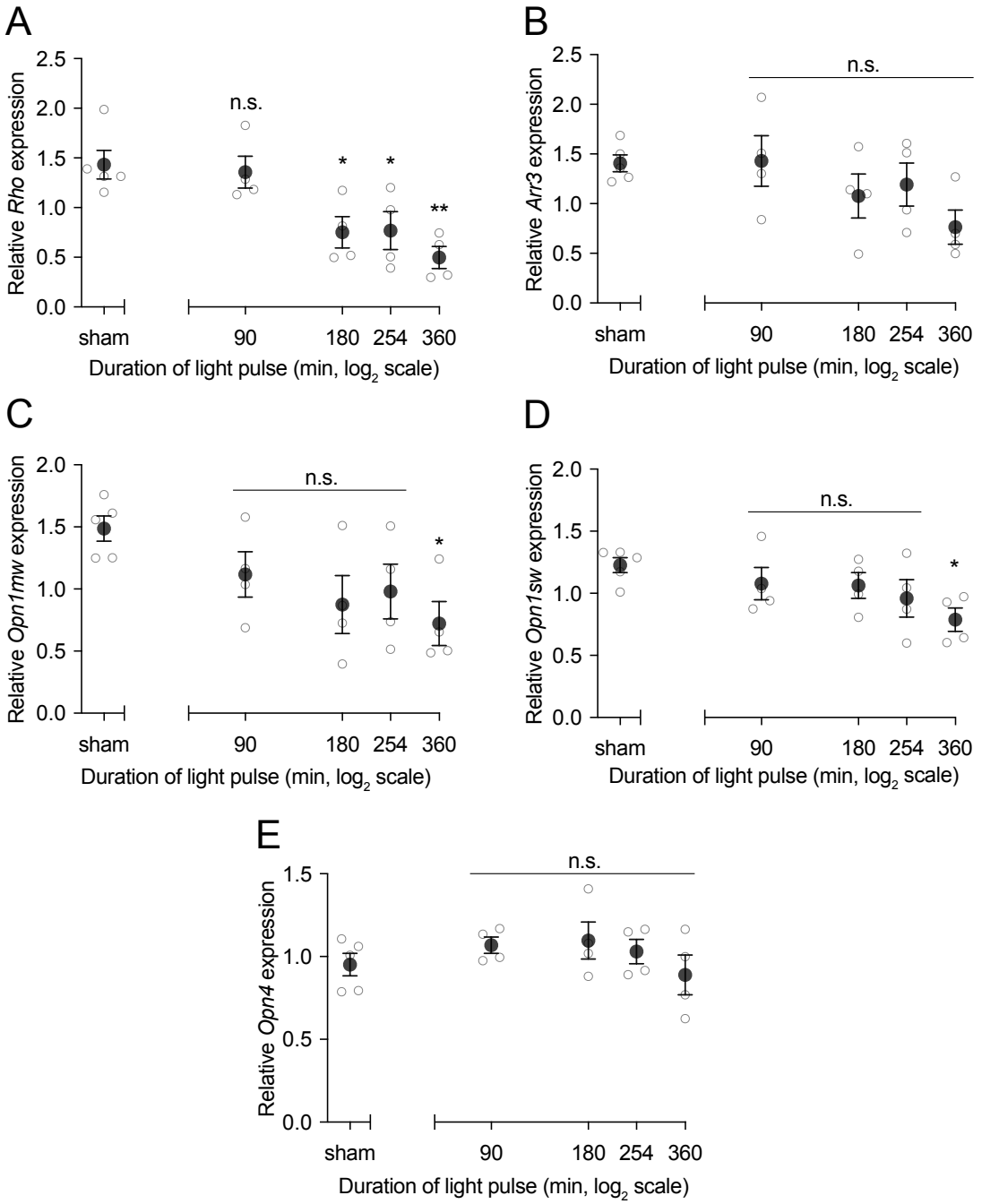


Figure 4.9: Expression of photoreceptor genes after exposure to 20,000 lux light pulses. Expression of rhodopsin (A), cone arrestin (B), M-opsin (C), S-opsin (D), and melanopsin (E) in the eyes of sham-treated mice and of those exposed to a 20,000 lux light pulse of different durations with prior pupil dilation. Data are mean ± SEM, n = 4-5. Statistical analysis was performed using one-way ANOVA with Dunnett's correction for multiple comparisons, expression values were compared to those of sham-treated eyes. n.s., not significant, * $p < 0.05$, ** $p < 0.01$.

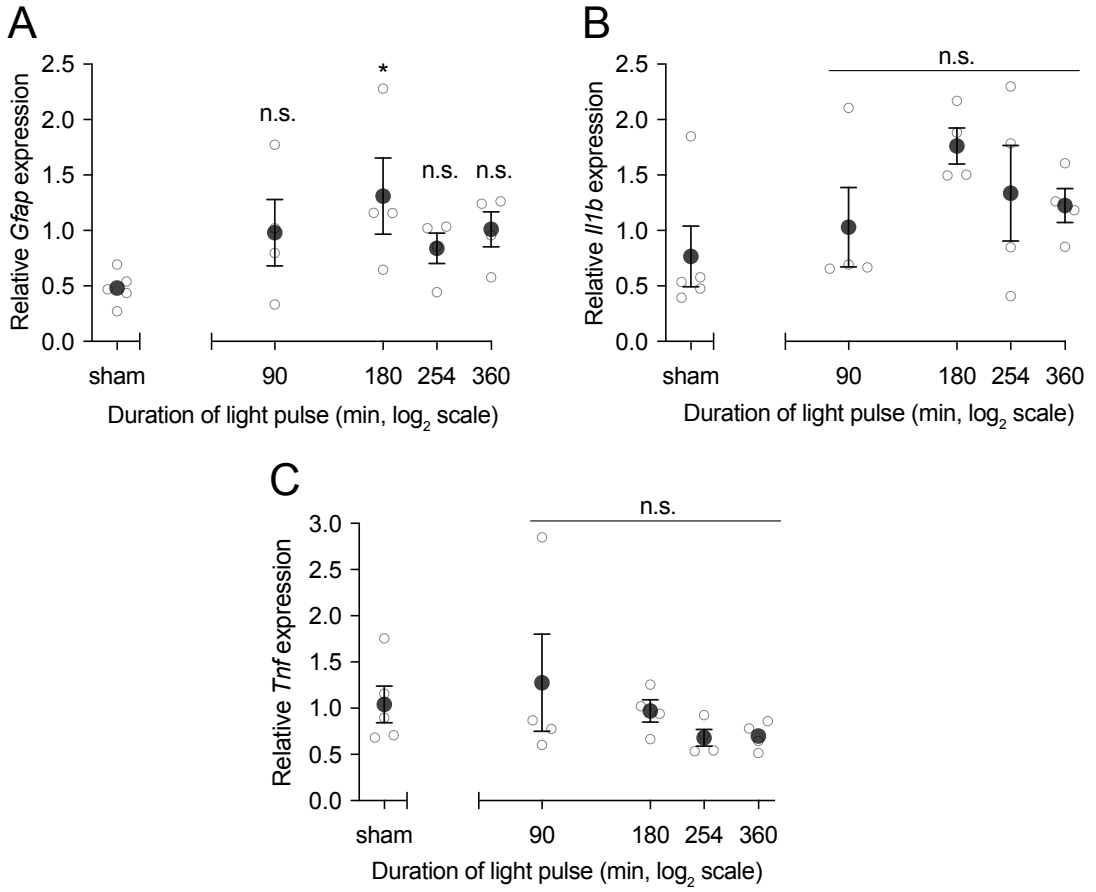


Figure 4.10: Expression of pro-inflammatory genes after exposure to 20,000 lux light pulses of different durations. Expression of *Gfap* (A), *Il1b* (B), and *Tnfa* (C) in the eyes of sham-treated mice and of those exposed to a 20,000 lux light pulse of different durations with prior pupil dilation. Data are mean ± SEM, n = 4-5. Statistical analysis was performed using one-way ANOVA with Dunnett's correction for multiple comparisons, expression values were compared to those of sham-treated eyes. n.s., not significant, * $p < 0.05$.

The bright light pulse did affect the expression of retinal opsins in WT animals. Rhodopsin levels were significantly reduced in eyes exposed to a 3-hour or longer light pulse compared to controls (Fig. 4.9A). The longest light pulse also resulted in a decline in the cone opsin levels and a trend towards a reduction of the cone arrestin *Arr3* transcript (Fig. 4.9B-D). At the same time, the expression of melanopsin was not affected in any experimental group (Fig. 4.9E). These results suggest that a 3-hour 20,000 lux light pulse may be sufficient to induce light damage in WT animals.

To evaluate the extent of inflammation in the eyes, I next analysed the retinas for the levels of pro-inflammatory genes *Gfap*, interleukin 1 beta *(Il1b)* and tumour

necrosis factor (*Tnf*). Interestingly, only the *Gfap* levels were differentially expressed between the light-pulsed and sham-pulsed eyes, showing higher expression values after a 3-hour light pulse (Fig. 4.10A). The levels of *Il1b* and *Tnf* were not affected by the bright light exposure (Fig. 4.10B, C). IL1B and TNF are acute pro-inflammatory cytokines, and their expression peaks 24-48 hours after the initiation of inflammation [243]. In contrast, GFAP is induced later in the process, approximately a week after damaging insult [244]. Since the retinal tissue was harvested seven days after light exposure, the immediate inflammatory response may have subsided.

The opsin transcript levels suggested that the retinas may have experienced some distress in response to the longer duration 20,000 lux light pulses. Alternatively, the gene expression changes may have reflected an adaptive response without any structural consequences to the retina. Therefore, I also studied the retinal morphology of these animals. I used an improved tissue processing procedure to track the location of each retinal section [245] to get a more accurate overview of retinal morphology across the different retinal regions. I analysed sagittal retinal sections containing the optic nerve head (ONH) and measured the thicknesses of the ONL, INL, and the distance between the outer margin of the ONL to the inner border of the GCL (referred to as ONL to GCL distance) every 400 µm from the ONH (Fig. 4.11D).

While the sham-pulsed retinas were normal, the retinas of mice pulsed with bright light showed noticeable morphological abnormalities manifested by a thinner ONL containing apoptotic photoreceptor nuclei (Fig. 4.11A-F). Quantification of the layer thicknesses revealed a significant reduction of the ONL to GCL distance and ONL thickness in eyes exposed to a 3-hour and a 6-hour light pulse. The areas immediately superior and inferior to the ONH were most affected (Fig. 4.11G, H). The retinas of the 6-hour light pulse group were more severely damaged and these also exhibited thinning of the INL immediately superior to the ONH, suggesting degeneration of the second-order neurons. Consequently, the INL/ONL ratios of light-damaged retinas were significantly reduced compared to sham-pulsed eyes. However, as the INL of the superior retina itself was affected by a 6-hour light

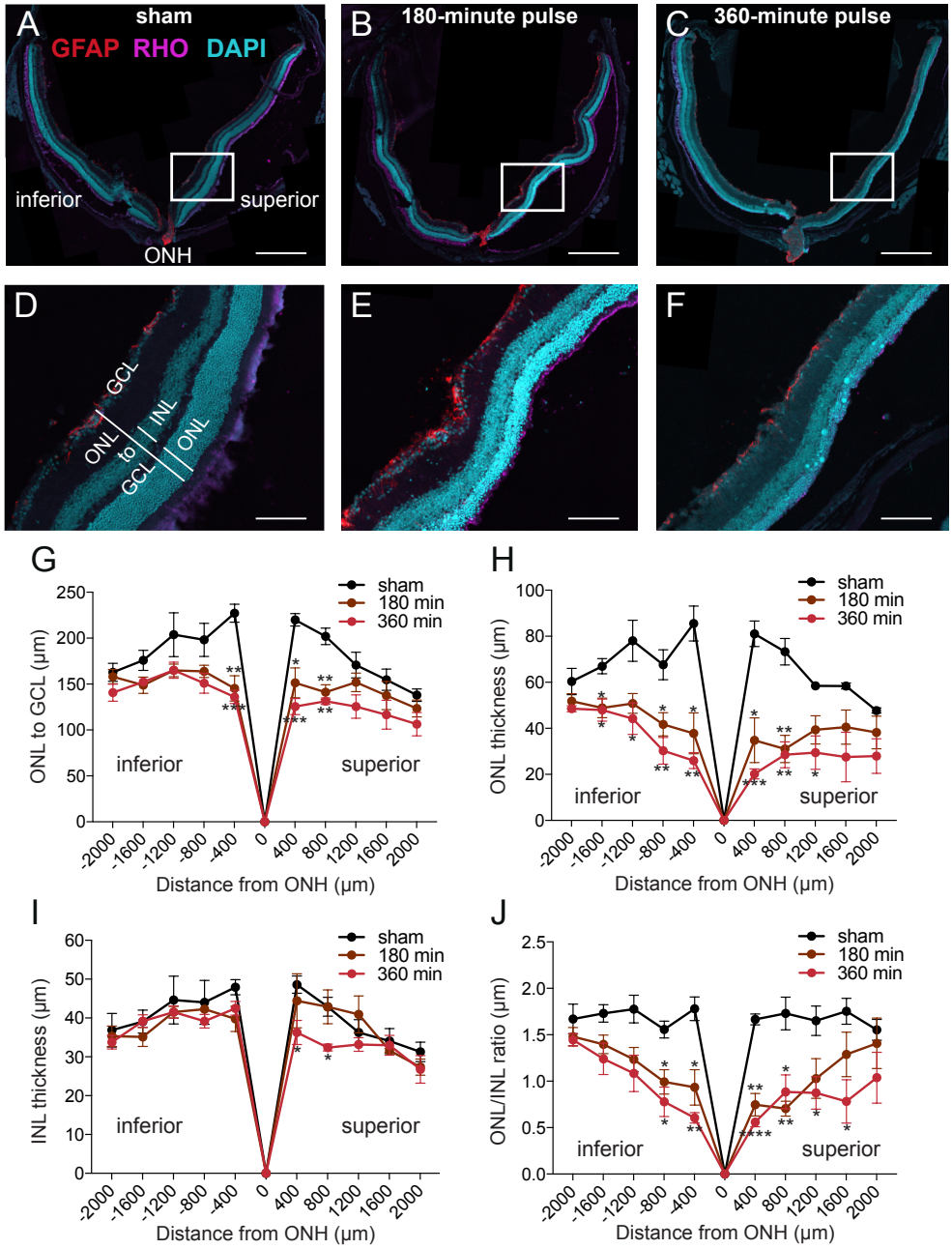


Figure 4.11: Retinal morphology of WT animals after exposure to 20,000 lux light pulses of different durations. Representative images of sham-treated retinas (A, D), those exposed to a 20,000 lux light pulse for 180 minutes (B, E), and a 360 minutes (C, F) seven days after the light pulse. The different measurements analysed are depicted on (D). Distance between ONL and GCL (G), ONL thickness (H), INL thickness (I), and ONL/INL ratio (J) at different distances from the ONH on sagittal retinal sections. Data are mean ± SEM, n = 4-5. Statistical analysis was performed using two-way ANOVA with Dunnett's correction for multiple comparisons, retinal thickness values at each position were compared to those of sham-treated eyes. Scale bars in (A-C) are 500 μm, in (D-F) 100 μm. ONH, optic nerve head; ONL, outer nuclear layer; INL, inner nuclear layer; GCL, ganglion cell layer. * $p < 0.05$, ** $p < 0.01$, *** $p < 0.001$, **** $p < 0.0001$.

pulse, the normalisation may not be appropriate for this retinal area. Overall, the immunohistochemical analysis revealed that 3- and 6-hour light pulses of 20,000 lux were sufficient to cause retinal damage, in line with the RT-qPCR analysis showing a reduction in visual opsin transcript levels.

In conclusion, the light doses I could expose mice to were high enough to cause retinal damage in WT retinas. Since the 3-hour 20,000 lux light pulse with pupil dilation induced retinal damage in WT mice, I decided to use this light dose in my further experiments.

4.3.5 Retinal transcriptomes of WT and *Opn4*$^{-/-}$ mice are similar after a 20,000 lux light pulse

One finding leading to the hypothesis of this chapter was that melanopsin might regulate upregulation of retinal crystallins. The light dose used in that particular experiment was 400 lux, which is considerably lower than the light dose able to cause retinal damage. Therefore, to study the effect of melanopsin signalling on the retinal transcriptome at a damaging light dose, I dilated the pupils WT and *Opn4*$^{-/-}$ animals and exposed them to a 3-hour 20,000 lux light pulse at night. I collected their eyes immediately at the end of the light pulse and analysed the entire transcriptome with RNA-seq.

First, I determined the overall quality of the sequencing runs. An average of 5.2 M reads (79%) per sample mapped uniquely to the mouse genome (Fig. 4.12A, B) and out of those, an average of 3.4 M reads mapped to unique exons and these counts were used for downstream analysis (Fig. 4.12C, D). The sequencing depth was slightly lower than in the retinal circadian time course samples presented in the previous chapter, but this enabled me to increase the number of biological replicates in each group to 5-6, increasing the overall power to detect differentially expressed genes [246].

I then used DESeq2 [169] to analyse the genes differentially expressed between WT and *Opn4*$^{-/-}$ retinas. There were altogether 448 genes that showed differential expression, 198 of those more highly expressed in WT and 250 in *Opn4*$^{-/-}$ retinas.

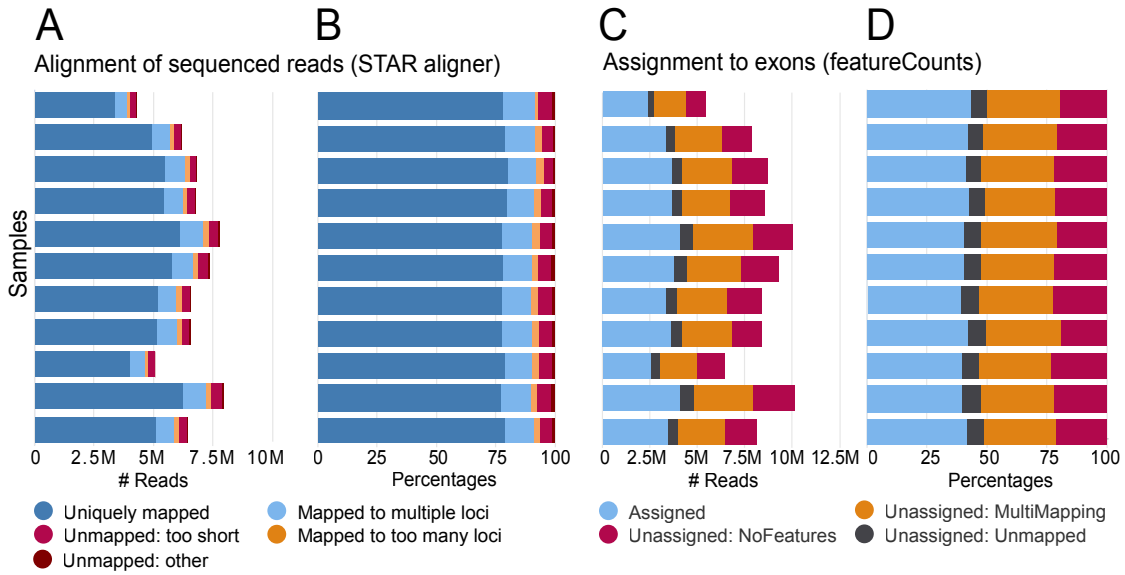


Figure 4.12: Quality control metrics of the bright light exposed retinal RNA-seq samples. (A-B) Sequenced reads were aligned to the mouse genome using the STAR alignment tool and an average of 5.2 M (79%) reads were uniquely mapped to the mouse genome. (C-D) Reads mapping to exons were counted with featureCounts, yielding an average of 3.4 M reads per sample, which were used for downstream analysis. Data were summarised with MultiQC [194].

The most significantly differentially expressed gene, with a higher expression value in WT retinas, was γ-synuclein (*Sncg*), a marker of all RGCs [247] (Fig. 4.13A). Furthermore, two crystallins, *Cryba1* and *Cryba2* were also more highly expressed in WT retinas (Fig. 4.13A).

To analyse the functions of the differentially expressed genes, I performed pathway analysis using the KEGG database [171]. The pathways enriched for genes more highly expressed in *Opn4*$^{-/-}$ retinas were apoptosis, circadian entrainment and various intracellular signalling pathways (Fig. 4.13B). Interestingly, another pathway was sphingolipid signalling, which was also enriched for genes with an overall higher expression in *Opn4*$^{-/-}$ retinas over the circadian day (Fig. 3.18 in chapter 3). The genes more highly expressed in WT retinas were not enriched for any meaningful pathways from a retinal damage perspective (Fig. 4.13B).

Due to their immediate relevance to retinal damage, I was next interested in seeing what genes constituted the apoptosis and circadian entrainment pathways. The apoptosis pathway genes with higher expression in *Opn4*$^{-/-}$ retinas contained

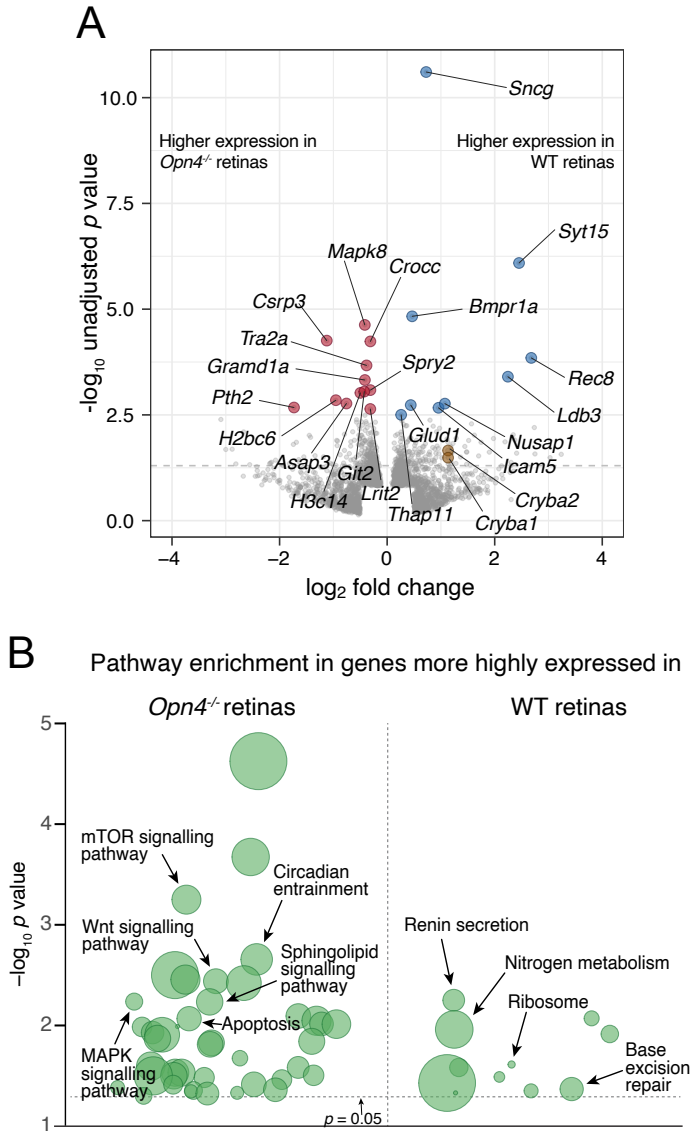


Figure 4.13: The genes and pathways differentially regulated between WT and *Opn4*$^{-/-}$ retinas after bright light exposure. (A) The genes differentially expressed between WT and *Opn4*$^{-/-}$ retinas after a 3-hour 20,000 lux light pulse. The most significantly and highly differentially expressed genes are highlighted. (C) KEGG pathways enriched for genes with higher expression in either WT or *Opn4*$^{-/-}$ retinas. The dashed lines indicate a p value of 0.05.

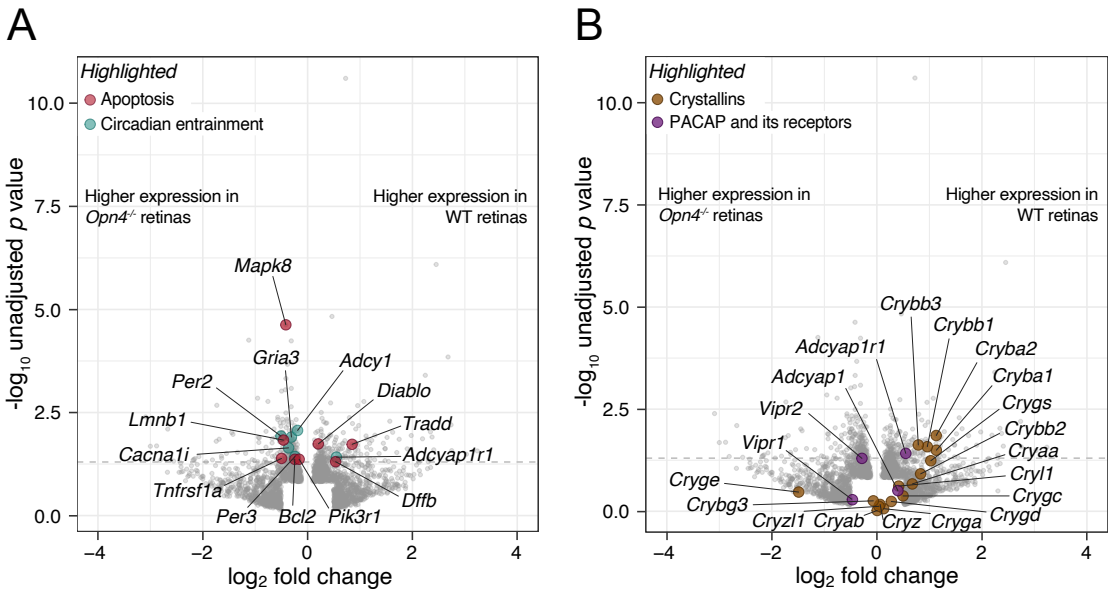


Figure 4.14: The genes of selected pathways differentially regulated between WT and *Opn4*$^{-/-}$ retinas after bright light exposure. (A) The expression differences of genes in apoptosis and circadian entrainment pathways. (B) The expression differences of crystallin genes, PACAP and its receptors. The dashed lines indicate a p value of 0.05.

pro-apoptotic factors such as a tumour necrosis factor receptor *Tnfrsf1a*, but also an anti-apoptotic factor Bcl-2 apoptosis regulator (*Bcl2*) (Fig. 4.14A). Some pro-apoptotic factors, e.g. DNA fragmentation factor (*Dffb*) and tumour necrosis factor receptor type 1-associated DEATH domain protein (*Tradd*) showed slightly higher levels in WT retinas (Fig. 4.14A). These findings make it difficult to interpret whether the genes associated with apoptosis would overall be more damaging in WT or *Opn4*$^{-/-}$ retinas.

Among the genes in the circadian entrainment pathway with higher expression in the *Opn4*$^{-/-}$ retinas was *Per2* (Fig. 4.14A). In my previous chapter, I tested the hypothesis that the absence of melanopsin in the retina leads to attenuated light responses, and a higher level of *Per2* in *Opn4*$^{-/-}$ retinas seems to speak against this hypothesis. However, the light dose used in the current experiment was significantly higher than the 30-minute 100 lux light pulse used in the previous chapter. In addition, the analysis at hand does not show a change from a baseline value, but only the transcript levels immediately after the light pulse.

Since two of the crystallins showed a higher expression in WT than *Opn4*$^{-/-}$ retinas, I analysed the expression of the different crystallin genes further. I saw that four crystallin genes, *Cryba1*, *Cryba2*, *Crybb1* and *Crybb3* showed a 2-fold higher expression in WT retinas (Fig. 4.14B). In addition, most other crystallin genes were also expressed at slightly higher levels in WT retinas. Therefore, as a group of genes, the crystallins show higher expression in WT than *Opn4*$^{-/-}$ retinas after a 3-hour 20,000 lux light pulse.

The other factor contributing to the hypothesis of a reduced damage susceptibility of *Opn4*$^{-/-}$ retinas was the knowledge that the pRGCs contain PACAP and therefore, I also analysed the expression of PACAP-related transcripts in the retinas. PACAP acts on three G protein-coupled receptors: the PACAP receptor, type I (PAC1); and since PACAP is structurally highly similar to vasoactive intestinal peptide (VIP), PACAP also acts on VIP receptors 1 and 2 (VPAC1/2). While the transcript for PAC1 receptor (*Adcyap1r1*) showed a higher expression in WT retinas, the expression of PACAP (*Adcyap1*) or the VIP receptor gene levels were not different between WT and *Opn4*$^{-/-}$ retinas (Fig. 4.14B).

To gain insight into the cell types involved in mediating the gene expression differences between WT and *Opn4*$^{-/-}$ retinas, I analysed the retinal cell types the differentially regulated genes were enriched in, using the dataset by Siegert et al. [184] as outlined in section 2.10. The cell profiles showing enrichment for genes more highly expressed in WT or *Opn4*$^{-/-}$ retinas displayed marked differences. In particular, WT retinas had higher expression of genes enriched in pRGCs while there was a depletion of pRGC-related genes in *Opn4*$^{-/-}$ retinas (Fig. 4.15). The genes more highly expressed in WT retinas were also enriched in microglia and direction-selective RGCs, while genes more highly expressed in *Opn4*$^{-/-}$ retinas were enriched in different subtypes of amacrine cells. This analysis suggests that melanopsin signalling mediates gene expression across the retina, and has the most pronounced effect on pRGC and microglia-specific genes.

In conclusion, the retinas of WT and *Opn4*$^{-/-}$ mice showed differential expression in 448 genes. As a group of genes, crystallins were more highly expressed in WT

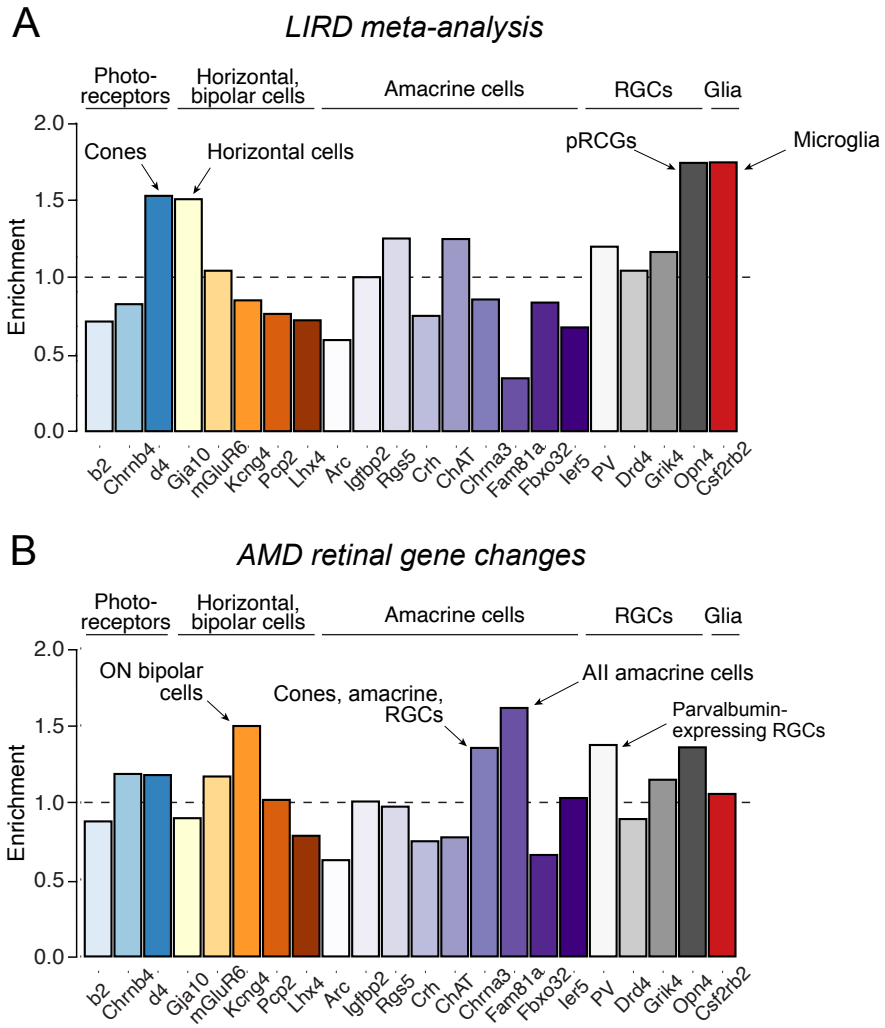


Figure 4.15: Enrichment of differentially expressed genes in retinal cell subpopulations. Enrichment in each retinal cell subpopulation was calculated as the number of genes expressed more than 2 SD higher than the mean expression of that gene across all subpopulations normalised to the number of genes enriched in each subpopulation across the entire transcriptome. Data are displayed for genes with significantly higher expression levels in WT (A) and *Opn4*$^{-/-}$ retinas (B).

retinas, and some factors relating to apoptosis were more highly expressed in WT, some in *Opn4*$^{-/-}$ retinas. Therefore, there is some evidence that melanopsin could regulate retinoprotective mechanisms, but the evidence is not concrete.

4.3.6 The retinal function of WT and *Opn4*$^{-/-}$ mice deteriorates after exposure to a 20,000 lux light pulse

The retinal transcriptome analysis demonstrated that *Opn4*$^{-/-}$ retinas might be more susceptible to light damage, but the results were far from conclusive. Therefore, to

fully understand whether melanopsin can protect the retina from damage at these light levels I analysed the retinal function of WT and *Opn4*$^{-/-}$ mice before and after exposure to a 3-hour 20,000 lux light pulse with pupil dilation. As in the previous set of experiments, I used pupillometry to test retinal function, however this time I also used electroretinography (ERG), which we had set up in the lab with Dr Moritz Lindner. I decided not to use the optomotor response or the visuospatial context recognition tasks as the results of these behavioural tests were relatively variable, and the experiments time-consuming.

The maximum pupil constriction of WT animals remained the same after the bright light pulse as it was at baseline (Fig. 4.16A, C). However, the *Opn4*$^{-/-}$ animals developed a pupil constriction deficit, which was evident at 4 and 7 days after light exposure (Fig. 4.16A, C). The maximum pupil constriction was determined by measuring the pupil area after a 10-second light stimulus. In addition, I also determined how much the pupil had constricted at 2 seconds, as this measure has been used to estimate the preferential activation of rods and cones [248]. Intriguingly, both WT and *Opn4*$^{-/-}$ mice showed a 2-second pupil constriction deficit compared to the baseline measures after bright light exposure (Fig. 4.16B, D). In conclusion, while bright light exposure resulted in a maximum pupil constriction deficit in only *Opn4*$^{-/-}$ animals, both WT and *Opn4*$^{-/-}$ mice showed deficits in pupil constriction at 2 seconds, which may suggest that both genotypes developed damage to classical photoreceptors.

To gain a more thorough insight into the retinal function, I used ERG and measured the retinal electrical responses to a series of light flashes administered to dark-adapted retinas. I performed the same measurements before and 7 days after bright light exposure and calculated the amplitudes of the a- and b-waves. Representative ERG traces are depicted in Figure 4.17A. The b-wave amplitudes showed a reduction in the majority of WT (Fig. 4.17B) and all *Opn4*$^{-/-}$ animals (Fig. 4.17C). However, there was considerable variability between the b-wave amplitudes across the animals. Therefore, I normalised the b-wave amplitudes of each mouse to the b-wave amplitude in response to the highest light intensity at baseline.

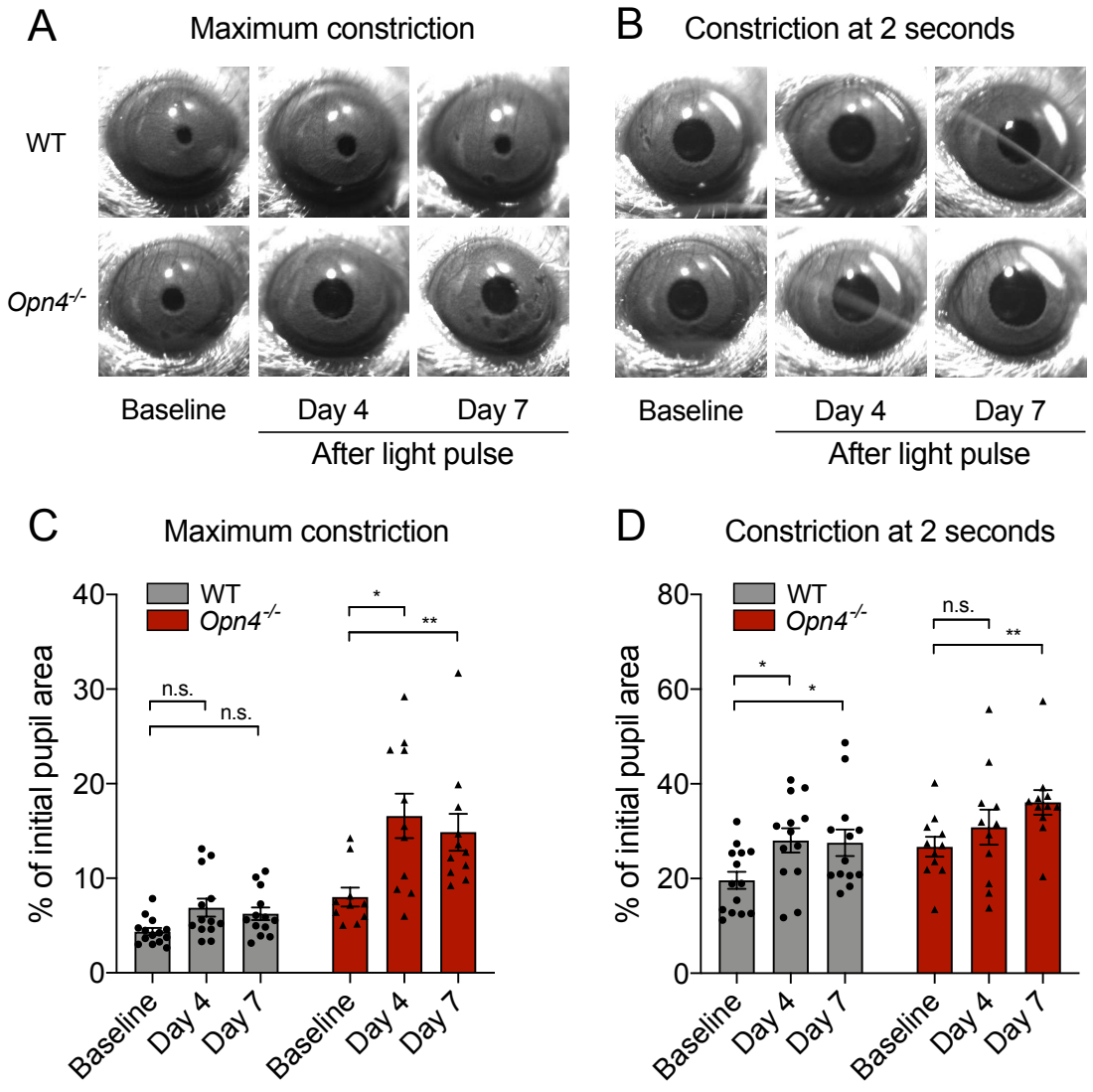


Figure 4.16: Pupil response before and after a 20,000 lux light pulse. Representative images of maximum pupil constriction (A) and constriction at 2 seconds (B) at baseline and several days after a 3-hour 20,000 lux light pulse in WT and *Opn4*$^{-/-}$ animals. Quantification of maximum pupil constriction (C) and constriction at 2 seconds (D) at baseline, 4 and 7 days after the light pulse. Data are mean ± SEM, n = 11-14. Statistical analysis was performed using two-way ANOVA with Dunnett's correction for multiple comparisons. n.s., not significant, * $p < 0.05$, ** $p < 0.01$.

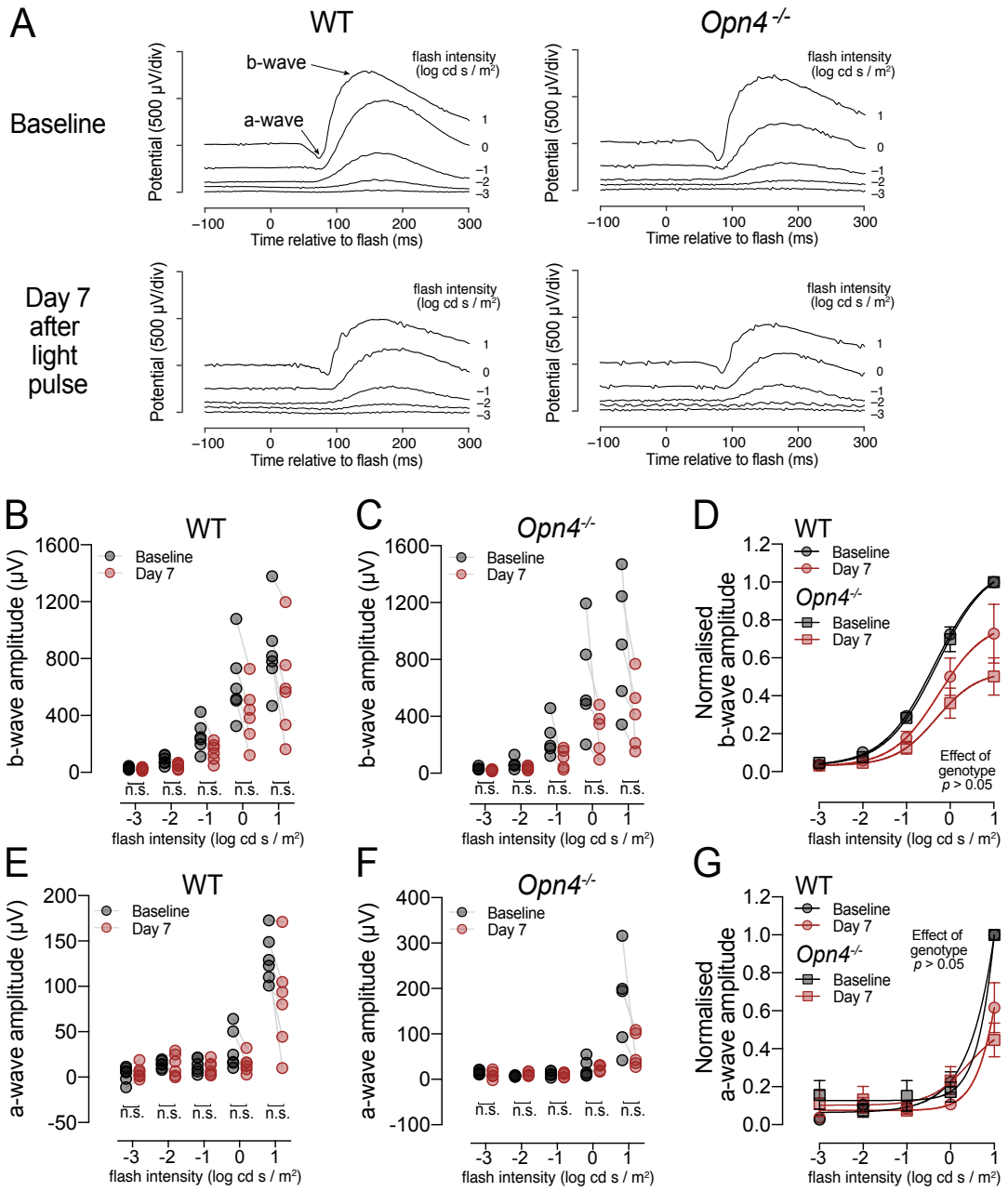


Figure 4.17: Electroretinogram before and after bright light exposure: first experiment. (A) Representative ERG traces to all light intensities used. The b-wave amplitudes of individual WT (B) and *Opn4*$^{-/-}$ mice (C) at baseline and seven days after bright light exposure. (D) The normalised b-wave amplitudes before and after light exposure. The a-wave amplitudes of individual WT (E) and *Opn4*$^{-/-}$ mice (F) at baseline and seven days after bright light exposure. (G) The normalised a-wave amplitudes before and after light exposure. Data in (D, G) are mean ± SEM, n = 6. Statistical analysis in (B, C, E, F) was performed using two-way ANOVA with Šidák's correction for multiple comparisons. n.s., not significant. Statistical analysis in (D, G) was performed using three-way ANOVA.

It can be seen that the b-wave amplitudes of WT and *Opn4*$^{-/-}$ animals were lower after the bright light pulse than at baseline (Fig. 4.17D). However, a three-way ANOVA of the b-wave amplitudes before and after light damage across the flashes of different intensities did not show a significant effect of genotype ($p = 0.026$). The a-wave amplitude showed a similar pattern. Although most animals had a reduced a-wave amplitude after light exposure (Fig. 4.17E, F), there was no significant effect of genotype (Fig. 4.17G).

In this ERG experiment, I prioritised the sensitivity to detect changes at low light levels, but the highest light flash did not elicit a maximum electrical response. Therefore, I modified the experiment slightly to increase the range of flash intensities, and since the electrical response to the lowest light intensity was undetectable, I shifted the flash intensity range and used -2.5 to 2.5 log cd $\cdot$ s/m^2 flashes.

This modified protocol allowed me to record maximum retinal electrical responses (Fig. 4.18A), and in line with the results of the previous experiment, the ERG a- and b-wave amplitudes showed a reduction in WT (Fig. 4.18B, E) and *Opn4*$^{-/-}$ mice (Fig. 4.18C, F) after bright light exposure. However, when comparing the a- and b-wave amplitudes across the genotypes, there were no differences between WT and *Opn4*$^{-/-}$ mice (Fig. 4.18D, G). In conclusion, the ERG results demonstrated that the retinal function of mice was reduced after bright light exposure, but the lack of melanopsin did not result in a more severe phenotype.

4.3.7 A 20,000 lux light pulse induces retinal degeneration in WT and *Opn4*$^{-/-}$ mice

The *in vivo* analyses suggested that the retinas of WT and *Opn4*$^{-/-}$ mice developed a functional deficit after bright light exposure, but did not suggest any differences between the genotypes. To analyse whether the functional deficit was complemented by changes on a molecular level, I studied the retinal gene expression morphology of the retinas 7 days after bright light exposure. To start with, I analysed the expression of photoreceptor genes and *Gfap* with RT-qPCR and saw no gene expression differences between WT and *Opn4*$^{-/-}$ retinas (Fig. 4.19).

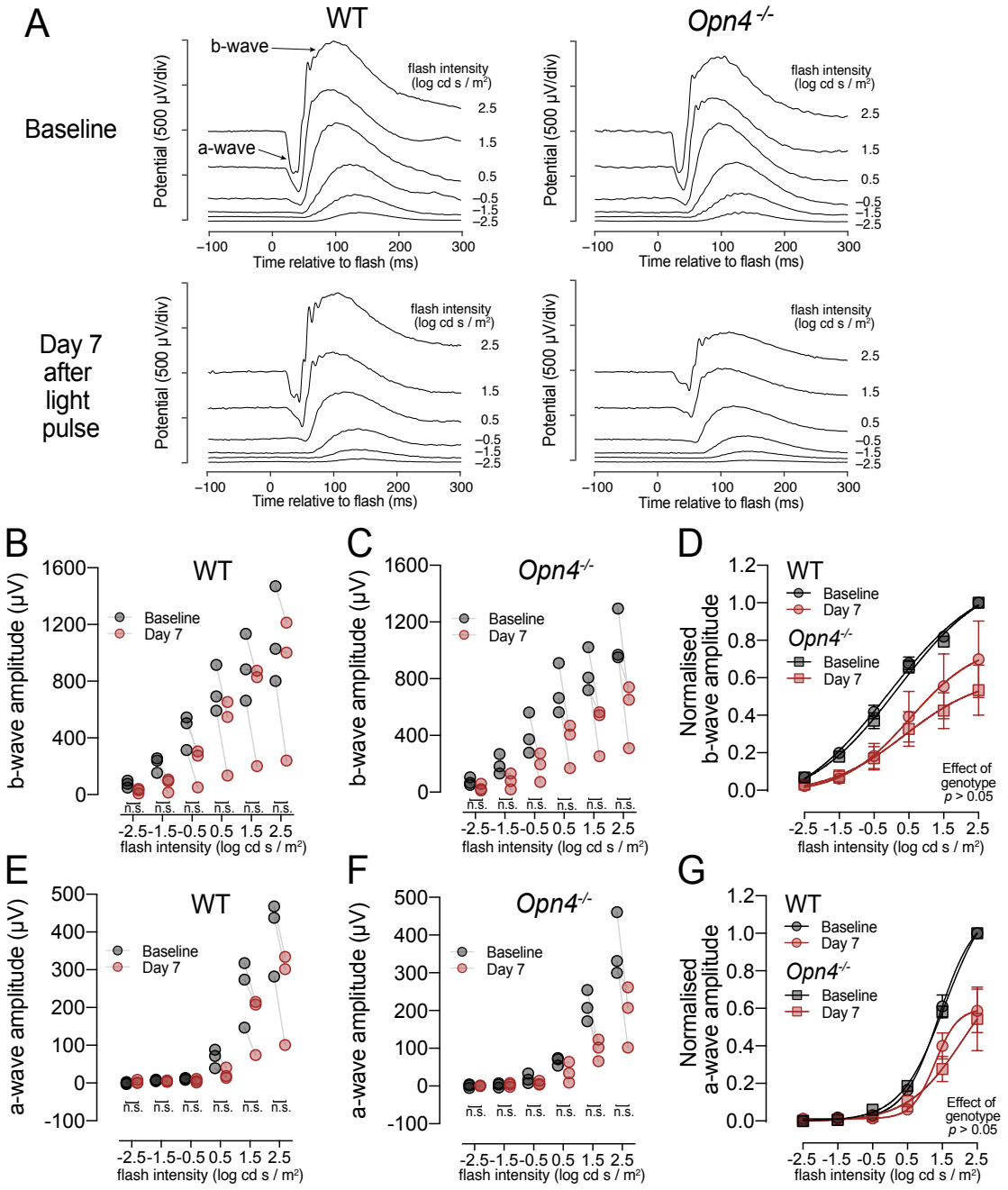


Figure 4.18: Electroretinogram before and after bright light exposure: second experiment. (A) Representative ERG traces to all light intensities used. The b-wave amplitudes of individual WT (B) and *Opn4*$^{-/-}$ mice (C) at baseline and seven days after bright light exposure. (D) The normalised b-wave amplitudes before and after light exposure. The a-wave amplitudes of individual WT (E) and *Opn4*$^{-/-}$ mice (F) at baseline and seven days after bright light exposure. (G) The normalised a-wave amplitudes before and after light exposure. Data in (D, G) are mean ± SEM, n = 3. Statistical analysis in (B, C, E, F) was performed using two-way ANOVA with Šidák's correction for multiple comparisons. n.s., not significant. Statistical analysis in (D, G) was performed using three-way ANOVA.

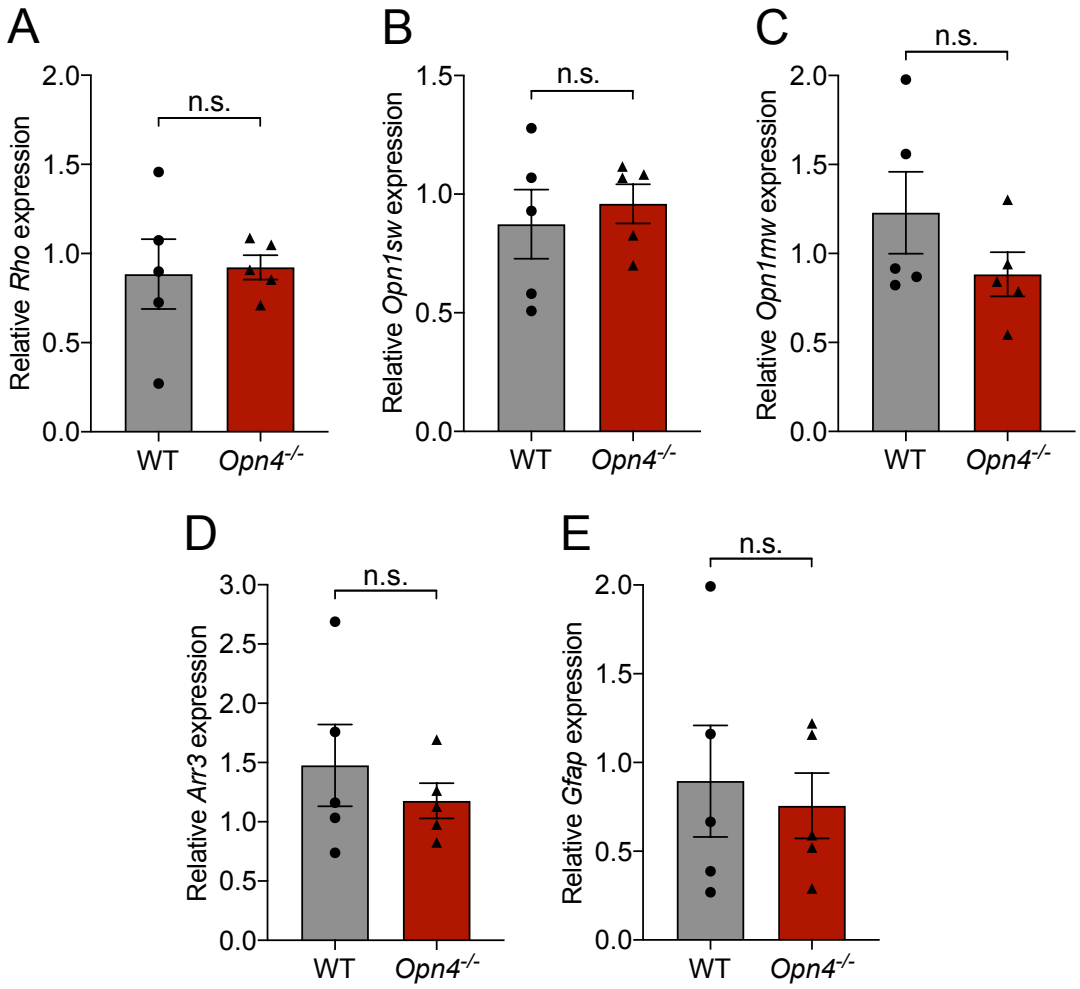


Figure 4.19: Retinal gene expression after exposure to a 20,000 lux light pulse. Relative expression of rhodopsin (A), S-opsin (B), M-opsin (C), cone arrestin (D), and *Gfap* (E) in retinas seven days after bright light exposure. Statistical analysis was performed using two-tailed t-tests. n.s., not significant.

Some photoreceptor outer segments can remain attached to the RPE during the retinal dissection procedure, and consequently influence the expression values of retinal photoreceptor genes. Therefore, to minimise any such error, I also analysed the gene expression of the same genes in entire eyes. However, similarly to the previous experiment, there were no significant differences in the levels of photoreceptor transcripts between the two genotypes (Fig. 4.20A-D). The *Gfap* levels were, surprisingly, lower in the *Opn4*$^{-/-}$ eyes than in WT eyes (Fig. 4.20E). Since the *Gfap* levels were similar in WT and *Opn4*$^{-/-}$ retinas, this indicated that the expression of *Gfap* might be lower in some other *Opn4*$^{-/-}$ ocular tissue. However,

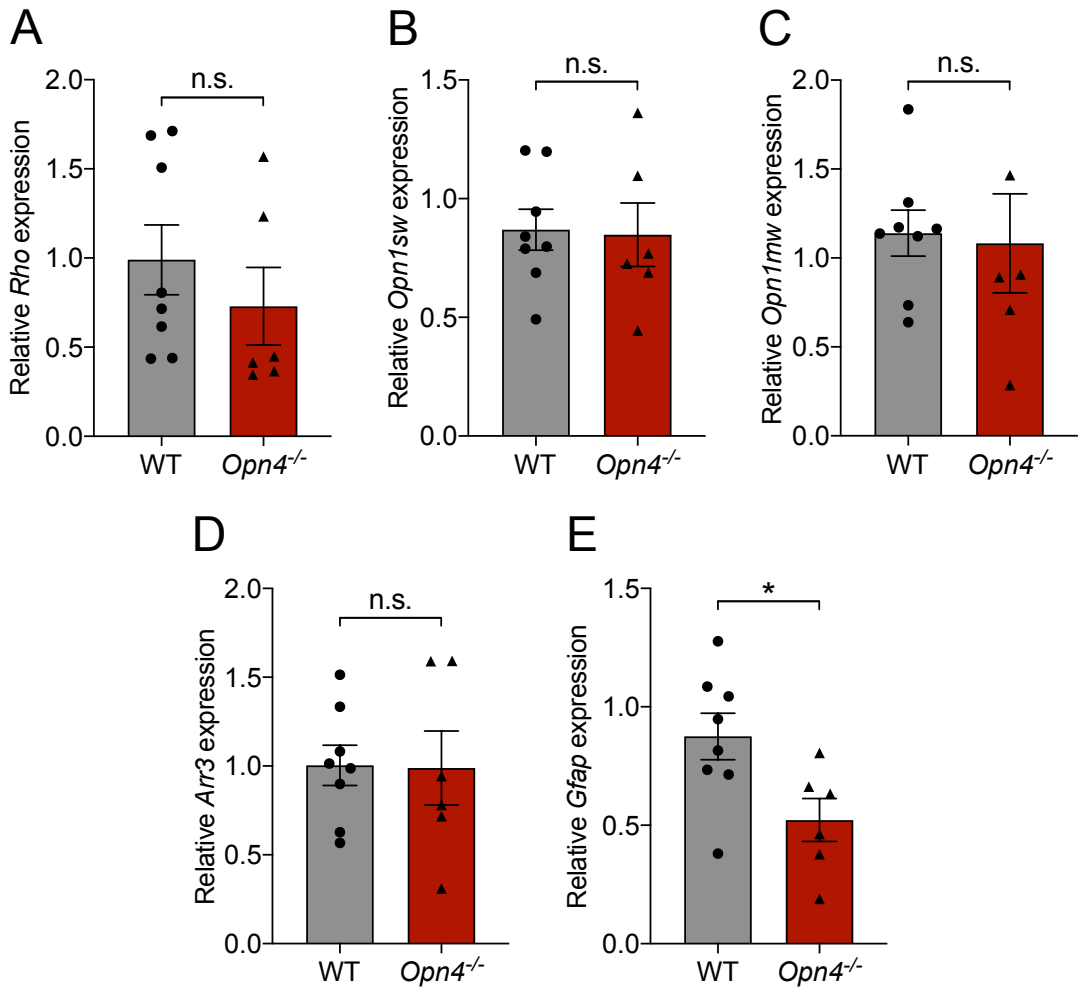


Figure 4.20: Gene expression in whole eyes after exposure to a 20,000 lux light pulse. Relative expression of rhodopsin (A), S-opsin (B), M-opsin (C), cone arrestin (D), and *Gfap* (E) in whole eyes seven days after bright light exposure. Statistical analysis was performed using two-tailed t-tests. n.s., not significant., * $p < 0.05$.

the similar expression of opsins in the retinas and entire eyes suggested that the retinal photoreceptors of the two genotypes were not differentially affected by the bright light pulse.

To analyse whether the retinal morphology of WT and *Opn4*$^{-/-}$ mice differed, I carried out an immunohistochemical analysis measuring the thicknesses of the ONL, INL and the ONL to GCL distance (see Fig. 4.11D for the measurement definitions). WT and *Opn4*$^{-/-}$ retinas showed abnormal morphology and thinning of retinal layers (Fig. 4.21A-D). GFAP immunostaining, which is usually restricted to the endfeet of Müller cells (see Fig. 4.11D for comparison), showed high immunoreactivity

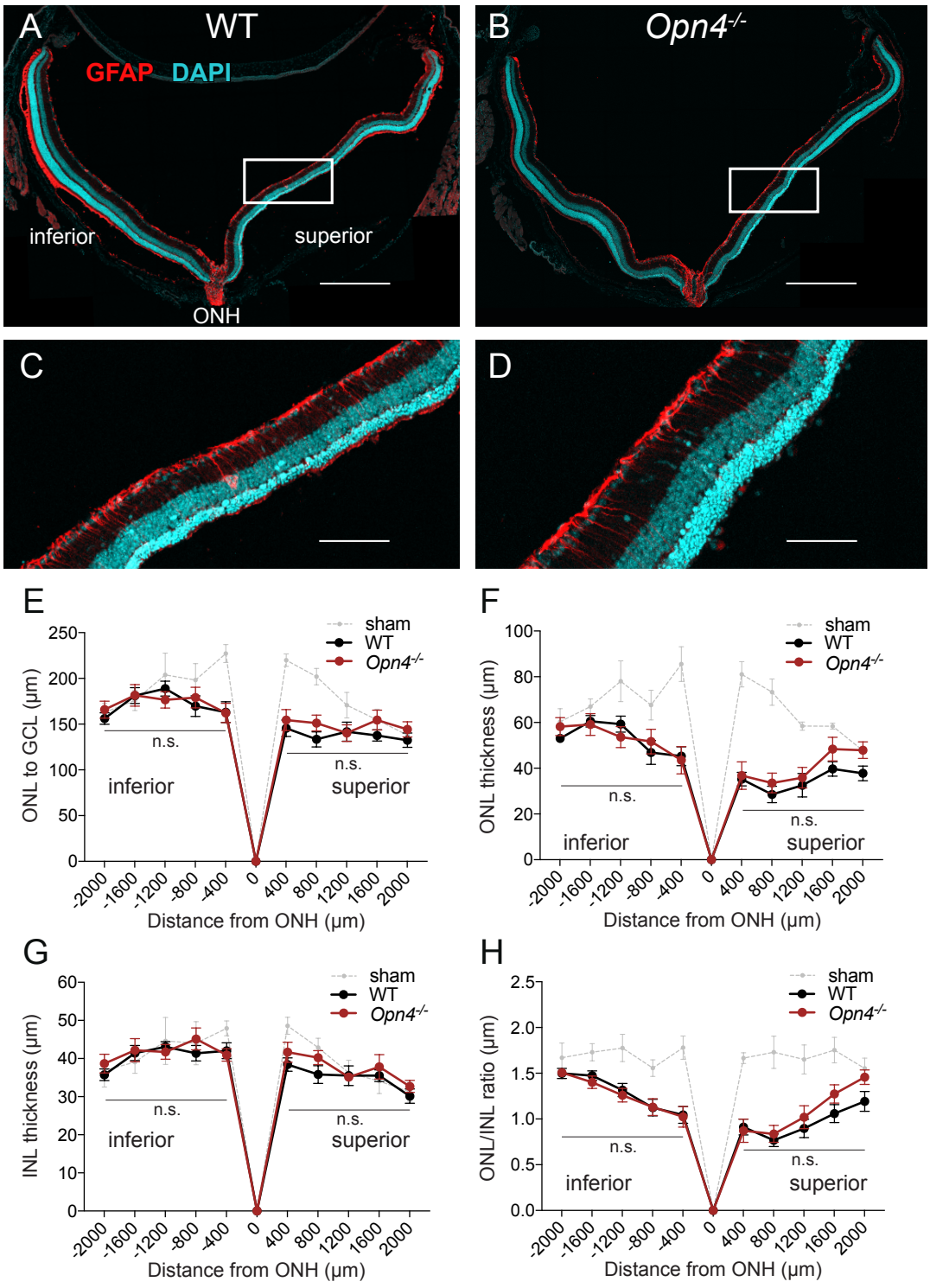


Figure 4.21: Retinal morphology after bright light exposure. Representative images of WT (A, C) and *Opn4*$^{-/-}$ retinas (B, D). Distance between ONL and GCL (E), ONL thickness (F), INL thickness (G), and ONL/INL ratio (H) at different distances from the ONH on sagittal retinal sections. Data are mean ± SEM, n = 4-6. The measurements of WT sham-pulsed retinas from the previous experiment are included for reference with dashed lines. Statistical analysis was performed using two-way ANOVA with Dunnett's correction for multiple comparisons, values at each position were compared between WT and *Opn4*$^{-/-}$ eyes. Scale bars in (A-B) are 500 μm, in (C-D) 100 μm. ONH, optic nerve head; ONL, outer nuclear layer; INL, inner nuclear layer; GCL, ganglion cell layer. n.s., not significant.

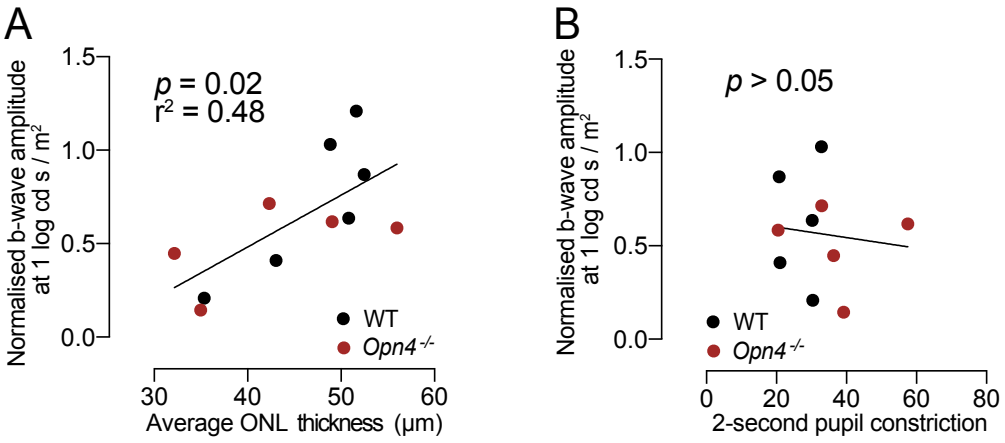


Figure 4.22: Correlations of retinal function measures after light damage The correlation between normalised ERG b-wave amplitude and average ONL thickness (A) and 2-second pupil constriction (B). Data were analysed with Pearson correlation analysis.

in the radial stalks of Müller cells, indicative of their activation (Fig. 4.21A-D). However, there were no statistically significant differences in any of the retinal layer thicknesses between WT and *Opn4*$^{-/-}$ retinas (Fig. 4.21E-H). Interestingly, there was a slight trend toward a thicker ONL in the far superior region of the *Opn4*$^{-/-}$ retinas compared to WT retinas, which also resulted in a larger ONL/INL ratio. In conclusion, there was no evidence of differential retinal light damage susceptibility between WT and *Opn4*$^{-/-}$ animals on a histological level.

Since I used several measures to quantify retinal function after light damage induction, I was interested to know how well the measurements of ERG, immunohistochemistry and 2-second pupil response correlate. I found that the normalised b-wave amplitude in response to the highest intensity light flash was in correlation with the average ONL thickness of the retina (Fig. 4.22A). The 2-second pupil constriction, which also showed a reduction 7 days after the light pulse, did not correlate with the normalised ERG b-wave amplitude (Fig. 4.22B). Therefore, the extent of pupil constriction after a 2-second light exposure might not be a reliable method for detecting a functional retinal deficit.

4.4 Discussion

In this chapter, I addressed the second aim of my thesis and tested the hypothesis that the lack of melanopsin leads to an increased retinal susceptibility to light damage.

In the first set of experiments, I exposed WT and *Opn4*$^{-/-}$ mice to a 3-hour 10,000 lux white light pulse and did not dilate their pupils. I saw that *Opn4*$^{-/-}$ mice developed a deficit in their pupillary light reflex and optomotor response, which showed slight recovery at the end of the follow-up period, approximately one week after the light pulse. However, light exposure did not lead to a reduction in the ONL/INL ratio. The retinal changes causing retinal and visual defects may have been transient and recovered by 12 days after the light pulse when the retinal tissue was collected. Another possibility is that the immunohistochemistry protocol I used for this set of experiments was not sensitive enough to detect the retinal damage. I averaged the ONL/INL ratio of retinal sections across the retina and may have missed smaller and more localised changes.

I chose the maximum pupillary light response as one of the readouts of retinal function. Pupil response is driven by the rods, cones and melanopsin. Since *Opn4*$^{-/-}$ retinas contain no melanopsin, any deficit in maximum pupil constriction can be attributed to classical photoreceptor dysfunction. As WT retinas express melanopsin, which is able to drive the maximum pupil constriction on its own [82], any potential damage in the classical photoreceptors in WT animals could be masked by melanopsin activation. Therefore, the maximum pupil constriction is not a suitable measure to quantify differences in retinal function between WT and *Opn4*$^{-/-}$ animals. In addition, the 2-second pupil response did not correlate with the ERG b-wave amplitude, and further experiments are needed to determine whether pupil constriction is a suitable method to detect retinal damage.

I further determined that the pupil response of *Opn4*$^{-/-}$ mice was not sustained in response to a 10,000 lux nocturnal light pulse, as the literature suggested that melanopsin is mediating the sustained pupil response [83]. Therefore, *Opn4*$^{-/-}$

animals received a retinal light dose approximately 18 times higher than WT animals, making it challenging to compare the retinal and visual function between WT and *Opn4*$^{-/-}$ mice after the 10,000 lux light pulse. The presence of melanopsin is necessary for a sustained pupil constriction, limiting the amount of light reaching the retina and providing protection from any potential damage. As it has been demonstrated that the iris sphincter muscle constricts *in vitro* in a melanopsin-dependent way [84], this function might be to further ensure that the pupil constriction is sustained at bright light levels.

In the second set of light damage experiments, I kept the light dose reaching the animals' retinas the same by dilating their pupils before administering the bright light pulse. I first determined the dose of light required to damage WT retinas and saw a reduction of retinal ONL thickness in response to a 3-hour 20,000 lux light pulse, which I decided to use for further experiments. This light pulse is relatively mild compared to what is being used in other research groups. Among the smallest light dose in pigmented animals is a 6-hour light pulse of 18,000 lux [235]. The difference between my experiment and most light damage literature is that I administered the bright light pulse at night for reasons discussed in section 4.3.1. There are several reasons why this relatively low light dose was able to cause retinal degeneration in our WT mouse colony. First, the retinas are more susceptible to damage at night [158]; second, our colony carries the RPE65 450L variant, which is known to lead to an increased retinal light damage susceptibility [249]; and third, there may be contributions from other unidentified genetic factors.

I was interested to see whether the immediate bright light induced transcriptome of the retina was influenced by melanopsin and whether there were indications of a lack of protective mechanisms upregulated in *Opn4*$^{-/-}$ retinas. More than 400 genes showed differential expression between WT and *Opn4*$^{-/-}$ retinas. Several apoptosis-related transcripts showed higher expression levels in *Opn4*$^{-/-}$ and also WT retinas. The crystallin genes, which drove the hypothesis of this chapter, showed a higher expression in WT retinas. The PACAP transcript levels were not different between WT and *Opn4*$^{-/-}$ retinas, although the PACAP receptor transcript

levels were slightly higher in WT retinas. Overall, there were no very obvious targets from the transcriptome analysis that would indicate whether *Opn4*$^{-/-}$ retinas were more susceptible to light damage.

After exposing WT and *Opn4*$^{-/-}$ animals to a 3-hour 20,000 lux light pulse with pupil dilation, I saw that both genotypes developed a functional defect as their pupil constriction after a 2-second light stimulation was reduced and their ERG a- and b-wave amplitudes were lower compared to baseline. Additionally, the retinas of WT and *Opn4*$^{-/-}$ mice showed significant damage on a morphological level. However, on a functional and structural level, there were no differences between the genotypes. Therefore, I did not find any evidence to suggest that melanopsin plays a protective role in the retina by using this particular model of retinal light damage. There were several limitations of this study, which I discuss in the section below.

The potential protective role of melanopsin in the retina has also been studied in the context of other models of retinal damage, and several reports have shown that pRGCs are more resistant to damage than other RGCs. For example, in response to optic nerve transection, the M1 pRGCs comprise 82% of the total RGCs surviving 60 days after the axonal injury [250]. Furthermore, inherited optic neuropathies, which lead to the loss of RGCs, are also characterised by the preferential survival of the pRGCs [251]. There is also evidence to suggest the contrary. For example, Alzheimer's disease seems to affect pRGCs more severely than other RGCs, and pRGC loss occurs even at stages when there is no loss of conventional RGCs [252].

The role of melanopsin in retinal damage has also been studied. It was reported that the pRGCs were more resistant to damage in a mouse model of dominant optic atrophy [253]. However, the pRGCs of animals lacking melanopsin were similarly resistant to damage, indicating that the preferential survival of pRGCs may not be mediated by melanopsin [253]. The reason for the preferential survival of pRGCs in optic neuropathies may instead have to do with their morphology as it is known that RGCs with larger cell bodies are more resistant to damage [254]. Another report investigated the possible protective role of melanopsin in an *in vitro* model. The human embryonic kidney cell line (HEK-293) stably

expressing melanopsin under a specific promoter was challenged with drugs that induce oxidative stress. The expression of melanopsin alone or in the presence of retinal did not change the viability of the cells in response to oxidative stress [255]. Moreover, the cell viability was no different from control cells when exposed to blue or white light, which activates melanopsin phototransduction [255]. Collectively, these data suggest that melanopsin expression and its light responses may not provide a protective signal, and the resistance of pRGCs to damage may instead have to do with their morphology.

4.4.1 Limitations of this study and future work

While melanopsin may not show a protective effect from light damage in response to a 3-hour 20,000 lux light pulse administered at night, it does not necessarily mean that melanopsin does not mediate retinoprotection. There light exposure protocol I chose may have been too severe to see a protective effect of melanopsin. Further, melanopsin as an irradiance detector may be eliciting a protective effect in a more sustained light exposure paradigm. As discussed in the previous chapter, *Opn4*$^{-/-}$ retinas seem to be in a constant "day-like" state and the phase of the retinal clock may have counteracted any retinoprotective effect of melanopsin in my experiments. Therefore, it would be interesting to investigate the role of melanopsin in different retinal light damage paradigms. One could use a lower intensity more sustained light pulse, or examine the effect of melanopsin on preconditioning light pulses. In addition, to control for the potential differences in retinal clock phases, the administration of light pulses at daytime could also be considered.

Another limitation of this study was that I did not have a control group in the retinal transcriptomics experiment, but I only compared the transcriptomes of WT and *Opn4*$^{-/-}$ retinas at the end of the light pulse. This analysis did not determine which genes were induced by the light pulse in either genotype and which genes were more highly expressed before the light pulse. Therefore, to uncover what changes are specifically a result of a light pulse, it would be appropriate to include a matched group of animals not exposed to the light pulse. In addition,

the collection of tissue immediately after the light pulse might have been too soon to determine all gene expression changes and future experiments could consider leaving additional time between the end of the light exposure and tissue harvesting.

A third limitation was that I only studied the transcript levels of retinal PACAP. However, the release of PACAP from the pRGCs might not be complemented by increased transcription of the peptide precursor gene. Further research on the release of PACAP in the retina is needed to determine whether the process is mediated by melanopsin and whether it has a functional significance in retinal function.

5

Light-induced retinal damage as a model of human retinal degenerative diseases: a meta-analysis of transcriptome profiling studies

5.1 Introduction

In the UK, approximately 2 million people, or 3% of the population, were affected by vision loss in 2013, and this figure is estimated to double by 2050 [256]. The leading cause of vision loss is age-related macular degeneration (AMD), accounting for a fourth of the cases, thus presenting a considerable burden on the healthcare system [256]. The most common causes of blindness in working-age adults in the UK, on the other hand, are inherited retinal degenerations (IRDs), comprising 20% of the total cases [257]. Therefore, a detailed understanding of these diseases is vital and would enable the development of better treatments for these patients. Much of our knowledge of the molecular mechanisms of these diseases is derived from studies conducted on animal models. One model of retinal degenerative diseases is the mouse model of light-induced retinal damage (LIRD). However, to what extent it mimics the human disease processes, is not entirely known.

In this chapter, I am addressing the second part of the second aim of my thesis. Its purpose is to study the molecular mechanisms involved in the mouse model of LIRD and to determine to what extent its molecular signature mirrors the molecular mechanisms implicated in IRDs and AMD. These results will enable us to understand the benefits and limitations of the animal model and allow more accurate translation of basic research into clinical benefit.

5.1.1 Inherited and acquired retinal degenerations

Retinal degenerations can broadly be divided into IRDs and acquired retinal diseases, the most common of the latter being AMD. IRDs are caused by pathological variants of single genes and lead to progressive photoreceptor death and eventual vision loss. To date, 271 IRD genes have been identified and documented in the Retinal Information Network (RetNet) database [258]. IRDs are a heterogeneous group of conditions that cause a range of clinical phenotypes, varying in the age at symptom onset, progression rate and inheritance pattern. Interestingly, different pathological variants of a single gene can cause a wide range of phenotypes, and conversely, mutations in different genes can result in very similar phenotypes, highlighting the complexities of the disease mechanisms [259].

There are multiple ways to classify IRDs, one of which is based on the photoreceptors most affected. Consequently, diseases affecting primarily rods are termed rod and rod-cone dystrophies while cone or cone-rod dystrophies cause primary degeneration of cones. The most common IRD, estimated to affect 1 in 3,500 individuals, is retinitis pigmentosa (RP), a rod-cone dystrophy that has been associated with mutations in more than 80 genes [258, 260]. The clinical presentation of RP is initially characterised by reduced vision in dim light and progressive loss of peripheral vision. Cone function is often affected at later stages, resulting in severely reduced visual acuity and ultimately blindness [261]. On the other hand, cone-dominated diseases are characterised by the loss of central vision and severe reduction in visual acuity, while peripheral retina can be affected in later stages.

One condition that may have cone dysfunction is Stargardt disease, which is most often caused by mutations in the ATP-binding cassette, sub-family A member 4 (*ABCA4*) gene.

ABCA4 codes for a transmembrane protein located in the cone and rod outer segments and is involved in the visual cycle. In fact, there are more than 900 different disease-associated sequence variants of the *ABCA4* gene and while one form of *ABCA4* retinopathy is Stargardt disease, there are other phenotypes, including cone-rod dystrophies and RP [262]. Altogether, mutations in *ABCA4* are estimated to account for 30% of all IRD cases [262]. Although IRDs are genetic diseases, there is also evidence of environmental factors modifying the disease process. For example, a recent report suggests that increased sunlight exposure may result in a faster progression of Stargardt disease [263], although further work is required to confirm this finding.

In contrast to the IRDs, multiple environmental risk factors have been identified for AMD, including older age, smoking, hypertension and increased sunlight exposure [264, 265]. The initial stages of AMD are characterised by the deposition of extracellular debris known as drusen to the Bruch's membrane, leading to retinal and RPE atrophy. These changes result primarily in a gradual loss of central vision. In some cases, the disease is further complicated by the formation of abnormal blood vessels invading the subretinal space, termed neovascular or wet AMD, and leads to rapid vision loss. AMD is a complex disease with both genetic and environmental factors playing a role in its pathogenesis. To date, studies have identified polymorphisms in thirteen genes, which increase the susceptibility to AMD [258].

5.1.2 Molecular mechanisms of retinal degenerations

Understanding the molecular mechanisms involved in IRDs and AMD has been the focus of a significant amount of research. The more than 300 genes with variants leading to IRDs have a wide variety of functions, a number of them are involved in the two critical processes of the retina: phototransduction, e.g. rhodopsin

(*RHO*), phosphodiesterases (*PDE6A* and *PDE6B*); and the visual cycle, e.g. *RPE65*, *ABCA4* and *LRAT* (see Figs. 1.2 and 1.3 for overviews of the processes). Other IRD genes affect the development of the retina, e.g. the transcription factors cone-rod homeobox (*CRX*) and nuclear receptor subfamily 2 group E member 3 (*NR2E3*); take part in mRNA splicing, e.g. pre-mRNA processing factors 3, 8, and 31 (*PRPF3*, *PRPF8*, *PRPF31*) and RP9 pre-mRNA splicing factor (*RP9*); or are essential structural components of photoreceptors, e.g. rod outer segment membrane protein 1 (*ROM1*) and peripherin 2 (*PRPH2*) [259, 266]. The diverse functions of genes causing IRDs indicate the wide variety of processes necessary for the proper functioning of retinal photoreceptors.

The molecular events leading to AMD development are not fully understood. Nonetheless, they seem to involve oxidative stress, abnormal lipid homeostasis, and inflammation. The factors initiating the retinal and RPE damage trigger a systemic immune response, which fails to restore tissue homeostasis and instead propagates the disease process. The importance of inflammation in AMD pathogenesis is highlighted by the multiple inflammatory components present in the drusen [267]. Additionally, several AMD risk genes have a role in the innate immune system, particularly in the complement pathway, including complement factors H and B (*CFH* and *CFB*), and complement components 2 and 3 (*C2* and *C3*). Notably, approximately 50% of the genetic risk can be attributed to a polymorphism in *CFH* [268].

Furthermore, some AMD risk genes code for molecules involved in recognising pathogenic molecules, e.g. toll-like receptors 3 and 4 (*TLR3* and *TLR4*) [258]. Oxidative stress, another hallmark of AMD, is primarily the result of retina's high oxygen consumption. Photoreceptors consume the most oxygen per gram of cells in the human body [269] and cellular respiration results inevitably in the formation of ROS, which in the absence of sufficient antioxidative mechanisms cause damage to cellular components [270].

In conclusion, the causes, clinical presentation and mechanisms whereby IRDs and AMD lead to photoreceptor degeneration are distinct, but there are a few

similarities. First, increased sunlight exposure has been suggested as a factor accelerating both disease processes. And second, there is an overlap in the genes associated with IRDs and AMD. Namely, there are several genes whose pathological variants cause IRDs and whose polymorphisms also increase the risk for developing AMD, e.g. *ABCA4*, *C2*, *C3*, *TLR3* and *TLR4* [258].

And second, there is overlap in the disease-associated genes as pathological variants of several genes, including *ABCA4*, lead to different IRDs, and some polymorphisms in the same genes confer an increased risk for developing AMD [258].

5.1.3 Mouse models of retinal degenerations

The mechanistic understanding of IRDs and AMD has benefitted considerably from work conducted on mouse models. There are several advantages of using mice to model retinal diseases. First, the genetic tools available make it an excellent model to investigate the effects of various genetic factors. Second, mice are small and keeping them is relatively cost-efficient, facilitating high-throughput studies. Finally, the structure and cellular composition of the mouse retina is similar to the human retina. The mouse and human retinas are composed of the same neural and glial cell types organised similarly into three cellular layers. However, there are also several differences in the retinal structure. Notably, the mouse retina lacks a macula, the central part of the retina involved in AMD and macular dystrophies. Furthermore, the photoreceptor composition between mice and humans is slightly different: while cones comprise 5% of human photoreceptors, they amount to only 1% in mice [271]. Despite these disadvantages, the mouse model continues to be widely used for retinal degeneration research [272]. Recent years have seen a wider use of *in vitro* models where patient-specific induced pluripotent stem cells are differentiated into retinal cells [273] or retinal organoids [274]. Zebrafish, whose retinas are actively regenerating, are also more commonly studied to uncover potential therapeutic strategies for retinal degenerations [275].

There are several approaches to modelling retinal degenerative diseases in mice. IRDs are mainly investigated using transgenic animals carrying gene variants known

to cause human disease, and mouse models are already available for 40% of the known IRD mutations [272]. Likewise, mouse models used for AMD research also include transgenic animals with mutations in AMD risk genes. Additionally, modelling AMD involves replicating particular aspects of the disease process, e.g. increased oxidative stress or deficits in the innate immune system [276]. As both IRDs and AMD lead ultimately to photoreceptor apoptosis, models inducing global photoreceptor damage, such as LIRD, are also used to study the fundamental mechanisms of retinal degenerations.

Light-induced retinal damage model

One method of inducing photoreceptor apoptosis, the final common pathway of retinal degenerations, is by exposing mice to a bright light pulse over a short period. The primary mechanism leading to photoreceptor apoptosis in LIRD is the overstimulation of the visual cycle, which leads to the accumulation of all-*trans*-retinal. The latter is toxic to the retina because of its reactive properties as an aldehyde and as a mediator for ROS generation [223]. As discussed in the previous chapter in section 4.1.1, the induction of retinal damage is dependent on an intact visual cycle and the sufficient supply of 11-*cis*-retinal. The downstream molecular pathways of LIRD are known to involve activator protein 1 (AP-1) [277] and differential regulation of pathways associated with phototransduction, apoptosis and metal homeostasis [278–280].

The LIRD model has several advantages. It is easy to set up in a research laboratory, since administering a bright light pulse does not require complicated equipment. Moreover, photoreceptor damage is induced in a synchronised way, enabling the research of the temporal characteristics of apoptosis. In addition, while retinal degeneration takes several months to develop in some transgenic models, LIRD leads to retinal damage within a few weeks [277]. Besides, by modelling a pathway common to retinal degenerations in general, the results obtained can be extrapolated more broadly than the results of a more specific disease model. And finally, since increased light exposure is known to increase

susceptibility to AMD and some IRDs, LIRD can be regarded as not merely an artificial stimulus inducing photoreceptor apoptosis, but as a model mimicking a risk factor of retinal degenerations [277].

However, there are also several disadvantages to the model. In addition to the aforementioned anatomical differences between human and murine retinas, it is known that rods are more vulnerable to light-induced damage than cones [281], which means the results should be interpreted cautiously in the context of cone-dominated retinal degenerations. Furthermore, IRDs and AMD are chronic conditions evolving over time, whereas exposing animals to a single bright light pulse is an acute treatment, more similar in its mechanism to solar retinopathy than to chronic neurodegenerations. Therefore, the molecular processes involved in LIRD might not be similar to the mechanisms involved in photoreceptor degeneration in IRDs and AMD. In conclusion, the mouse model of LIRD has several advantages. However, it remains unknown to what extent it mimics the human retinal degenerations, which is essential for the accurate extrapolation of the results obtained from this model to human diseases.

5.2 Aims of this chapter

LIRD is a commonly used animal model for retinal degenerative diseases due to its ability to induce photoreceptor apoptosis. The model has several advantages, and it replicates some aspects of human retinal degenerations, but it is currently unknown to what extent the molecular processes affected by LIRD are comparable to changes in human diseases. Therefore, the overarching objective of this chapter is to determine what aspects of human retinal degenerations, the IRDs and AMD, are mimicked by LIRD. Furthermore, it remains unknown to what extent the retinal cell types other than photoreceptors are affected by LIRD and human retinal degenerations, which would provide further insight into how well the LIRD model mimics the cell-specific aspects of human diseases. The recent availability of retinal cell-specific transcriptome datasets, however, now enables this investigation. In addition, and as discussed in section 1.4.5, there is evidence of an interplay between

retinal circadian rhythms and retinal degenerative processes, highlighted by the neuroprotective properties of the circadian hormone melatonin [151–153], the higher retinal susceptibility to damage at night [158], and the reduced photoreceptor function in aged mice lacking core molecular clock components [155–157]. The presence of a dataset of rhythmic retinal transcriptome allows exploring how LIRD affects the rhythmic retinal genes.

With this in mind, the experimental aims of this chapter are to:

1. Conduct a meta-analysis of all publicly available mouse LIRD transcriptome profiling studies to identify the genes and pathways affected in this model
2. Determine whether the genes and pathways differentially regulated in LIRD are enriched for genes involved in IRDs and AMD
3. Determine the retinal cell enrichment and diurnal rhythmicity profiles of genes differentially regulated in LIRD and AMD

5.3 Results

5.3.1 Six publicly available LIRD transcriptomics datasets were identified

To identify studies that analysed global retinal gene expression in response to LIRD, I conducted systematic searches in PubMed, GEO and ArrayExpress (see section 2.9 for methodology). The searches yielded 66, 284 and 291 results, respectively. Out of these, eight studies met the inclusion criteria of using mice as experimental animals, exposing them to a single high-intensity light pulse (>1,000 lux) and subjecting their retinas to a transcriptome profiling analysis [278–280, 282–286] (see Table 5.1 for a detailed overview). Two of the studies [285, 286] had not made their raw data available and could not, therefore, be included in further analysis. The six remaining studies investigated the effect of a genetic mutation or treatment on light damage susceptibility and included WT animals as a control group. Since

this chapter aims to get an overview of the genes and pathways affected by LIRD in general, I included only the transcriptome data of genetically unmodified WT animals in my analysis. The six studies included 43 WT retinal samples, 23 from animals exposed to a bright light pulse and 20 from control animals.

The studies varied in the platforms used to evaluate gene expression: two used Affymetrix Gene 1.0 ST Arrays, two Affymetrix Mouse Genome 430 2.0 Arrays and the remaining two RNA-seq analysis. Most of the studies (five out of six) were conducted on non-pigmented BALB/c mice, whereas one study used pigmented C57 BL/6 NRj animals. The light intensity mice were exposed to ranged from 2,500 to 15,000 lux, and pulse duration varied between 1 hour to 24 hours. Five out of the six studies stated that mouse pupils were dilated before light exposure, while this was not mentioned in one study. Tissue was collected either immediately or up to 4 days after the end of the light pulse. Studies also differed in how the control animals were treated. Some studies pulsed them with a lower intensity light, some kept them in darkness, and some retained them under a normal 12:12 hour LD cycle.

After extracting the gene expression data and importing them into NetworkAnalyst [178], principal component analysis of the 43 samples was performed both before and after the normalisation procedure. Notably, before normalisation across the datasets, the samples clustered based on the transcriptomics platform used. The microarray samples were clearly separated from the samples analysed with RNA-seq, and the two microarray platforms were also distinctly clustered (Fig. 5.1A). However, robust empirical Bayes normalisation [179] across the samples eliminated this platform effect and samples clustered based on whether they were harvested from control or light-damaged retinas (Fig. 5.1B). Therefore, there were no significant batch effects in the resulting normalised dataset, which could confound further analysis, and I went on to analyse the genes changing in response to LIRD.

Table 5.1: Light-induced retinal damage transcriptome profiling studies identified

	Author, year	Accession no	Platform	Mouse strain	Light intensity	Pulse duration	Tissue harvested	Control group	Number of animals
1	Li et al., 2020	GSE146176	Illumina NovaSeq 6000	BALB/c	15,000 lux white LED light with pupils dilated	24 hours after 12-hour dark adaptation	Immediately after the end of pulse	Exposed to 200 lux light for 24 hours	5 control, 5 damaged
2	Scholz et al., 2015	GSE71025	Illumina HiSeq 1000	BALB/cJ	10,000 lux white light with pupils dilated	1 hour after 16-hour dark adaptation	4 days after the pulse	Not stated	2 control, 2 damaged
3	Elachouri et al., 2015	GSE54886	Affymetrix Mouse Genome 430 2.0 Array	BALB/c	2,500 and 5,000 lux cool white fluorescent light with pupils dilated	1 hour after 16-hour dark adaptation	24 hours after light exposure	Exposed to 50 lux light	2 control, 6 damaged (3 in 2,500 lux, 3 in 5,000 lux group)
4	Egger et al., 2012	GSE80265	Affymetrix Mouse Gene 1.0 ST Array	C57 BL/6 NRj	15,000 lux with pupils dilated	2 hours after 16-hour dark adaptation	Immediately after the end of pulse	Not exposed to light	4 control, 3 damaged
5	Hadziahmetovic et al., 2012	GSE37773	Affymetrix Mouse Gene 1.0 ST Array	BALB/c	10,000 lux cool white fluorescent light, no mention of pupil dilation	18 hours after 24-hour dark adaptation	4 hours after light exposure	12:12 light-dark cycle at 200 lux	4 control, 4 damaged
6	Rattner et al., 2008	GSE10528	Affymetrix Mouse Genome 430 2.0 Array	BALB/c	6,000 lux cool white light with pupils dilated	1.5 hours after one-week dark adaptation	24 hours after light exposure	Dark-adapted, not exposed to light	3 control, 3 damaged
7	Krishnan et al., 2008	Not available	Affymetrix GeneChip U74Av2 array	Mixed 129Sv and C57BL/6	2,000 lux cool white fluorescent light without pupil dilation, 6,000 lux with pupils dilated	24 hours (2,000 lux) and 80 minutes (6,000 lux)	Immediately after the end of pulse	Not stated	Pooled retinas of three to four mice
8	Demos et al., 2008	Not available	Affymetrix oligonucleotide MGU74AV2 array	BALB/c	1,500 lux fluorescent light, no mention of pupil dilation	24 and 48 hours	Immediately after the end of pulse	Not stated	Pooled retinas of four mice

5.3.2 Meta-analysis revealed 2,944 retinal genes differentially regulated in LIRD

By combining the gene expression values of the 43 retinal samples, I identified 2,944 genes that were differentially expressed between control and light-damaged retinas (Benjamini-Hochberg multiple comparisons adjusted p value < 0.05). Of those, 1,219 genes were downregulated and 1,726 upregulated in response to the bright light pulse. To understand the molecular mechanisms involved in LIRD, I carried out a network analysis of the 2,944 genes using the IMEx Interactome [180]. The resulting interactome, depicted in Figure 5.2A, illustrates the interactions between the differentially regulated genes and highlights those with the highest number of connections, termed as "hubs". Interestingly, one of the gene hubs was *Tnf*, a key regulator of the innate inflammatory response [277]. The hubs also included other genes associated with chemokine signalling and inflammation, for example, *Tlr3*, the interferon regulatory factors 1 and 8 (*Irf1* and *Irf8*), the interleukin-1 receptor-associated kinase 1 (*Irak1*) and myeloid differentiation primary response protein 88 (*Myd88*). These factors are part of the innate immune system and act as initiators or effectors of the TLR signalling pathway, leading to the activation of innate immune cells and the propagation of pro-inflammatory pathways [287, 288]. Ultimately, these pathways result in the activation of transcription factors such as Jun proto-oncogene (*Jun*), which was also one of the hubs and a known contributor to retinal degenerative processes in multiple diseases, including AMD and RP [287, 289]. In conclusion, this interactome demonstrates that LIRD leads to the activation of the inflammatory response and degenerative processes.

To further characterise the cellular processes involved in LIRD, I carried out a pathway analysis of the differentially regulated genes. The genes were enriched for a wide array of pathways, including those associated with immune function, cellular senescence, and cancer (Fig. 5.2B). The high number of cancer pathways could result from the similarities in the molecular effectors involved in cancer and inflammation [290] and the dysregulation of apoptosis in cancer [291]. Two interesting pathways

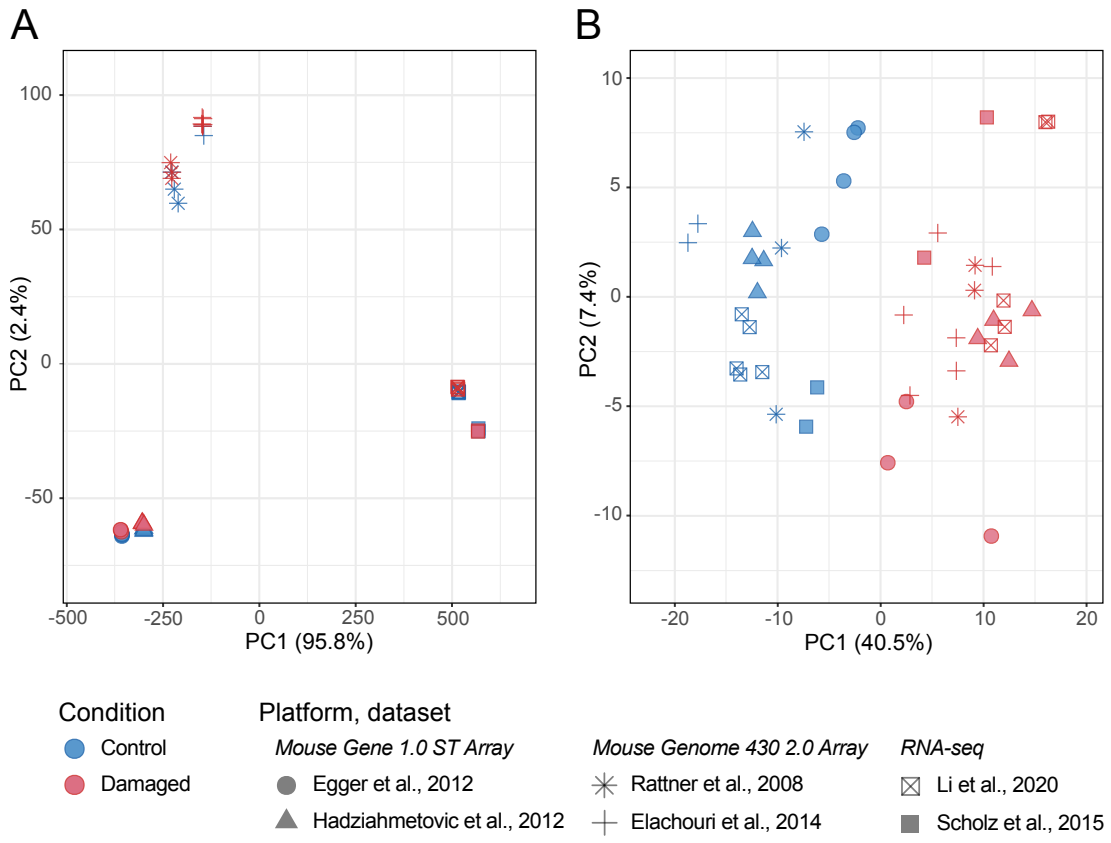


Figure 5.1: Principal component analysis of the six studies included in the LIRD meta-analysis. (A) Before correcting for batch effects, the samples clustered based on the experiment platform used. (B) After robust empirical Bayes regression normalisation, there was a clear separation between control and light-damaged retinas.

from the light damage perspective that showed enrichment for the differentially regulated genes were apoptosis and phototransduction, and I studied these further.

Interestingly, there was a dichotomy in the regulation of genes associated with apoptosis. The factors involved in the induction of apoptosis, such as pro-apoptotic members of the Bcl-2 family *Bid* and *Bax*, pro-inflammatory genes of the tumour necrosis factor pathway and lysosomal proteases cathepsins (*Cts*) were all upregulated in LIRD. On the other hand, genes with anti-inflammatory properties, such as interferon-α and -β (*Infa* and *Infb*), were downregulated (Fig. 5.2C). Genes related to visual function showed similar directionality and were all downregulated in light-damaged retinas (Fig. 5.2D). Since LIRD leads to retinal damage through the overstimulation of the visual cycle and phototransduction [223], this finding could indicate a compensatory mechanism to limit the activation of

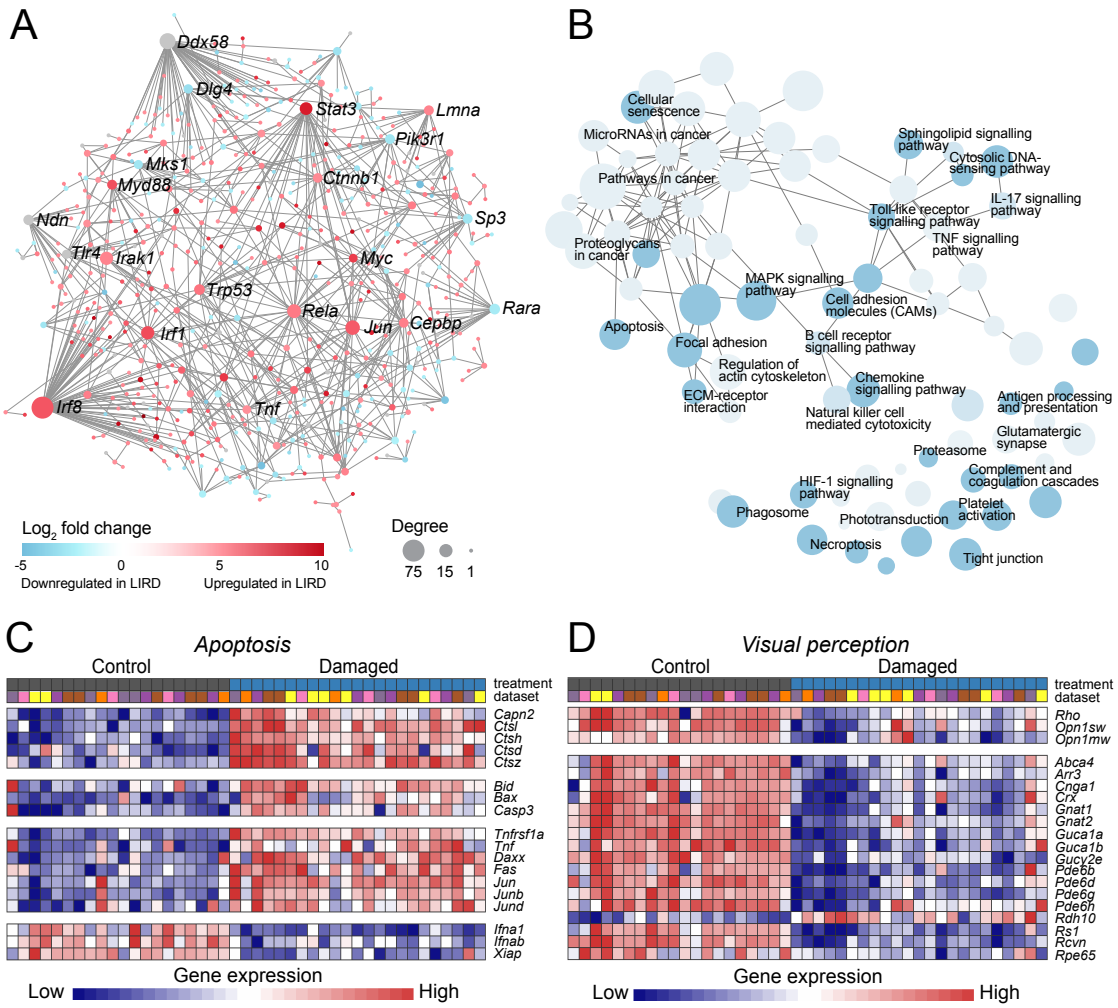


Figure 5.2: Differentially regulated genes and pathways in LIRD. (A) The network of genes differentially regulated in LIRD, produced with IMEx Interactome and visualised in NetworkAnalyst. Degree denotes the number of interactions of a gene. (B) Pathway analysis of differentially regulated genes in LIRD. Pathway size indicates the number of genes in the pathway, darkness indicates more significant enrichment. The expression of genes associated with apoptosis (C) and phototransduction (D). Samples in (C, D) are clustered by unsupervised complete-linkage hierarchical clustering.

photoreceptors. Altogether, the genes and pathways differentially regulated by LIRD, particularly the induction of inflammation and apoptosis, and the downregulation of photoreceptor genes, agree with our knowledge of the processes leading to photoreceptor stress in LIRD.

5.3.3 LIRD leads to the differential regulation of genes implicated in IRDs and AMD

It is crucial to understand which processes of the human diseases each animal model replicates and what are the model's limitations. As I identified the genes and pathways that were reliably changing in the mouse model of LIRD, I went on to analyse whether these genes were overlapping with those known to be associated with retinal degenerations in humans. I retrieved the genes associated with IRDs and the genes with polymorphisms predisposing to AMD from RetNet [258], which lists 301 IRD genes and thirteen AMD risk genes (accessed on August 23, 2020). Out of the 301 genes associated with IRDs, 288 genes have a homolog in the mouse genome, as do 11 of the 13 AMD risk genes.

Notably, almost a third of the IRD risk genes (90 genes, or 31%) were among the 2,944 genes identified in the LIRD meta-analysis (Fig. 5.3), which was significantly more than would be expected by chance ($p < 0.0001$, Fisher's exact test). In addition, nearly half of the AMD risk genes (5 genes, 45%) were differentially expressed in the light-damaged retinas, also showing a significant overrepresentation ($p < 0.05$, Fisher's exact test). Interestingly, all of the AMD risk genes were also among the genes leading to IRDs. This analysis demonstrated that the genes differentially regulated in LIRD are significantly enriched for both IRD and AMD risk genes, indicating that LIRD affects the genes involved in the initiation of both IRDs and AMD.

5.3.4 LIRD affects the cellular pathways, but not genes differentially regulated in AMD

Although the genes differentially expressed in LIRD were enriched for IRD and AMD risk genes, this does not indicate whether LIRD mirrors the retinal gene expression changes seen in these conditions. To analyse this, I used a publicly available dataset by Kim et al. [292]. They performed RNA-seq analysis on human donor retinas harvested from individuals with AMD and age-matched controls. The study included eight normal retinas and seven retinas with a confirmed diagnosis

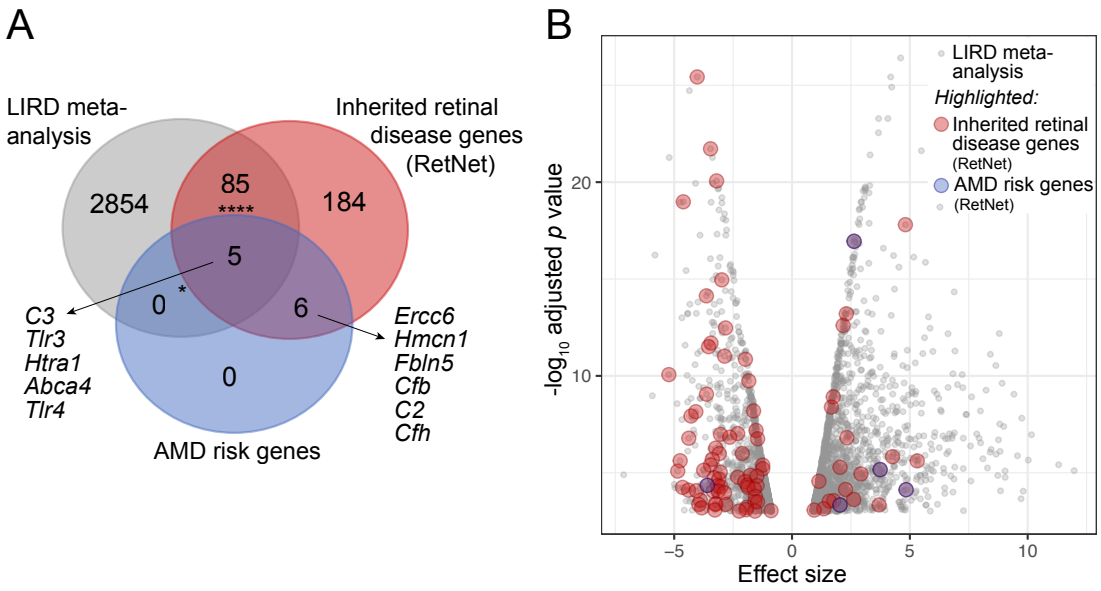


Figure 5.3: Overlap of differentially expressed genes in LIRD with genes associated with IRDs and AMD. (A) A Venn diagram of mouse retinal genes differentially regulated in LIRD and their overlap with human IRD and AMD risk genes. Overrepresentation was analysed with Fisher's exact tests and the results marked in the overlapping area of the Venn diagram circles. (B) A volcano plot of genes differentially regulated in LIRD, illustrating the effect size and p value with IRD and AMD risk genes highlighted. * $p < 0.05$, **** $p < 0.0001$.

of either early or late AMD. Clustering of the samples before and after filtering and $\log_2$ normalisation revealed that the samples clustered based on whether they belonged to the control or disease group, but also on the level of sex (Fig. 5.4). This clustering profile illustrated that the gene expression of AMD retinas differed from control retinas on a global scale, and these changes were also partly modified by sex.

Next, I carried out a differential analysis of gene expression and discovered 1,102 genes that showed differential expression between the control and AMD retinas (Benjamini-Hochberg multiple comparisons adjusted p value < 0.05). Network analysis revealed gene hubs such as the extracellular matrix component fibronectin (*FN1*), which is known to take part in the remodelling of extracellular matrix in AMD, promoting the development of aberrant retinal vessels characteristic of advanced disease [293] (Fig. 5.5A). Another upregulated gene hub was the androgen receptor (*AR*), which might be related to the finding that the retinal sample clustering was modified by sex.

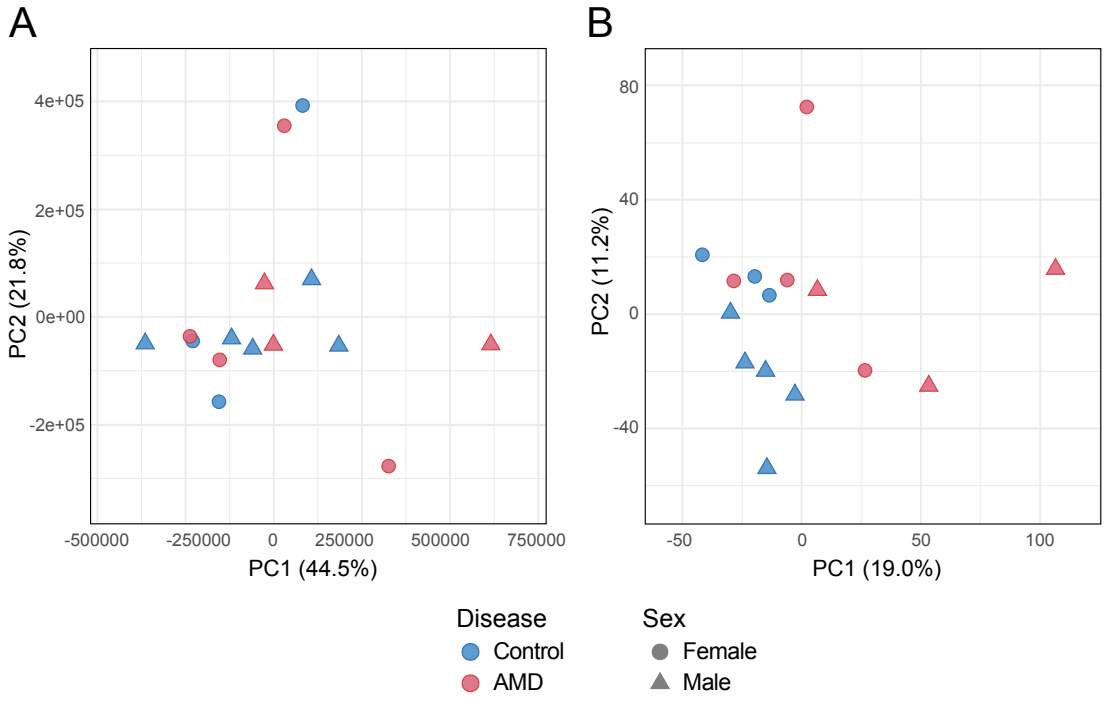


Figure 5.4: Principal component analysis of control and AMD retinas. (A) Before filtering the dataset for genes expressed at a low level and $\log_2$ normalisation, there was no distinct clustering of samples. (B) After filtering and normalisation, samples clustered by disease and sex.

To further understand the cellular processes involved in AMD, I conducted a pathway analysis of the 1,102 genes whose expression differed between AMD and control retinas. The results indicated the involvement of inflammation, apoptosis and collagen remodelling (Fig. 5.5B). Since apoptosis pathway was also enriched for genes differentially regulated in LIRD, and collagen remodelling could refer to late-stage AMD changes, I further analysed these pathways. Contrary to the finding in LIRD retinas, the genes related to apoptosis, including multiple pro-apoptotic factors, were significantly downregulated in AMD retinas compared to controls (Fig. 5.5C). Various collagens and related transcripts also showed significant downregulation in AMD retinas (Fig. 5.5D), possibly indicating the lack of active remodelling in the AMD retinas.

I then analysed to what extent the molecular signature of AMD was replicated in LIRD and how it compared to the genes involved in IRDs. Interestingly, the genes differentially regulated in AMD were not overrepresented in the genes identified in

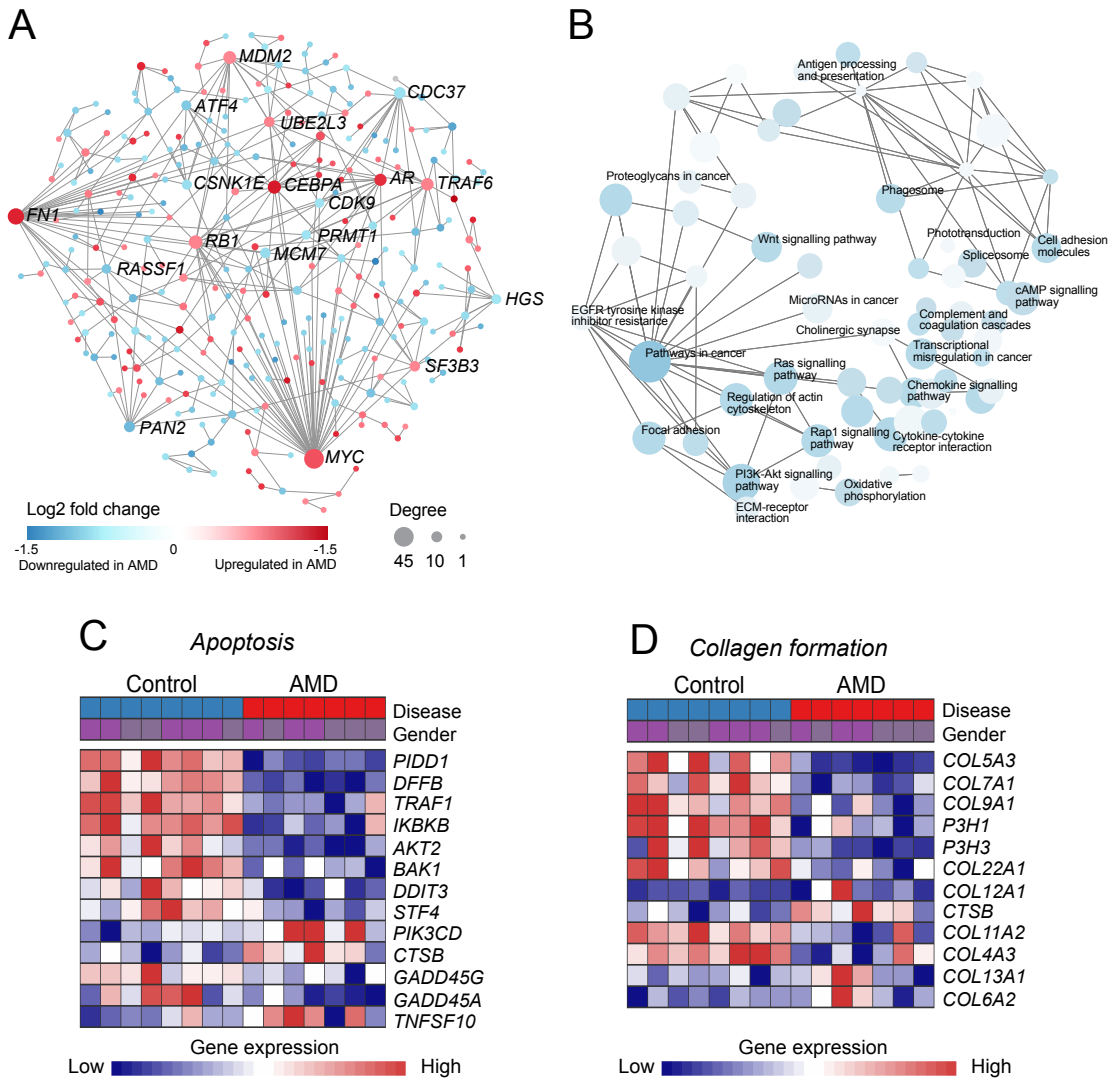


Figure 5.5: Differentially regulated genes and pathways in AMD retinas. (A) The network of retinal genes differentially regulated in AMD retinas, produced with IMEx Interactome and visualised in NetworkAnalyst. Degree denotes the number of interactions of a gene. (B) Pathway analysis of differentially regulated genes in AMD retinas. Pathway size indicates the number of genes in the pathway; darkness indicates a more significant enrichment. The expression of genes involved in apoptosis (C) and collagen formation (D) in AMD retinas. Samples in (C, D) are clustered by unsupervised complete-linkage hierarchical clustering.

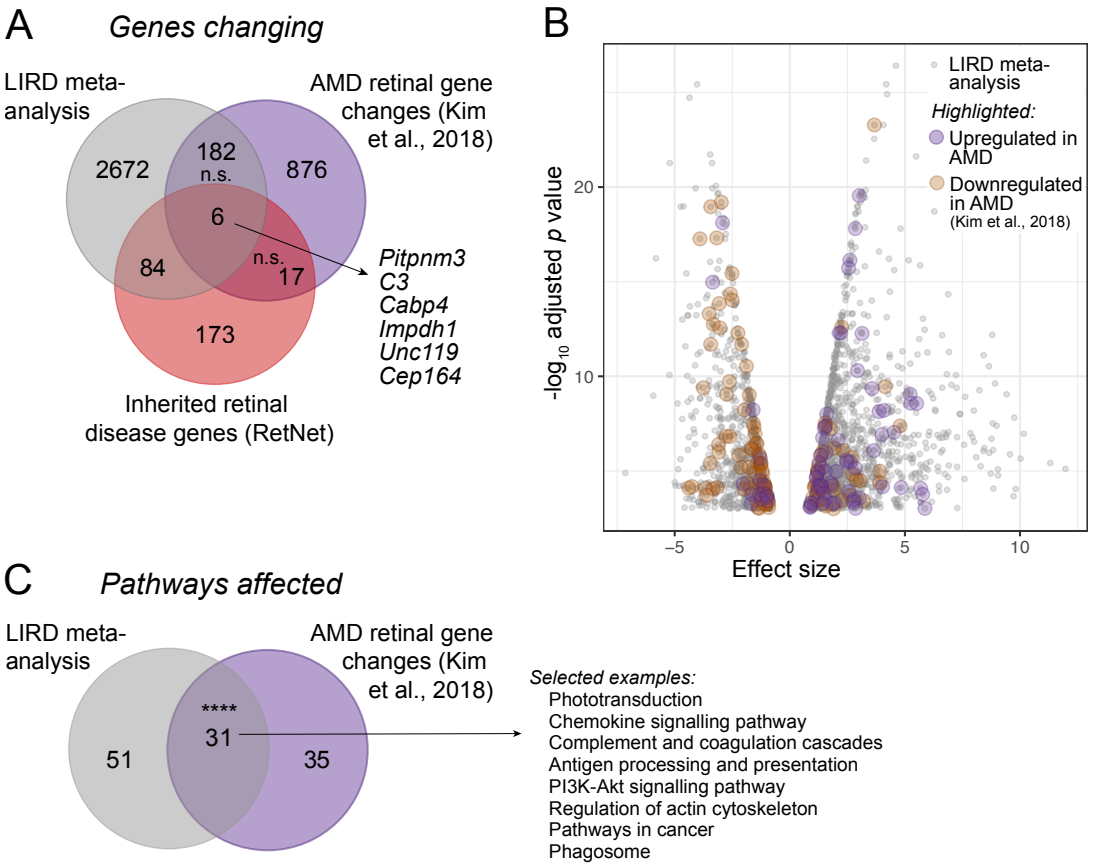


Figure 5.6: Gene expression and pathway overlap between LIRD and AMD retinal changes. (A) A Venn diagram of genes changing in human AMD retinas and their overlap with IRD risk genes and genes differentially regulated in a mouse model of LIRD. (B) A volcano plot of genes identified in the meta-analysis with genes changing in AMD retinas highlighted. (C) The overlap between pathways affected in the LIRD model and AMD retinas. (A, C) Overrepresentation was analysed with Fisher's exact tests and the results marked in the overlapping areas of the Venn diagram circles. n.s., not significant; **** $p < 0.0001$.

the LIRD meta-analysis nor was there a significant overlap with IRD risk genes (Fig. 5.6A). However, 72% of the genes that did show differential regulation in both LIRD and AMD changed in a similar direction, i.e. the genes upregulated in AMD retinas were also upregulated in LIRD (Fig. 5.6B). This finding suggests that LIRD does not model the transcriptional changes seen in AMD retinas. While LIRD is an acute model of retinal degeneration and the retinal tissue was collected shortly after the light damage induction, AMD is a disease developing over years and even decades. It may be that the chronic changes of AMD result in a different gene expression pattern than that of an acute intervention.

Despite the lack of similarities on a gene expression level, the two processes, LIRD and AMD, may still involve similar pathways. Therefore, I analysed the pathways enriched for the genes changing in LIRD and AMD and found that they showed significant overlap, with phototransduction and various inflammatory pathways affected in both (Fig. 5.6C). Overall, these results demonstrated that although the genes differentially regulated in AMD were not overrepresented in the genes differentially regulated in LIRD, both processes affected similar cellular pathways.

As seen from the results above, the genes initiating a disease may not necessarily be involved in the later stages of a disease. Therefore, I wanted to further examine whether the retinal transcriptional changes of AMD reflect the genes known to increase AMD risk. For this analysis, I used the genes listed as AMD risk genes in the RetNet database [258], as well as the AMD risk genes identified in a recent genome-wide association study (GWAS) study [294]. Indeed, the group of genes differentially regulated in AMD retinas was not enriched for either of the gene sets (Fig. 5.7). However, genes related to the complement cascade, e.g. *C2*, *C3*, *CFH* and *CFB* were listed as AMD risk genes in RetNet and also identified in the GWAS study, indicating an essential role for this process in AMD pathogenesis. This finding further confirms that the molecular mechanisms initiating AMD are distinct from the gene expression changes the process ultimately leads to.

The clustering of AMD retinal samples based on sex and the presence of the androgen receptor in the interactome analysis suggested the involvement of sex hormones in AMD pathogenesis. To understand the sex-mediated differences in AMD, I carried out further analysis and found that a total of 58 genes were differentially regulated between male and female AMD retinas. They all showed a similar expression pattern: these genes were upregulated in female AMD retinas compared to controls, and this upregulation was missing in male AMD retinas (Fig. 5.8A). The pathways these genes belonged to involved inflammatory processes, but interestingly also oestrogen signalling (Fig. 5.8B). I further carried out an interactome analysis (Fig. 5.8C) and saw that among the differentially regulated genes were histone genes (*HIST1H1*), fibronectin (*FN1*), and heat shock protein

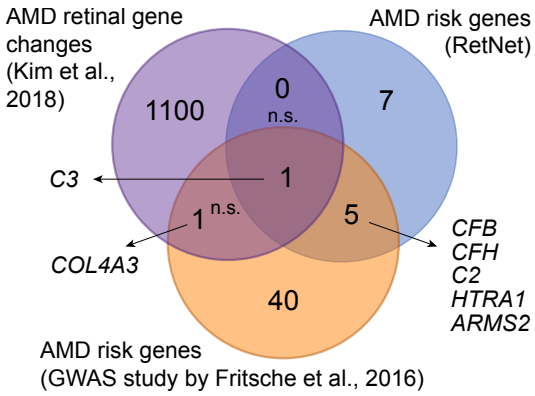


Figure 5.7: The overlap between retinal genes differentially regulated in AMD and AMD risk genes. A Venn diagram depicting genes differentially expressed in human AMD retinas and their overlap with published AMD risk genes listed on RetNet and genes associated with AMD in a recent GWAS study. Overrepresentation was analysed with Fisher's exact tests and the results marked in the overlapping areas of the Venn diagram circles. n.s., not significant.

A6 (*HSPA6*). The latter has anti-apoptotic properties and is known to be induced by oestrogen signalling and also in response to cellular stress [295]. However, whether the 58 genes as a group would result in retinal protection or, conversely, in more severe degeneration, was not clear. In conclusion, a cluster of genes was differentially regulated in male and female AMD retinas, which can partly be explained by differential oestrogen signalling.

5.3.5 Retinal cell populations enriched for genes differentially regulated in LIRD and AMD show limited similarity

The retina is composed of multiple cell types, and the changes on a retinal level do not indicate what cell types are involved in the disease processes. To understand which retinal cells LIRD and AMD affect, I carried out an analysis using a publicly available dataset by Siegert et al. [184] who performed microarray analysis on a variety of retinal cell populations. I calculated the cell-specific enrichment of the genes differentially regulated in LIRD and AMD as outlined in section 2.10.

This analysis demonstrated that the genes differentially regulated in LIRD were enriched in microglia, pRGCs, cones and horizontal cells (Fig. 5.9A). The genes changing in AMD, on the other hand, showed enrichment in AII amacrine cells,

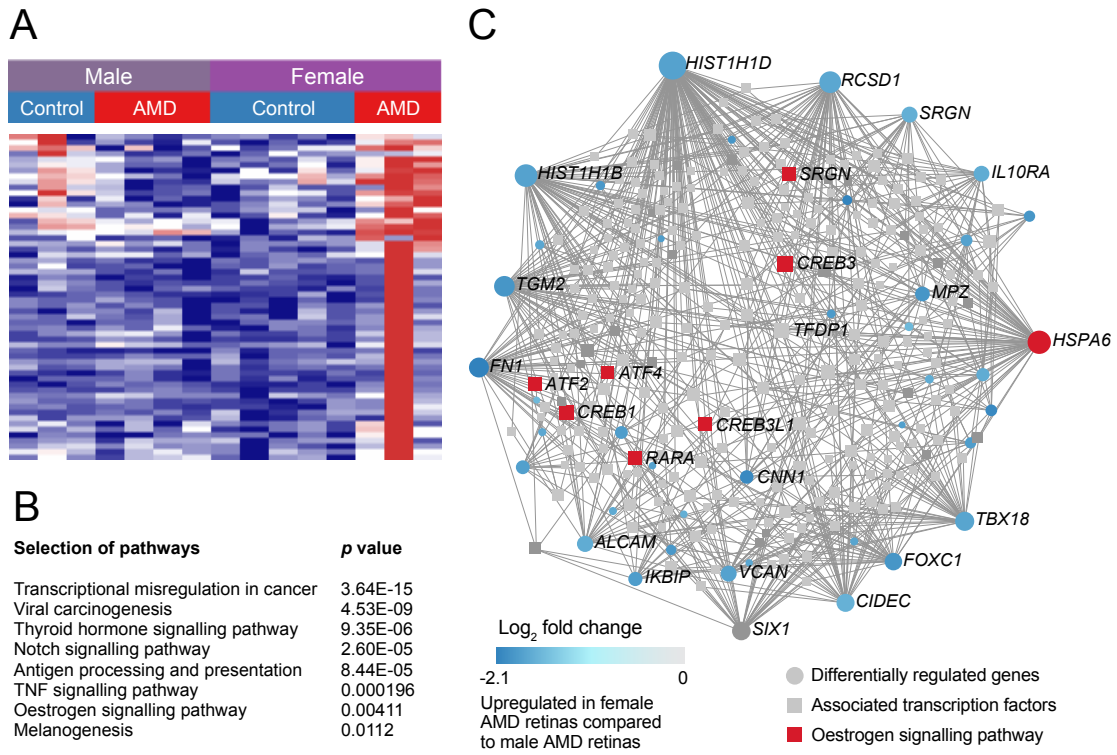


Figure 5.8: Differentially regulated genes and pathways in male and female AMD retinas. (A) A heatmap of all differentially regulated genes in AMD retinas between sexes and (B) the selection of pathways enriched for these genes. (C) The network of genes differentially regulated and associated transcription factors. Genes and transcription factors related to oestrogen signalling pathway are highlighted in red. Interaction network was produced with IMEx Interactome and visualised in NetworkAnalyst. Samples in (A) are clustered by unsupervised complete-linkage hierarchical clustering.

ON bipolar cells, parvalbumin (PV) positive RGCs and a cell population marked by neuronal acetylcholine receptor subunit alpha-3 (CHRNA3), which labels cones, amacrine cells and RGCs [184] (Fig. 5.9D). Overall, these data suggest that LIRD and AMD lead to changes in genes, which are enriched in distinct cell types. These differences might be explained by the acute nature of LIRD, which leads to the activation of retinal microglia, and light stimulation would activate photosensitive cells such as cones and pRGCs. The chronic disease process of AMD would instead have led to the remodelling of retinal circuits and affected the gene expression profiles of retinal interneurons, including bipolar and amacrine cells.

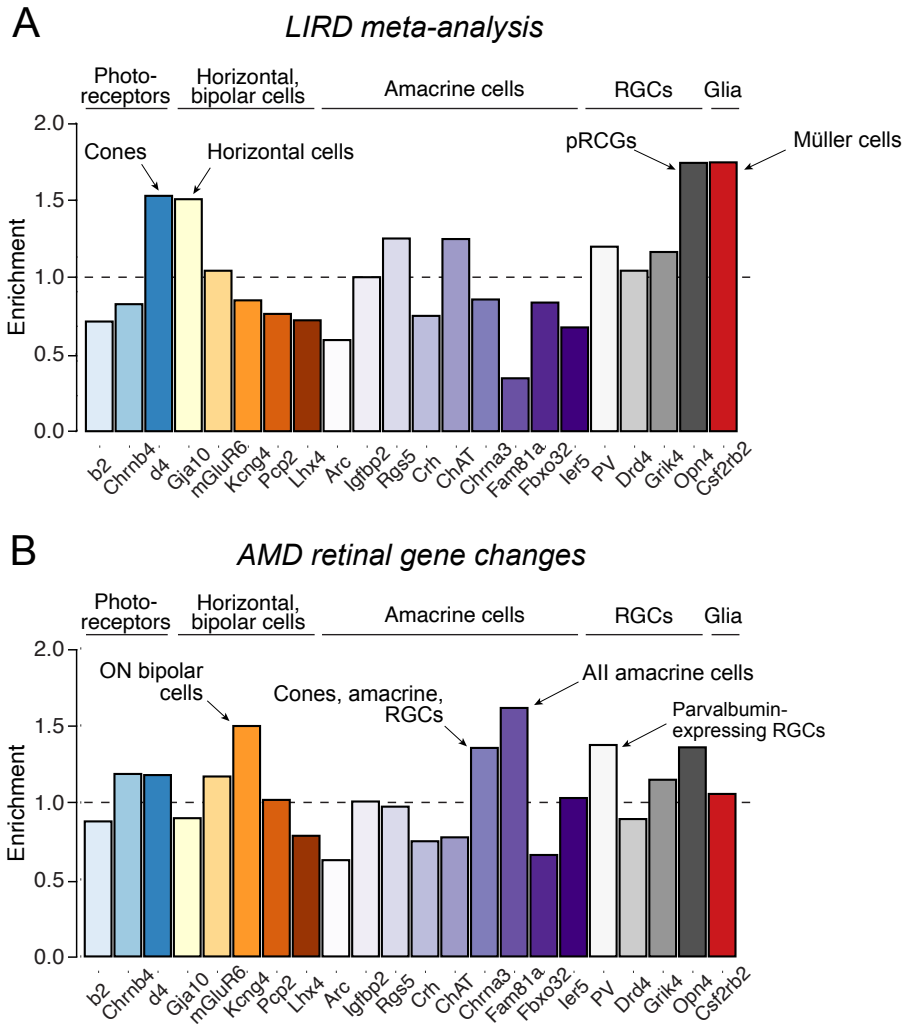


Figure 5.9: Enrichment of differentially regulated genes in retinal cell types. Enrichment of genes in each retinal cell subpopulation was calculated as the number of genes expressed more than 2 SD higher than the mean expression of that gene across all subpopulations, and was normalised to the number of genes enriched in each subpopulation across the entire transcriptome. Data are displayed for genes differentially regulated in LIRD (A) and AMD (B).

5.3.6 LIRD and AMD do not differentially affect rhythmic retinal genes

Several neurodegenerations are associated with the disruption of circadian rhythms, and there is also evidence of interactions between circadian rhythms and retinal degenerations. To investigate whether LIRD and AMD preferentially affect the rhythmic retinal transcriptome, I determined how many of the differentially regulated genes show rhythmic expression in the retina. Since at the writing of this chapter, there were no retinal circadian datasets available on mice, I made use of the dataset

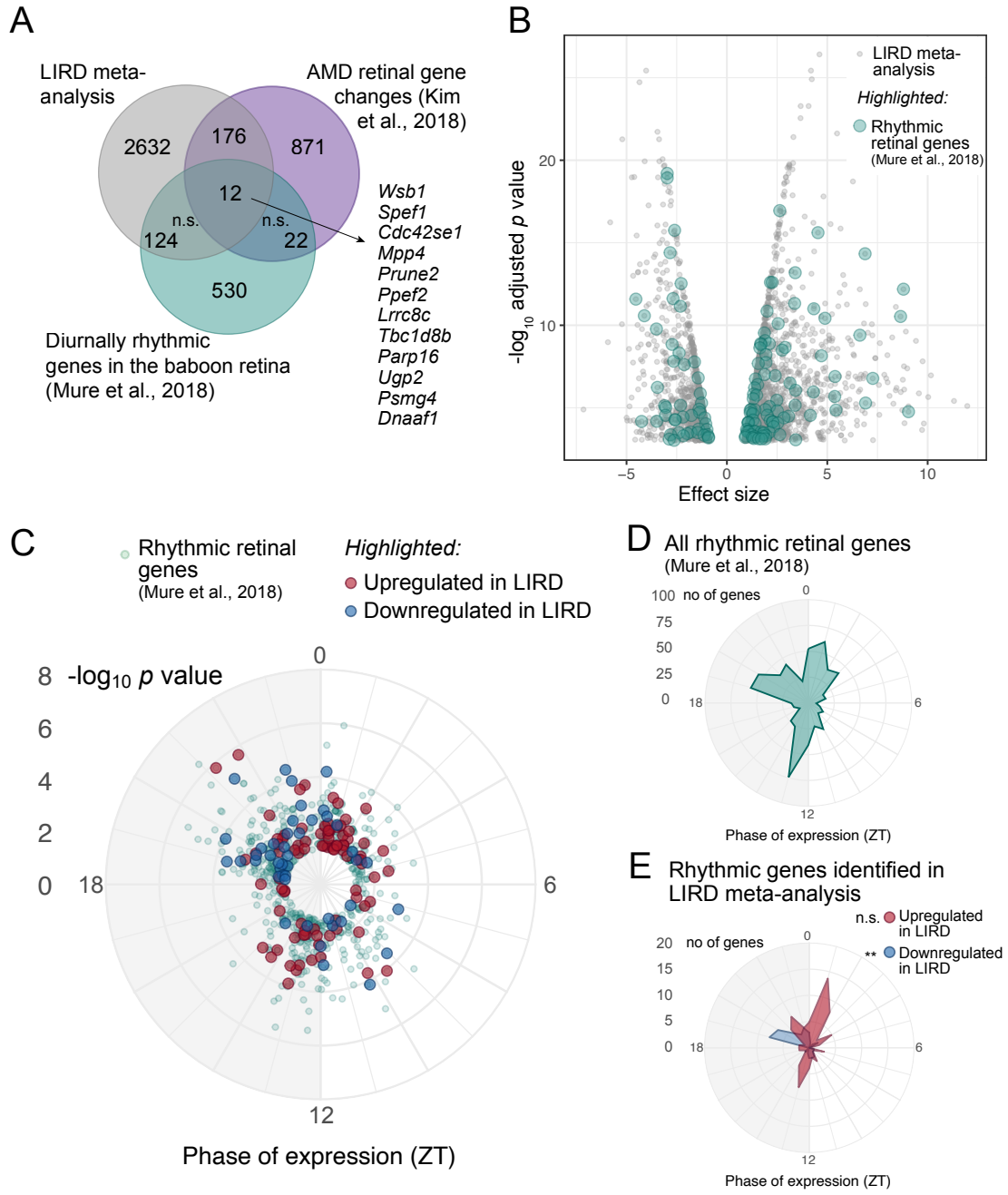


Figure 5.10: Representation of diurnally rhythmic genes in LIRD and AMD retinas. (A) The overlap between genes differentially regulated in LIRD and AMD with genes showing diurnal rhythmicity in the mammalian retina. Overrepresentation was analysed with Fisher's exact tests and the results marked in the overlapping areas of the Venn diagram circles. (B) A volcano plot of genes identified in the LIRD meta-analysis with genes showing diurnal rhythmicity highlighted. (C) A radial plot of all rhythmic genes in the retina with genes differentially regulated in LIRD highlighted. (D) The distribution of the peak expression phases of all rhythmic genes in the retina and (E) the rhythmic genes differentially regulated in LIRD. There was a statistically significant difference in the distribution of phases between all retinal rhythmic genes and those downregulated in LIRD ($p < 0.01$, two-tailed t-test). n.s., not significant; ** $p < 0.01$.

by Mure et al. [199] who harvested retinal tissue from olive baboons every two hours over a diurnal day and subjected these samples to RNA-seq analysis. I analysed the expression rhythmicity of the genes changing in LIRD and AMD and discovered that the retinal genes affected by these processes were not enriched for rhythmic genes ($p > 0.05$, Fisher's exact test, Fig. 5.10A). Furthermore, the rhythmic genes did not show a preferential up- or downregulation in LIRD (Fig. 5.10B).

Since genes with a similar peak phase are often involved in similar tissue processes [296], I analysed the phases of the rhythmic genes that were up- and downregulated in LIRD. Intriguingly, while the phases of upregulated LIRD genes showed two distinct phases at ZT1 and ZT13, the majority of genes downregulated in LIRD showed a peak around ZT19 (Fig. 5.10C). Quantification of the number of genes with phases in 1-hour bins revealed that the genes upregulated in LIRD had an overall similar phase distribution to all rhythmic retinal genes ($p > 0.05$, two-tailed t-test of the phases, Fig. 5.10D, E). However, the phases of downregulated genes were significantly different from the average phase of rhythmic retinal genes ($p < 0.01$, two-tailed t-test). The finding that the directionality of gene changes was related to the diurnal phase of the genes increased the confidence that the genes up- and downregulated in LIRD belonged to distinct cellular pathways.

5.4 Discussion

The objective of this chapter was to determine to what extent the mouse model of LIRD mimics the IRDs and AMD on a gene and pathway level. A meta-analysis of six publicly available LIRD datasets resulted in the identification of 2,944 genes differentially regulated in LIRD. Investigation of the pathways suggested the involvement of the innate immune system, apoptosis and visual cycle. Furthermore, the differentially regulated genes were enriched for genes known to cause IRDs and increase AMD risk, implying that the cellular pathways set in motion by LIRD are similar to those initiating human retinal degenerations. Therefore, on a gene expression level, the mouse model of LIRD seems to replicate human diseases.

Despite these similarities, I found that the genes differentially regulated in LIRD were not enriched for genes changing in AMD retinas. This result may not be surprising as LIRD is an acute model of retinal distress and the retinal samples included in the meta-analysis were collected either immediately after light exposure or up to 4 days after the end of the light pulse, the majority were collected 24 hours after the end of the light pulse. Therefore, the gene changes seen in LIRD would mirror the initial, not chronic effect of the human retinal degenerations. Throughout AMD, the retina undergoes considerable remodelling, photoreceptor degeneration and can in later stages also result in the development of abnormal blood vessels [297]. Retinal remodelling and vascular changes are unlikely to occur in a short time frame of the LIRD model. To uncover how well the mouse model of LIRD mirrors changes seen in human AMD, it would be interesting to investigate the transcriptional changes of light-damaged mouse retinas after several months when the photoreceptors have undergone apoptosis, and the retinal circuits have started to remodel.

The pathways enriched for the genes differentially regulated in LIRD and AMD displayed significant overlap, and most of the genes that changed in both LIRD and AMD showed similar directionality. Surprisingly however, various pro-apoptotic genes were upregulated after LIRD but downregulated in AMD retinas. Postmortem analysis of AMD retinas has demonstrated increased terminal deoxynucleotidyl transferase dUTP nick end labeling (TUNEL) staining in macular photoreceptors, indicative of apoptosis [298], which seems to contradict my findings. Nevertheless, it might be that the pro-apoptotic factors, which set the degenerative processes in motion are downregulated at later stages of apoptosis, which is instead characterised by DNA fragmentation, detected by TUNEL staining.

The cell types affected by LIRD and AMD show limited overlap as microglia, pRGCs, cones, and horizontal cells were involved in LIRD and bipolar and amacrine cells in AMD. The damaging effect of LIRD could explain the enrichment of differentially expressed genes in microglia and the increased light stimulation the involvement of pRGCs and photoreceptors. Horizontal cells provide lateral

inhibition to surrounding photoreceptors [2] and could also be activated as a result. On the other hand, AMD is characterised by retinal remodelling and rewiring, which could explain the enrichment of differentially regulated genes in bipolar and amacrine cells. In conclusion, the cell types enriched for genes involved in LIRD and AMD are distinct.

The analysis of AMD retinas showed that several genes were differentially regulated between male and female AMD retinas, and pathway analysis referred to oestrogen signalling in this process. There is a considerable amount of data available on the role of sex hormones in retinal protection as both female sex hormones, oestrogen and progesterone, have been demonstrated to exhibit neuroprotective properties. For example, 17b-oestradiol and a synthetic progesterone progestin have both shown a protective effect in LIRD [299, 300]. Furthermore, female sex hormones seem to also have a retinoprotective effect in AMD. A study by Snow et al. [301] demonstrated that the use of oestrogen replacement therapy in postmenopausal women significantly lowered the risk of developing advanced AMD. Whether sex itself is an independent risk factor for AMD, has also been studied, but there is no clear consensus in the field. Some studies have determined that women have a higher risk for developing AMD [264], others have shown men to have a higher risk [302], and some studies have found no effect of sex [303].

In light of this literature, it is perhaps not surprising that the AMD retinal samples clustered by sex and female and male AMD retinas had differences in gene expression. The retinas of the two sexes would have been exposed to different amounts of oestrogen, progesterone, and testosterone throughout their lifetime, which could account for the findings. It would have also been interesting to analyse the sex-dependent retinal gene changes in light-damaged mouse retinas. Unfortunately, only two of the six studies included data on which samples were collected from male and female mice [278, 279]. The sex of animals was not mentioned at all in two studies [280, 284], and two said they used a combination of male and female mice, but did not indicate in their sample information sheet, which samples were from male and which from female animals [282, 283].

The genes changing in LIRD and AMD retinas were not enriched for the rhythmic transcriptome of baboon retinas. One might hypothesise that since the retinas of aged mice lacking components of the core molecular clock develop retinal photoreceptor abnormalities [155–157], retinal degenerations may preferentially affect the circadian retinal transcriptome suggesting a broader role for circadian rhythm disruptions in retinal degenerations. In addition, as the retina is better adjusted to manage damaging insults at day [158], the rhythmic genes providing this protection would be differentially regulated in response to damaging stimuli. However, the results of this study do not confirm these hypotheses. Interestingly however, the genes that were up- or downregulated in LIRD showed distinct phase distributions, suggesting perhaps that they participate in similar cellular processes [296].

In conclusion, in this chapter, I set out to determine to what extent the mouse model of LIRD, which is widely used to study the molecular mechanisms of retinal degenerations, mimics the molecular mechanisms known to be involved in human retinal degenerations. I demonstrated that the acute gene expression changes in light-damaged mouse retinas mirror the initiation phase of human retinal degenerations, both IRDs and AMD, but do not overlap with the transcriptomic landscape characteristic of later stages of AMD. Therefore, the results obtained with the mouse model of LIRD are applicable to human retinal degenerative diseases.

5.4.1 Limitations of this study and future work

One limitation of this investigation is that the meta-analysis was conducted on studies using different protocols to induce LIRD, varying in when the retinal tissue was harvested, how the control group was treated, and the genetic background of the mice used. By combining the gene expression data of all studies, the analysis was biased towards detecting transcripts that were consistently elevated across the different treatments. As five out of the six studies analysed retinal gene expression 24 hours after the start of the bright light exposure, the more immediate and acute light-induced gene expression changes were missed. A larger number of studies

with more varied times of tissue collection would enable to determine the temporal characteristics of light-induced transcripts in more detail.

Another limitation of the study is the assumption that the genes known to have pathological variants leading to IRD and AMD initiate the disease process by having a primary role in the retina. The pathogenesis of retinal degenerations is strongly influenced by the function of the underlying RPE and defects in its function, as pathological variants of visual cycle genes, e.g. *LRAT*, *RPE65* and *RDH5* are known to lead to IRDs [258]. Furthermore, the disease processes are modulated by the innate immune system and other systemic factors. In my transcriptome meta-analysis, I only investigated the gene changes taking place in the retina and compared these results to all IRD and AMD risk genes. However, some of the risk genes may have a more critical function in the RPE or immune system, and LIRD may not influence their expression levels in the retina. Nonetheless, by including all IRD and AMD risk genes in my comparison, I avoided any potential bias I would have introduced by classifying IRD and AMD risk genes to having a role in the retina or not.

A further limitation is that I did not consider whether the pathological variants of genes causative of IRDs are loss- or gain-of-function mutations. It could be argued that for LIRD to mimic human diseases, the genes with loss-of-function variants and gain-of-function variants causing IRDs should be regulated in opposite directions. The genes with gain-of-function pathological variants should be upregulated to result in a similar retinal effect as the genes have in IRDs. Alternatively, one might hypothesise that the retinal changes upon LIRD should reflect retinal adaptation and lead to gene expression changes in the opposite direction. It would be interesting to analyse which direction the genes with loss- and gain-of-function pathological variants were changing in LIRD. Unfortunately, the matter is complicated by the notion that several genes have multiple pathological variants, some of which are loss- and some gain-of-function variants [259], making this comparison challenging to conduct.

In addition, I base all my analysis on gene expression data. While gene expression is a relatively accessible and cost-effective way to study the global changes in response

to a stimulus, the proteins, not the transcripts, carry out cellular functions and protein abundance is not directly correlated with transcript abundance. The function of proteins themselves is regulated by post-translational mechanisms, controlled by other proteins, which are difficult to account for in my analysis. Therefore, although I identify almost 3,000 genes differentially regulated in LIRD, these results do not indicate protein abundance and do not reflect post-translational modifications, both of which would be interesting targets for future investigations.

An important confounding factor in my analysis of whether the rhythmic genes were more likely to be affected in LIRD and AMD was that I compared the mouse retinal gene changes in LIRD to genes rhythmic in the baboon retina. As I discovered in chapter 3, there is limited overlap between the rhythmic genes in mouse and baboon retinas (Fig. 3.19). Future work will include the comparison of the LIRD transcriptomics results to the circadian transcriptome of the mouse retina. It would also be interesting to analyse the rhythmicity of gene expression in degenerate retinas to further uncover the implications of circadian rhythms in retinal degenerations.

6

Characterisation of the key circadian protein salt-inducible kinase 1 in the mammalian retina

6.1 Introduction

The retina adjusts its function to the environmental light levels to enable the visual system to function over a range of irradiances and prepare the retina for the potentially damaging effect of bright light [210, 225, 226]. Similarly, light input to the SCN is responsible for communicating environmental changes to the entire organism by modulating the central circadian rhythms [22, 109]. The absence of melanopsin results in dampened light responses in the SCN [32, 33, 64] and also the retina [78, 192], indicating a level of similarity between how these two tissues sense light. However, the extent to which the SCN and retinal light responses correlate is not known. Therefore, to further investigate the interplay between circadian rhythms and retinal light responses, I used a mouse model with an opposite circadian phenotype to mice lacking melanopsin, one that is more sensitive to light [186]. The animals lacking functional salt-inducible kinase 1 (SIK1) have enhanced circadian responses to light on the SCN level (Dr Lewis Taylor, unpublished data), suggesting that their retinas might also show heightened light sensitivity.

In this chapter, I am addressing the final aim of my thesis to study the retinal light sensitivity of mice lacking functional SIK1, a model that shows increased light responses of the central circadian clock.

6.1.1 Function of SIK1 in the core molecular clock

The core molecular clocks of the retina and the SCN are both responsive to light, enabling the tissues to align their circadian phases to the external world. However, light exposure can shift the clocks only to a certain extent, and the adjustment to a new light schedule takes several days [145, 186]. The extent of light-induced clock shifts in the SCN is regulated by SIK1 [186]. Light information is relayed to the SCN by the pRGCs that release glutamate and PACAP from their axon terminals [53, 83]. Neurotransmitter release leads to the rise of intracellular Ca^{2+} and cyclic AMP (cAMP) in the SCN neurons, the phosphorylation of cAMP-response element-binding protein (CREB) and its binding to CREB-regulated transcription coactivator 1 (CRTC1). The CREB–CRTC complex translocates to the nucleus, binds to cAMP response elements (CRE) and induces the expression of their target genes, including *Per1*. The increased levels of PER1 protein, a component of the negative arm of the core molecular clock, modulates the time it takes for the circadian clock to complete one cycle, thus shifting the phase of the clock [186] (Fig. 6.1).

Another gene induced in the SCN by light and the CREB-CRTC1 complex is *Sik1*. Once translated, the SIK1 protein phosphorylates CRTC1, which is unable to bind CREB, in its phosphorylated state, resulting in the dissociation of the CREB-CRTC1 complex. This, in turn, limits the expression of target genes controlled by the CRE regulatory element, including *Per1*. Therefore, SIK1 limits the extent the SCN clock can shift in response to light [186] (Fig. 6.1). As would be expected from the impact of SIK1 on *Per1* expression, animals lacking *Sik1* display exaggerated light sensitivity. Upon *Sik1* knock-down in the SCN, mice show larger circadian phase-shifting response to a nocturnal light pulse and entrain to a shifted light schedule considerably faster than WT animals [186]. While WT mice take approximately 5 days to adjust a 6-hour shift in the light schedule, mice lacking *Sik1* expression in the

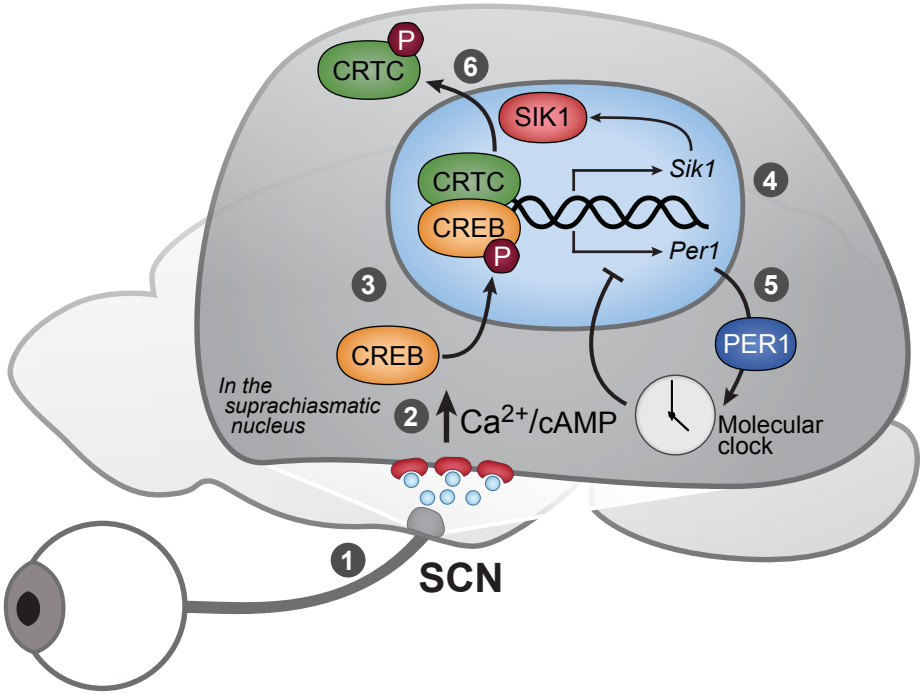


Figure 6.1: SIK1 acts as a brake on light-induced clock shifts in the SCN. 1) Light input reaches the suprachiasmatic nucleus (SCN) via photosensitive retinal ganglion cells (pRGCs). 2) Neurotransmitter release leads to intracellular Ca^{2+} influx and increased levels of cAMP. 3) CREB is phosphorylated and binds to its co-factor CRTC1, translocates to the nucleus and interacts with its response elements. 4) This leads to the transcription of CREB target genes, *Per1* and *Sik1* among others. 5) PER1 protein acts to shift the phase of the molecular clock. 6) SIK1 phosphorylates CRTC1, resulting in its dissociation from CREB, therefore limiting CREB-mediated transcription of its target genes, including *Per1*. This mechanism thus limits the extent the central circadian clock can shift in response to light.

SCN take only 2-3 days. The phenotype is indeed dependent on the kinase activity of SIK1 as mice expressing a variant of SIK1 that lacks the ability to phosphorylate its targets, show a similar phenotype (Dr Lewis Taylor, unpublished data).

6.1.2 The SIK family and signalling cascade

The discovery of SIK1 was relatively recent. Twenty-two years ago, Wang et al. [304] characterised *Sik1* as a transcript upregulated in the rat adrenal gland in response to a high salt diet [304]. Two other SIK family members, SIK2 and SIK3, have been identified since and shown to have physiological roles in several tissues. SIK2 is present in high abundance in murine adipocytes, and its function has been studied

with regard to its contribution to the development of insulin resistance in type 2 diabetes [305]. SIK3 is crucial for metabolism, and the development of the skeletal system. Mice lacking SIK3 exhibit abnormal cartilage formation, have severe skeletal abnormalities and develop hypoglycemia and hypoglycemia [306]. Furthermore, SIK3 is also important for proper sleep function as a gain-of-function variant of SIK3 has been identified to cause increased sleep need in mice [307].

The signalling cascade of SIKs involves several key proteins. SIK1-3 are activated by serine/threonine kinase 11 (STK11), also known as liver kinase B1 (LKB1) [308]. SIK proteins themselves exert their function by phosphorylating their substrates, most importantly the CRTC1-3 [309], and class IIa histone deacetylases (HDACs 4, 5, 7, and 9) [310]. Phosphorylation by SIKs plays an important role in determining the subcellular localisation and thus the biological activity of their targets. When phosphorylated, the CRTC proteins and class IIa HDACs are localised to the cytoplasm and associated with 14-3-3 chaperones. Upon dephosphorylation, they translocate to the nucleus to regulate their target genes [309, 310]. CRTC proteins function as CREB coactivators and mediate CREB target gene activation [309]. Class IIa HDACs have a conserved binding site for the transcription factor myocyte-specific enhancer factor 2 (MEF2) and act to repress its activity [310].

6.1.3 The possible function of SIK1 in the retina

The mechanisms limiting light-induced shifts in the retina are not known. Since the clock machinery of the retina and the SCN involve the core molecular clock, the role of SIK1 in the retina may be similar to its function in the SCN to limit light responses. Furthermore, as several core clock genes affect retinal development [174], this could also be the case for SIK1. The function of SIK1 in the mammalian retina has not been studied to date. However, the two fly homologs of SIKs, *Sik2* and *Sik3*, were recently studied. It was reported that the overexpression and knock-down of either gene led to ocular developmental abnormalities [311]. Knock-down of *Sik2* resulted in the most severe phenotype as those flies lost the entire ventral half of

the eye [311]. Therefore, SIK1 could play a role in the light responses of the retina, similarly to its role in the SCN, but also affect retinal development.

6.2 Aims of this chapter

SIK1 is an essential component of the core molecular clock, limiting the light-induced circadian clock shifts in the SCN by limiting the extent of *Per1* induction. Animals lacking functional SIK1 thus exhibit increased SCN light responses, manifested in enhanced circadian phase-shifting response and rapid re-entrainment to a new environmental light-dark cycle, a phenotype opposite to mice lacking melanopsin. In mice lacking melanopsin, the dampened light responses of the SCN are coupled with slight decrease in retinal light responses. However, to what extent the retinal and SCN light responses are regulated in a similar fashion, is not known. Therefore, the animals lacking functional SIK1 provide an exciting model to further investigate the interplay between the retinal light responses and the circadian clock. Should the light responses of the retina and SCN be similarly regulated, the lack of functional SIK1 should also result in increased retinal light responses.

Therefore, the overarching objective of this chapter is to explore the function of SIK1 in the retina, and the specific experimental aims of this chapter are to:

1. Characterise the expression of *SIK1* and related transcripts in mammalian ocular tissues

2. Investigate retinal morphology in the absence of functional SIK1

3. Analyse the retinal light responses of gene expression and pupil constriction in the absence of functional SIK1

6.3 Results

6.3.1 SIK family and related transcripts are expressed in the retina and other ocular tissues

To understand the role of SIK1 in the retina, I first set out to investigate its expression in ocular tissues. To get a more holistic overview, I analysed the expression of the genes in the SIK family and the genes associated with their function: the *CRTCs*, *CREB* isoforms, CREB binding protein (*CREBBP*) and *STK11*. I made use of the dataset by Mure et al. [199] who harvested several tissues from olive baboons over a diurnal day and subjected these samples to RNA-seq analysis. I calculated the average expression of each gene of interest in all ocular tissues included in this dataset: the iris, cornea, ONH, retina and RPE. Since the function of SIK1 has been well characterised in the SCN and adrenal cortex, and SIK2 is known to play an essential role in white adipose tissue, I also included these three tissues in the analysis as a comparison.

In this dataset, the *SIK1-3* and *STK11* transcripts were detected in all five ocular tissues (Fig. 6.2A). The gene expression differed substantially between the tissues, but as a general pattern, the levels of *SIK1* were the lowest, followed by *SIK2*, then *SIK3*. An exception to this pattern was the cornea where *SIK1* was the most abundant of the transcripts. As a general observation, the transcripts of *SIK1-3* and *STK11* were not depleted or particularly enriched in ocular tissues compared to their levels in non-ocular tissues with a known role for the SIK system (Fig. 6.2A).

I then analysed the expression levels of the three *CRTC* isoforms. Similarly to the *SIK* transcripts, these were all detected in all five ocular tissues (Fig. 6.2B). The tissues with the lowest expression values were the retina and ONH, while the iris and cornea showed a higher expression of some *CRTC* isoforms. The *CRTCs* isoforms were expressed in the same order of magnitude as in the non-ocular tissues.

Similarly, the transcript levels of *CREB* isoforms and *CREBBP* were comparable between ocular and non-ocular tissues (Fig. 6.2C). On average, *CREB3* levels were the highest, followed by *ATF2* (or *CREB2*), *CREB1*, and *CREBBP*. Therefore,

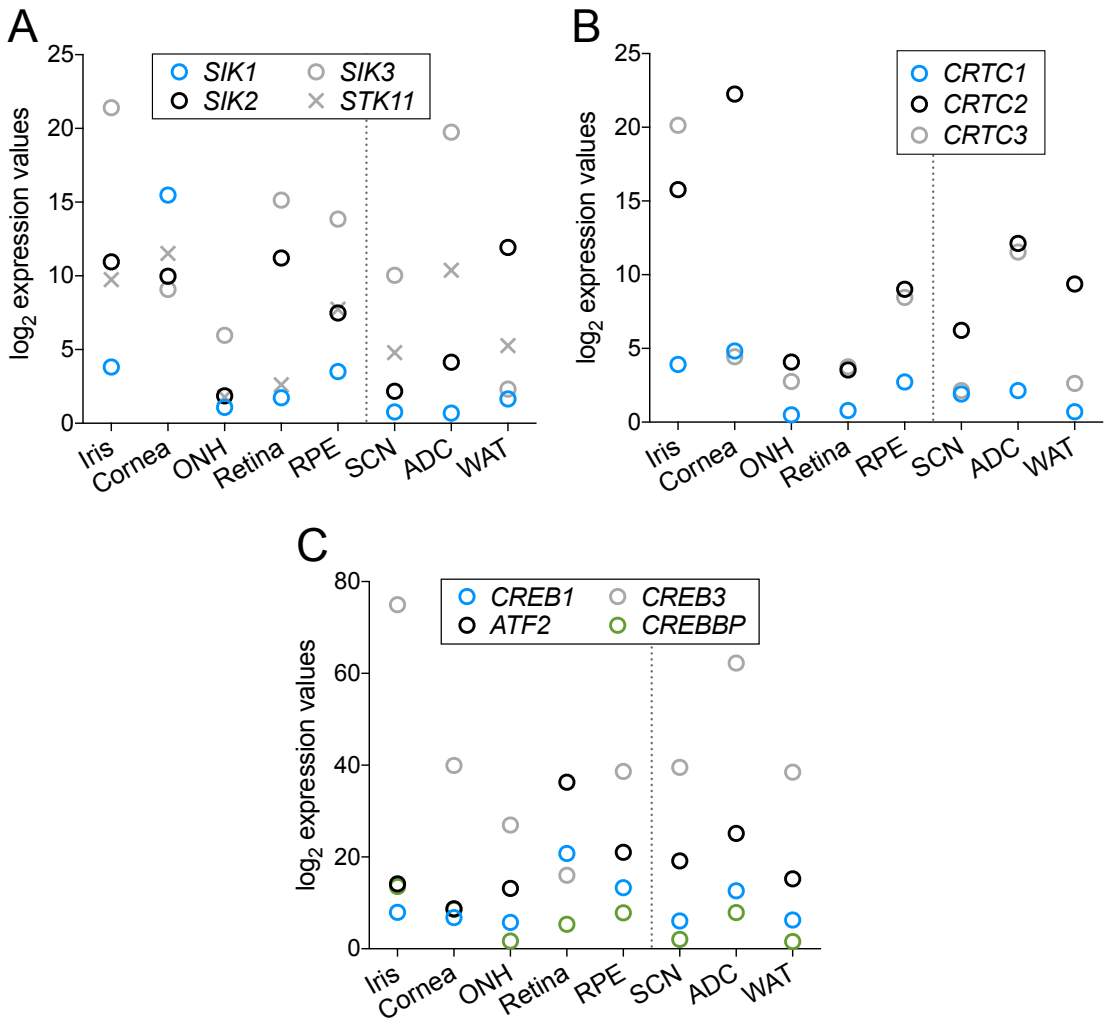


Figure 6.2: Expression of SIK family and related transcripts in baboon ocular tissues. Transcript levels of (A) *SIK1-3* and their activating kinase *STK11*, (B) *CRTC1-3*, (C) *CREB1-3* and *CREBBP* in the iris, cornea optic nerve head (ONH), retina and retinal pigment epithelium (RPE). Transcript levels in the SCN, adrenal cortex (ADC) and white adipose tissue (WAT) are included for comparison. Data are mean expression over a diurnal day, n=12.

on a transcript level, the *SIKs*, their activating kinase, and the molecules in their signalling cascade were overall present at a similar level to tissues where the SIK system is known to play a role, laying the grounds for a potential role of the system in ocular tissues.

Some of the SIK genes and molecules in their signalling cascade are expressed rhythmically in the SCN. For example, *Sik1* and *Crtc1* transcripts display diurnal rhythmicity [312] and *Sik1* also a circadian rhythm in the mouse SCN [296].

Therefore, to assess the potential of the SIK system to mediate circadian rhythms in ocular tissues, I analysed the diurnal rhythmicity of the SIKs and related transcripts in the dataset by Mure et al. [199]. I studied rhythmicity with the MetaCycle package in R [170].

Most of the SIK family and related genes did not display a diurnal rhythm in their expression pattern in any ocular tissues (Table 6.1). In particular, none of the 11 transcripts were rhythmically expressed in the iris, retina or RPE. The only genes with a diurnal rhythm were *CRTC1* and *CRTC3*, which showed rhythmic expression in the cornea and ONH, respectively. In conclusion, the SIK1 and related transcripts did not show diurnal rhythmicity in most ocular tissues analysed. Therefore, should these genes play a role in the circadian rhythms in constant conditions, their action may be independent of their transcript levels and could involve protein abundance rhythmicity or post-translational modifications.

In conclusion, *SIK1* is expressed in the retina and other ocular tissues, as are the genes in the SIK1 signalling cascade, indicating it may have a functional role in the retinal tissue.

Table 6.1: Statistical significance of diurnal rhythmicity of individual genes in ocular tissues

Gene	Iris	Cornea	ONH	Retina	RPE	Description
SIK1	1	0.78	0.63	0.83	0.73	Salt-inducible kinase 1
SIK2	0.75	0.16	1	0.9	1	Salt-inducible kinase 2
SIK3	0.69	0.92	0.11	1	0.99	Salt-inducible kinase 3
STK11	0.87	0.1	0.09	1	0.93	Serine/threonine kinase 11
CRTC1	0.2	**0.01**	0.1	0.96	0.47	CREB regulated transcription coactivator 1
CRTC2	0.89	0.12	0.2	0.98	0.23	CREB regulated transcription coactivator 2
CRTC3	0.51	1	**0.01**	0.87	0.36	CREB regulated transcription coactivator 3
CREB1	1	0.81	0.89	0.81	0.98	cAMP responsive element binding protein 1
ATF2	0.99	0.95	1	0.69	0.99	Activating transcription factor 2
CREB3	0.95	0.98	1	1	0.89	cAMP responsive element binding protein 3
CREBBP	0.47	0.52	0.3	0.98	0.9	CREB binding protein

Note:
Diurnal rhythmicity of genes was analysed with MetaCycle package in R and the corresponding p values are represented here. $p < 0.05$ denotes statistically significant diurnal rhythmic expression pattern and is formatted in bold.

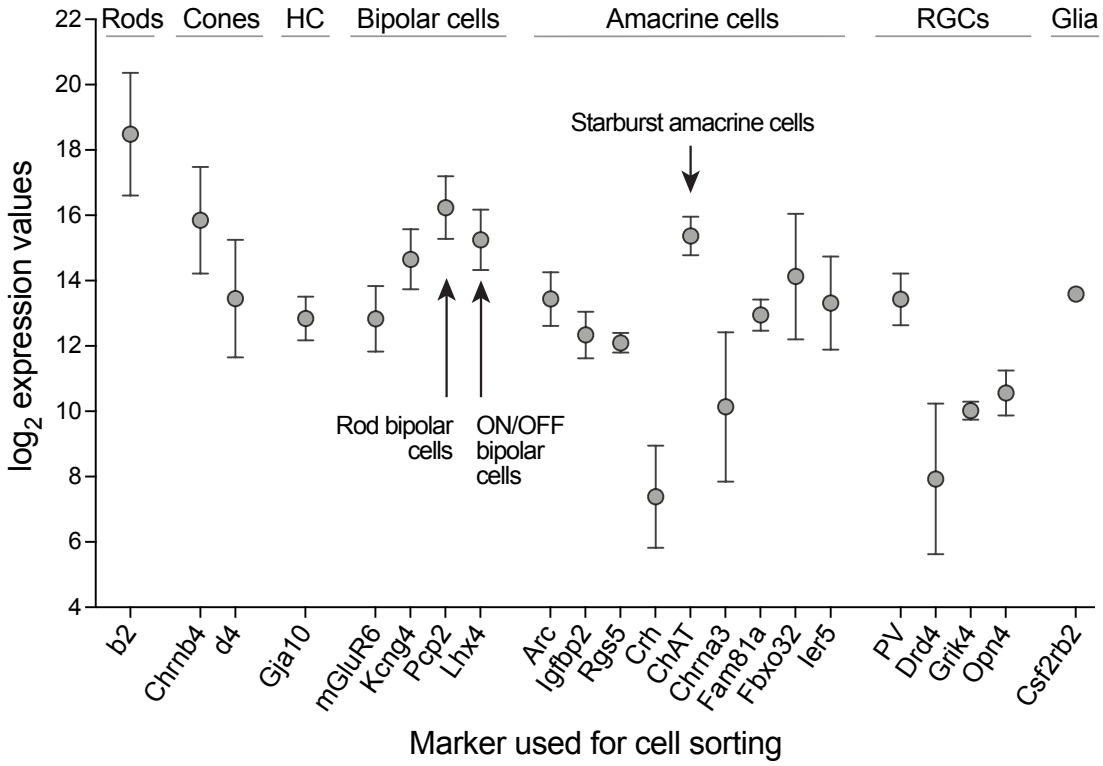


Figure 6.3: Expression of *Sik1* in murine retinal cell populations. Log_2 expression values of *Sik1* across 22 retinal cell populations as analysed by Siegert et al. [184]. Data are mean ± SEM, n = 3-9. HC, horizontal cells.

6.3.2 SIK1 is expressed ubiquitously in the mouse retina

To start to unravel the role of SIK1 in the retina, I first set out to determine which retinal cells express the transcript and protein. To begin with, I used another publicly available dataset by Siegert et al. [184], who characterised the transcriptome of 22 mouse retinal cell populations. In this dataset, the expression of *Sik1* was not confined to any particular cell type, but instead expressed in various cells (Fig. 6.3). The most abundant expression was detected in rods, rod bipolar cells, cones, cholinergic starburst amacrine cells and LIM homeobox 4 (LHX4) expressing bipolar cells. *Sik1* levels were the lowest in Crh-positive GABAergic amacrine cells and Drd4-positive direction-sensitive RGCs. These results indicate that SIK1 could play a role in various retinal cells as its expression is not confined to any particular cell type.

As transcript levels are not directly correlated with protein abundance, I next aimed to characterise the localisation of the SIK1 protein in the retina. I performed

immunohistochemical analysis of WT mouse retinas using two different dilutions of a rabbit anti-SIK1 primary antibody (1:100 and 1:300). I detected considerable staining in the photoreceptor inner segments, the inner and outer plexiform layers, and the retinal ganglion cell layer (Fig. 6.4A, B). The staining intensity was dependent on antibody dilution with only the higher concentration resulting in detectable immunofluorescence (Fig. 6.4A, B vs 6.4C). In addition, using only the secondary antibody resulted in minimal background immunofluorescence (Fig. 6.4D). Therefore, the retinal SIK1 immunofluorescence pattern resulted from the primary antibody binding to an antigen, which was present in multiple retinal layers.

In the retinal immunohistochemical analysis, the SIK1 staining was high in the plexiform layers and considerably lower in the nuclear layers. This finding was somewhat surprising as the SIK1 protein shuttles between the cytoplasm and nucleus, depending on its phosphorylation status [313]. While the mechanism of SIK1 regulation might be different in the retina from other cell types, I was nevertheless curious to investigate this phenomenon further to ensure the SIK1 immunohistochemical staining pattern was not an artefact.

It is known that *Sik1* transcript is enriched in the SCN compared to whole brain tissue [314, 315]. Therefore, I used the same SIK1 antibody to stain mouse coronal brain sections containing the SCN, expecting to detect higher SIK1 immunostaining in the SCN area. Since *Sik1* levels peak at around ZT4-5 [296, 312], I used mouse brain tissue harvested at ZT10 for this analysis, accounting for the approximate time it would take to produce the protein. The tissue I used was harvested and sectioned by Dr Jovi Wong. My analysis showed uniform SIK1 immunostaining in the brain sections with no visibly higher staining in the SCN region (Fig. 6.5). The immunofluorescence was more intense at the higher antibody dilution (1:100, Fig. 6.5A) than at the lower dilution (1:300, Fig. 6.5C), and barely detectable when no primary antibody was used (Fig. 6.5D). Despite there being no enrichment in the SCN region, I detected slightly higher immunofluorescence in the optic chiasm area. Interestingly, as in the retina, the SIK1 immunofluorescence was absent from the cell nuclei, as illustrated in a magnified image of the SCN (Fig. 6.5B).

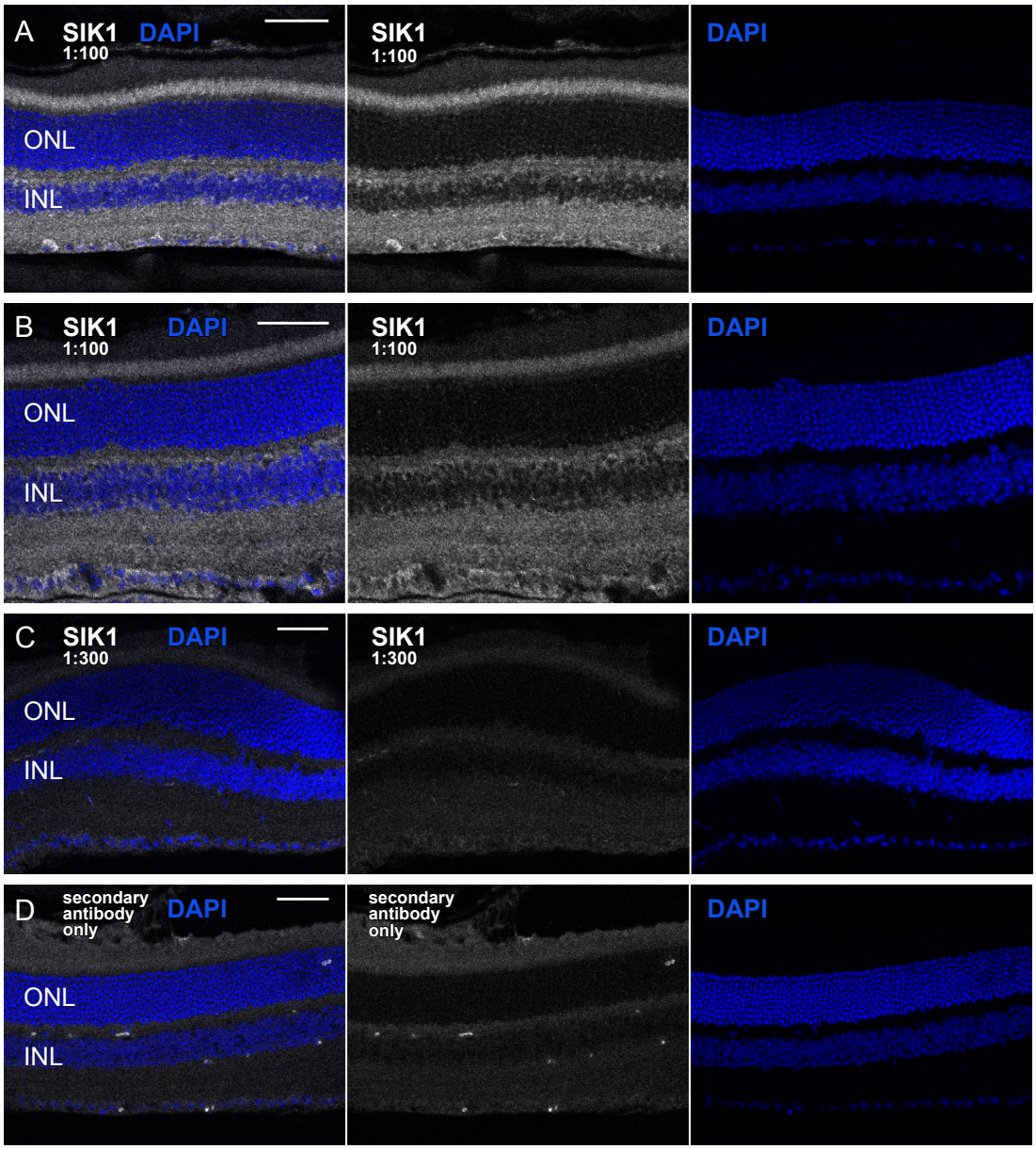


Figure 6.4: Immunohistochemical staining pattern of SIK1 in the retina. Primary rabbit anti-SIK1 antibody was used at two dilutions, 1:100 (A, B) and 1:300 (C). (D) No primary antibody control revealed secondary antibody background fluorescence. Scale bars 50 μm.

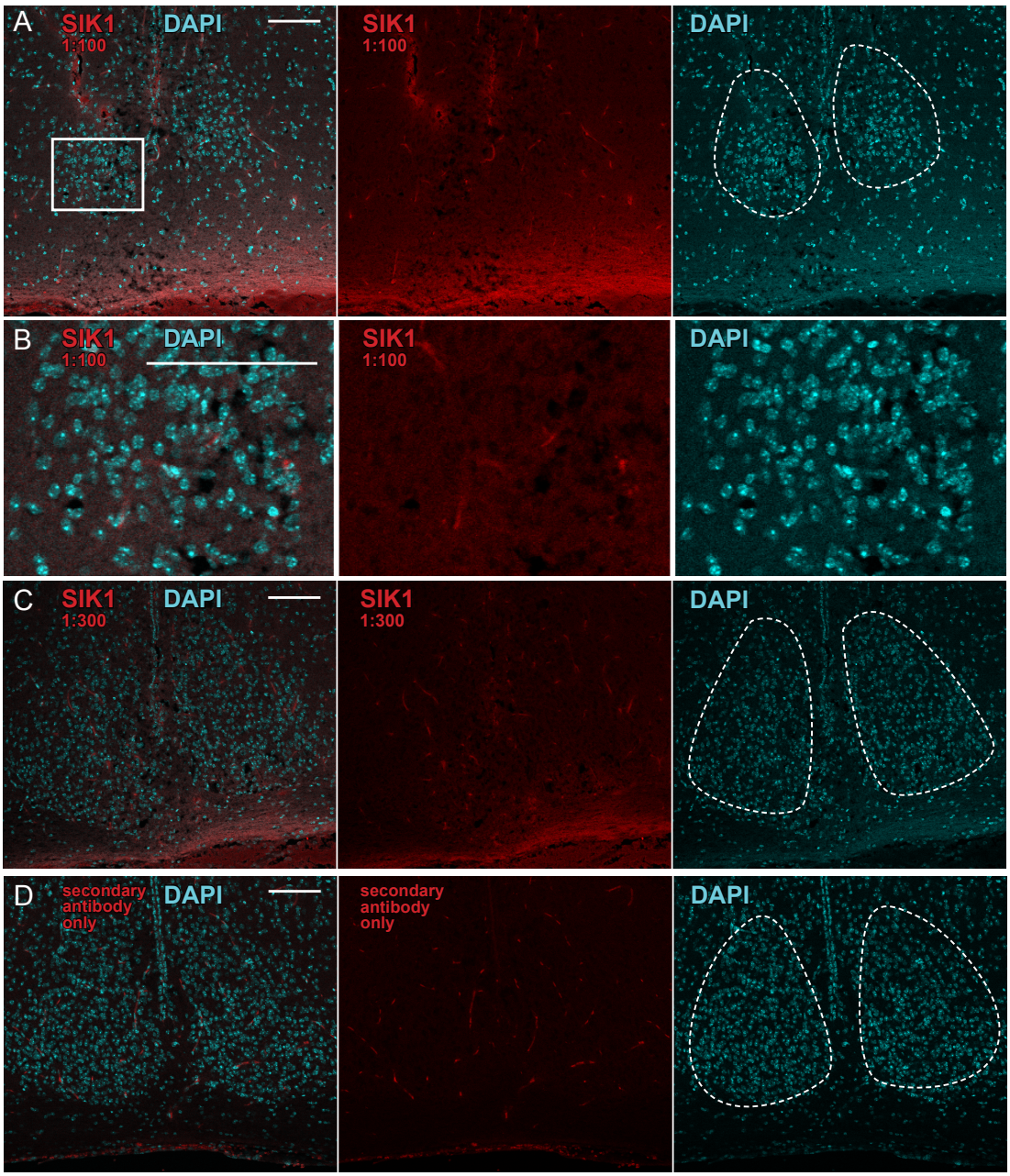


Figure 6.5: Immunohistochemical staining pattern of SIK1 in the SCN. (A) An SCN slice immunostained for SIK1 with a primary rabbit anti-SIK1 antibody at a dilution of 1:100. (B) A magnified image of the box in (A). (C) Antibody staining at a dilution of 1:300. (D) No primary antibody control reveals secondary antibody background fluorescence. The SCNs are outlined with dashed lines. Scale bars 100 μm.

The results from the SIK1 immunofluorescence in the retina and SCN were unexpected. First, there was minimal staining in cell nuclei, and second, the primary antibody immunofluorescence was not enriched in the SCN. Therefore, I decided to study the antibody staining further to validate the immunohistochemistry results. I transfected NIH3T3 mouse fibroblast cells with an overexpression vector of SIK1-GFP fusion protein and subsequently immunostained the cells with the same SIK1 antibody as above, expecting to see an overlap of the GFP and immunostaining signal.

The analysis showed that the SIK1-GFP signal was localised to the cell nuclei and the cytoplasm (Fig. 6.6A, B, D). In contrast, SIK1 immunofluorescence originated mainly from the cytoplasm with very limited staining present in the cell nuclei, similarly to what I saw in the retinas and the SCN tissue (Fig. 6.6A, B, C, E). Intriguingly, the SIK1-GFP and the SIK1 immunostaining patterns were distinct with minimal overlap (Fig. 6.6A, B). This finding may result from unspecific binding of the SIK1 antibody to other cellular components. Alternatively, the GFP tag could potentially change the conformation of the SIK1 protein such that the antibody is no longer able to recognise it. Therefore, the SIK1 antibody may recognise another cellular target

To test the hypothesis that the SIK1-GFP is conformationally different from the native SIK1 protein, I transfected another set of cells with a native SIK1 overexpression vector and subsequently immunostained the cells for SIK1. The overexpression of SIK1 did not lead to a marked increase in SIK1 immunofluorescence, or any detectable staining in the cell nuclei (Fig. 6.6E). Overall, the limited co-localisation of the SIK1-GFP and SIK1 antibody staining indicated that the SIK1 antibody I used might not have recognised the native SIK1 protein.

In this part of the chapter, I characterised the expression of SIK1 in mammalian ocular tissues. Using publicly available datasets, I found that *SIK1* and its related transcripts were present in the baboon retina, RPE, cornea, iris and ONH. At the same time, a limited subset showed diurnally rhythmic expression pattern. There was no cell type in the mouse retina with particularly high levels of *Sik1*; the

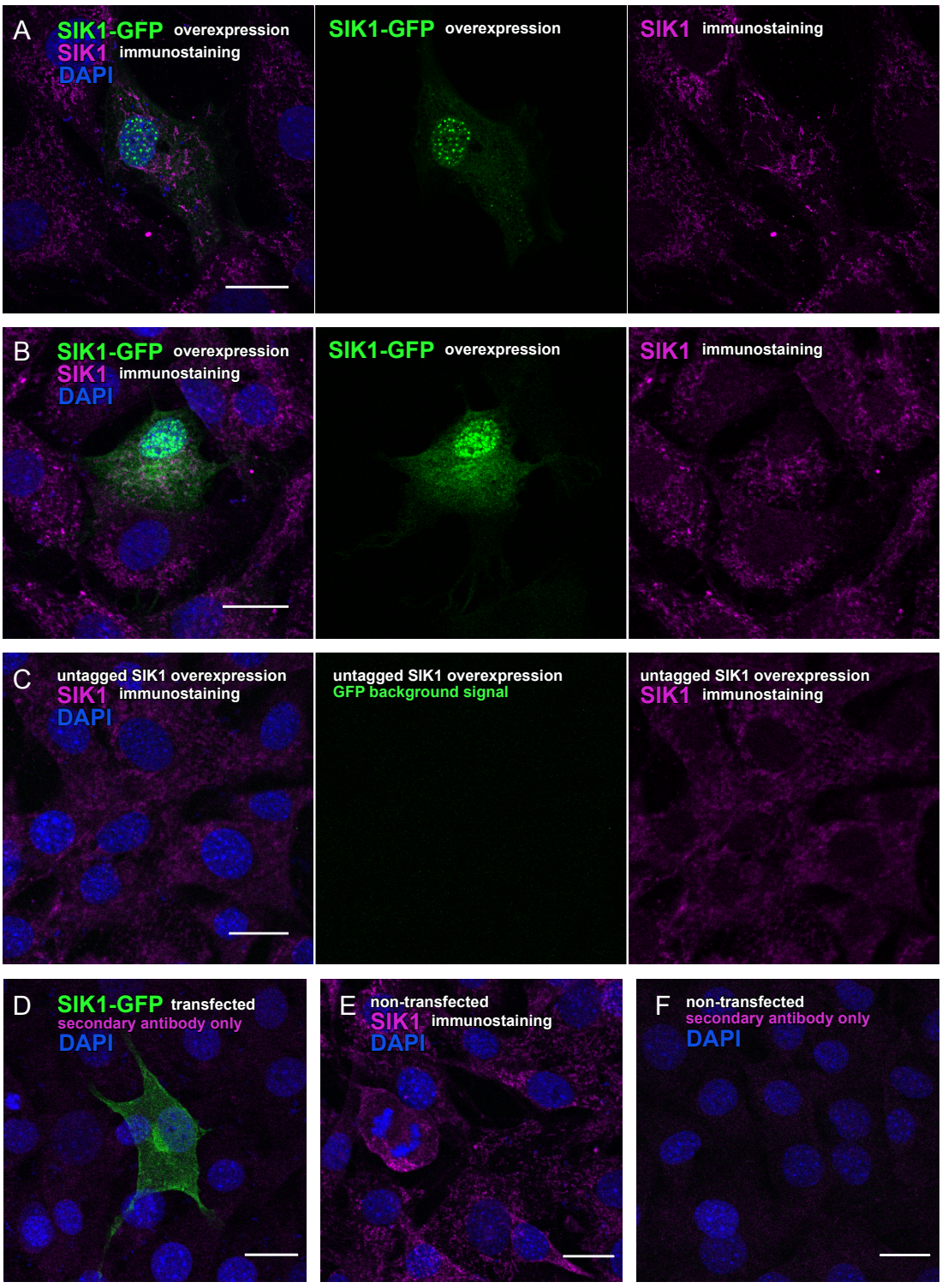


Figure 6.6: Immunocytochemical staining pattern of SIK1 in NIH3T3 cells overexpressing SIK1. (A, B) Cells transfected with an overexpression vector of SIK1-GFP fusion protein and immunostained for SIK1. (C) Cells transfected with an untagged overexpression vector of SIK1, followed by SIK1 immunostaining. (D) Cells transfected with SIK1-GFP plasmid, no primary antibody was used during immunostaining. (E) Non-transfected cells immunostained for SIK1. (F) Non-transfected cells, no primary antibody was during immunostaining. Scale bars 20 μm.

highest expression was detected in rods and rod bipolar cells. I also attempted to analyse the localisation of SIK1 protein in the retina, but am not confident that the antibody was reliably detecting SIK1.

6.3.3 Retinal morphology is unaffected by the lack of functional SIK1

Since *Sik1* was present in the retina, I was then interested in understanding whether the absence of functional SIK1 affects the gross retinal morphology. For this, I used SIK1 knock-in (KI) mice that express a mutated SIK1 protein, which is unable to phosphorylate its targets [159]. I stained the retinal tissue of these mice and their WT littermates for several retinal cell markers. I found that on a broad anatomical level, the morphology of retinal cones (Fig. 6.7A, B), bipolar cells (Fig. 6.7C, F), RGCs and pRGCs (Fig. 6.7G, H) appeared indistinguishable between the WT and SIK1 KI retinas.

Furthermore, I did not detect any marked differences in amacrine cells (Fig. 6.8A, B), horizontal cells (Fig. 6.8C, D) or retinal glial cells (Fig. 6.7E, F). Therefore, on a gross anatomical level, the lack of functional SIK1 in the retina did not lead to obvious abnormalities in the principal retinal cell types. However, these analyses were not quantitative, and I cannot exclude more subtle defects.

6.3.4 The distribution of cones is not affected by the lack of functional SIK1

The absence of core circadian clock components has been reported to affect cone distribution in the retina: *Bmal1*$^{-/-}$ animals display ectopic expression of S-opsin in the dorsal retina and the absence of *Per2*, conversely, leads to a decrease in retinal S-opsin levels [174]. Therefore, I was curious to investigate whether the lack of functional SIK1 affects the distribution of retinal cones.

I first analysed the expression of different opsins and core clock components in the retinas of SIK1 KI mice. I found that the expression of all opsins, the cone opsins, melanopsin and rhodopsin were not different between the WT and SIK1 KI

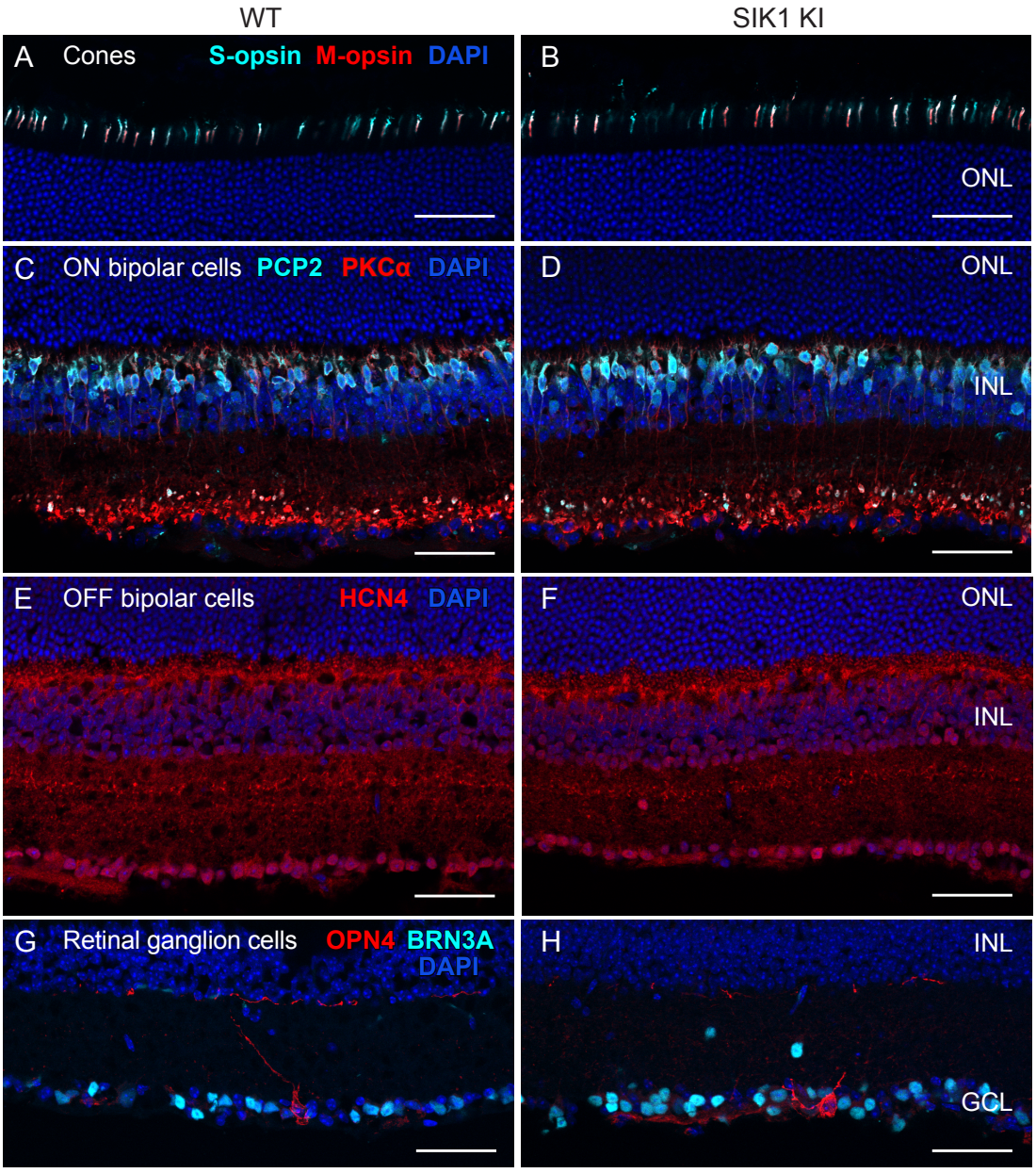


Figure 6.7: Morphology of cones, bipolar and retinal ganglion cells in WT and SIK1 KI retinas. Immunohistochemical labelling of S- and M-opsin in retinal cones (A, B); Purkinje cell protein-2 (PCP2) and protein kinase C α (PKCα) in subsets of ON bipolar cells (C, D); hyperpolarisation-activated cyclic nucleotide-gated potassium channel 4 (HCN4) in OFF bipolar cells (E, F); OPN4 and brain-specific homeobox/POU domain protein 3A (BRN3A) in retinal ganglion cells (G, H). Panels A, C, E, G are images of WT retinas; B, D, F, H of SIK1 KI retinas. Scale bars 50 μm.

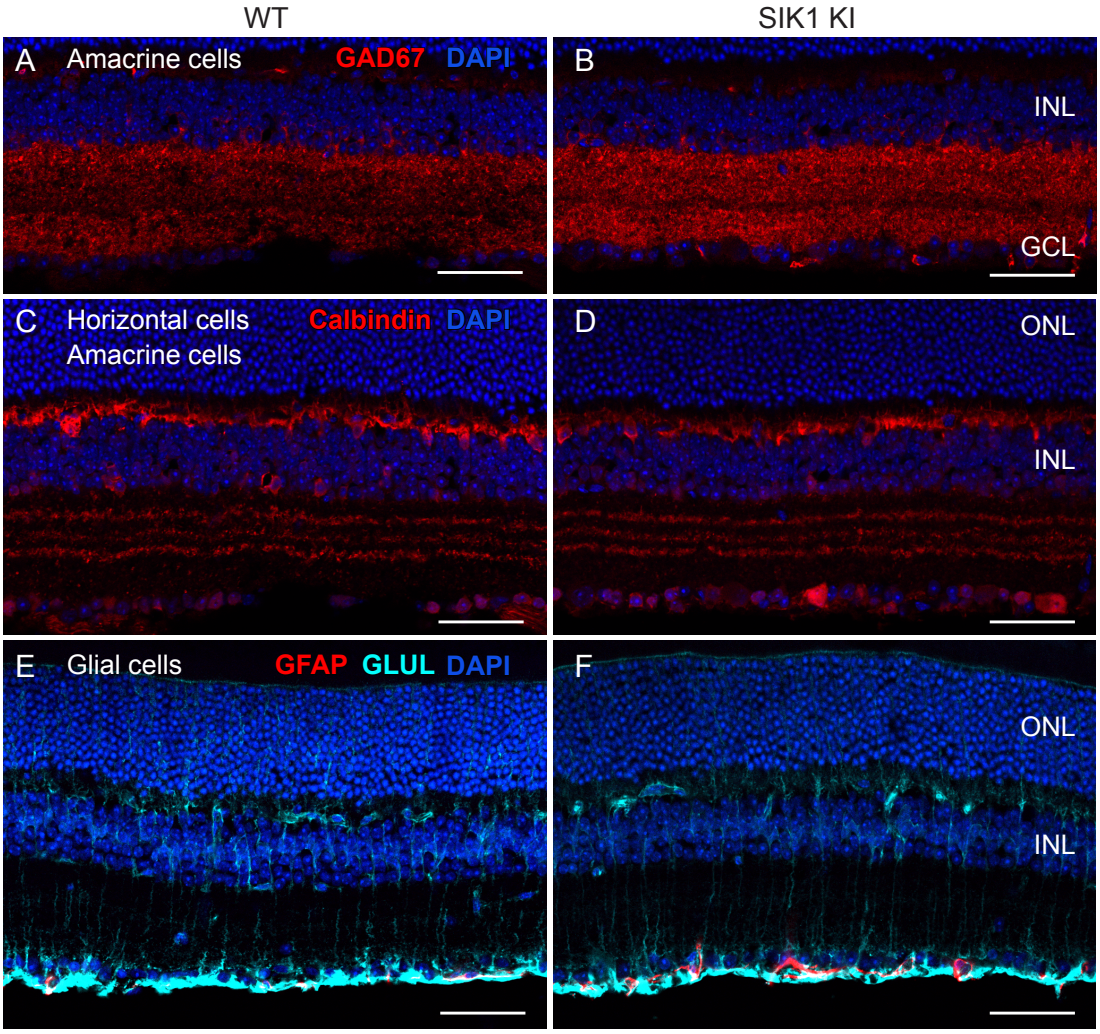


Figure 6.8: Morphology of amacrine, horizontal and glial cells in WT and SIK1 KI retinas. Immunohistochemical labelling of glutamate decarboxylase (GAD67) in amacrine cells (A, B); calbindin in subsets of horizontal and amacrine cells (C, D); GFAP and glutamine synthetase (GLUL) in retinal glial cells (E, F). Panels A, C, E are images of WT retinas; B, D, F of SIK1 KI retinas. Scale bars 50 μm.

animals (Fig. 6.9A). Furthermore, the levels of the retinal core clock genes *Clock*, *Bmal1*, *Per1/2* and *Cry1/2* were also similar between the two genotypes.

Although the transcript levels of cone opsins and core molecular clock components were not affected in SIK1 KI animals, the cones could display altered retina distribution. Therefore, I analysed flat-mount retinas of WT and SIK1 KI animals immunostained for S- and M-opsins. I saw that the proportion of retina with high S-opsin expression was approximately 57% in both WT and SIK1 KI animals and there were no differences between the genotypes (Fig. 6.10A). Furthermore, there

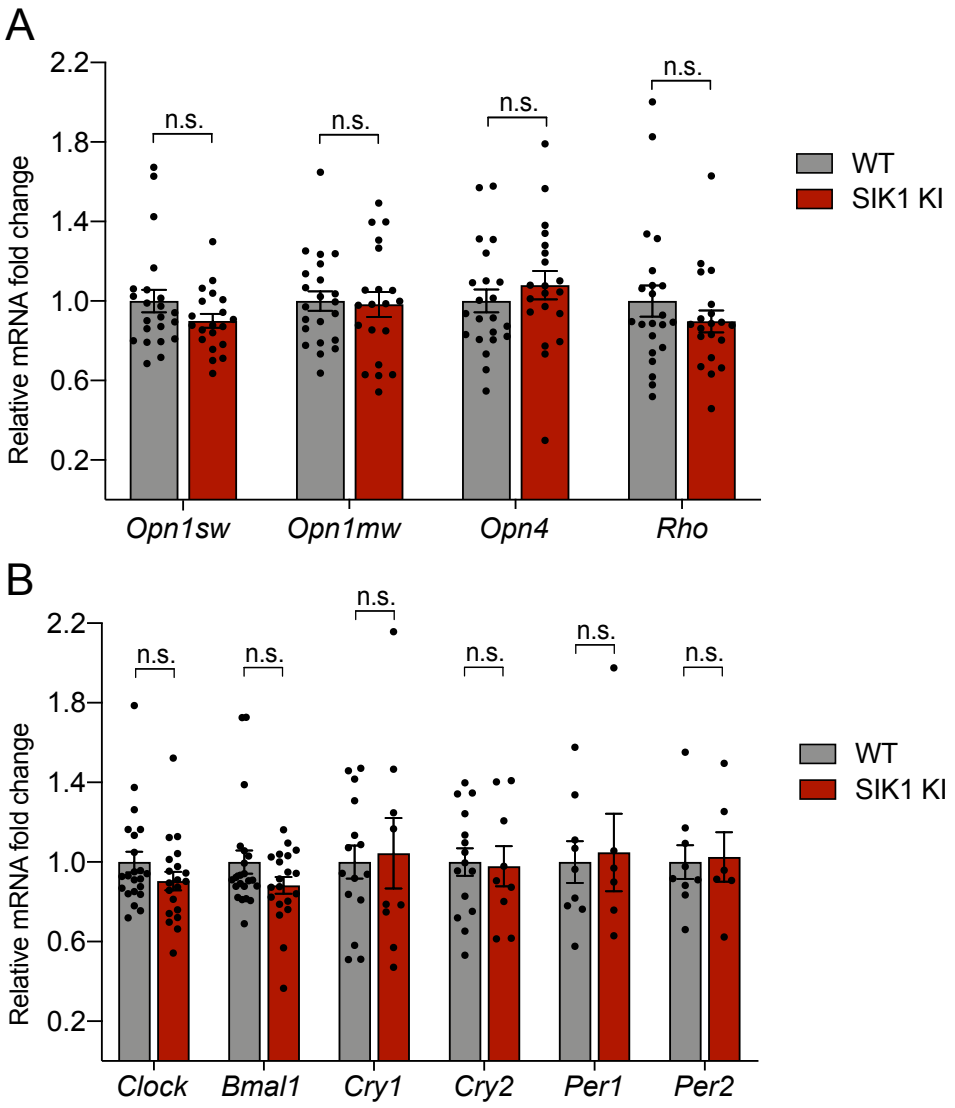


Figure 6.9: Expression of opsins and core clock genes in WT and SIK1 KI retinas. (A) Gene expression of retinal opsins: S-opsin *Opn1sw*, M-opsin *Opn1mw*, melanopsin *Opn4* and rhodopsin *Rho*. (B) Expression levels of core clock components *Clock*, *Bmal1*, *Per1/2* and *Cry1/2*. Values are shown as fold change compared to WT expression levels. Data are mean ± SEM, n = 6-22. Statistical analysis was performed with pair-wise student t-tests and statistical significance determined using the Holm-Šidák method, with alpha = 0.05. n.s., not significant.

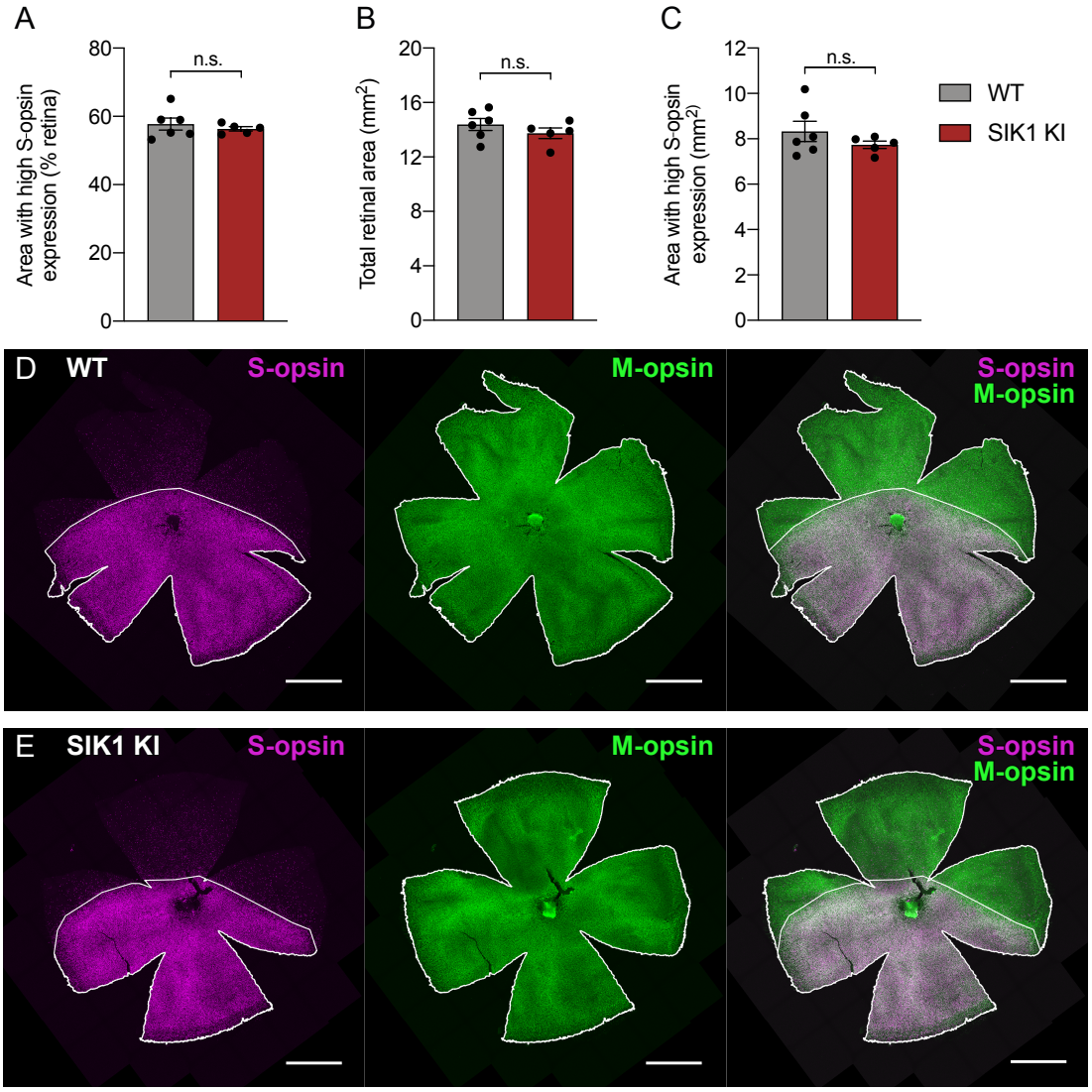


Figure 6.10: Cone distribution in WT and SIK1 KI retinas. Proportion of the retina expressing high levels of S opsin (A), total retinal area (B) and total area with high S opsin expression (C). (D) Representative immunohistochemistry images of S and M opsin expression in a WT retina and (E) SIK1 KI retina. Outlines surrounding the areas of high S opsin expression and the entire retina were used for quantification. Scale bars 1 mm. Data are mean ± SEM, n = 5-6. Statistical analysis was performed using Student's t-tests. n.s., not significant.

were no statistically significant differences in the total retinal area (Fig. 6.10B) or the area with high S-opsin expression (Fig. 6.10C), which could have affected the result.

In this part of the chapter, I characterised the retinal morphology in the absence of functional SIK1. Immunohistochemical analysis of retinal cross-sections and the study of retinal cone distribution revealed no gross morphological abnormalities

in SIK1 KI retinas.

6.3.5 Retinal gene induction in response to a light pulse is not enhanced in the absence of functional SIK1

As mentioned above, SIK1 KI animals have an increased circadian phase shifting response and display rapid re-entrainment (Dr Lewis Taylor, unpublished data), which can be attributed to the increased induction of *Per1* [186]. To determine whether SIK1 plays a similar role in the retina, I exposed WT and SIK1 KI animals to a 60-minute or a 120-minute 400 lux white light pulse at CT16, and analysed the expression of light-induced retinal genes *Fos* and *Dio2*. In the WT retinas, I saw that *Fos* was induced upon both a 60- and 120-minute light pulse. In SIK1 KI retinas, *Fos* induction was significant only after a 60-minute pulse (Fig. 6.11A), but not after a 120-minute pulse, which might have been influenced by the higher level of *Fos* before the light exposure (Fig. 6.11B). The levels of *Dio2* increased after the light pulse in both WT and SIK1 KI retinas (Fig. 6.11C, D). Therefore, there were no major deficits in light-induced gene expression in SIK1 KI retinas.

Since the role of SIK1 in the SCN is mediated by its negative feedback on *Per1* expression, I next quantified the light-induced retinal expression of *Per1*, *Per2* and *Sik1*. Should the function of SIK1 in the retina be similar to its role in the SCN, one would expect a higher upregulation of *Per1* in the retinas of SIK1 KI animals. In response to a 60-minute light pulse, none of the three transcripts were significantly induced in WT or SIK1 KI retinas, although there was a trend towards upregulation of all these transcripts in both genotypes (Fig. 6.12A, C, E). Unexpectedly, after a 120-minute light pulse, the *Per1* and *Sik1* transcripts were significantly induced in WT retinas, but not in SIK1 KI retinas (Fig. 6.12B, F). Therefore, SIK1 does not seem to inhibit the light-mediated upregulation of *Per1* in the retina.

In conclusion, the light-regulated induction of retinal *Fos* and *Dio2* and core clock genes was overall similar between the WT and SIK1 KI mice. The data were variable, and the sample size might have been too small to detect the induction of some of the genes. However, the *Per1* transcript, whose induction is limited by

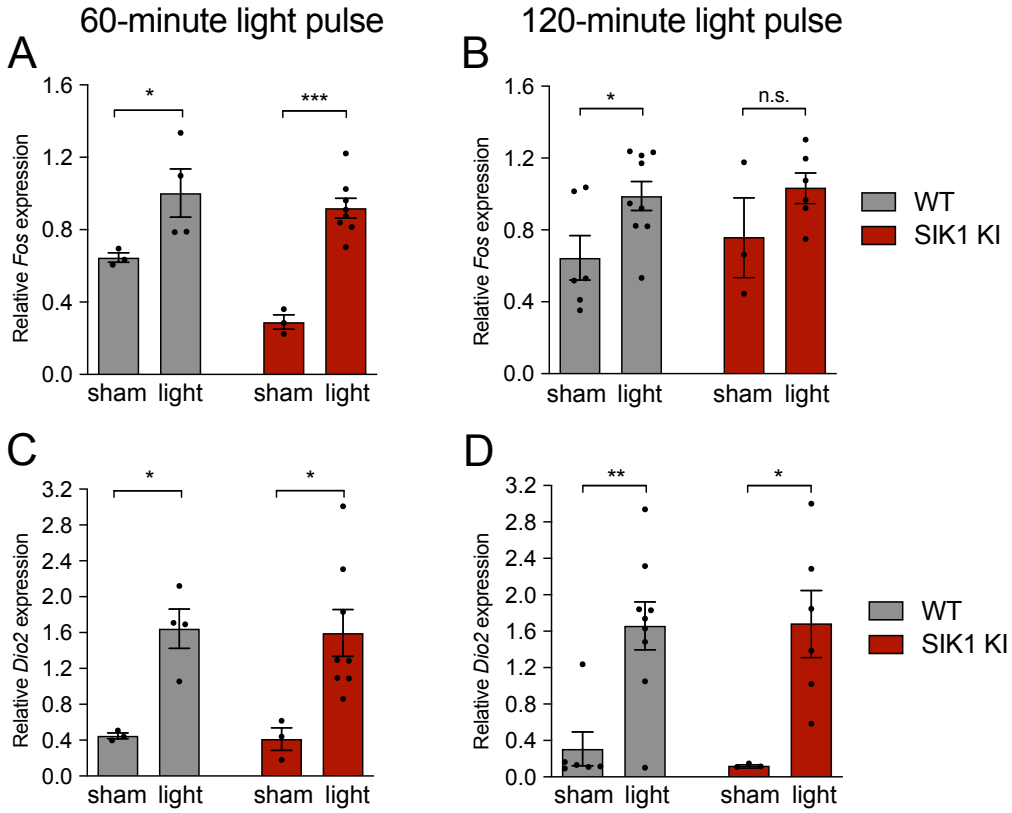


Figure 6.11: Light-regulation of immediate early genes in SIK1 KI retinas. Expression of *Fos* (A, B), and *Dio2* (C, D) upon exposure to a 60-minute (A, C) or 120-minute (B, D) white 100 lux light pulse at CT16. Data are mean ± SEM, n = 3-8. Statistical analysis was performed using two-way ANOVA with Šidák's correction for multiple comparisons. n.s., not significant, * $p < 0.05$, ** $p < 0.01$, *** $p < 0.001$.

SIK1 in the SCN, was upregulated in WT, but not in SIK1 KI retinas. This finding is opposite to what one would expect if the role of SIK1 in the retina and the SCN was similar. Therefore, the regulation of retinal light-induced clock components might be distinct between the retina and the SCN.

6.3.6 Maximum pupil constriction and its diurnal regulation is normal in animals lacking functional SIK1

To analyse the role of SIK1 in retinal function, I measured the pupil reflex of SIK1 KI animals in response to a blue light pulse of different intensities. The maximum pupil constriction of SIK1 KI animals was not different from their WT littermates at any light intensity tested (Fig. 6.13A-F).

Maximum pupil constriction shows circadian and diurnal rhythmicity in mice,

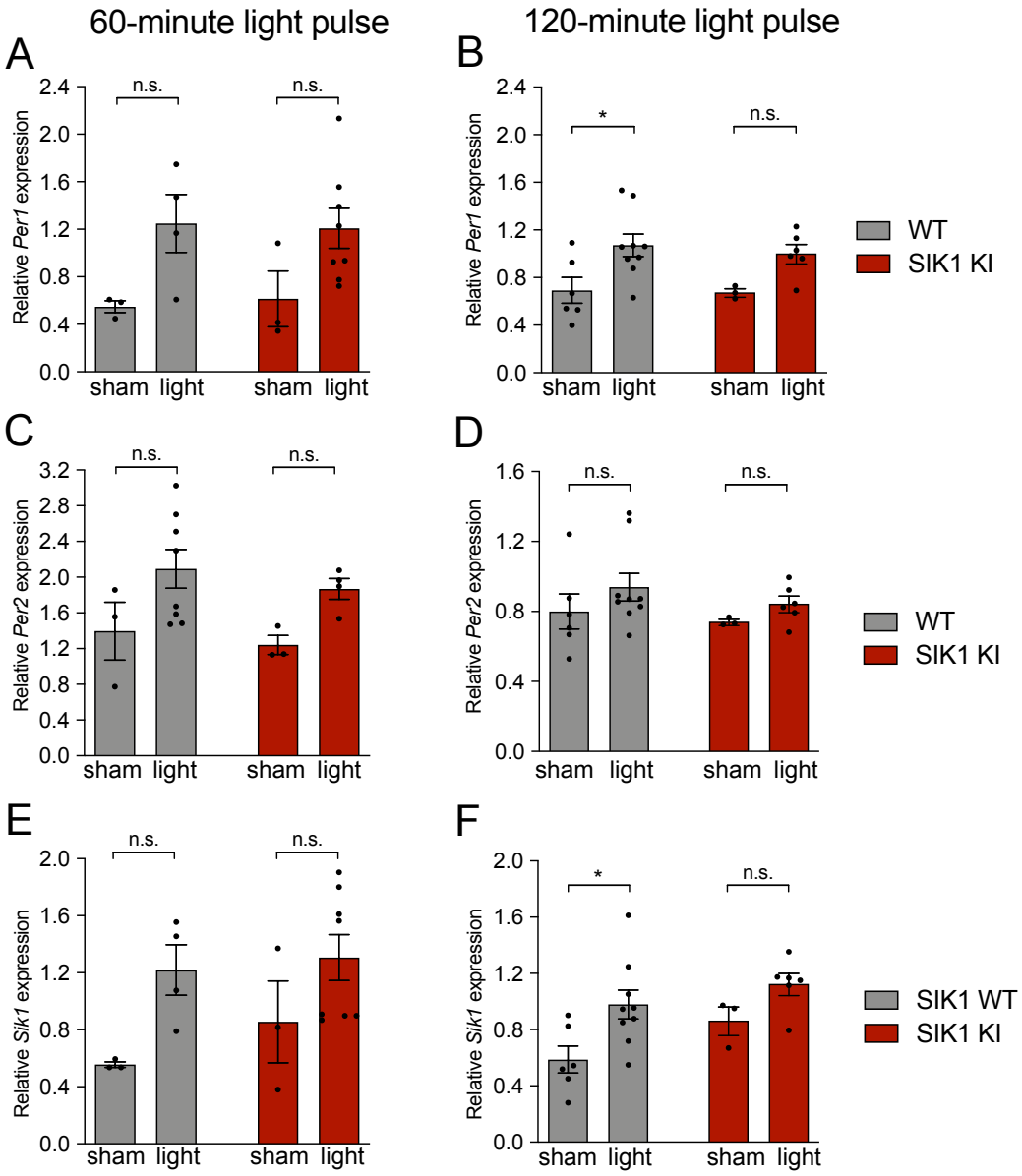


Figure 6.12: Light-induced expression of clock genes in SIK1 KI retinas. Expression of *Per1* (A, B) and *Per2* (C, D) and *Sik1* (E, F) upon exposure to a 60-minute (A, C, E) or 120-minute (B, D, F) white 100 lux light pulse at CT16. Data are mean ± SEM, n = 3-8. Statistical analysis was performed using two-way ANOVA with Šidák's correction for multiple comparisons. n.s., not significant, * $p < 0.05$.

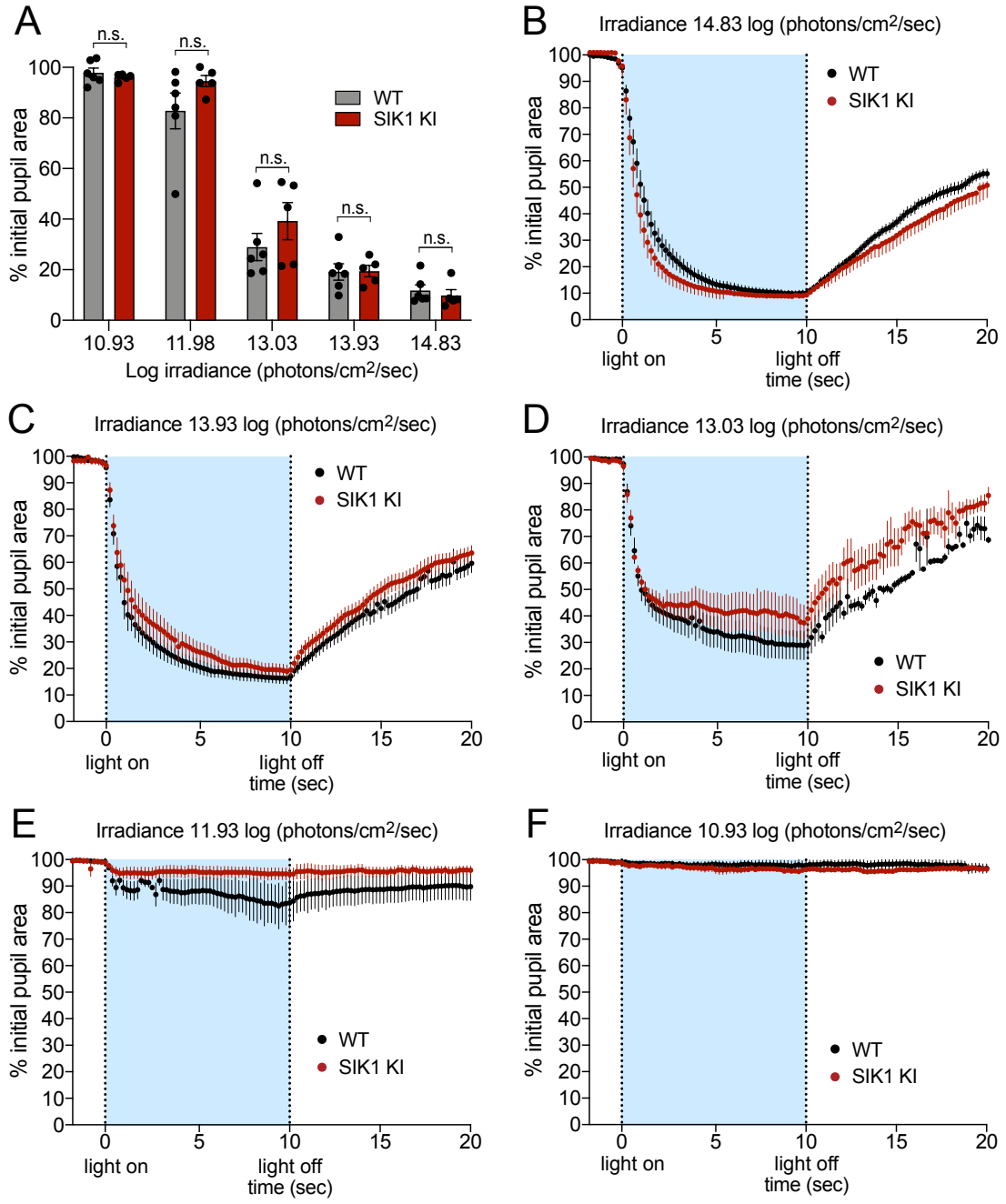


Figure 6.13: Characterisation of pupil response in SIK1 KI animals. (A) Maximum pupil constriction of WT and SIK1 KI animals in response to a 10-second blue light pulse of different intensities at diurnal day. (B-F) Pupil constriction dynamics at the intensities of 14.83 (B), 13.93 (C), 13.03 (D), 11.93 (E) and 10.93 log quanta (log photons/cm^2/sec) (F). A two-second baseline pupil recording is followed by a 10-second light pulse and a 10-second post-illumination recording. Pupil constriction values at the end of the 10-second pulse from (B-F) are used for the analysis in (A). Data are mean ± SEM, n = 5-6. Statistical analysis was performed using two-way ANOVA with Šidák's correction for multiple comparisons. n.s., not significant.

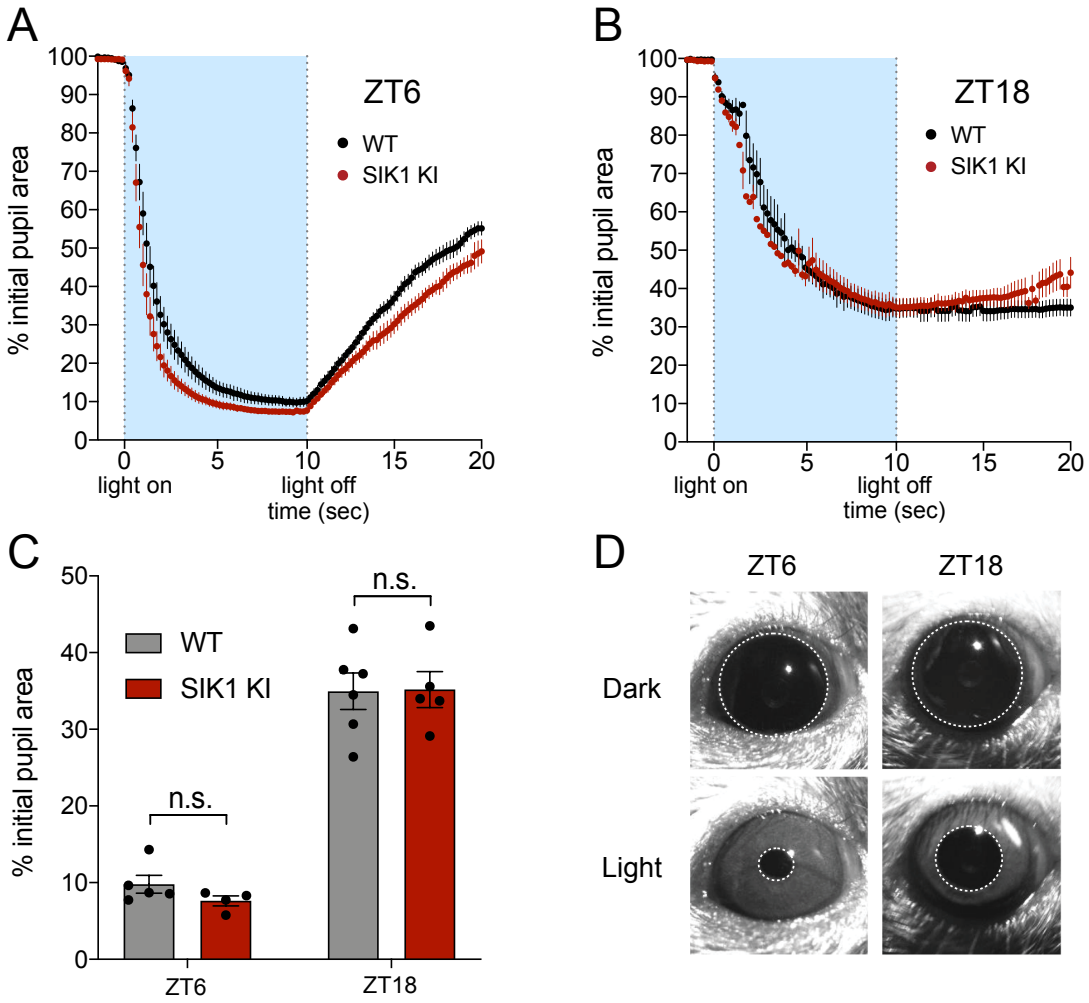


Figure 6.14: Diurnal rhythmicity of pupil response in SIK1 KI animals. Pupil constriction dynamics in response to a 10-second 480 nm wavelength light pulse at the intensity of 14.83 log quanta at ZT6 (A) and ZT18 (B). (C) Quantification of maximum pupil constriction at ZT6 and ZT18. (D) Representative images of WT pupils at day and night before the start of light pulse (dark) and at maximum pupil constriction. Data are mean ± SEM, n = 5-6. Statistical analysis was performed using two-way ANOVA with Šidák's correction for multiple comparisons. n.s., not significant.

and this rhythm is known to be lost in mice lacking the core clock component *Cry1* [134]. To see whether SIK1 also influences the pupil constriction rhythmicity, I measured the pupil response at diurnal midday and midnight (ZT6 and ZT18, respectively). The analysis demonstrated that the maximum pupil constriction did not differ between WT and SIK1 KI animals at ZT6 or ZT18 (Fig. 6.14). Thus the SIK1 KI animals retained their diurnal rhythmicity in pupillary light reflex.

In this part of the chapter, I determined the pupil constriction dynamics and its

diurnal regulation in SIK1 KI animals. The maximum pupil constriction in response to blue light did not differ between WT and SIK1 KI animals. Furthermore, the animals lacking functional SIK1 retained their diurnal regulation of pupillary light reflex.

6.4 Discussion

In this chapter, I addressed the third aim of my thesis. I investigated the retinal light responses of SIK1 KI mice that display enhanced central circadian light responses in order to uncover the similarities and differences between retinal and SCN light signalling.

As the SIK family of proteins has not been investigated in the mammalian eye, I first analysed the expression of all SIK family members, *SIK1-3* and their downstream targets *CRTCs* and *CREBs* in different baboon ocular tissues. The tissue with the highest levels of *SIK1* and a diurnal rhythm of *CRTC1* expression was the cornea. The cornea shows robust diurnal rhythms in core clock gene expression, and the efficiency of corneal epithelium repair is dependent on when the corneal wound was inflicted [316]. The high levels of *SIK1* could indicate a functional role for the system in the cornea and could be an exciting avenue for future research.

The role of SIK1 in the SCN is to limit the light-induced clock shifts by limiting the induction of *Per1* and the lack of *Sik1* results in an increased induction of *Per1* [186]. However, I did not detect an enhanced light-induced *Per1* transcription in SIK1 KI retinas. In fact, there were indications to the opposite, as the *Per1* transcript was significantly induced in the WT retinas, but not in SIK1 KI retinas after a 120-minute light pulse. Therefore, from these data, it does not appear that SIK1 has a similar role in the retina as it has in the SCN and other mechanisms could act as a brake on light-induced retinal clock shifts.

6.4.1 Limitations of this study and future work

One limitation of this study was that I was unable to detect the SIK1 protein in the retina. The retinal location of the protein would have allowed me to speculate which retinal cells the lack of SIK1 would primarily affect, and thus create hypotheses for

the further study of the retinal morphology of SIK1 KI animals. On a transcript level, *SIK1* seemed to be present across the retina, and therefore, the protein level characterisation would have been particularly interesting. I am sceptical of the quality of the SIK1 antibody I used. In fact, a recent paper reported that they attempted to immunostain for the SIK1 protein in the SCN. While they saw high enrichment of *Sik1* in the SCN with in situ hybridisation, they were unsuccessful in detecting SIK1 with commercially available antibodies [315]. These scientists then produced an antibody in house, which was also unsuccessful in detecting the endogenous SIK1 [315]. As seen from the expression levels of *SIK1* in the baboon ocular tissues [200], and as has been reported by others [315], the transcript levels of *Sik1* are extremely low, which is likely to result in a low protein abundance, making it a challenging protein to analyse with immunohistochemistry.

One limitation of this study is that the analysis of the morphology of retinal cell types was not quantitative. Although I did not see any apparent abnormalities in SIK1 KI retinas, there might have been more subtle changes I did not detect because of the lack of a more thorough investigation. As the analysis of retinal cell morphology was exploratory, it was difficult to determine which retinal cells to focus on. Since the core clock proteins influence cone development, I quantified the retina area covered by the two cone opsins and did not see any differences between the WT and SIK1 KI retinas. However, there might have been more subtle changes that would only have been revealed with a more detailed analysis. Since *Sik1* is expressed in multiple retinal cells, future research into its role will determine the function of the kinase in the retina.

A further limitation was that while I did not detect exaggerated light responses of SIK1 KI retinas, I did not study whether the pupil response of SIK1 KI animals was sustained throughout the light pulses. As shown in chapter 3, pupil constriction differences can lead to significant discrepancies in the light doses received by the retinas. Therefore, the sustained pupil response of SIK1 KI animals should be investigated in future studies. If pupil constriction is not sustained in SIK1 KI animals, the light-induced retinal gene expression changes presented in this chapter

would be difficult to interpret. In addition, a lack of a sustained pupil response could contribute to the circadian phenotype seen in SIK1 KI animals as it would result in more light information reaching the SCN.

7

Thesis summary and final discussion

7.1 Key findings

The first aim of my thesis was to investigate the mechanisms of how melanopsin affects the retinal circadian clock, and its light responses, drawing parallels to its role in the light responses of the SCN. With regards to this aim, I made the following findings:

1. Melanopsin regulates the circadian rhythmicity of phototransduction genes and sphingolipid signalling pathways, while the rhythmicity of dopaminergic signalling and gap junction pathways remain intact in the absence of melanopsin.

2. Circadian rhythmicity of core clock gene expression is dampened in retinas lacking melanopsin.

3. The lack of sustained pupil constriction can lead to significant differences in retinal light doses in experiments where light responses are studied. For example, the melanopsin-null animals receive several times higher light doses than their wild-type littermates in conventional circadian experiments.

4. The retinal light responses are slightly attenuated in the absence of melanopsin, similarly to what has been shown about their SCN light responses.

5. The aberrant retinal circadian clock in the absence of melanopsin is not a result of an apparent deficit in cone development.

My next experimental aim was to examine whether melanopsin light responses mediate retinoprotection in a mouse model of light-induced retinal degeneration and I made the following observations:

1. Melanopsin mediates sustained pupil constriction at high light intensities, and the lack of melanopsin results in a significantly higher light dose received by the retina. By limiting retinal light dose by enabling adequate and appropriate pupil constriction, melanopsin does limit retinal damage.

2. The retinal function of wild-type and melanopsin-null animals deteriorates to a similar extent in response to a 3-hour 20,000 lux nocturnal light pulse. Therefore, in this particular model, melanopsin does not seem to mediate retinoprotection.

My next aim was to study to what extent the mouse model of light-induced retinal degeneration replicates the human disease processes, and I made the following observations:

1. The genes differentially regulated in mouse retinas after exposure to a bright light pulse are enriched for genes known to cause or increase the risk of human retinal degenerations. Therefore, on a gene expression level, the model replicates the initiation phase of the human disease processes.

2. The mouse retinal genes differentially regulated in response to a bright light pulse are not enriched for genes known to be involved in the later stages of age-related macular degeneration. However, there is significant overlap in the cellular processes.

3. The genes affected by light damage or age-related macular degeneration are not enriched for rhythmic retinal genes, therefore suggesting that the circadian processes of the retina are not preferentially affected by retinal degenerations.

My final aim was to determine to what extent the retinal and SCN light responses are regulated similarly by using an animal model with enhanced SCN light sensitivity, resulting from the absence of a functional SIK1 protein. With these experiments I found the following:

1. SIK family and related transcripts are expressed in the retina and other ocular tissues. In the mouse retina, *Sik1* is most abundant in rods and rod bipolar cells.

2. The gross retinal morphology and distribution of retinal cones are not affected by the lack of a functional SIK1 protein.

3. Mice lacking functional SIK1 do not display enhanced retinal light sensitivity, measured by their pupil response and induction of light-regulated genes in the retina. Therefore, the mechanisms limiting the retinal and SCN light responses are regulated differently.

7.2 Future directions

In addition to the future work listed at the end of each chapter, this thesis raises several considerations for future research on the retina and circadian rhythms.

The complexities of the retinal structure make it extremely difficult to investigate the contributions of each cell type to retinal circadian rhythms. Therefore, there is scepticism in the field for using whole retinal assays to study the retinal clocks [317]. Indeed, analysing entire retinas is far from perfect as it cannot provide information on cell-specific contributions to the circadian processes. Nevertheless, the whole retinal omics analyses may identify attractive targets and create hypotheses for future studies. Certainly, the study of individual retinal cells will be key to uncovering the precise regulation of the retinal circadian clocks. With the single-cell

omics approaches becoming increasingly affordable, the analysis of the circadian transcriptomes of individual retinal cell types may not be unrealistic.

The entire retinal transcriptomics analysis can be complemented by cross-referencing the results with other available studies, which allows us to speculate over the functional implications of the findings. With more public datasets being deposited, such post-analyses may become incredibly powerful. However, public datasets are not always deposited in a very user-friendly format. They often consist of extensive spreadsheets or raw microarray or sequencing files that frequently require further processing and analysis. Therefore, I believe that the scientific community would benefit greatly from innovative approaches to data deposition and visualisation. By ensuring that the available datasets are accessible to every scientist regardless of their bioinformatics skills, we would create a truly collaborative global scientific community.

In my view, the field of retinal circadian rhythms would greatly benefit from applying omics approaches more widely. For example, it was only shown a month ago that adenosine release from the goldfish retina displays a robust circadian rhythm *in vitro* [127], challenging the prevailing view that the retinal rhythms are mainly governed by the opposing actions of melatonin and dopamine [317]. The available metabolomics and peptidomics techniques allow the detection and precise quantification of hundreds of metabolites [318] and peptides [318, 319], and could potentially uncover other molecules that function as mediators of retinal circadian clocks.

The study of genetically modified mice is essential in discovering the functions of different genes in retinal processes. However, the field would also benefit from using more targeted genetic models. Should a gene be essential in guiding the development of the tissue, as is the case of melanopsin in the retina, these developmental abnormalities are significant confounding factors for studying the function of a gene in the adult tissue. Current genomics techniques enable the inactivation of genes in a temporal and tissue-specific manner, allowing to circumvent any developmental defects and focus the study on the role of genes specifically in adult tissues.

In this thesis I provide evidence for melanopsin regulating the circadian transcriptome of the retina by affecting sphingolipid signalling and phototransduction processes, I dissect the differential regulation of retinal and SCN light responses and find that the mouse model of light-induced retinal damage mimics the human retinal degenerations on a molecular level. The novel scientific methodologies have the potential to further elucidate the implications of these findings.

Appendices

A

Spectra of lights used in this thesis

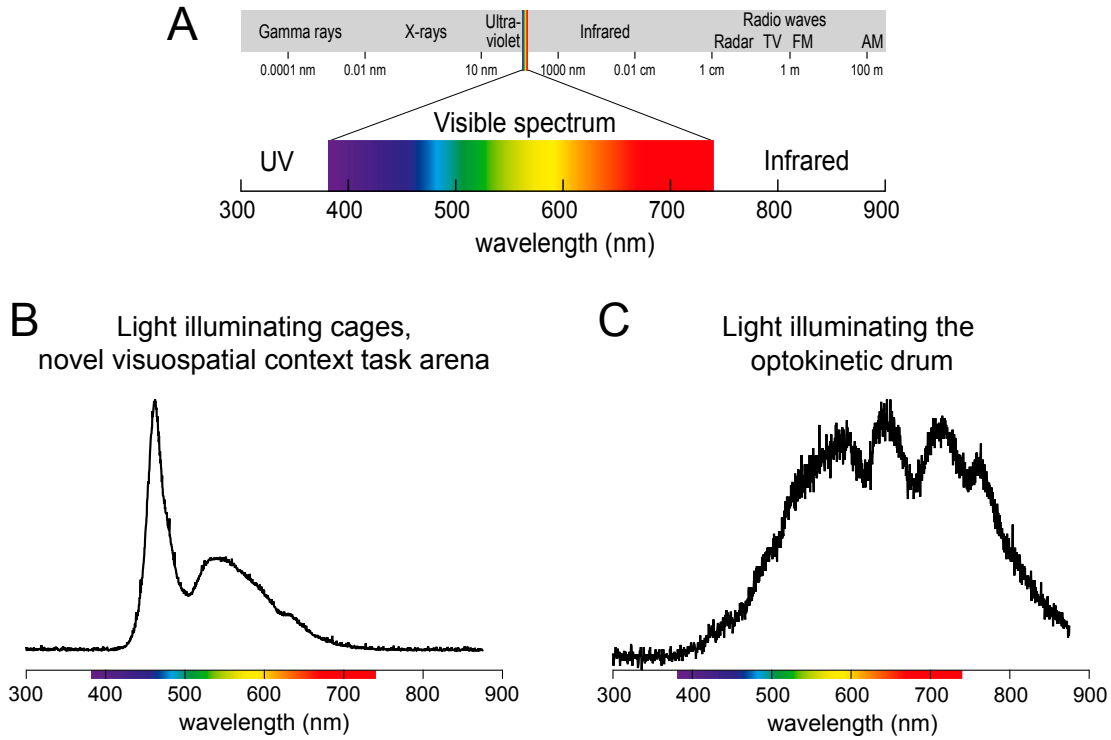


Figure A.1: Spectra of lights used in this thesis. (A) The electromagnetic spectrum with the visible spectrum expanded. The spectrum of lights illuminating animal cages and the novel visuospatial context task arena (B), and the optokinetic drum (C).

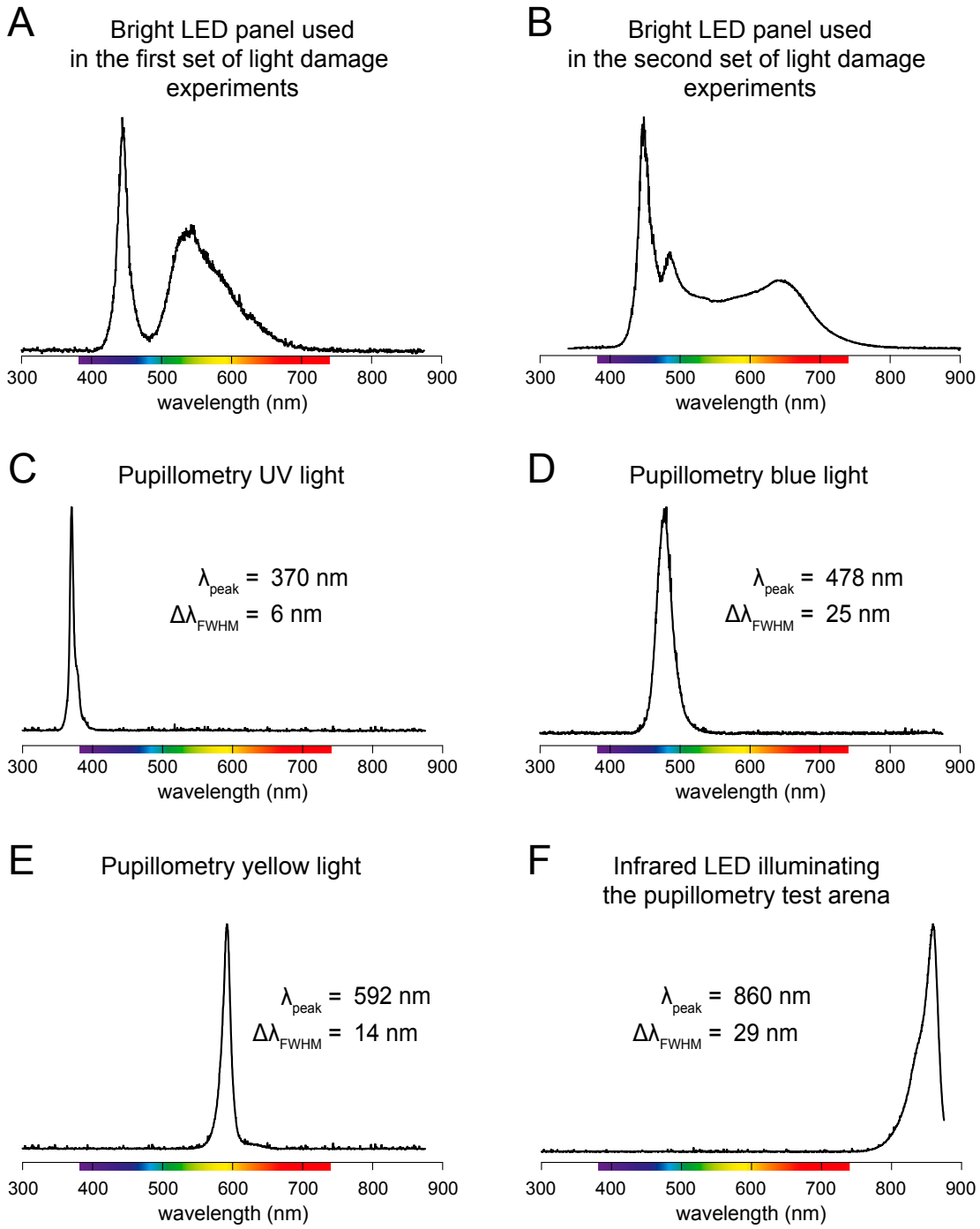


Figure A.2: Spectra of lights used in this thesis *(continued)*. (A) The spectrum of the light panel used for the first set of light damage experiments (10,000 lux light without pupil dilation), and (B) the second set of light damage experiments (20,000 lux with pupil dilation). The UV (C), blue (D), and yellow (E) light used for pupillometry recordings, and the infrared light illuminating the pupillometry test arena (F). Peak wavelength λ_{peak} and spectral width $\Delta\lambda_{\text{FWHM}}$ are indicated for single colour LEDs.

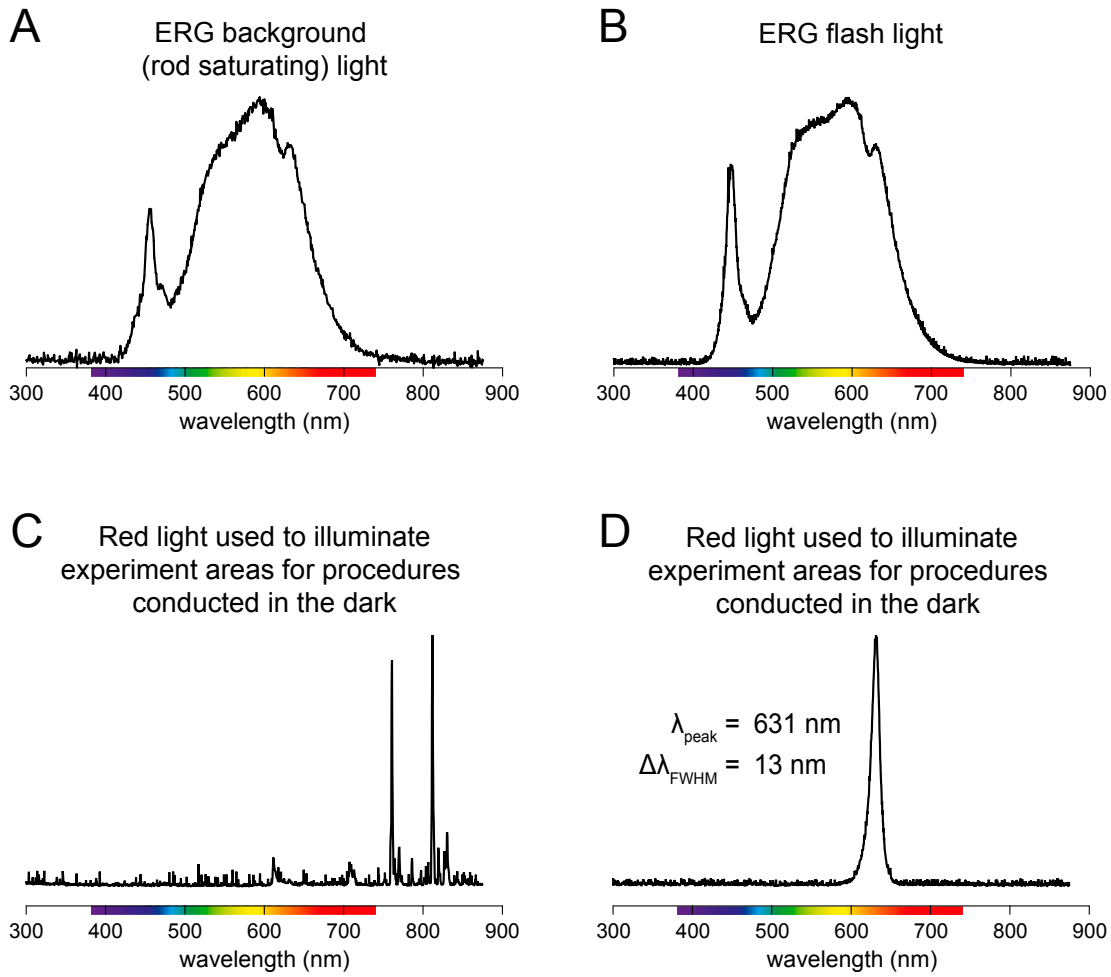


Figure A.3: Spectra of lights used in this thesis *(continued).* The spectra of electroretinography background (A) and flash lights (B). (C-D) The spectra of red lights used during experimental procedures and tissue collections performed in the darkness. Peak wavelength λ_{peak} and spectral width $\Delta\lambda_{\text{FWHM}}$ are indicated for the single colour LED.

B

Primers used for RT-qPCR

Gene name	Strand	Primer sequence 5' -> 3'
Arr3	Forward	TGGGGAAACGAGACTTCGTG
	Reverse	GGAGCCACTTGCTTGGTTTG
B2m	Forward	GCTATCCAGAAAACCCCTCAA
	Reverse	GATGTCTCGATCCCAGTAGACGGT
Bmal1	Forward	GAGGTGCCACCAACCCATAC
	Reverse	AGTCAAACAAGCTCTGGCCAA
Clock	Forward	TTGCTCCACGGGAATCCTT
	Reverse	GGAGGGAAAGTGCTCTGTTGTAG
Cry1	Forward	GCGGTTGCCTGTTTCCTGACTC
	Reverse	CCACATCCAACTTCCAGCATTTATG
Cry2	Forward	GATGTGTTCCCAAGGCTGTTCAAG
	Reverse	GAGTTCTCAGTCACCACCTCCACG
Cryaa tv 1	Forward	ACCCCGTCAAGGCAAGTTAC
	Reverse	ATTGGAAGGCAGACGGTAGC
Cryba1	Forward	TCTCATGTCCTTCCGACCCA
	Reverse	CCATGGTGGTCACACTCCAA
Crygd	Forward	GGATCAGACTGTACGAGAGGG
	Reverse	AATCGGTCCTGGAGAGAGGG
Crygs	Forward	CAACTACCGTGGCAGACAGT
	Reverse	CCAGGCCATCACTCCACAAT
Dbp	Forward	GGAAACAGCAAGCCCAAAGAA
	Reverse	CAGCGGCGCAAAAAGACTC

(continued)

Gene name	Strand	Primer sequence 5' -> 3'
Dio2	Forward	TTGCTGATCACCCTGCAGAT
	Reverse	GCACCACACTGGAATTGGGA
Dusp1	Forward	GGGGCACCTCTACTACCACA
	Reverse	GTGGCAAGTGAAACTCCACA
Egr1	Forward	CCTGACCACAGAGTCCTTTTCT
	Reverse	ATAGGTGATGGGAGGCAACC
Fos	Forward	ATCGGCAGAAGGGGAAAGTAG
	Reverse	GCAACGCAGACTTCTCATCTTCAAG
Gapdh	Forward	TGCACCACCAACTGCTTAG
	Reverse	GATGCAGGGATGATGTTC
Gfap	Forward	TCCTGGAACAGCAAAACAAG
	Reverse	CAGCCTCAGGTTGGTTTCAT
Gusb	Forward	CCAGAGCGAGTATGGAGCAG
	Reverse	TCGTCATGAAGTCGGCGAAA
Il1b	Forward	GCAGGCAGTATCACTCATTG
	Reverse	CGTTGCTTGGTTCTCCTTGT
Opn1mw	Forward	ATGGTGGTGGTGATGGTCTTCG
	Reverse	TGTCTTGGAGGTGCTGGAAAGTTC
Opn1sw	Forward	TCTTCACAGTCTTCATCGCCAGC
	Reverse	TTCAAAAGCCAGGAAAGCCAATG
Opn4 isoform 2	Forward	GCTACCGCTCTACCCACC
	Reverse	CTACATCCCGAGATCCAGACT
Per1	Forward	AGTTCCTGACCAAGCCTCGTTAG
	Reverse	CCTGCCCTCTGCTTGTCATC
Per2	Forward	GGGGTGAGATTCGTCATTGAACTTG
	Reverse	AGGACATTGGCACACTGGAAAGAG
Rho	Forward	TGTTCCTGCTCATCGTGCTGG
	Reverse	GGAAGTTGCTCATCGGCTTGC
Rplp0	Forward	CTCTCGCTTTCTGGAGGGTG
	Reverse	ATTGATGATGGAGTGTGGCA
Sik1	Forward	TGGACGTCTGGAGCCTCGGT
	Reverse	AGAGTGGGGTCGGCCTGCAT
Tnfa	Forward	CGTCGTAGCAAACCACCAAG
	Reverse	GAGAACCTGGGAGTAGACAAGG

References

1. Palumaa T, Gilhooley M, Jagannath A, Hankins MW, Hughes S, and Peirson SN. Melanopsin: Photoreceptors, Physiology and Potential. Curr Opin Physiol 2018;5:68–74.
2. Demb JB and Singer JH. Functional Circuitry of the Retina. Annu Rev Vis Sci 2015;1:263–89.
3. Cameron MA, Morley JW, and Pérez-Fernández V. Seeing the Light: Different Photoreceptor Classes Work Together to Drive Adaptation in the Mammalian Retina. Curr Opin Physiol 2020;16:43–9.
4. Vecino E, Rodriguez FD, Ruzafa N, Pereiro X, and Sharma SC. Glia-Neuron Interactions in the Mammalian Retina. Prog Retin Eye Res 2016;51:1–40.
5. Lamb TD and Pugh EN. Phototransduction, Dark Adaptation, and Rhodopsin Regeneration The Proctor Lecture. Invest Ophthalmol Vis Sci 2006;47:5138–52.
6. Larhammar D, Nordström K, and Larsson TA. Evolution of Vertebrate Rod and Cone Phototransduction Genes. Philos Trans R Soc Lond B Biol Sci 2009;364:2867–80.
7. Arshavsky VY and Burns ME. Current Understanding of Signal Amplification in Phototransduction. Cell Logist 2014;4:e29390.
8. Lamb TD. Why Rods and Cones? Eye 2016;30:179–85.
9. Knudsen E. Evolution of Neural Processing for Visual Perception in Vertebrates. J Comp Neurol 2020;528:2888–901.
10. Krauzlis RJ, Lovejoy LP, and Zénon A. Superior Colliculus and Visual Spatial Attention. Annu Rev Neurosci 2013;36.
11. Mueller T. What Is the Thalamus in Zebrafish? Front Neurosci 2012;6.
12. Keeler CE. Iris Movements in Blind Mice. Am J Physiol 1927;81:107–12.
13. Bowes C, Li T, Danciger M, Baxter LC, Applebury ML, and Farber DB. Retinal Degeneration in the Rd Mouse Is Caused by a Defect in the β Subunit of Rod cGMP-Phosphodiesterase. Nature 1990;347:677–80.
14. Zucker I. Light-Dark Rhythms in Rat Eating and Drinking Behavior. Physiol Behav 1971;6:115–26.
15. Bertolucci C and Foà A. Extraocular Photoreception and Circadian Entrainment in Nonmammalian Vertebrates. Chronobiol Int 2004;21:501–19.
16. Nelson RJ and Zucker I. Absence of Extraocular Photoreception in Diurnal and Nocturnal Rodents Exposed to Direct Sunlight. Comp Biochem Physiol Part A Mol Integr Physiol 1981;69:145–8.
17. Foster RG, Provencio I, Hudson D, Fiske S, De Grip W, and Menaker M. Circadian Photoreception in the Retinally Degenerate Mouse (Rd/Rd). J Comp Physiol A 1991;169:39–50.
18. Freedman MS, Lucas R, Soni B, et al. Regulation of Mammalian Circadian Behavior by Non-Rod, Non-Cone, Ocular Photoreceptors. Science 1999;284:502–4.

19. Lucas RJ, Freedman MS, Muñoz M, Garcia-Fernández JM, and Foster RG. Regulation of the Mammalian Pineal by Non-Rod, Non-Cone, Ocular Photoreceptors. Science 1999;284:505–7.

20. Lucas RJ, Douglas RH, and Foster RG. Characterization of an Ocular Photopigment Capable of Driving Pupillary Constriction in Mice. Nat Neurosci 2001;4:621–6.

21. Mrosovsky N, Lucas RJ, and Foster RG. Persistence of Masking Responses to Light in Mice Lacking Rods and Cones. J Biol Rhythms 2001;16:585–7.

22. Moore RY and Eichler VB. Loss of a Circadian Adrenal Corticosterone Rhythm Following Suprachiasmatic Lesions in the Rat. Brain Res 1972;42:201–6.

23. Lehman MN, Silver R, Gladstone WR, Kahn RM, Gibson M, and Bittman EL. Circadian Rhythmicity Restored by Neural Transplant. Immunocytochemical Characterization of the Graft and Its Integration with the Host Brain. J Neurosci 1987;7:1626–38.

24. Berson DM, Dunn FA, and Takao M. Phototransduction by Retinal Ganglion Cells That Set the Circadian Clock. Science 2002;295:1070–3.

25. Sekaran S, Foster RG, Lucas RJ, and Hankins MW. Calcium Imaging Reveals a Network of Intrinsically Light-Sensitive Inner-Retinal Neurons. Curr Biol 2003;13:1290–8.

26. Okano T, Yoshizawa T, and Fukada Y. Pinopsin Is a Chicken Pineal Photoreceptive Molecule. Nature 6501 1994;372:94–7.

27. Thresher RJ, Vitaterna MH, Miyamoto Y, et al. Role of Mouse Cryptochrome Blue-Light Photoreceptor in Circadian Photoresponses. Science 1998;282:1490–4.

28. Campbell SS and Murphy PJ. Extraocular Circadian Phototransduction in Humans. Science 1998;279:396–9.

29. Provencio I, Jiang G, Grip WJD, Hayes WP, and Rollag MD. Melanopsin: An Opsin in Melanophores, Brain, and Eye. Proc Natl Acad Sci USA 1998;95:340–5.

30. Provencio I, Rodriguez IR, Jiang G, Hayes WP, Moreira EF, and Rollag MD. A Novel Human Opsin in the Inner Retina. J Neurosci 2000;20:600–5.

31. Hattar S, Liao HW, Takao M, Berson D, and Yau K. Melanopsin-Containing Retinal Ganglion Cells: Architecture, Projections, and Intrinsic Photosensitivity. Science 2002;295:1065–70.

32. Hattar S, Lucas RJ, Mrosovsky N, et al. Melanopsin and Rod-Cone Photoreceptive Systems Account for All Major Accessory Visual Functions in Mice. Nature 2003;424:76–81.

33. Panda S, Provencio I, Tu DC, et al. Melanopsin Is Required for Non-Image-Forming Photic Responses in Blind Mice. Science 2003;301:525–7.

34. Peirson S and Foster RG. Melanopsin: Another Way of Signaling Light. Neuron 2006;49:331–9.

35. Panda S, Nayak SK, Campo B, Walker JR, Hogenesch JB, and Jegla T. Illumination of the Melanopsin Signaling Pathway. Science 2005;307:600–4.

36. Qiu X, Kumbalasiri T, Carlson SM, et al. Induction of Photosensitivity by Heterologous Expression of Melanopsin. Nature 2005;433:745–9.

37. Sonoda T, Lee SK, Birnbaumer L, and Schmidt TM. Melanopsin Phototransduction Is Repurposed by ipRGC Subtypes to Shape the Function of Distinct Visual Circuits. Neuron 2018;99:754–67.

38. Jiang Z, Yue WWS, Chen L, Sheng Y, and Yau KW. Cyclic-Nucleotide- and HCN-Channel-Mediated Phototransduction in Intrinsically Photosensitive Retinal Ganglion Cells. Cell 2018;175:652–64.

39. Sexton TJ and Gelder RNV. G-Protein Coupled Receptor Kinase 2 Minimally Regulates Melanopsin Activity in Intrinsically Photosensitive Retinal Ganglion Cells. PLoS One 2015;10:e0128690.

40. Blasic JR, Lane Brown R, and Robinson PR. Light-Dependent Phosphorylation of the Carboxy Tail of Mouse Melanopsin. Cell Mol Life Sci 2012;69:1551–62.

41. Cameron EG and Robinson PR. β-Arrestin-Dependent Deactivation of Mouse Melanopsin. PLoS One 2014;9:e113138.

42. Valdez-Lopez JC, Gulati S, Ortiz EA, Palczewski K, and Robinson PR. Melanopsin Carboxy-Terminus Phosphorylation Plasticity and Bulk Negative Charge, Not Strict Site Specificity, Achieves Phototransduction Deactivation. PLoS One 2020;15:e0228121.

43. Davies WIL, Foster RG, and Hankins MW. The Evolution and Function of Melanopsin in Craniates. In: *Evolution of Visual and Non-Visual Pigments*. Ed. by Hunt DM, Hankins MW, Collin SP, and Marshall NJ. Springer Series in Vision Research. Boston, MA: Springer US, 2014:23–63.

44. Melyan Z, Tarttelin EE, Bellingham J, Lucas RJ, and Hankins MW. Addition of Human Melanopsin Renders Mammalian Cells Photoresponsive. Nature 2005;433:741–5.

45. Emanuel AJ and Do MTH. Melanopsin Tristability for Sustained and Broadband Phototransduction. Neuron 2015;85:1043–55.

46. Chew KS, Renna JM, McNeill DS, et al. A Subset of ipRGCs Regulates Both Maturation of the Circadian Clock and Segregation of Retinogeniculate Projections in Mice. eLife 2017;6:e22861.

47. Güler AD, Ecker JL, Lall GS, et al. Melanopsin Cells Are the Principal Conduits for Rod-Cone Input to Non-Image-Forming Vision. Nature 2008;453:102–5.

48. Beier C, Zhang Z, Yurgel M, and Hattar S. Projections of ipRGCs and Conventional RGCs to Retinorecipient Brain Nuclei. J Comp Neurol 2020:1–13.

49. Hattar S, Kumar M, Park A, et al. Central Projections of Melanopsin-Expressing Retinal Ganglion Cells in the Mouse. J Comp Neurol 2006;497:326–49.

50. Ecker JL, Dumitrescu ON, Wong KY, et al. Melanopsin-Expressing Retinal Ganglion-Cell Photoreceptors: Cellular Diversity and Role in Pattern Vision. Neuron 2010;67:49–60.

51. Morin LP and Studholme KM. Retinofugal Projections in the Mouse. J Comp Neurol 2014;522:3733–53.

52. Baver SB, Pickard GE, Sollars PJ, and Pickard GE. Two Types of Melanopsin Retinal Ganglion Cell Differentially Innervate the Hypothalamic Suprachiasmatic Nucleus and the Olivary Pretectal Nucleus. Eur J Neurosci 2008;27:1763–70.

53. Ding JM, Chen D, Weber ET, Faiman LE, Rea MA, and Gillette MU. Resetting the Biological Clock: Mediation of Nocturnal Circadian Shifts by Glutamate and NO. Science 1994;266:1713–7.

54. Hannibal J, Hindersson P, Knudsen SM, Georg B, and Fahrenkrug J. The Photopigment Melanopsin Is Exclusively Present in Pituitary Adenylate Cyclase-Activating Polypeptide-Containing Retinal Ganglion Cells of the Retinohypothalamic Tract. J Neurosci 2002;22:1–7.

55. Sonoda T, Li JY, Hayes NW, et al. A Noncanonical Inhibitory Circuit Dampens Behavioral Sensitivity to Light. Science 2020;368:527–31.

56. Schmidt TM and Kofuji P. Structure and Function of Bistratified Intrinsically Photosensitive Retinal Ganglion Cells in the Mouse. J Comp Neurol 2011;519:1492–504.

57. Quattrochi LE, Stabio ME, Kim I, et al. The M6 Cell: A Small-Field Bistratified Photosensitive Retinal Ganglion Cell. J Comp Neurol 2018;527:297–311.

58. Estevez ME, Fogerson PM, Ilardi MC, et al. Form and Function of the M4 Cell, an Intrinsically Photosensitive Retinal Ganglion Cell Type Contributing to Geniculocortical Vision. J Neurosci 2012;32:13608–20.

59. Zhao X, Stafford BK, Godin AL, King WM, and Wong KY. Photoresponse Diversity among the Five Types of Intrinsically Photosensitive Retinal Ganglion Cells. J Physiol 2014;592:1619–36.

60. Sonoda T, Okabe Y, and Schmidt TM. Overlapping Morphological and Functional Properties between M4 and M5 Intrinsically Photosensitive Retinal Ganglion Cells. J Comp Neurol 2020;528:1028–40.

61. Aranda ML and Schmidt TM. Diversity of Intrinsically Photosensitive Retinal Ganglion Cells: Circuits and Functions. Cell Mol Life Sci 2020.

62. Schmidt TM, Alam NM, Chen S, et al. A Role for Melanopsin in Alpha Retinal Ganglion Cells and Contrast Detection. Neuron 2014;82:781–8.

63. Pires SS, Hughes S, Turton M, et al. Differential Expression of Two Distinct Functional Isoforms of Melanopsin (Opn4) in the Mammalian Retina. J Neurosci 2009;29:12332–42.

64. Jagannath A, Hughes S, Abdelgany A, et al. Isoforms of Melanopsin Mediate Different Behavioral Responses to Light. Curr Biol 2015;25:2430–4.

65. Van Hook MJ, Wong KY, and Berson DM. Dopaminergic Modulation of Ganglion-Cell Photoreceptors in Rat. Eur J Neurosci 2012;35:507–18.

66. Vuong HE, Hardi CN, Barnes S, and Brecha NC. Parallel Inhibition of Dopamine Amacrine Cells and Intrinsically Photosensitive Retinal Ganglion Cells in a Non-Image-Forming Visual Circuit of the Mouse Retina. J Neurosci 2015;35:15955–70.

67. Stabio ME, Sabbah S, Quattrochi LE, et al. The M5 Cell: A Color-Opponent Intrinsically Photosensitive Retinal Ganglion Cell. Neuron 2018;97:150–63.

68. Sodhi P and Hartwick ATE. Adenosine Modulates Light Responses of Rat Retinal Ganglion Cell Photoreceptors through a cAMP-Mediated Pathway. J Physiol 2014;592:4201–20.

69. Pack W, Hill DD, and Wong KY. Melatonin Modulates M4-Type Ganglion-Cell Photoreceptors. Neuroscience 2015;303:178–88.

70. Cleymaet AM, Gallagher SK, Tooker RE, et al. μ-Opioid Receptor Activation Directly Modulates Intrinsically Photosensitive Retinal Ganglion Cells. Neuroscience 2019;408:400–17.

71. Barnard AR, Appleford JM, Sekaran S, et al. Residual Photosensitivity in Mice Lacking Both Rod Opsin and Cone Photoreceptor Cyclic Nucleotide Gated Channel 3 α Subunit. Vis Neurosci 2004;21:675–83.

72. Pérez de Sevilla Müller L, Do MTH, Yau KW, He S, and Baldridge WH. Tracer Coupling of Intrinsically Photosensitive Retinal Ganglion Cells to Amacrine Cells in the Mouse Retina. J Comp Neurol 2010;518:4813–24.

73. Reifler AN, Chervenak AP, Dolikian ME, et al. All Spiking, Sustained on Displaced Amacrine Cells Receive Gap-Junction Input from Melanopsin Ganglion Cells. Curr Biol 2015;25:2763–73.

74. Zhang DQ, Wong KY, Sollars PJ, Berson DM, Pickard GE, and McMahon DG. Intraretinal Signaling by Ganglion Cell Photoreceptors to Dopaminergic Amacrine Neurons. Proc Natl Acad Sci USA 2008;105:14181–6.

75. Zhang DQ, Belenky MA, Sollars PJ, Pickard GE, and McMahon DG. Melanopsin Mediates Retrograde Visual Signaling in the Retina. PLoS One 2012;7:e42647.

76. Joo HR, Peterson BB, Dacey DM, Hattar S, and Chen SK. Recurrent Axon Collaterals of Intrinsically Photosensitive Retinal Ganglion Cells. Vis Neurosci 2013;30:175–82.

77. Prigge CL, Yeh PT, Liou NF, et al. M1 ipRGCs Influence Visual Function through Retrograde Signaling in the Retina. J Neurosci 2016;36:7184–97.

78. Milosavljevic N, Storchi R, Eleftheriou CG, Colins A, Petersen RS, and Lucas RJ. Photoreceptive Retinal Ganglion Cells Control the Information Rate of the Optic Nerve. Proc Natl Acad Sci USA 2018;115:E11817–E11826.

79. Hatori M, Le H, Vollmers C, et al. Inducible Ablation of Melanopsin-Expressing Retinal Ganglion Cells Reveals Their Central Role in Non-Image Forming Visual Responses. PLoS One 2008;3:e2451.

80. Ruby NF, Brennan TJ, Xie X, et al. Role of Melanopsin in Circadian Responses to Light. Science 2002;298:2211–3.

81. Panda S, Sato TK, Castrucci AM, et al. Melanopsin (Opn4) Requirement for Normal Light-Induced Circadian Phase Shifting. Science 2002;298:2213–6.

82. Lucas RJ, Hattar S, Takao M, Berson DM, Foster RG, and Yau KW. Diminished Pupillary Light Reflex at High Irradiances in Melanopsin-Knockout Mice. Science 2003;299:245–7.

83. Keenan WT, Rupp AC, Ross RA, et al. A Visual Circuit Uses Complementary Mechanisms to Support Transient and Sustained Pupil Constriction. eLife 2016;5:e15392.

84. Wang Q, Yue WWS, Jiang Z, et al. Synergistic Signaling by Light and Acetylcholine in Mouse Iris Sphincter Muscle. Curr Biol 2017;27:1791–800.

85. Lupi D, Oster H, Thompson S, and Foster RG. The Acute Light-Induction of Sleep Is Mediated by OPN4-Based Photoreception. Nat Neurosci 2008;11:1068–73.

86. Milosavljevic N, Cehajic-Kapetanovic J, Procyk CA, and Lucas RJ. Chemogenetic Activation of Melanopsin Retinal Ganglion Cells Induces Signatures of Arousal and/or Anxiety in Mice. Curr Biol 2016;26:2358–63.

87. Pilorz V, Tam SKE, Hughes S, et al. Melanopsin Regulates Both Sleep-Promoting and Arousal-Promoting Responses to Light. PLoS Biol 2016;14:1–24.

88. Golden RN, Gaynes BN, Ekstrom RD, et al. The Efficacy of Light Therapy in the Treatment of Mood Disorders: A Review and Meta-Analysis of the Evidence. Am J Psychiatry 2005;162:656–62.

89. LeGates TA, Altimus CM, Wang H, et al. Aberrant Light Directly Impairs Mood and Learning through Melanopsin-Expressing Neurons. Nature 2012;491:594–8.

90. Brown TM, Gias C, Hatori M, et al. Melanopsin Contributions to Irradiance Coding in the Thalamo-Cortical Visual System. PLoS Biol 2010;8:e1000558.

91. Brown TM, Tsujimura Si, Allen AE, et al. Melanopsin-Based Brightness Discrimination in Mice and Humans. Curr Biol 2012;22:1134–41.

92. Zaidi FH, Hull JT, Peirson SN, et al. Short-Wavelength Light Sensitivity of Circadian, Pupillary, and Visual Awareness in Humans Lacking an Outer Retina. Curr Biol 2007;17:2122–8.

93. Sekaran S, Lupi D, Jones SL, et al. Melanopsin-Dependent Photoreception Provides Earliest Light Detection in the Mammalian Retina. Curr Biol 2005;15:1099–107.

94. Tu DC, Owens LA, Anderson L, et al. Inner Retinal Photoreception Independent of the Visual Retinoid Cycle. Proc Natl Acad Sci USA 2006;103:10426–31.

95. Tarttelin EE, Bellingham J, Bibb LC, et al. Expression of Opsin Genes Early in Ocular Development of Humans and Mice. Exp Eye Res 2003;76:393–6.

96. Rao S, Chun C, Fan J, et al. A Direct and Melanopsin-Dependent Fetal Light Response Regulates Mouse Eye Development. Nature 2013;494:243–6.

97. Renna JM, Chellappa DK, Ross CL, Stabio ME, and Berson DM. Melanopsin Ganglion Cells Extend Dendrites into the Outer Retina during Early Postnatal Development. Dev Neurobiol 2015;75:935–46.

98. Tufford AR, Onyak JR, Sondereker KB, et al. Melanopsin Retinal Ganglion Cells Regulate Cone Photoreceptor Lamination in the Mouse Retina. Cell Rep 2018;23:2416–28.

99. Chai Z, Silverman D, Li G, Williams D, Raviola E, and Yau KW. Light-Dependent Photoreceptor Orientation in Mouse Retina. Sci Adv 2020;6:eabe2782.

100. Renna JM, Weng S, and Berson DM. Light Acts through Melanopsin to Alter Retinal Waves and Segregation of Retinogeniculate Afferents. Nat Neurosci 7 2011;14:827–9.

101. Vitaterna MH, Takahashi JS, and Turek FW. Overview of Circadian Rhythms. Alcohol Res Health 2001;25:85–93.

102. Pittendrigh CS. Circadian Rhythms and the Circadian Organization of Living Systems. Cold Spring Harb Symp Quant Biol 1960;25:159–84.

103. Aschoff J. Circadian Control of Body Temperature. J Therm Biol 1983;8:143–7.

104. Aschoff J. Circadian Timing. Ann N Y Acad Sci 1984;423:442–68.

105. Buhr ED and Takahashi JS. Molecular Components of the Mammalian Circadian Clock. Handb Exp Pharmacol 2013;217:3–27.

106. Abrahamson EE and Moore RY. Suprachiasmatic Nucleus in the Mouse: Retinal Innervation, Intrinsic Organization and Efferent Projections. Brain Res 2001;916:172–91.

107. Hofman MA, Fliers E, Goudsmit E, and Swaab DF. Morphometric Analysis of the Suprachiasmatic and Paraventricular Nuclei in the Human Brain: Sex Differences and Age-Dependent Changes. J Anat 1988;160:127–43.

108. Meijer JH, Groos GA, and Rusak B. Luminance Coding in a Circadian Pacemaker: The Suprachiasmatic Nucleus of the Rat and the Hamster. Brain Res 1986;382:109–18.

109. Stephan FK and Zucker I. Circadian Rhythms in Drinking Behavior and Locomotor Activity of Rats Are Eliminated by Hypothalamic Lesions. Proc Natl Acad Sci USA 1972;69:1583–6.

110. Inouye ST and Kawamura H. Persistence of Circadian Rhythmicity in a Mammalian Hypothalamic "Island" Containing the Suprachiasmatic Nucleus. Proc Natl Acad Sci USA 1979;76:5962–6.

111. Welsh DK, Logothetis DE, Meister M, and Reppert SM. Individual Neurons Dissociated from Rat Suprachiasmatic Nucleus Express Independently Phased Circadian Firing Rhythms. Neuron 1995;14:697–706.

112. Ralph MR and Menaker M. A Mutation of the Circadian System in Golden Hamsters. Science 1988;241:1225–7.

113. Ralph MR, Foster RG, Davis FC, and Menaker M. Transplanted Suprachiasmatic Nucleus Determines Circadian Period. Science 1990;247:975–8.

114. Konopka RJ and Benzer S. Clock Mutants of Drosophila Melanogaster. Proc Natl Acad Sci USA 1971;68:2112–6.

115. Zehring WA, Wheeler DA, Reddy P, et al. P-Element Transformation with Period Locus DNA Restores Rhythmicity to Mutant, Arrhythmic Drosophila Melanogaster. Cell 1984;39:369–76.

116. Vitaterna MH, King DP, Chang AM, et al. Mutagenesis and Mapping of a Mouse Gene, Clock, Essential for Circadian Behavior. Science 1994;264:719–25.

117. Lowrey PL and Takahashi JS. Chapter 6 - Genetics of Circadian Rhythms in Mammalian Model Organisms. In: *The Genetics of Circadian Rhythms*. Ed. by Brody S. Vol. 74. Advances in Genetics. Academic Press, 2011:175–230.

118. Brown SA and Azzi A. Peripheral Circadian Oscillators in Mammals. In: *Circadian Clocks*. Ed. by Kramer A and Merrow M. Handbook of Experimental Pharmacology. Berlin, Heidelberg: Springer, 2013:45–66.

119. Yoo SH, Yamazaki S, Lowrey PL, et al. PERIOD2:: LUCIFERASE Real-Time Reporting of Circadian Dynamics Reveals Persistent Circadian Oscillations in Mouse Peripheral Tissues. Proc Natl Acad Sci USA 2004;101:5339–46.

120. Besharse JC and Iuvone PM. Circadian Clock in Xenopus Eye Controlling Retinal Serotonin N-Acetyltransferase. Nature 1983;305:133–5.

121. Terman JS, Remé CE, and Terman M. Rod Outer Segment Disk Shedding in Rats with Lesions of the Suprachiasmatic Nucleus. Brain Res 1993;605:256–64.

122. Tosini G and Menaker M. Circadian Rhythms in Cultured Mammalian Retina. Science 1996;272:419–21.

123. Ribelayga C and Mangel SC. Absence of Circadian Clock Regulation of Horizontal Cell Gap Junctional Coupling Reveals Two Dopamine Systems in the Goldfish Retina. Journal of Comparative Neurology 2003;467:243–53.

124. Ribelayga C, Cao Y, and Mangel SC. The Circadian Clock in the Retina Controls Rod-Cone Coupling. Neuron 2008;59:790–801.

125. Tikidji-Hamburyan A, Reinhard K, Storchi R, et al. Rods Progressively Escape Saturation to Drive Visual Responses in Daylight Conditions. Nature Communications 2017;8:1813.

126. Zhang Z, Li H, Liu X, O'Brien J, and Ribelayga CP. Circadian Clock Control of Connexin36 Phosphorylation in Retinal Photoreceptors of the CBA/CaJ Mouse Strain. Vis Neurosci 2015;32.

127. Cao J, Ribelayga CP, and Mangel SC. A Circadian Clock in the Retina Regulates Rod-Cone Gap Junction Coupling and Neuronal Light Responses via Activation of Adenosine A2A Receptors. Front Cell Neurosci 2021;14:467.

128. Penn RD and Hagins WA. Signal Transmission along Retinal Rods and the Origin of the Electroretinographic A-Wave. Nature 5202 1969;223:201–5.

129. Robson JG and Frishman LJ. Dissecting the Dark-Adapted Electroretinogram. Doc Ophthalmol 1998;95:187–215.

130. Storch KF, Paz C, Signorovitch J, et al. Intrinsic Circadian Clock of the Mammalian Retina: Importance for Retinal Processing of Visual Information. Cell 2007;130:730–41.

131. Cameron MA, Barnard AR, Hut RA, et al. Electroretinography of Wild-Type and Cry Mutant Mice Reveals Circadian Tuning of Photopic and Mesopic Retinal Responses. J Biol Rhythms 2008;23:489–501.

132. Jackson CR, Ruan GX, Aseem F, et al. Retinal Dopamine Mediates Multiple Dimensions of Light-Adapted Vision. J Neurosci 2012;32:9359–68.

133. Umino Y, Solessio E, and Barlow RB. Speed, Spatial, and Temporal Tuning of Rod and Cone Vision in Mouse. J Neurosci 2008;28:189–98.

134. Wong JCY, Smyllie NJ, Banks GT, et al. Differential Roles for Cryptochromes in the Mammalian Retinal Clock. FASEB J 2018;32:4302–14.

135. Hall CA and Chilcott RP. Eyeing up the Future of the Pupillary Light Reflex in Neurodiagnostics. Diagnostics 2018;8.

136. Ruan GX, Zhang DQ, Zhou T, Yamazaki S, and McMahon DG. Circadian Organization of the Mammalian Retina. Proc Natl Acad Sci USA 2006;103:9703–8.

137. Liu X, Zhang Z, and Ribelayga CP. Heterogeneous Expression of the Core Circadian Clock Proteins among Neuronal Cell Types in Mouse Retina. PLoS One 2012;7:e50602.

138. Dkhissi-Benyahya O, Coutanson C, Knoblauch K, et al. The Absence of Melanopsin Alters Retinal Clock Function and Dopamine Regulation by Light. Cell Mol Life Sci 2013;70:3435–47.

139. Doyle SE, Grace MS, McIvor W, and Menaker M. Circadian Rhythms of Dopamine in Mouse Retina: The Role of Melatonin. Vis Neurosci 2002;19:593–601.

140. Tosini G and Menaker M. The Clock in the Mouse Retina: Melatonin Synthesis and Photoreceptor Degeneration. Brain Res 1998;789:221–8.

141. Sakamoto K, Liu C, Kasamatsu M, Iuvone PM, and Tosini G. Intraocular Injection of Kainic Acid Does Not Abolish the Circadian Rhythm of Arylalkylamine N-Acetyltransferase mRNA in Rat Photoreceptors. Mol Vis 2006;12:117–24.

142. Jaliffa CO, Saenz D, Resnik E, Keller Sarmiento MI, and Rosenstein RE. Circadian Activity of the GABAergic System in the Golden Hamster Retina. Brain Res 2001;912:195–202.

143. Ruan GX, Allen GC, Yamazaki S, and McMahon DG. An Autonomous Circadian Clock in the Inner Mouse Retina Regulated by Dopamine and GABA. PLoS Biol 2008;6:e249.

144. Ebihara S, Marks T, Hudson DJ, and Menaker M. Genetic Control of Melatonin Synthesis in the Pineal Gland of the Mouse. Science 1986;231:491–3.

145. Buhr ED and Van Gelder RN. Local Photic Entrainment of the Retinal Circadian Oscillator in the Absence of Rods, Cones, and Melanopsin. Proc Natl Acad Sci USA 2014;111:8625–30.

146. Buhr ED, Yue WWS, Ren X, et al. Neuropsin (OPN5)-Mediated Photoentrainment of Local Circadian Oscillators in Mammalian Retina and Cornea. Proc Natl Acad Sci USA 2015;112:13093–8.

147. Buhr ED, Vemaraju S, Diaz N, Lang RA, and Van Gelder RN. Neuropsin (OPN5) Mediates Local Light-Dependent Induction of Circadian Clock Genes and Circadian Photoentrainment in Exposed Murine Skin. Curr Biol 2019;29:3478–87.

148. Liang FQ, Green L, Wang C, Alssadi R, and Godley BF. Melatonin Protects Human Retinal Pigment Epithelial (RPE) Cells against Oxidative Stress. Exp Eye Res 2004;78:1069–75.

149. Baba K, Pozdeyev N, Mazzoni F, et al. Melatonin Modulates Visual Function and Cell Viability in the Mouse Retina via the MT1 Melatonin Receptor. Proc Natl Acad Sci USA 2009;106:15043–8.

150. Yi C, Pan X, Yan H, Guo M, and Pierpaoli W. Effects of Melatonin in Age-Related Macular Degeneration. Ann N Y Acad Sci 2005;1057:384–92.

151. Rosen R, Hu DN, Perez V, et al. Urinary 6-Sulfatoxymelatonin Level in Age-Related Macular Degeneration Patients. Mol Vis 2009;15:1673–9.

152. Tosini G, Chaurasia SS, and Iuvone PM. Regulation of Arylalkylamine N-Acetyltransferase (AANAT) in the Retina. Chronobiol Int 2006;23:381–91.

153. Baba K, Mazzoni F, Owino S, Contreras-Alcantara S, Strettoi E, and Tosini G. Age-Related Changes in the Daily Rhythm of Photoreceptor Functioning and Circuitry in a Melatonin-Proficient Mouse Strain. PLoS One 2012;7:e37799.

154. Tabandeh H, Lockley SW, Buttery R, et al. Disturbance of Sleep in Blindness. American Journal of Ophthalmology 1998;126:707–12.

155. Baba K, Piano I, Lyuboslavsky P, et al. Removal of Clock Gene Bmal1 from the Retina Affects Retinal Development and Accelerates Cone Photoreceptor Degeneration during Aging. Proc Natl Acad Sci USA 2018:201808137.

156. Baba K, Ribelayga CP, Michael Iuvone P, and Tosini G. The Retinal Circadian Clock and Photoreceptor Viability. Adv Exp Med Biol 2018;1074:345–50.

157. Jun G, Nicolaou M, Morrison MA, et al. Influence of ROBO1 and RORA on Risk of Age-Related Macular Degeneration Reveals Genetically Distinct Phenotypes in Disease Pathophysiology. PLoS One 2011;6:e25775.

158. Vaughan DK, Nemke JL, Fliesler SJ, Darrow RM, and Organisciak DT. Evidence for a Circadian Rhythm of Susceptibility to Retinal Light Damage. Photochem Photobiol 2002;75:547–53.

159. Darling NJ, Toth R, Arthur JSC, and Clark K. Inhibition of SIK2 and SIK3 during Differentiation Enhances the Anti-Inflammatory Phenotype of Macrophages. Biochem J 2017;474:521–37.

160. Wenzel A, Reme CE, Williams TP, Hafezi F, and Grimm C. The Rpe65 Leu450Met Variation Increases Retinal Resistance Against Light-Induced Degeneration by Slowing Rhodopsin Regeneration. J Neurosci 2001;21:53–8.

161. Hughes S, Pothecary CA, Jagannath A, Foster RG, Hankins MW, and Peirson SN. Profound Defects in Pupillary Responses to Light in TRPM-Channel Null Mice: A Role for TRPM Channels in Non-Image-Forming Photoreception. Eur J Neurosci 2012;35:34–43.

162. Schindelin J, Arganda-Carreras I, Frise E, et al. Fiji: An Open-Source Platform for Biological-Image Analysis. Nat Methods 2012;9:676–82.

163. Tam SKE, Hasan S, Hughes S, et al. Modulation of Recognition Memory Performance by Light Requires Both Melanopsin and Classical Photoreceptors. Proc Royal Soc B 2016;283:20162275.

164. Hurst JL and West RS. Taming Anxiety in Laboratory Mice. Nat Methods 2010;7:825–6.

165. Afgan E, Baker D, Batut B, et al. The Galaxy Platform for Accessible, Reproducible and Collaborative Biomedical Analyses: 2018 Update. Nucleic Acids Res 2018;46:W537–W544.

166. Andrews S. FastQC: A Quality Control Tool for High Throughput Sequence Data [Online]. 2010. URL: `http://www.bioinformatics.babraham.ac.uk/projects/fastqc/`.

167. Dobin A, Davis CA, Schlesinger F, et al. STAR: Ultrafast Universal RNA-Seq Aligner. Bioinformatics 2013;29:15–21.

168. Liao Y, Smyth GK, and Shi W. featureCounts: An Efficient General Purpose Program for Assigning Sequence Reads to Genomic Features. Bioinformatics 2014;30:923–30.

169. Love MI, Huber W, and Anders S. Moderated Estimation of Fold Change and Dispersion for RNA-Seq Data with DESeq2. Genome Biol 2014;15:550.

170. Wu G, Anafi RC, Hughes ME, Kornacker K, and Hogenesch JB. MetaCycle: An Integrated R Package to Evaluate Periodicity in Large Scale Data. Bioinformatics 2016;32:3351–3.

171. Kanehisa M and Goto S. KEGG: Kyoto Encyclopedia of Genes and Genomes. Nucleic Acids Res 2000;28:27–30.

172. Raudvere U, Kolberg L, Kuzmin I, et al. G:Profiler: A Web Server for Functional Enrichment Analysis and Conversions of Gene Lists (2019 Update). Nucleic Acids Res 2019;47:W191–W198.

173. Ortín-Martínez A, Nadal-Nicolás FM, Jiménez-López M, et al. Number and Distribution of Mouse Retinal Cone Photoreceptors: Differences between an Albino (Swiss) and a Pigmented (C57/BL6) Strain. PLoS One 2014;9:e102392.

174. Sawant OB, Horton AM, Zucaro OF, et al. The Circadian Clock Gene Bmal1 Controls Thyroid Hormone-Mediated Spectral Identity and Cone Photoreceptor Function. Cell Rep 2017;21:692–706.

175. Lucas RJ, Peirson SN, Berson DM, et al. Measuring and Using Light in the Melanopsin Age. Trends Neurosci 2014;37:1–9.

176. Carvalho BS and Irizarry RA. A Framework for Oligonucleotide Microarray Preprocessing. Bioinformatics 2010;26:2363–7.

177. Huber W, Carey VJ, Gentleman R, et al. Orchestrating High-Throughput Genomic Analysis with Bioconductor. Nat Methods 2015;12:115–21.

178. Zhou G, Soufan O, Ewald J, Hancock REW, Basu N, and Xia J. NetworkAnalyst 3.0: A Visual Analytics Platform for Comprehensive Gene Expression Profiling and Meta-Analysis. Nucleic Acids Res 2019;47:W234–W241.

179. Johnson WE, Li C, and Rabinovic A. Adjusting Batch Effects in Microarray Expression Data Using Empirical Bayes Methods. Biostatistics 2007;8:118–27.

180. Orchard S, Kerrien S, Abbani S, et al. Protein Interaction Data Curation: The International Molecular Exchange (IMEx) Consortium. Nat Methods 2012;9:345–50.

181. Subramanian A, Tamayo P, Mootha VK, et al. Gene Set Enrichment Analysis: A Knowledge-Based Approach for Interpreting Genome-Wide Expression Profiles. Proc Natl Acad Sci USA 2005;102:15545–50.

182. Durinck S, Spellman PT, Birney E, and Huber W. Mapping Identifiers for the Integration of Genomic Datasets with the R/Bioconductor Package biomaRt. Nat Protoc 2009;4:1184–91.

183. Bult CJ, Blake JA, Smith CL, Kadin JA, Richardson JE, and Mouse Genome Database Group. Mouse Genome Database (MGD) 2019. Nucleic Acids Res 2019;47:D801–D806.

184. Siegert S, Cabuy E, Scherf BG, et al. Transcriptional Code and Disease Map for Adult Retinal Cell Types. Nat Neurosci 2012;15:487–95.

185. Barnard AR, Hattar S, Hankins MW, and Lucas RJ. Melanopsin Regulates Visual Processing in the Mouse Retina. Curr Biol 2006;16:389–95.

186. Jagannath A, Butler R, Godinho SI, et al. The CRTC1-SIK1 Pathway Regulates Entrainment of the Circadian Clock. Cell 2013;154:1100–11.

187. Cameron MA, Pozdeyev N, Vugler AA, Cooper H, Iuvone PM, and Lucas RJ. Light Regulation of Retinal Dopamine That Is Independent of Melanopsin Phototransduction. J Neurosci 2009;29:761–7.

188. Pérez-Fernández V, Milosavljevic N, Allen AE, et al. Rod Photoreceptor Activation Alone Defines the Release of Dopamine in the Retina. Curr Biol 2019;29:763–774.e5.

189. Wong JCY, Pothecary CA, Banks GT, et al. Melanopsin Regulates Circadian Rhythms in Contrast Sensitivity but Not Pupillary Light Responses. Invest Ophthalmol Vis Sci 2018;59:1980.

190. Hwang CK, Chaurasia SS, Jackson CR, Chan GCK, Storm DR, and Iuvone PM. Circadian Rhythm of Contrast Sensitivity Is Regulated by a Dopamine–Neuronal PAS-Domain Protein 2–Adenylyl Cyclase 1 Signaling Pathway in Retinal Ganglion Cells. J Neurosci 2013;33:14989–97.

191. Sengupta A, Baba K, Mazzoni F, et al. Localization of Melatonin Receptor 1 in Mouse Retina and Its Role in the Circadian Regulation of the Electroretinogram and Dopamine Levels. PLoS One 2011;6:e24483.

192. Allen AE, Storchi R, Martial FP, et al. Melanopsin-Driven Light Adaptation in Mouse Vision. Curr Biol 2014;24:2481–90.

193. Sawant OB, Jidigam VK, Fuller RD, et al. The Circadian Clock Gene Bmal1 Is Required to Control the Timing of Retinal Neurogenesis and Lamination of Müller Glia in the Mouse Retina. FASEB J 2019;33:8745–58.

194. Ewels P, Magnusson M, Lundin S, and Käller M. MultiQC: Summarize Analysis Results for Multiple Tools and Samples in a Single Report. Bioinformatics 2016;32:3047–8.

195. Glynn EF, Chen J, and Mushegian AR. Detecting Periodic Patterns in Unevenly Spaced Gene Expression Time Series Using Lomb–Scargle Periodograms. Bioinformatics 2006;22:310–6.

196. Hughes ME, Hogenesch JB, and Kornacker K. JTK_CYCLE: An Efficient Non-Parametric Algorithm for Detecting Rhythmic Components in Genome-Scale Datasets. J Biol Rhythms 2010;25:372–80.

197. Klitten LL, Rath MF, Coon SL, Kim JS, Klein DC, and Møller M. Localization and Regulation of Dopamine Receptor D4 Expression in the Adult and Developing Rat Retina. Exp Eye Res 2008;87:471–7.

198. Ballouz S, Pavlidis P, and Gillis J. Using Predictive Specificity to Determine When Gene Set Analysis Is Biologically Meaningful. Nucleic Acids Res 2017;45:e20.

199. Mure LS, Le HD, Benegiamo G, et al. Diurnal Transcriptome Atlas of a Primate across Major Neural and Peripheral Tissues. Science 2018;359:eaao0318.

200. Mure LS, Hatori M, Ruda K, Benegiamo G, Demas J, and Panda S. Sustained Melanopsin Photoresponse Is Supported by Specific Roles of β-Arrestin 1 and 2 in Deactivation and Regeneration of Photopigment. Cell Rep 2018;25:2497–2509.e4.

201. Daan S and Pittendrigh CS. A Functional Analysis of Circadian Pacemakers in Nocturnal Rodents. J Comp Physiol 1976;106:253–66.

202. Caputto BL and Guido ME. Immediate Early Gene Expression Within the Visual System: Light and Circadian Regulation in the Retina and the Suprachiasmatic Nucleus. Neurochem Res 2000;25:153–62.

203. Bedolla DE and Torre V. A Component of Retinal Light Adaptation Mediated by the Thyroid Hormone Cascade. PLoS One 2011;6:e26334.

204. Jones KA, Hatori M, Mure LS, et al. Small Molecule Antagonists of Melanopsin-Mediated Phototransduction. Nat Chem Biol 2013;9:630–5.

205. Park SJH, Pottackal J, Ke JB, et al. Convergence and Divergence of CRH Amacrine Cells in Mouse Retinal Circuitry. J Neurosci 2018;38:3753–66.

206. Maceyka M, Harikumar KB, Milstien S, and Spiegel S. Sphingosine-1-Phosphate Signalling and Its Role in Disease. Trends Cell Biol 2012;22:50–60.

207. Porter H, Qi H, Prabhu N, et al. Characterizing Sphingosine Kinases and Sphingosine 1-Phosphate Receptors in the Mammalian Eye and Retina. Int J Mol Sci 2018;19:3885.

208. Skoura A, Sanchez T, Claffey K, Mandala SM, Proia RL, and Hla T. Essential Role of Sphingosine 1–Phosphate Receptor 2 in Pathological Angiogenesis of the Mouse Retina. J Clin Invest 2007;117:2506–16.

209. Noell WK, Walker VS, Kang BS, and Berman S. Retinal Damage by Light in Rats. Invest Ophthalmol Vis Sci 1966;5:450–73.

210. Liu C, Peng M, Laties AM, and Wen R. Preconditioning with Bright Light Evokes a Protective Response against Light Damage in the Rat Retina. J Neurosci 1998;18:1337–44.

211. Van Norren D and Vos JJ. Light Damage to the Retina: An Historical Approach. Eye 2016;30:169–72.

212. Lyubarsky AL, Falsini B, Pennesi ME, Valentini P, and Pugh EN. UV- and Midwave-Sensitive Cone-Driven Retinal Responses of the Mouse: A Possible Phenotype for Coexpression of Cone Photopigments. J Neurosci 1999;19:442–55.

213. Van Norren D and Gorgels TGMF. The Action Spectrum of Photochemical Damage to the Retina: A Review of Monochromatic Threshold Data. Photochem Photobiol 2011;87:747–53.

214. Ham WT, Mueller HA, and Sliney DH. Retinal Sensitivity to Damage from Short Wavelength Light. Nature 1976;260:153–5.

215. Gorgels TG and Van Norren D. Ultraviolet and Green Light Cause Different Types of Damage in Rat Retina. Invest Ophthalmol Vis Sci 1995;36:851–63.

216. Marie M, Bigot K, Angebault C, et al. Light Action Spectrum on Oxidative Stress and Mitochondrial Damage in A2E-Loaded Retinal Pigment Epithelium Cells. Cell Death Dis 3 2018;9:1–13.

217. Rezai KA, Gasyna E, Seagle BLL, Norris JR, and Rezaei KA. AcrySof Natural Filter Decreases Blue Light-Induced Apoptosis in Human Retinal Pigment Epithelium. Graefes Arch Clin Exp Ophthalmol 2008;246:671–6.

218. Yanagi Y, Inoue Y, Iriyama A, and Jang WD. Effects of Yellow Intraocular Lenses on Light-Induced Upregulation of Vascular Endothelial Growth Factor. J Cataract Refract Surg 2006;32:1540–4.

219. Keller C, Grimm C, Wenzel A, Hafezi F, and Remé CE. Protective Effect of Halothane Anesthesia on Retinal Light Damage: Inhibition of Metabolic Rhodopsin Regeneration. Invest Ophthalmol Vis Sci 2001;42:476–80.

220. Grimm C, Wenzel A, Williams TP, Rol PO, Hafezi F, and Remé CE. Rhodopsin-Mediated Blue-Light Damage to the Rat Retina: Effect of Photoreversal of Bleaching. Invest Ophthalmol Vis Sci 2001;42:497–505.

221. Chen J, Simon MI, Matthes MT, Yasumura D, and LaVail MM. Increased Susceptibility to Light Damage in an Arrestin Knockout Mouse Model of Oguchi Disease (Stationary Night Blindness). Invest Ophthalmol Vis Sci 1999;40:2978–82.

222. Chen CK, Burns ME, Spencer M, et al. Abnormal Photoresponses and Light-Induced Apoptosis in Rods Lacking Rhodopsin Kinase. Proc Natl Acad Sci USA 1999;96:3718–22.

223. Maeda T, Golczak M, and Maeda A. Retinal Photodamage Mediated by All-Trans-Retinal. Photochem Photobiol 2012;88:1309–19.

224. Grimm C, Remé CE, Rol PO, and Williams TP. Blue Light's Effects on Rhodopsin: Photoreversal of Bleaching in Living Rat Eyes. Invest Ophthalmol Vis Sci 2000;41:3984–90.

225. Penn JS, Naash MI, and Anderson RE. Effect of Light History on Retinal Antioxidants and Light Damage Susceptibility in the Rat. Exp Eye Res 1987;44:779–88.

226. Penn JS and Williams TP. Photostasis: Regulation of Daily Photon-Catch by Rat Retinas in Response to Various Cyclic Illuminances. Exp Eye Res 1986;43:915–28.

227. Shioda S, Takenoya F, Wada N, Hirabayashi T, Seki T, and Nakamachi T. Pleiotropic and Retinoprotective Functions of PACAP. Anat Sci Int 2016;91:313–24.

228. Slingsby C and Wistow GJ. Functions of Crystallins in and out of Lens: Roles in Elongated and Post-Mitotic Cells. Prog Biophys Mol Biol 2014;115:52–67.

229. Sakaguchi H, Miyagi M, Darrow RM, et al. Intense Light Exposure Changes the Crystallin Content in Retina. Exp Eye Res 2003;76:131–3.

230. Organisciak D, Darrow R, Barsalou L, Rapp C, McDonald B, and Wong P. Light Induced and Circadian Effects on Retinal Photoreceptor Cell Crystallins. Photochem Photobiol 2011;87:151–9.

231. Yaung J, Kannan R, Wawrousek EF, Spee C, Sreekumar PG, and Hinton DR. Exacerbation of Retinal Degeneration in the Absence of Alpha Crystallins in an in Vivo Model of Chemically Induced Hypoxia. Exp Eye Res 2008;86:355–65.

232. Johnson PT, Brown MN, Pulliam BC, Anderson DH, and Johnson LV. Synaptic Pathology, Altered Gene Expression, and Degeneration in Photoreceptors Impacted by Drusen. Invest Ophthalmol Vis Sci 2005;46:4788–95.

233. Organisciak D, Darrow R, Gu X, Barsalou L, and Crabb JW. Genetic, Age and Light Mediated Effects on Crystallin Protein Expression in the Retina. Photochem Photobiol 2006;82:1088–96.

234. Philp AR, Jin M, Li S, et al. Predicting the Pathogenicity of RPE65 Mutations. Human Mutation 2009;30:1183–8.

235. Luke MPs, LeVatte TL, Rutishauser U, Tremblay F, and Clarke DB. Polysialylated Neural Cell Adhesion Molecule Protects Against Light-Induced Retinal Degeneration. Invest Ophthalmol Vis Sci 2016;57:5066–75.

236. Bai S and Sheline CT. NAD+ Maintenance Attenuates Light Induced Photoreceptor Degeneration. Exp Eye Res 2013;108:76–83.

237. Schroeder MM, Harrison KR, Jaeckel ER, et al. The Roles of Rods, Cones, and Melanopsin in Photoresponses of M4 Intrinsically Photosensitive Retinal Ganglion Cells (ipRGCs) and Optokinetic Visual Behavior. Front Cell Neurosci 2018;12:203.

238. Van Alphen B, Winkelman BHJ, and Frens MA. Age- and Sex-Related Differences in Contrast Sensitivity in C57Bl/6 Mice. Invest Ophthalmol Vis Sci 2009;50:2451–8.

239. Vecino E, Rodriguez F, Ruzafa N, Pereiro X, and Sharma SC. Glia–Neuron Interactions in the Mammalian Retina. Prog Retin Eye Res 2016;51:1–40.

240. Read SP, Cashman SM, and Kumar-Singh R. POD Nanoparticles Expressing GDNF Provide Structural and Functional Rescue of Light-Induced Retinal Degeneration in an Adult Mouse. Mol Ther 2010;18:1917–26.

241. Tao Y, Chen T, Fang W, et al. The Temporal Topography of the N-Methyl- N-Nitrosourea Induced Photoreceptor Degeneration in Mouse Retina. Sci Rep 2015;5:18612.

242. Organisciak DT and Vaughan DK. Retinal Light Damage: Mechanisms and Protection. Prog Retin Eye Res 2010;29:113–34.

243. Gruys E, Toussaint M, Niewold T, and Koopmans S. Acute Phase Reaction and Acute Phase Proteins. J Zhejiang Univ Sci B 2005;6:1045–56.

244. Raad S de, Szczesny PJ, Munz K, and Remé CE. Light Damage in the Rat Retina: Glial Fibrillary Acidic Protein Accumulates in Müller Cells in Correlation with Photoreceptor Damage. Ophthalmic Res 1996;28:99–107.

245. Hanif AM, Lawson EC, Prunty M, et al. Neuroprotective Effects of Voluntary Exercise in an Inherited Retinal Degeneration Mouse Model. Invest Opthalmol Vis Sci 2015;56:6839–46.

246. Liu Y, Zhou J, and White KP. RNA-Seq Differential Expression Studies: More Sequence or More Replication? Bioinformatics 2014;30:301–4.

247. Laboissonniere LA, Goetz JJ, Martin GM, et al. Molecular Signatures of Retinal Ganglion Cells Revealed through Single Cell Profiling. Sci Rep 1 2019;9:15778.

248. De Silva SR, Barnard AR, Hughes S, et al. Long-Term Restoration of Visual Function in End-Stage Retinal Degeneration Using Subretinal Human Melanopsin Gene Therapy. Proc Natl Acad Sci USA 2017;114:11211–6.

249. Danciger M, Matthes MT, Yasamura D, et al. A QTL on Distal Chromosome 3 That Influences the Severity of Light-Induced Damage to Mouse Photoreceptors. Mamm Genome 2000;11:422–7.

250. Pérez de Sevilla Müller L, Sargoy A, Rodriguez AR, and Brecha NC. Melanopsin Ganglion Cells Are the Most Resistant Retinal Ganglion Cell Type to Axonal Injury in the Rat Retina. PLoS One 2014;9:e93274.

251. La Morgia C, Ross-Cisneros FN, Sadun AA, et al. Melanopsin Retinal Ganglion Cells Are Resistant to Neurodegeneration in Mitochondrial Optic Neuropathies. Brain 2010;133:2426–38.

252. Morgia CL, Ross-Cisneros FN, Koronyo Y, et al. Melanopsin Retinal Ganglion Cell Loss in Alzheimer Disease. Ann Neurol 2016;79:90–109.

253. González-Menéndez I, Reinhard K, Tolivia J, Wissinger B, and Münch TA. Influence of Opa1 Mutation on Survival and Function of Retinal Ganglion Cells. Invest Ophthalmol Vis Sci 2015;56:4835–45.

254. Sadun AA, Win PH, Ross-Cisneros FN, Walker SO, and Carelli V. Leber's Hereditary Optic Neuropathy Differentially Affects Smaller Axons in the Optic Nerve. Trans Am Ophthalmol Soc 2000;98:223–35.

255. Georg B, Ghelli A, Giordano C, et al. Melanopsin-Expressing Retinal Ganglion Cells Are Resistant to Cell Injury, but Not Always. Mitochondrion 2017;36:77–84.

256. Pezzullo L, Streatfeild J, Simkiss P, and Shickle D. The Economic Impact of Sight Loss and Blindness in the UK Adult Population. BMC Health Serv Res 2018;18:63.

257. Liew G, Michaelides M, and Bunce C. A Comparison of the Causes of Blindness Certifications in England and Wales in Working Age Adults (16–64 Years), 1999–2000 with 2009–2010. BMJ Open 2014;4:e004015.

258. RetNet. URL: `https://sph.uth.edu/RetNet/` (visited on 01/10/2020).

259. Broadgate S, Yu J, Downes SM, and Halford S. Unravelling the Genetics of Inherited Retinal Dystrophies: Past, Present and Future. Prog Retin Eye Res 2017;59:53–96.

260. Verbakel SK, van Huet RAC, Boon CJF, et al. Non-Syndromic Retinitis Pigmentosa. Prog Retin Eye Res 2018;66:157–86.

261. Hartong DT, Berson EL, and Dryja TP. Retinitis Pigmentosa. Lancet 2006;368:1795–809.

262. Hanany M, Rivolta C, and Sharon D. Worldwide Carrier Frequency and Genetic Prevalence of Autosomal Recessive Inherited Retinal Diseases. Proc Natl Acad Sci USA 2020;117:2710–6.

263. Teussink MM, Lee MD, Smith RT, et al. The Effect of Light Deprivation in Patients With Stargardt Disease. Am J Ophthalmol 2015;159:964–72.

264. Age-Related Eye Disease Study Research Group. Risk Factors Associated with Age-Related Macular Degeneration: A Case-Control Study in the Age-Related Eye Disease Study: Age-Related Eye Disease Study Report Number 3. Ophthalmology 2000;107:2224–32.

265. Sui GY, Liu GC, Liu GY, et al. Is Sunlight Exposure a Risk Factor for Age-Related Macular Degeneration? A Systematic Review and Meta-Analysis. Br J Ophthalmol 2013;97:389–94.

266. Parmeggiani F, S. Sorrentino F, Ponzin D, Barbaro V, Ferrari S, and Di Iorio E. Retinitis Pigmentosa: Genes and Disease Mechanisms. Curr Genomics 2011;12:238–49.

267. Johnson LV, Leitner WP, Staples MK, and Anderson DH. Complement Activation and Inflammatory Processes in Drusen Formation and Age Related Macular Degeneration. Exp Eye Res 2001;73:887–96.

268. Edwards AO, Ritter R, Abel KJ, Manning A, Panhuysen C, and Farrer LA. Complement Factor H Polymorphism and Age-Related Macular Degeneration. Science 2005;308:421–4.

269. Wangsa-Wirawan ND. Retinal Oxygen: Fundamental and Clinical Aspects. Arch Ophthalmol 2003;121:547.

270. Rozing MP, Durhuus JA, Krogh Nielsen M, et al. Age-Related Macular Degeneration: A Two-Level Model Hypothesis. Prog Retin Eye Res 2019;76:100825.

271. Seabrook TA, Burbridge TJ, Crair MC, and Huberman AD. Architecture, Function, and Assembly of the Mouse Visual System. Annu Rev Neurosci 2017;40:499–538.

272. Collin GB, Gogna N, Chang B, et al. Mouse Models of Inherited Retinal Degeneration with Photoreceptor Cell Loss. Cells 2020;9:931.

273. Jin ZB, Okamoto S, Osakada F, et al. Modeling Retinal Degeneration Using Patient-Specific Induced Pluripotent Stem Cells. PLOS ONE 2011;6:e17084.

274. Gao ML, Lei XL, Han F, et al. Patient-Specific Retinal Organoids Recapitulate Disease Features of Late-Onset Retinitis Pigmentosa. Front Cell Dev Biol 2020;8.

275. Angueyra JM and Kindt KS. Leveraging Zebrafish to Study Retinal Degenerations. Front Cell Dev Biol 2018;6.

276. Pennesi ME, Neuringer M, and Courtney RJ. Animal Models of Age Related Macular Degeneration. Mol Aspects Med 2012;33:487–509.

277. Wenzel A, Grimm C, Samardzija M, and Remé CE. Molecular Mechanisms of Light-Induced Photoreceptor Apoptosis and Neuroprotection for Retinal Degeneration. Prog Retin Eye Res 2005;24:275–306.

278. Hadziahmetovic M, Kumar U, Song Y, et al. Microarray Analysis of Murine Retinal Light Damage Reveals Changes in Iron Regulatory, Complement, and Antioxidant Genes in the Neurosensory Retina and Isolated RPE. Invest Ophthalmol Vis Sci 2012;53:5231–41.

279. Egger A, Samardzija M, Sothilingam V, et al. PGC-1α Determines Light Damage Susceptibility of the Murine Retina. PLoS One 2012;7:e31272.

280. Li H, Lian L, Liu B, et al. KIT Ligand Protects against Both Light-Induced and Genetic Photoreceptor Degeneration. eLife 2020;9:e51698.

281. Cicerone CM. Cones Survive Rods in the Light-Damaged Eye of the Albino Rat. Science 1976;194:1183–5.

282. Scholz R, Sobotka M, Caramoy A, Stempfl T, Moehle C, and Langmann T. Minocycline Counter-Regulates pro-Inflammatory Microglia Responses in the Retina and Protects from Degeneration. J Neuroinflammation 2015;12:209.

283. Elachouri G, Lee-Rivera I, Clérin E, et al. Thioredoxin Rod-Derived Cone Viability Factor Protects against Photooxidative Retinal Damage. Free Radic Biol Med 2015;81:22–9.

284. Rattner A, Toulabi L, Williams J, Yu H, and Nathans J. The Genomic Response of the Retinal Pigment Epithelium to Light Damage and Retinal Detachment. J Neurosci 2008;28:9880–9.

285. Krishnan J, Chen J, Shin KJ, et al. Gene Expression Profiling of Light-Induced Retinal Degeneration in Phototransduction Gene Knockout Mice. Exp Mol Med 2008;40:495–504.

286. Demos C, Bandyopadhyay M, and Rohrer B. Identification of Candidate Genes for Human Retinal Degeneration Loci Using Differentially Expressed Genes from Mouse Photoreceptor Dystrophy Models. Mol Vis 2008;14:1639–49.

287. Deguine J and Barton GM. MyD88: A Central Player in Innate Immune Signaling. F1000Prime Rep 2014;6:97.

288. Masuda T, Iwamoto S, Mikuriya S, et al. Transcription Factor IRF1 Is Responsible for IRF8-Mediated IL-1β Expression in Reactive Microglia. J Pharmacol Sci 2015;128:216–20.

289. Kim BJ and Zack DJ. The Role of C-Jun N-Terminal Kinase (JNK) in Retinal Degeneration and Vision Loss. In: *Retinal Degenerative Diseases*. Ed. by Ash JD, Anderson RE, LaVail MM, Bowes Rickman C, Hollyfield JG, and Grimm C. Vol. 1074. Cham: Springer International Publishing, 2018:351–7.

290. Cui J, Chen Y, Wang HY, and Wang RF. Mechanisms and Pathways of Innate Immune Activation and Regulation in Health and Cancer. Hum Vaccin Immunother 2015;10:3270–85.

291. Wong RS. Apoptosis in Cancer: From Pathogenesis to Treatment. J Exp Clin Cancer Res 2011;30:87.

292. Kim EJ, Grant GR, Bowman AS, Haider N, Gudiseva HV, and Chavali VRM. Complete Transcriptome Profiling of Normal and Age-Related Macular Degeneration Eye Tissues Reveals Dysregulation of Anti-Sense Transcription. Sci Rep 2018;8:3040.

293. Miller CG, Budoff G, Prenner JL, and Schwarzbauer JE. Minireview: Fibronectin in Retinal Disease. Exp Biol Med (Maywood) 2017;242:1–7.

294. Fritsche LG, Igl W, Bailey JNC, et al. A Large Genome-Wide Association Study of Age-Related Macular Degeneration Highlights Contributions of Rare and Common Variants. Nat Genet 2016;48:134–43.

295. Ito YA, Goping IS, Berry F, and Walter MA. Dysfunction of the Stress-Responsive FOXC1 Transcription Factor Contributes to the Earlier-Onset Glaucoma Observed in Axenfeld-Rieger Syndrome Patients. Cell Death Dis 2014;5:e1069.

296. Zhang R, Lahens NF, Ballance HI, Hughes ME, and Hogenesch JB. A Circadian Gene Expression Atlas in Mammals: Implications for Biology and Medicine. Proc Natl Acad Sci USA 2014;111:16219–24.

297. Gehrs KM, Anderson DH, Johnson LV, and Hageman GS. Age-related Macular Degeneration—Emerging Pathogenetic and Therapeutic Concepts. Ann Med 2006;38:450–71.

298. Dunaief JL, Dentchev T, Ying GS, and Milam AH. The Role of Apoptosis in Age-Related Macular Degeneration. Arch Ophthalmol 2002;120:1435–42.

299. Zhu C, Wang S, Wang B, et al. 17β-Estradiol up-Regulates Nrf2 via PI3K/AKT and Estrogen Receptor Signaling Pathways to Suppress Light-Induced Degeneration in Rat Retina. Neuroscience 2015;304:328–39.

300. Doonan F, O'Driscoll C, Kenna P, and Cotter TG. Enhancing Survival of Photoreceptor Cells in Vivo Using the Synthetic Progestin Norgestrel. J Neurochem 2011;118:915–27.

301. Snow KK, Cote J, Yang W, Davis NJ, and Seddon JM. Association between Reproductive and Hormonal Factors and Age-Related Maculopathy in Postmenopausal Women. American Journal of Ophthalmology 2002;134:842–8.

302. Fraser-Bell S, Donofrio J, Wu J, Klein R, Azen SP, and Varma R. Sociodemographic Factors and Age-Related Macular Degeneration in Latinos: The Los Angeles Latino Eye Study. Am J Ophthalmol 2005;139:30–8.

303. Friedman DS, O'Colmain BJ, Muñoz B, et al. Prevalence of Age-Related Macular Degeneration in the United States. Arch Ophthalmol 2004;122:564–72.

304. Wang Zn, Takemori H, Halder SK, Nonaka Y, and Okamoto M. Cloning of a Novel Kinase (SIK) of the SNF1/AMPK Family from High Salt Diet-Treated Rat Adrenal. FEBS Lett 1999;453:135–9.

305. Horike N, Takemori H, Katoh Y, et al. Adipose-Specific Expression, Phosphorylation of Ser^{794} in Insulin Receptor Substrate-1, and Activation in Diabetic Animals of Salt-Inducible Kinase-2. J Biol Chem 2003;278:18440–7.

306. Uebi T, Itoh Y, Hatano O, et al. Involvement of SIK3 in Glucose and Lipid Homeostasis in Mice. PLoS One 2012;7:e37803.

307. Funato H, Miyoshi C, Fujiyama T, et al. Forward-Genetics Analysis of Sleep in Randomly Mutagenized Mice. Nature 2016;539:378–83.

308. Lizcano JM, Göransson O, Toth R, et al. LKB1 Is a Master Kinase That Activates 13 Kinases of the AMPK Subfamily, Including MARK/PAR-1. EMBO J 2004;23:833–43.

309. Altarejos JY and Montminy M. CREB and the CRTC Co-Activators: Sensors for Hormonal and Metabolic Signals. Nat Rev Mol Cell Biol 2011;12:141–51.

310. Haberland M, Montgomery RL, and Olson EN. The Many Roles of Histone Deacetylases in Development and Physiology: Implications for Disease and Therapy. Nat Rev Genet 2009;10:32–42.

311. Şahin HB, Sayın S, Holder M, Buğra K, and Çelik A. Salt Inducible Kinases as Novel Notch Interactors in the Developing Drosophila Retina. PLoS One 2020;15:e0234744.

312. Pembroke WG, Babbs A, Davies KE, Ponting CP, and Oliver PL. Temporal Transcriptomics Suggest That Twin-Peaking Genes Reset the Clock. eLife 2015;4:e10518.

313. Katoh Y, Takemori H, Min L, et al. Salt-Inducible Kinase-1 Represses cAMP Response Element-Binding Protein Activity Both in the Nucleus and in the Cytoplasm. Eur J Biochem 2004;271:4307–19.

314. Brown LA, Williams J, Taylor L, et al. Meta-Analysis of Transcriptomic Datasets Identifies Genes Enriched in the Mammalian Circadian Pacemaker. Nucleic Acids Res 2017;45:9860–73.

315. Park M, Miyoshi C, Fujiyama T, et al. Loss of the Conserved PKA Sites of SIK1 and SIK2 Increases Sleep Need. Sci Rep 2020;10:8676.

316. Xue Y, Liu P, Wang H, et al. Modulation of Circadian Rhythms Affects Corneal Epithelium Renewal and Repair in Mice. Invest Ophthalmol Vis Sci 2017;58:1865–74.

317. Tosini G, Pozdeyev N, Sakamoto K, and Iuvone PM. The Circadian Clock System in the Mammalian Retina. BioEssays 2008;30:624–33.

318. Fuhrer T and Zamboni N. High-Throughput Discovery Metabolomics. Curr Opin Biotechnol. Analytical Biotechnology 2015;31:73–8.

319. Soloviev M. Peptidomics: Divide et Impera. In: *Peptidomics: Methods and Protocols.* Ed. by Soloviev M. Methods in Molecular Biology. Totowa, NJ: Humana Press, 2010:3–9.